Republic of Iraq
Ministry of Higher Education
And Scientific Research
University of Babylon
College of Engineering
Department of Mechanical Engineering

Investigation of the Three-dimensional Natural Convection Flow inside a Cavity with Different Geometries filled with Nanofluids

A Dissertation Submitted to the College of Engineering, University of Babylon in Partial Fulfillment of the Requirements of the Degree of Doctorate of Philosophy in Mechanical Engineering

By

Zainab Kareem Ghoben

B.Sc. & M.Sc., Mechanical Power Engineering

Supervised by:
Prof. Dr. Ahmed Kadhim Hussein

2023 A.D – 1444 A.H

Abstract

Due to the wide applications of the laminar natural convection inside cavities like cooling systems, solar collecting systems and else. Laminar convective heat transfer inside cavities with 3D partially heated walls was studied numerically and experimentally. The study was performed through the use of different domain configurations, boundary conditions and insertion of solid bodies inside domains.

Numerically, the software package (COMSOL Multiphysics) that adopts the finite difference method (FDM) was used to simulate four different 3D cavity geometries which are parallelogrammical, hexagonal, octagonal and elliptical according to the shape of the cross-section between the hot and cold walls. The cavities are filled with nanofluid (alumina-water / Al_2O_3-H_2O) and pure water. The nanoparticle solid volume fraction range was ($0.01 \leq \varphi \leq 0.05$) and Rayleigh number range ($10^3 \leq Ra \leq 10^6$).

The parallelogrammical cavity was studied for three different skew angles to determine the best one (γ=30º, 45º, 60º). Also, optimization of the best arrangements for the heated and cooled walls (left-right, right-left and bottom-up) was studied. It was concluded that the angle (60º) with the left wall hot and the right wall cold gives the best results. The results of the study were presented through the isotherm surfaces, the streamlines, the horizontal and vertical velocities, the local and the average Nusselt number (Nu). There is a modification of the parallelogram cavity where which cylindrical inserted bodies with different size, distribution and dimensions inside the cavity. It was

observed that, the size of these objects, their number, their distribution, and their overall surface areas have an effect on the thermal behavior inside this cavity.

The experimental work was fabricating a parallelogrammical cavity of constant lateral length walls (15 cm) except the front horizontal length was (16 cm) filled with nanofluid (alumina-deionized water) with three different solid volume fraction (φ=0.01, 0.03, and 0.05) and ($Ra=10^5$ and 10^6). It is worth noting that the alumina nanoparticles were of gamma type and had ($d_{np} \leq 45$ nm). The heat transfer was studied by temperature distribution along the three axes from the hot wall to the cold wall and the average (Nu) on the hot wall. It appeared that there is a good agreement between the numerical and the experimental results with about (0.03%) deviation. Also, the results of the study were compared with previous published studies, and good agreement was noted between the results.

Both the numerical and the experimental results of the parallelogrammical cavity proved that the increase in (φ) and (Ra) increases the average (Nu) or enhances the convective heat transfer. Whereas, increasing the solid volume fraction to (φ=0.05) over water (φ=0) leads to an increase in the average (Nu) by about (13) times for the same conditions. While the improvement in the average (Nu) of hexagonal, octagonal and elliptical cavities was about (17.6%, 18% and 17.2%), respectively, relative to the improvement in the parallelogrammical cavity at ($Ra=10^6$). The best improvement was recorded from the central location and higher overall surface area cases. In general, the insertion of three elements improves convection by about twice (200%) as much as the one-body improvement for all (Ra) adopted in this study.

Chapter One: Introduction

1.1. General Concept of the Natural Convection Heat Transfer

The convection heat transfer represents one of the major modes of the three basic types of heat transfer associated with fluid flow. The convection is considered forced when it is accelerated by external tools like fans or pumps [1].

It is termed natural when occurs spontaneously and mixed when it initiated by the two manners [2]. The natural or free convection can be classified into external and internal flows. In the external flow, the solid object is surrounded by the flowing fluid like the flows over the flat plate.

For the internal flow, the fluid is surrounded by the solid objects like the flow inside cavities and pipes. In energy related applications, the natural convection plays a dominant role because of its simplicity, low cost and reliability. Since the fluid movement is generated by density variation which accomplished naturally without an additional effort [3].

The density variation in the natural convection flows may have initiated by different physical phenomena; either temperatures difference, difference in the concentrations of fluid or the presence of multiple flow phases [4].

The Natural convection inside a closed cavity is a representation of the internal flow which is a common practical application in cooling and energy transportation. It is important to mention that, the proper

design of the cavities is a key parameter in order to achieve best performance [5]. There are two main classes of natural convection flows that are driven by temperature differences: the first in which the basic temperature gradient is parallel to the direction of gravity (heating from below) and the other in which this gradient is orthogonal to the direction of gravity (heating from the side) which is known as a differentially heated cavities [6].

1.2. Nanotechnology and Nanofluid Concept

Nanofluid is a two-phase (liquid-solid) mixture flow that formed by suspension of solid particles have high thermal, rheological and wettability properties in a fluid named as the base fluid. These particles must have at least one dimension below (100 nm). The base fluids are water, alcohol, oil and etc. [7].

Nanofluids are now have a great interest for improving heat transfer performance that are related to energy saving. Among the several thermophysical properties of a fluid, the thermal conductivity and dynamic viscosity have more significant role on heat transfer behavior [8].

Adding nano particles increasing the thermal conductivity and dynamic viscosity. The higher thermal conductivity has a favorable effect on convective heat transfer of fluids, while the increase in dynamic viscosity has a worse effect on it.

So, these parameters are controlled by specifying ranges of the particles solid volume fraction in base fluids that do not activating the worse effect of high viscosity. The enhanced thermal conductivity of nanofluids offers several benefits that makes the nanofluids promising for many applications such as [9]:

1. Higher cooling rates
2. A decreased power needs for pumping.
3. Smaller and lighter cooling systems, reduced inventory of heat transfer fluids.
4. Reduced friction coefficients, and improved wear resistance.

1.3. Applications of the Natural Convection inside Cavities

One of the most significant applicable challenges in the industrial area is cooling. Also, it is very important to design the cooling systems in most efficient manners and minimum power requirement. Effective cooling of electronic components has become increasingly important as power dissipation to be up to date with the fast growth of technology.

The applications of such cooling technique are the passive cooling of computers, smart mobile devices, microelectronic devices operating at high speeds and brighter optical devices, laser technology and electronic circuit boards, etc. [10].

Besides cooling of the electronic components, there are numerous other practical applications of natural convection in cavities including, air conditioning systems, thermal insulation in buildings, high-power engines and pumps, heat exchangers and electrical transformers.

Also, it found in renewable energy processes like convective processes in lakes and reservoirs, solar energy applications like collectors, nuclear reactors, storage of nuclear waste, petrochemicals. Also, in the aerospace systems as like as food and dairy industries [11].

In the current study, the cavities are classified into two types called classical or cubical and complex or non-cubical cavities. Four different geometries are studied numerically in three dimensions (3D)

named as; parallelogrammical, hexagonal, octagonal and elliptical cavities. In addition to the mentioned applications, the practical application of the current work, parallelogrammical cavity is the large high-power pumps like the water push pumps of Al-Diwaniya Water Office that works inside buildings (indoor pumps).

These pumps are working at the indoor conditions which are rounded as (20ºC – 25ºC) and (28ºC – 35ºC) at summer and winter seasons, respectively. The longtime operation that reaches about (22 hour/day) makes some of the pump's parts fail repeatedly. This is due to the raise in temperature which reached about (40ºC – 55ºC).

In general, the considered cavities; hexagonal, octagonal and elliptical can be designated and manufactured to obey the demands of any of the mentioned applications. Where these cavities are featuring with special shapes that suitable to place in different locations without need for manufacturing adjustment especially for the applications of narrow regions.

The working fluid is water and nanofluid consists of alumina nanoparticles of (d_p<45nm) particle size that suspended in de-ionized water (Al_2O_3-water) base fluid which is selected due to its low cost and acceptable thermal enhancement.

The considered ranges of the nanoparticle solid volume fraction and the Rayleigh number for the numerical study are ($0.01 \leq \varphi \leq 0.05$) and ($10^3 \leq Ra \leq 10^6$) respectively. For the experimental study; the solid volume fractions are (φ=0.01, 0.03 and 0.05) while the temperature differences between the differentially heated walls are (ΔT= 16ºC and 26ºC) by considering two different values for the cold wall temperature (T_c=28ºC and 30ºC).

1.4. Objective of the Present Study

The present study focused on the effect of the following on the natural convection heat transfer enhancement both numerically and experimentally:

1. The cavity geometry where four different shapes of cavities are studied named according to the lateral cross section between the hot and cold walls.

2. the cavities are parallelogrammical, hexagonal, octagonal and elliptical which are studied for the first time with the selected dimensions and arrangements of walls.

3. The surface area of cavity by considering different skew angles for the parallelogrammical cavity.

4. The location, number and distribution of inserted bodies.

5. The parallelogrammical cavity considered the main geometry which in turn visualized experimentally.

Chapter Two: Literature Review

2.1. Introduction

The widespread applications of the natural convection or buoyancy driven heat transfer and fluid flow inside cavities led to the clear attention received over the recent years [1-5]. This field was investigated numerically and experimentally. Where the increasing importance of the computer techniques for modelling and simulation allows a quantitative and qualitative evaluation of the different complex phenomenon. Many works in the current field were viewed for different geometries of the cavities; square or non-square [3-7]. The accomplished cases were studied under various conditions which enhanced the heat transfer.

Different techniques were presented, which able to enhance the heat transferred through the cavities by natural convection. These techniques were either changing the shape or inclination of the cavity [12-14]. On the other hand, adding fins inside the closed cavities was one of these techniques. The fins used by researchers were varied in location and shape. These fins or baffles were either rigid or sometimes porous [15-18].

Enhancing the working fluid properties by using various (Ra) was considered as a technique also. The laminar natural convection (Ra) range of ($10^3 \leq Ra \leq 10^6$) was depended on by many researches. Recently, using the fluid additives by means of two-phase fluids (liquid – solid particles) was a common technique in this field. Adding particles

with nano scale to the base fluids improving the fluid thermal properties which enhance the heat transfer performance inside cavities [19, 20]. Researchers approved that, the thermal properties were enhanced by adding the nanoparticles of metals or other materials like ceramics by a specific volume fraction. This range was not to exceed ($0.01 \leq \varphi \leq 0.06$) to get the better enhancement [21-23] and avoid the problems of agglomeration of the solid particles at the same time.

Sometimes using the external magnetic field enhancement scheme is one of these techniques [24], which is of higher importance due to its wide application in metal casting and other industrial applications [25, 26]. From other side, number of researchers depend on the advantages of the porous media expected advantages in designing their cavities [27-29].

The following sections introduced a detailed literature review on the specific research region of the three-dimensional numerical and experimental natural convection heat transfer inside cavities for different geometries; classical (cubical) or complex (non-cubical), boundary conditions and filled with different working fluids, classical (single phase) or nanofluids (two phase).

2.2. Numerical and Experimental Studies inside Classical Cavities

The natural convection heat transfer inside the classical square or rectangle cavities had been studied in four groups that reviewed for the period (2010-2020) where (2020) is the year of starting the current study. For different working fluids; classical or nanofluids numerically and experimentally as presented in Table (2.1).

2.2.1. Numerical Studies in Classical Cavities filled with Classical Fluids

Zemani et al. [30], 2014, analyzed numerically the natural convection in a cubical and differentially heated air-filled cavity with ($10^5 \leq Ra \leq 10^6$). The geometry was a cube with wavy hot surface. Three undulations and three partitions introduced at the crests with constant hot temperature. The opposite wall was straight and has a constant cold temperature. The other walls were thermally insulated. The investigation has been performed for different partitions lengths. The results obtained show that the mean (Nu) decreases compared with the heat transfer in the undulated cubical cavity without partitions. This decrease was up (40%) in heat transfer at the same (Ra).

Li et al. [31], 2016, investigated numerically the natural convection of air in a cubical cavity heated partially for ($10^4 \leq Ra \leq 10^5$). Two opposite vertical walls were kept at different temperatures. While, the remained four walls were considered either adiabatic for the first case or had linear temperature variations for the second case. Whereas in the third case, the front and back walls have linearly variable temperature. The bottom and top walls were adiabatic for all cases. The results of the third type exhibited more enhancement in the average (Nu) than the other two types at the same (Ra).

Al-Rashed et al. [32], 2017, investigated the natural convection in a cubical cavity filled by air numerically at ($10^3 \leq Ra \leq 10^6$).. Both the left and right sidewalls were subjected to four different arrangements of partial cooling and heating sections. The remaining walls were assumed thermally insulated. It was found that the average (Nu) reached its peak value when both left and right sidewalls of the cavity were subjected to the partial heating and cooling at their middle position.

Wang et al. [33], 2017, performed the study of the natural convection of air in a differentially heated cubical cavity at ($10^3 \leq Ra \leq 10^{10}$). The left wall was cold and the right was hot while adiabatic lateral walls. It was found that the boundary layers of temperature and velocity were developed adjacent to the isothermal walls, and become thinner as (Ra) increases. Where the effect on the overall heat transfer decreases with increasing (Ra). Also, an exponential scaling law between (Nu) and (Ra) was found for the study range of (Ra).

Spizzichino et al. [34], 2019, investigated numerically the natural convection flow of air in a cold cubical cavity at ($10^4 \leq Ra \leq 10^6$). The cavity included a tandem of cold and hot vertically aligned cylinders inside it. It was found that the distance between the cylinders played an important role in determining the characteristics of the instability mechanisms governing the oscillatory flow. Also, in all the configurations studied in the framework the average and instantaneous (Nu) on the hot cylinder values are higher than the corresponding (Nu) on the cold cylinder.

Alnaqi et al. [35], 2020, investigated numerically the natural convection in an air-filled cubical cavity with active lateral walls at ($10^3 \leq Ra \leq 10^6$). The lateral front and right sidewalls were maintained at an isothermal cold temperature. While the back and left were subjected to an isothermal hot temperature. The upper and lower walls were kept adiabatic. It was shown that, the increase in (Ra) leads to increase of the average (Nu).

Alshomrani et al. [36], 2020, studied numerically the natural convection of the air inside a 3D inclined cavity at ($10^3 \leq Ra \leq 10^6$). The left and right walls were cooled partially whereas the other walls were

kept adiabatic. In the left and right walls, three different locations of the cooler were examined. While, the heater moved in three locations in the middle of the cavity. It was recognized that the inclination of the cavity and the locations of the coolers highly influenced the flow and thermal fields inside the cavity. Also, that the computed results were found to be very useful to design the cooling of electronic equipment.

Onyango et al. [37], 2013, focused on the numerical study of the natural convection in a square cavity. The two opposite vertical walls and the top wall were considered cold with constant temperature. A fixed heat source was attached at the middle bottom surface. The other two vertical walls and the non-heated part of the bottom surface were considered insulated. It was found that, the position of the heat source was one of the most important parameters that affecting flow and temperature fields and the heat transfer was very weak at the sides of the cavity. The flow and thermal fields were strongly affected by the cold surfaces.

Ahmadi M. [38], 2014, carried out a numerical study of the steady laminar natural convection in a cubical cavity numerically at ($10^3 \leq Ra \leq 10^6$). The left vertical wall had two elements, the larger upper was kept cold. While the smaller lower kept hot. Whereas the remaining walls were insulated. The results indicated that, by increasing the distance between heat sources, the average (Nu) significantly decreased. Also, the average temperature and maximum component of velocity in all directions were increased. Moreover, by increasing the length of the cold source ratio, the rate of heat transfer of the hot source was increased.

Kolsi et al. [33], 2016, investigated numerically the natural convection and the generated entropy with the internal heat generation

inside a cubical cavity. A partial cooler was located on the insulated bottom wall and the cavity was heated differentially. The horizontal walls were adiabatic. It was found that, the role of location and height of partition became less important with increasing the internal (Ra). The entropy generation was strongly dependent on the ratio of internal to external (Ra). Based on the values of geometrical parameter, (Nu) is increased with increasing of external (Ra).

Gibanov and Sheremet [39], 2017, numerically solved the transient natural convection inside a cubical cavity filled with a Newtonian fluid at ($10^4 \leq Ra \leq 10^6$). It was equipped by a hot partition as a heat source having a triangular cross section. The vertical opposite walls were cooled while the rest walls were adiabatic. It was found that, the extreme left position of the heater illustrated more essential cooling of the cavity. The increase in the distance between the heat source and the left vertical wall leads to non-monotonic changes of the average (Nu).

For the same cavity configuration and heating system **Gibanov and Sheremet** [40], 2018, investigated numerically five various shapes of the heater cross section (rectangular, three trapezoidal and one triangular). It was found that, trapezoidal shapes were more effective than other considered shapes. For high values of (Ra) the differences for the average (Nu) between the triangular shape and other configurations are increased.

Then, **Gibanov and Sheremet** [41], 2019, designated a discrete heater of a trapezoidal shape located at the bottom wall of a cubical cavity. The heater was maintained at constant temperature. It was detected that, an increase in the length of the local heat source did not have a strong effect compared with the increase in the height or the overall size on the average (Nu).

2.2.2. Numerical Studies in Classical Cavities filled with Nanofluids

Ravnik et al. [42] 2010, investigated numerically the free convection inside three-dimensional cavity filled with three different types of water based nanofluids (Cu-water, Al_2O_3-water and TiO_2-water) at ($10^3 \leq Ra \leq 10^6$) and ($\varphi \leq 20\%$). In their analysis, two cases were studied, the first case was a differentially heated cavity. While, the second one with a hot strip located in two locations in the cavity. the other walls for both cases, were kept thermally insulated. It was found that, the increase in (φ) enhanced the heat transfer rate and reach its peak value for (Cu-water) nanofluid.

Arefmanesh and Tavakoli [43], 2012, solved numerically the steady natural convection fluid flow and heat transfer in a cubical cavity filled with three different nanofluids (Al_2O_3-water, Cu-water, TiO_2-water) with ($10^3 \leq Ra \leq 10^5$) and (φ=0.05, 0.1). The left and right vertical sidewalls of the cavity were maintained at constant hot and cold temperatures. The remaining walls were insulated. The results showed that, the average (Nu) increased with increasing (φ) for all selected nanofluids.

Kolsi et al. [44], 2014, investigated numerically the natural convection heat transfer, fluid flow and entropy generation inside a cubical cavity filled with (Al_2O_3-water) nanofluid at ($10^3 \leq Ra \leq 10^6$) and ($0 < \varphi \leq 20\%$). Both, left and right sidewalls were maintained at isothermal hot and cold temperatures. The other walls were considered adiabatic. The results showed that, the local (Nu) increased when (φ) increased. While, the average (Nu) increased when both (φ) and (Ra) increase.

Ternik P. [45], 2015, solved numerically the steady natural convection in a cubical cavity filled with (Au-water) nanofluid at ($0 < \varphi \leq 5\%$). The vertical wall was heated, while the adjacent was cooled.

It was founded that, adding nanoparticles delays the onset of convection. It was found that the average (Nu) smaller than those obtained in the case of pure water with the same (Ra) unlike the other researchers.

Purusothaman et al. [46], 2016, investigated the numerical analysis of the natural convection cooling equipment with a (3×3) array of isothermal heaters which was mounted on one vertical wall of the cavity. The cavity was filled with various nanofluids (Cu-water and Al_2O_3-water) at ($10^5 \leq Ra \leq 10^7$) and ($0 < \varphi \leq 0.01$). It was observed that, (Cu-water) nanofluid had the greatest effect on the equipment performance compared with (Al_2O_3-water) nanofluid. As like as, the averaged (Nu) increased with the increase in both (Ra) and (φ).

Salari et al. [47], 2016, studied numerically the transient natural convection for cubical cavity with layered fluid system. The cavity was differentially heated and filled with two immiscible gas/liquid fluids (air/MWCNTs-water). Two heaters with constant heat flux were placed at the sides. The top and bottom walls were kept at constant cold temperature. The results showed that, the nanofluid interface aspect ratio had significant influences on the fluid flow, heat transfer performance. Also, it was shown that, the mean (Nu) was reduced by increasing the nanofluid interface aspect ratio and enhanced by increasing of (Ra).

For the same cavity and fluid conditions but with fillets on its bottom wall **Salari et al.** [48], 2017, investigated the transient natural convection. The results showed that, the curved corner an effective method to control the fluid flow and the energy consumption.

Kolsi et al. [49], 2016, presented a numerical simulation of natural convection inside a cubical cavity filled with (Al_2O_3-water) nanofluid at ($10^3 \leq Ra \leq 10^6$). The vertical walls were differentially heated. The cavity containing twin adiabatic blocks. The other walls were

adiabatic. The results showed that, the average (Nu) raised with the increase in (Ra) and (φ) while it was declined with the increase in the block size.

While **Kolsi et al.** [50], 2016, studied the laminar natural convection inside a cubical cavity with a solid conductive of inserts on the corners of triangular cross section. According to the number and location of these inserts, three cases were studied. The vertical left and right sidewalls of the cavity were assumed hot and cold respectively. The other sides were kept insulated. It was observed that, the heat transfer increased linearly according to the thermal conductivity ratio for the same geometrical parameters and (Ra).

Rahimi et al. [51], 2017, investigated numerically the natural convection of (CuO-water) nanofluid enclosed in a cubical cavity at ($10^3 \leq Ra \leq 10^6$) and ($0 < \varphi \leq 0.04$). The left and right sidewalls of it were assumed hot and cold respectively. While the other walls were assumed insulated. It was found that, the average (Nu) enhanced with increasing (Ra) and (φ).

Wang et al. [52], 2018, investigated numerically the natural convection of (Al_2O_3-water) nanofluid in a partially heated cubical cavity at ($10^4 \leq Ra \leq 10^6$) and ($0 < \varphi \leq 0.04$). The right sidewall was maintained at a constant low temperature, while a square heat source was located on the left sidewall. The remaining boundaries were thermally insulated. The results indicated that, the average (Nu) decreased with the increase of (φ). Also, it was found that the average (Nu) and the heat transfer enhancement were decreased with the increase of the heat source aspect ratio.

Benabderrahmane and Messadi [53], 2018, studied numerically the turbulent natural convection inside a rectangular cavity filled with

(Al_2O_3-water) nanofluid. The horizontal walls were considered isothermal where the bottom wall was hotter than the top one. The other walls were adiabatic. The results showed that, the average (Nu) increased with the increase of (Ra) and (φ). Also, in a comparison with pure water, nanofluid presented higher average (Nu) along the heating wall.

Sannad et al. [54], 2019, studied numerically the natural convection in a cavity containing (Cu-water) nanofluid. The cavity was included an isothermal heating block in the middle of the bottom as the first case and at the top in a second case. Both the right and the left vertical walls were kept at cold temperature and the other walls were insulated. The results illustrated that; the average (Nu) increased with (φ) for different values of (Ra). Also, the (Cu-water) nanofluid gave the best thermal transfer in the two considered configurations. Also, it was noticed that, the second case was the optimum choice for better heat transfer.

From other side, **Sannad et al.** [55], 2020, studied the transient laminar natural convection of (Al_2O_3, Cu, TiO_2) water based nanofluids inside a cubical partially heated cavity. It is heated by a partition maintained at a hot constant and uniform temperature. The right and left vertical walls were kept at cold temperature, while the others were kept adiabatic. The highlighted results were that the heat transfer in the presence of (Cu) nanoparticles was greater than that of (Al_2O_3) and (TiO_2). Also, as the length of the heat source increased the average (Nu) increased.

Then, for the same geometry of cavity but heated by two heating square portions on the left wall which maintained at hot temperature **Sannad et al.** [56], 2020, accomplished their study. The right wall and

the rest portion of the left vertical walls were kept at cold temperature, while the other walls were kept adiabatic. It was noticed that, the increase of the heating section size and (Ra) increased the heat removed by the same nanofluid. Also, increasing (φ) caused an increase in the heat exchange process.

Esfe et al. [35], 2020, investigated numerically the free convection flow of (CuO-water) nanofluid in a cubical cavity. A porous fins were embedded in different numbers on its right cold sidewall. Whereas, the left sidewall kept cold. The other walls were kept insulated. It was found that, the adding of nanoparticles possessed the greatest effect on the average (Nu). Also, it was observed that, the velocity of the nanofluids decreased when passing through the porous fins and noticed that, the pattern of temperature was very sensitive to the presence and number of porous fins at lowest ($Ra=10^3$).

Selimefendigil and Oztop [57], 2020, studied numerically the natural convection inside a cavity with one inclined side wall included a T-shaped heat source. The cold surface temperature of the cavity was controlled by using a thermoelectric cooler. While the hot surface of it was assumed inclined. It was found that, the average (Nu) was increased with increasing (φ). The variation in the average (Nu) versus (φ) was linear and the amount of enhancement was (128%) when compared to the pure water.

Moutaouakil et al. [58], 2020, studied numerically the natural convection inside a partially heated cubical cavity which was heated by using three identical and parallel elements on its left vertical wall. These elements had different inclinations. The cavity filled with different water based nanofluids (Cu-water, Al_2O_3-water, Ag-water, TiO_2-water). The results indicated that, the inclination angle had insignificant effect

on the average (Nu). The total (Nu) increased with (φ) and the aspect ratio of the heated elements. The numerical results also revealed that the (Cu-water) and (Ag-water) nanofluids offered a better heat exchange inside the cavity.

2.2.3. Experimental Studies in Classical Cavities filled with Classical Fluids

There are very little experimental studies in the current field, **Li and Tong** [59], 2016, studied the natural convection of air inside an inclined and vertical rectangular cavity with low width to height ratios experimentally and numerically. It was concluded that, increasing this ratio and cavity inclination accelerates the convective heat transfer. This ratio was insignificant when it became higher than (4). Also, the average (Nu) was correlated to the modified (Ra) and the adjusted aspect ratio with very little relative errors.

Nardini et al. [60], 2016, investigated the natural convection in a square cavity with partially active thermal sidewalls both numerically and experimentally. Four cold sources were placed on the vertical walls while the additional hot source placed on the base wall. Three different positions of the hot source varied along the base wall from the middle to the edge were investigated. The results showed that, different positions of the hot source enhanced the heat transfer. The best position of the hot source was on the middle.

Bharti et al. [61], 2018, studied experimentally the natural convective flow in a differentially heated cubical cavity filled with de-ionized water. An efficient use of (Z-type) schlieren technique for simultaneous measurement of ray-averaged velocity and temperature fields were considered. The velocity field was also determined by using laser-based (PIV) to compare with schlieren based technique. The

results showed that, the proposed technique was very robust and high accuracy in temperature measurements.

Karatas and Derbentli [62], 2018, studied experimentally the natural convection in six rectangular cavities with different (AR). All cavities had a united height and depth but different lengths. The cavities were closed, filled with air, and had one active vertical wall. The opposing vertical wall was inactive. The other four walls are adiabatic. The presented results showed that the mean (Nu) increased from (23.63 to 73.35) with decreasing aspect ratio from (6 to 1).

Whereas, **Karatas and Derbentli** [63], 2019, investigated the natural convection in differentially heated rectangular cavities. One of the vertical walls of the cavity was cooled, while the opposing vertical wall was heated. The cold and hot vertical walls were constant and time periodic temperatures, respectively. The other four walls were adiabatic. It was found that, the average (Nu) increases from (2.64 to 16.44) with decreasing aspect ratio from (6 to 1). The average (Nu) for the sinusoidally varying temperature was half of that for the constant temperature.

2.2.4. Experimental Studies in Classical Cavities filled with Nanofluids

Heris et al. [64], 2014, conducted an experimental study to investigate the effect of inclination angle on the natural convection inside a cubical cavity filled with various nanofluids as shown in **Fig.** (2.1). One of the surfaces was kept at a cold temperature and opposite side at a hot one. While the other four surfaces were insulated. The mixtures of three different types of nanoparticles (Al_2O_3, TiO2, CuO) within turbine oil were used as a heat transfer fluid. The results revealed that, the turbine oil had the highest (Nu) in any inclination angle of the

cavity compared to the nanofluids. Also, it was found that at the inclination angle of (90º) and the weight fraction of (0.2%) the (TiO_2) gives the maximum (Nu).

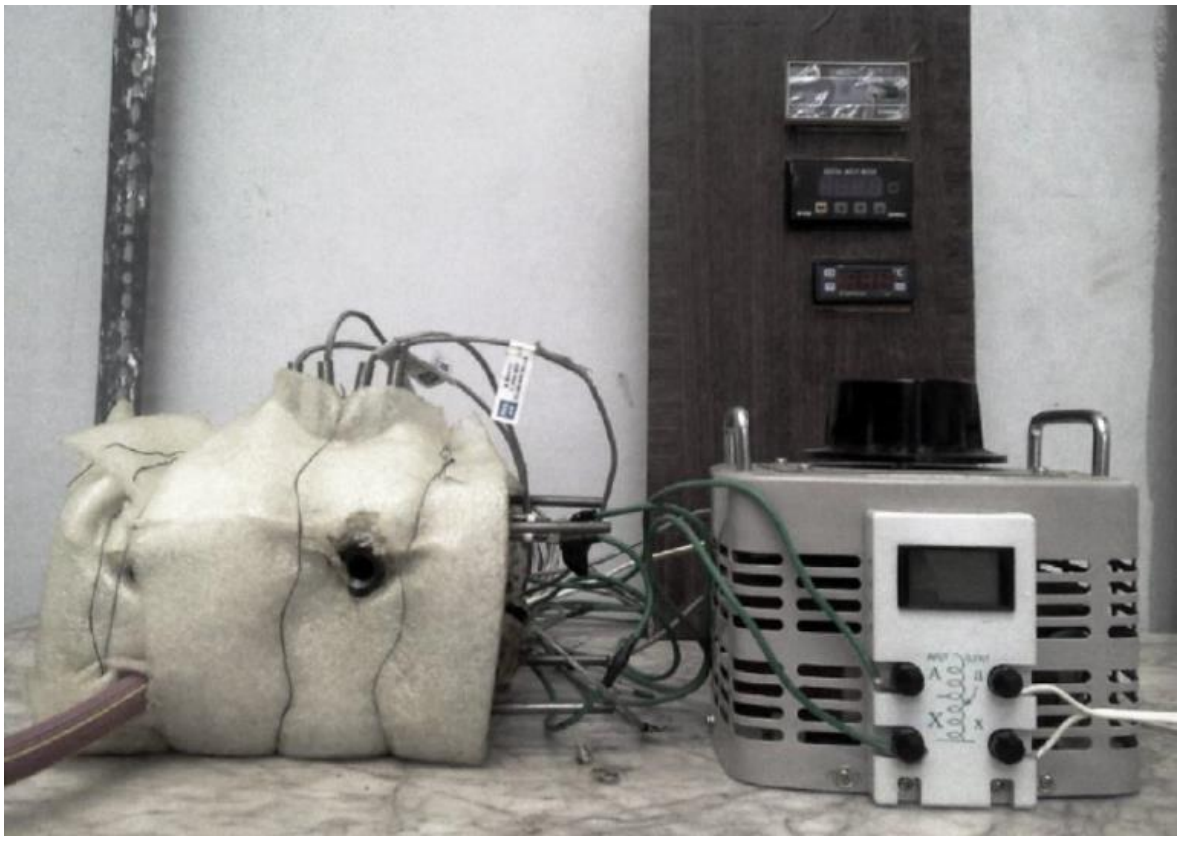

Figure (2.1): The experimental rig of Heris et al. [64].

Solomon et al. [65], 2017, studied experimentally the influence of (AR) of a rectangular cavity on the natural convection flow inside it. Three values of (AR) were adopted in their analysis. The cavity was filled with two different fluids; de-ionized water and Al_2O_3-water nanofluid. It was found that, the (AR) had a significant effect on (Nu). Also, it was concluded that, the optimum concentration of nanofluid for maximum heat transfer increases with increasing (AR).

Rahimi et al. [66], 2017, studied both experimentally and numerically the natural convection in a cuboid cavity filled with (DWCNTs-water) nanofluid. The cavity height, length and depth were equal. The left and right sidewalls had a constant uniform hot and cold

temperatures respectively. The other walls were insulated. It was found that, the average (Nu) enhanced with increasing (Ra) and (φ).

While **Rahimi et al.** [67], 2018, analyzed the natural convection heat transfer numerically and experimentally in the same cavity but filled with (MWCNT-MgO-water) hybrid nanofluid. It concluded from results that, the range of temperature of nanofluid is reduced with increasing of (φ). Increasing of temperature difference causes an enhancement of the average (Nu). The optimum value of (φ) for highest value of average (Nu) found to be (1%).

Torki and Etesami [68], 2020, investigated experimentally the natural convection heat transfer of (SiO_2-water) nanofluid inside inclined rectangular cavity with different inclination angles. It was made of two vertical copper plates as hot and cold walls, and the other sides were made of acrylic. The results showed that, the convection heat transfer is not enhanced by increasing (φ). The maximum (Nu) for all (φ) occurs when the cavity was in a horizontal status.

Giwa et al. [69], 2020, investigated experimentally the natural convection of the hybrid nanofluid (Al_2O_3-MWCNT/water) nanofluid in a square cavity. It was noticed that the (60:40) percent weight of (Al_2O_3: MWCNT) nanoparticles have the highest average (Nu) at each considered temperature. The maximum enhancement of (16.2%) was achieved at (T=50°C), in comparison to the base fluid. The average (Nu) is enhanced with increasing (Ra).

2.3. Numerical and Experimental Studies inside Complex Cavities

Lately, the researchers guided towards the modifications of the cavity shape from the simple classical to the more detailed complex configurations. This technique is to study the effect of these shapes on

the heat transfer enhancements. These studies are introduced in the following sections and limited to numerical works only as presented in Table (2.2).

2.3.1. Numerical Studies in Complex Cavities filled with Classical Fluids

For Air, **Hussein et al.** [70], 2016, performed the numerical computation of unsteady laminar natural convection and entropy generation in an inclined trapezoidal cavity filled with air. The vertical right and left sidewalls were maintained at constant cold temperatures. The lower wall was subjected to a constant hot temperature while the upper one was considered insulated. The results showed that, the average (Nu) increases with increasing (Ra). For other fluids, **Terekhov and Ekaid** [71], 2011, investigated numerically the laminar free convection in a parallelepiped cavity filled with incompressible gas. The two vertical side walls were kept at different temperatures hot and cold temperature respectively. The top, bottom and other walls were insulated. It was found that, the whole heat transfer through the cavities or through longer cavities (AR $\geq$ 1) was conservative to the action of the secondary flows. For (AR $\leq$ 1), the average (Nu) depends on the cavity thickness while for longer cavities it does not depend on it.

2.3.2. Numerical Studies in Complex Cavities filled with Nanofluids

Moura and Junior [72], 2012, analyzed numerically the transient natural convection of a 3D parallelopiped cavity had an equal sidewall dimension. Initially all the walls were kept at a specified temperature. Then, all the walls were heated to a temperature greater than the initial. A discussion of the topology, flow patterns and loss of symmetry within the cavity and the effects of natural convection are presented. It was

found that, the flow of fluid in the cavity has an oscillatory behavior in the first instants of simulation. **Al-Rashed et al.** [73], 2019, simulated numerically the natural convection in a parallelogrammical opened top side cavity. The cavity had a square heater on its bottom wall and the remaining part of it considered adiabatic. The heater was selected in different sizes. The cavity had an inclined front and back walls. Temperature of remaining walls was lower than that of heater. For all cases, heat transfer increased with increasing both (φ) and inclination angle. For lower inclination angle, it became almost constant for lower values of (Ra). It was concluded that, the (Nu) was depending on the heater side length.

2.4. Scope of the Present Study

The previous sections were introduced the recent studies of natural convection heat transfer inside cavities numerically and experimentally as shown in the flow chart that presented in Fig. (2.2). It was concluded that, there is a gap in the experimental studies for all cavities; classical or complex. Another conclusion is that, there is lakes in both numerical and experimental studies in the complex cavities' convection field. The current study is focused on the complex non-cubical configurations of cavities that filled with (Al_2O_3-water) nanofluid numerically and experimentally. Numerically; the considered cavities are of four different novel shapes or configurations that studied for the first time named as; parallelogrammical, hexagonal, octagonal and elliptical. The main cavity is the parallelogrammical which discovered for different skew angles (γ). As like as, many modifications are examined on it. These modifications are inserting bodies of different counts and shapes inside the cavity and/or drilling holes of different shapes and

orientations also. Experimentally, the parallelogrammical cavity that has skew angle of (60º) is designated and manufactured.

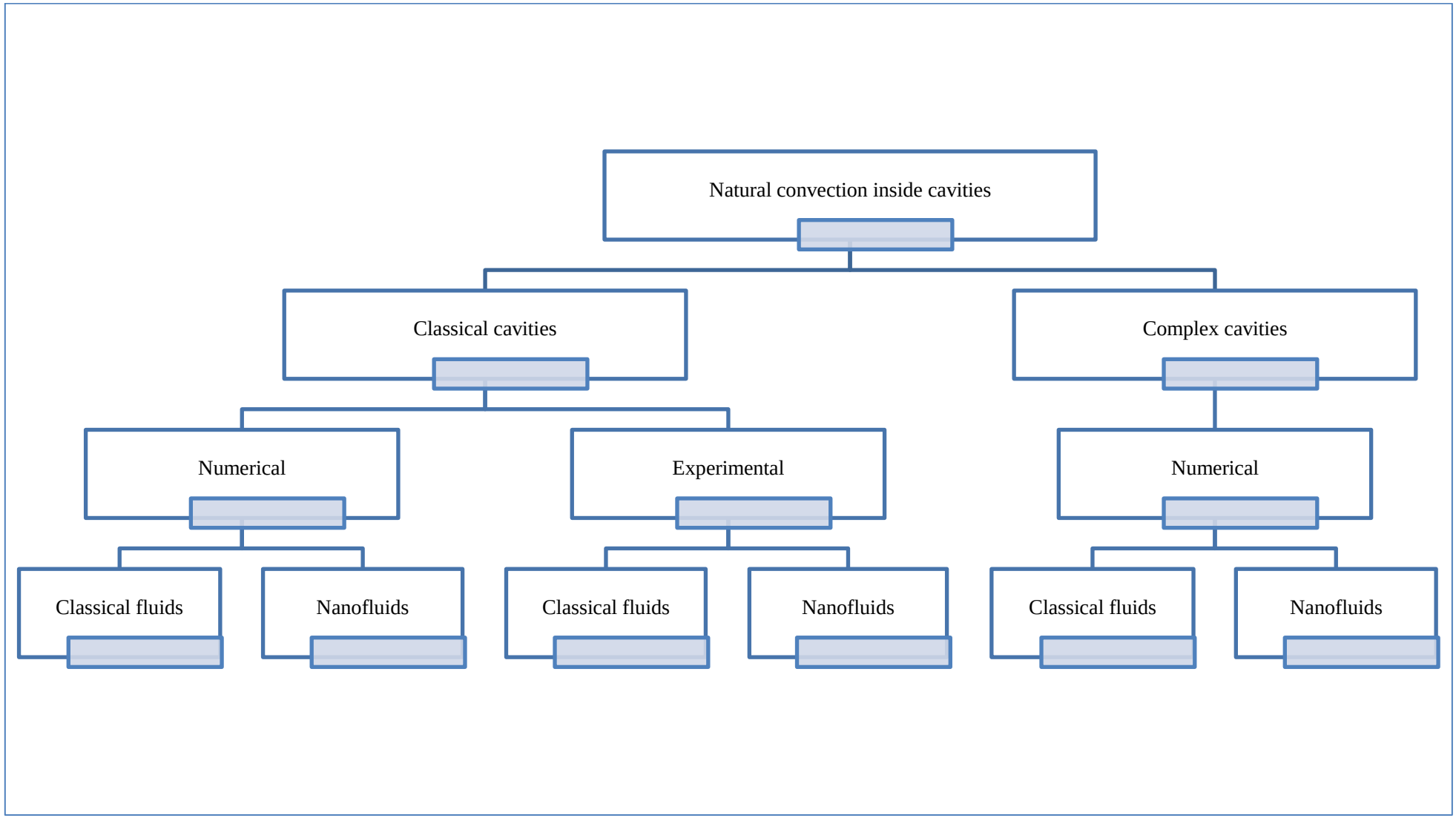

Figure (2.1): The literature review flow chart.

Table (2.1): Classical cavities

Author	Year	The model used	The study parameters	Cavity shape	Fluid type	Conclusions
Zemani et al. [30]	2014	FVM	$10^5 \leq Ra \leq 10^6$	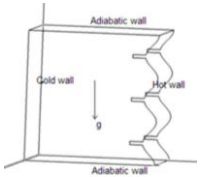	Air	These partitions caused decrease of up 40% in the heat transfer.
Li et al. [31]	2016	LBM	$10^4 \leq Ra \leq 10^5$	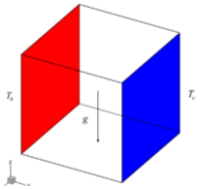	Air	The proposed double MRT is valid for 3D simulation.
Al-Rashed et al. [32]	2017	FVM	$10^3 \leq Ra \leq 10^6$	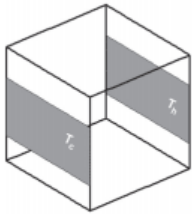	Air	The total entropy generation rate increases with Ra. The middle-middle arrangement produces higher average Nu.
Wang et al. [33]	2017	FVM	$10^3 \leq Ra \leq 10^{10}$	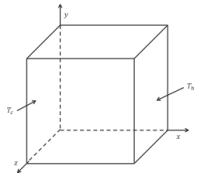	Air	An exponential scaling law between Nu and Ra was suggested.
Spizzichino et al. [34]	2019	FVM	$10^4 \leq Ra \leq 10^6$	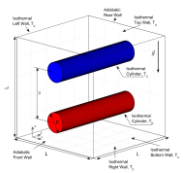	Air	Distance between cylinders had important role in determining the characteristics of the instability.

Alnaqi et al. [35]	2020	CVM	$10^3 \leq Ra \leq 10^6$	3D square 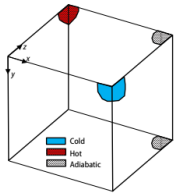	Air	Increase Ra leads to increase the average Nu and decrease Be.
Alshomrani et al. [36]	2020	FEM	$10^3 \leq Ra \leq 10^6$	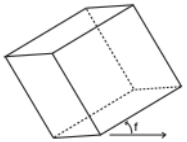	Air	The inclination of the cavity and the locations of the coolers influence the stream and energy transport.
Onyango et al. [37]	2013	FDM	$0^oC \leq \Delta T \leq 1^oC$	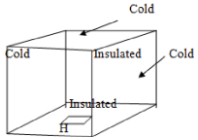	Newtonian incompressible of: Re=200 Pr=0.71	Heat transferred very weak at the sides. Flow and temperature fields were affected by the cold surfaces.
Ahmadi M. [38]	2014	FVM	$10^3 \leq Ra \leq 10^6$ L=1, H=1, W=0.875, $L_1=L_2$ =0.30, $L_3=L_4$ =0.2	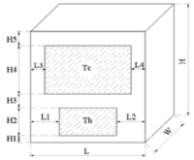	-	Increasing distance between heat sources, decreased average (Nu). Increasing length of cold source, causing heat transferred from hot source to increase.
Kolsi et al. [20]	2016	FDM	$10^3 \leq Ra_E \leq 10^5$ $10^3 \leq Ra_I \leq 10^6$ (h=0.25, 0.5, 0.75) (c=0.25, 0.5, 0.75)	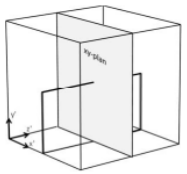	-	The role of location and height of partition became less important with increasing the inner (Ra).

Gibanov and Sheremet [39]	2017	FDM	$10^4 \leq Ra \leq 10^6$ $0.05 \leq l/L \leq 0.35$	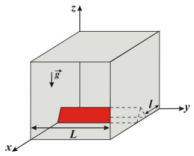	Newtonian fluid	The extreme left position of the heater illustrated more cooling.
Gibanov and Sheremet [40]	2018	FDM	$10^4 \leq Ra \leq 10^6$ $\pi/4 \leq \alpha \leq \pi/2$	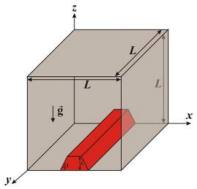	Newtonian fluid	Trapezoidal shape of heater was gave the more enhancement in (Nu).
Gibanov and Sheremet [41]	2019	FDM	$10^4 \leq Ra \leq 10^6$	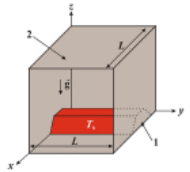	Newtonian fluid	The variation of height, length and size of the local heater influenced the temperature and fluid flow.
Ravnik et al. [42]	2010	FDM	$10^3 \leq Ra \leq 10^6$ $\varphi \leq 20\%$	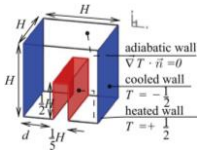 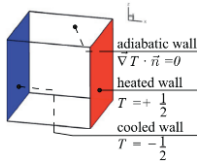	Al_2O_3-water Cu-water TiO_2-water	The best enhancement in heat transfer is that from Cu-water and it increased with increasing φ.
Arefmanesh and Tavakoli [43]	2012	MLPG	$10^3 \leq Ra \leq 10^5$ φ = 0.05, 0.1	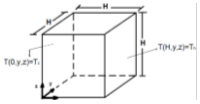	Al_2O_3-water Cu-water TiO_2-water	Average (Nu) increases with increasing (φ) for all selected nanofluids.

Kolsi et al. [44]	2014	FDM (FORTRAN)	$10^3 \leq Ra \leq 10^6$ $0\% \leq \varphi \leq 20\%$	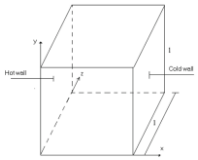	Al_2O_3-water	Average (Nu) increasing with both (φ) and (Ra).
Ternik [45]	2015	FVM	$10^1 \leq Ra_{water} \leq 10^6$ $0\% \leq \varphi \leq 5\%$	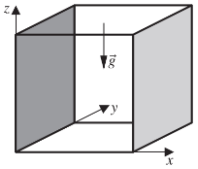	Au-water	Average (Nu) of nanofluid smaller than those of pure water at the same (Ra).
Purusothaman A. [46]	2016	FVM	$10^5 \leq Ra \leq 10^7$ $0 \leq \varphi \leq 0.01$ $1 \leq AR \leq 7.5$	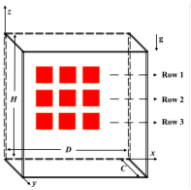	Cu-water Al_2O_3-water	Cu–water nanofluid has the greatest effect on the equipment performance.
Salari M. et al [47]	2016	FDM	$10^3 \leq Ra \leq 10^6$ $\varphi = \begin{pmatrix} 0.002, 0.004, \\ 0.01 \end{pmatrix}$ $AR = (0.125, 0.25, 0.375, 0.5)$	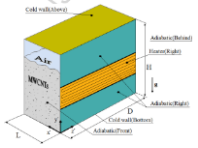	Air MWCNTs-water	Nanofluid interface (AR) had clear influences on the fluid flow, heat transfer and entropy generation.
Salari M. et al [48]	2017	FDM	$10^3 \leq Ra \leq 10^6$ $\varphi = (0.002, 0.01)$ $r = 0, 0.15, 0.20, 0.25$	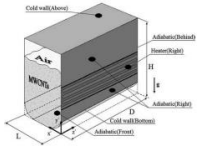	Air MWCNTs-water	The curved corner being an effective method to control fluid flow and energy consumption.

Kolsi et al. [49]	2016	FVM	$10^4 \leq Ra \leq 10^5$ $0 \leq \varphi \leq 0.15$ $L_b/L = \frac{1}{4}, \frac{1}{2}, \frac{1}{8}$	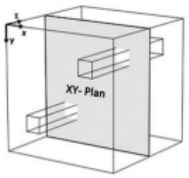	Al_2O_3-water	Average (Nu) raised with the increase in (Ra) and (φ) and declined with the increase in block size.
Kolsi et al. [50]	2016	FVM	$10^4 \leq Ra \leq 10^5$ $0 \leq \varphi \leq 0.15$ $0.01 \leq$ k ratio ≤ 100	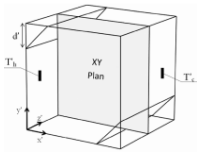	-	The heat transfer increased linearly according to (k) ratio for the same geometry and (Ra).
Rahimi et al. [51]	2017	LBM	$10^3 \leq Ra \leq 10^6$ $0 \leq \varphi \leq 0.04$	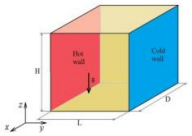	CuO-water	Average (Nu) enhanced with increasing (Ra) and (φ).
Wang et al. [52]	2018	LBM	$10^4 \leq Ra \leq 10^6$ $0 \leq \varphi \leq 0.04$ $10k \leq \Delta T \leq 50k$ $0.5 \leq AR \leq 1$	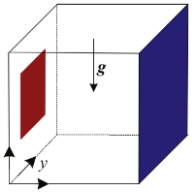	Al_2O_3-water	Average (Nu) decreased with (φ) increase and decreased with (AR) of heat source.
Benabderra-hmane and Messadi [53]	2018	FVM (FLUENT)	$10^7 \leq Ra \leq 3 \times 10^8$ φ=1%, 4%, 10%	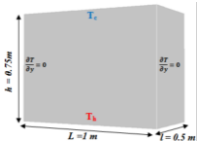	Al_2O_3-water	Using nanofluids increased (Nu) with increasing (Ra).
Sannad et al. [54]	2019	FVM	$10^3 \leq Ra \leq 10^5$ $0 \leq \varphi \leq 0.03$	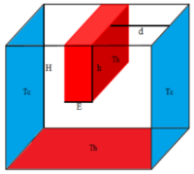	Cu-water	(Nu) increases with (φ) for different (Ra).

Sannad et al. [55]	2020	FVM	$10^3 \leq Ra \leq 10^6$ $0 \leq \varphi \leq 0.1$	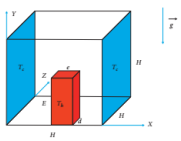	Cu-water	The increase of the heating section size and (Ra) led to an increase of heat transfer.
Sannad et al. [56]	2020	FVM	$10^3 \leq Ra \leq 10^6$ $0 \leq \varphi \leq 0.1$	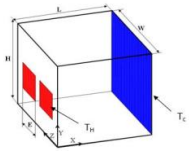	Al_2O_3-water	Increasing the heating section size and Ra increases the heat removed by the same nanofluid.
Esfe et al. [22]	2020	FVM	$10^3 \leq Ra \leq 10^5$ $0 \leq \varphi \leq 0.03$	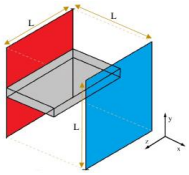	CuO-water	Average (Nu) enhanced by increasing (φ).
Selimefendigil and Oztop [57]	2020	FEM	$0 \leq \varphi \leq 0.04$	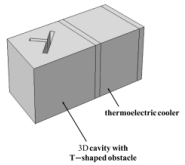	CNT-water	The size and inclination of the T-shaped obstacle have low effects on the variation of (Nu).
Moutaouakil et al. [58]	2020	FVM	$10^3 \leq Ra \leq 10^6$ $0 \leq \varphi \leq 0.1$ $0 \leq Rd \leq 0.5$ $\gamma = 0^o, 45^o, 90^o$	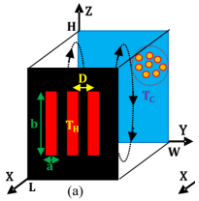	Cu-water Al_2O_3-water Ag-water TiO_2-water	Average (Nu) increased with (φ), radiation parameter and (AR) of the heating elements.
Li and Tong [59]	2016	Experiment and FVM (Fluent)	w/h= 1, 2, 4, 8	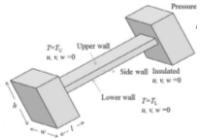	Air	Increasing (AR) and inclination angle enhanced the natural convection.

Nardini G. et al. [60]	2016	Experiment	$10^4 \leq Ra \leq 10^5$ D = 0.4, 0.5, 0.6	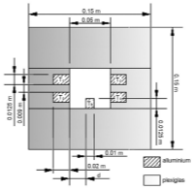	Air	Middle position of the hot source was the best to remove the heat generated in the cavity.
Bharti et al. [61]	2018	Experiment (PIV analysis)	Ra ($7.05x10^5$, $4.27x10^6$, $1.84x10^7$)	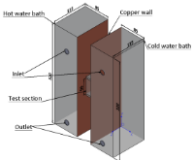	Deionized water	The technique was very robust and high accuracy in temperature measurement, within 1%.
Karatas and Delbentli [62]	2018	Experiment	$1.6x10^5 \leq Ra \leq 4.67x10^7$ $1 \leq AR \leq 6$	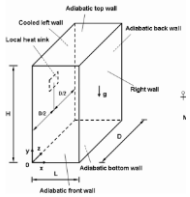	Air	Average (Nu) increases from 23.63 to 73.35 with decreasing (AR) from 6 to 1.
Karatas and Delbentli [63]	2019	Experiment	$4.51x10^5 \leq Ra \leq 1.13x10^8$ $1 \leq AR \leq 6$	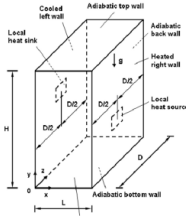	Air	(Nu) decreases when the heated wall temperature changed from constant to sinusoidally varying.
Heris et al. [64]	2014	Experiment	φ = 0.2%, 0.5%, 0.8% Θ= 0º, 45º, 90º	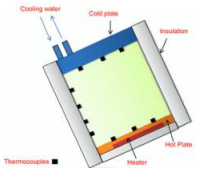	Al_2O_3, TiO_2, CuO with Turbine oil	At (90º) the maximum (Nu) was for TiO_2 at (φ=0.2%) while it was for CuO at (φ=0.8%)

Solomon et al. [65]	2017	Experiment	$0 \leq \varphi \leq 0.006$ AR (1, 2, 4)	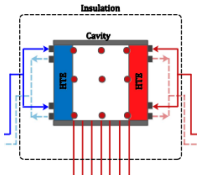	De-DI water Al_2O_3-water	(AR) had a clear effect on (Nu) where (φ) for maximum heat transfer was increased with increasing (AR).
Rahimi et al. [66]	2017	Experiment and FVM	ΔT=20º, 30º, 40º, 50º φ= (0.01, 0.02, 0.05, 0.1, 0.2, 0.5)%	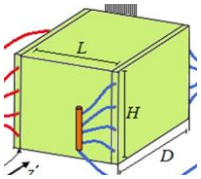	DWCNTs-water	Optimum (φ) for highest average (Nu) was (0.05 vol%).
Rahimi et al. [67]	2018	Experiment and LBM	MWCNT-MgO : (75–25)% φ = 0.25%, 0.5%, 1%, 1.5%, 2% 20°C ≤ΔT≤40°C	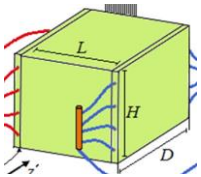	MWCNT-MgO/ water	Optimum (φ) for highest average (Nu) was (1 vol%).
Torki and Etesami [68]	2020	Experiment	$2.3º \leq \Delta T \leq 30.9º$	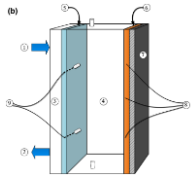	SiO_2-water	(Nu) increasing with (Ra) increasing and inclination effect was higher at low (φ).
Giwa et al. [69]	2020	Experiment	$1.65x10^8 \leq Ra \leq 3.8x10^8$ Al_2O_3: MWCNT (80:20, 60:40, 20:80)	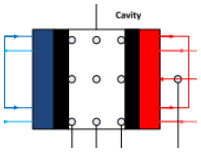	Al_2O_3-MWCNT-water (hybrid)	The using of hybrid nanofluid improved natural convection performance.

Table (2.2): Complex cavities

Author	Year	The model used	The study parameters	Cavity shape	Fluid type	Conclusions
Hussein et al. [70]	2016	CVFDM (FORTRAN)	$10^3 \leq Ra \leq 10^5$ $0^o \leq \emptyset \leq 180^o$	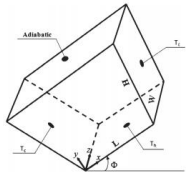	Air	The average (Nu) increased with increasing (Ra).
Terekhov and Ekaid [71]	2011	SIMPLE algorithm	$10^3 \leq Ra \leq 10^6$ $0.1 \leq AR \leq 5$	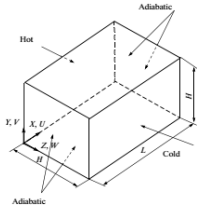	Incompressible gas	Average (Nu) depends on cavity thickness for (AR≤1) only.
Moura and Junior [72]	2012	FVM OpenFOAM	$Ra= 4.74\times10^7$, 9.48×10^8	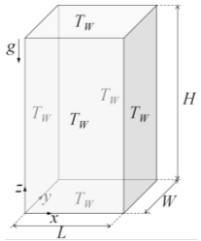	-	The initiation of the thermal stratification of the cavity bubbles formed mushroom-shaped in the bottom wall.
Al-Rashed et al. [73]	2019	FVM	$10^3 \leq Ra \leq 10^5$ $0 \leq \varphi \leq 0.05$ $5^o \leq \emptyset \leq 75^o$	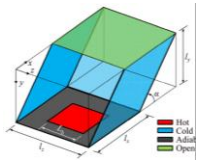	Al_2O_3-water	The inclination angle of the back and front walls and φ effect the flow structure and enhance the heat transfer.
Present (numerical)	2023	FDM	$10^3 \leq Ra \leq 10^6$ $0.01 \leq \varphi \leq 0.05$	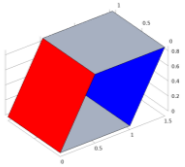	Water Al_2O_3-water	

				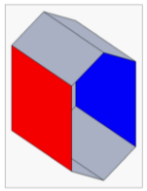 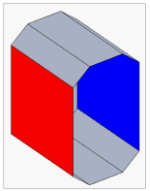 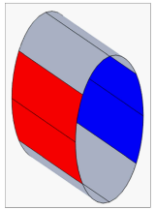	
Present	2023	Experiment	$10^5 \leq Ra \leq 10^6$ φ = 0.01, 0.03, 0.05	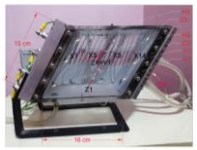	Al_2O_3-water

Chapter Three: Mathematical Modelling and Numerical Computation

3.1. Introduction

The Computational Fluid Dynamics (CFD) techniques which is a computer-based tool are used to solve and study complex fluid flow and heat transfer problems. The CFD can solve several system configurations at the same time at a reduced cost and high flexibility as an economical point of view compared with experiments. Due to the very involvement of a large number of variables, complex geometrical bodies, boundary conditions, and arbitrary boundary shapes can be considered [74-75].

The (CFD) is employed to solve the laminar natural convection and other related physical processes inside cavities. It works by solving the equations of fluid flow over a region of interest (the computational domain) inside the different geometry and 3D cavities with a specified conditions at the boundaries of that region.

This chapter includes the configuration of the studied cavities and its physical domains, the working fluid properties and its correlations. The governing equations together with the initial and boundary conditions, the computational tool and the validation of the code. In addition, the geometry, the mesh generation and grid independence test.

3.2. The Mathematical Model

Different cases of the cavity geometries are studied. These cases are classified according to the lateral cross section between the left and right walls. These novel cavities are studied for the first time with the selected dimensions and arrangements of walls. The main geometry is the parallelogrammical which is also classified according to: the changes of the walls dimension, the parallelogrammical walls skews, number and locations of the inserted bodies. The other selected geometries are with cross sections of: hexagonal, octagonal and elliptical.

To ensure best comparisons that give the optimum design of cavity, all the cavities have the same volume to contain the same amount of the working fluid. Also, the areas of the heating and cooling sections and their arrangements are the same, as presented in Appendix B.

The colors in figures for all the cases below are mean: the red and blue indicate hot and cold sections respectively, which are represented on the (Y-Z) plane. While the gray color indicates insulated region. The fronts walls are presented in the (X-Z) plane.

3.2.1. The Physical Domain of the Parallelogrammical Cavity

The main cavity configuration is the parallelogrammical front and back walls cavity which designed with skew angle (γ) from the horizon equals to (60^{o}). The effect of many cases of the cavity different configurations are examined in the following sections.

These effects are: the heating and cooling sections arrangements, the skew angle variation, the inner body's locations and distribution, the inner holes shape and orientations (annulus cavity).

3.2.1.1. The Parallelogrammical Cavity with Different (Heating / Cooling) Sections Arrangements

The schematic diagram of a 3D parallelogrammical cavity with the walls inclined by a specified angle from the horizon (along the X-axis) by skew angle of ($\gamma = 60^{o}$) are studied in two cases for the constant parameters as shown in Fig. (3.1).

Firstly, the constant side length at (L) and the changed volume as shown in Fig. (3.1). This case is designed to be the main case in the study and it is identical to the experimental cavity, which both have equal faces side lengths also.

Secondly, constant volume of cavity at (L^3), while the front and back walls have varied horizontal side lengths (along the -X axis) as shown in Fig. (3.2).

For both cases, the heating and cooling sections have the same side length (L) and the same area (L^2). To ensure the best differentially heating system arrangements, these cases of cavity geometry are examined in three cases for the heating and cooling sections.

Where, the differential heating means that one face of the cavity called hot which is kept at constant higher temperature (T_h). While, the opposite called cold and is kept at constant lower temperature (T_c). These arrangements as shown in Fig. (3.3) are:

1. Left hot and right cold.

2. Left cold and right hot.

3. Bottom hot and top cold.

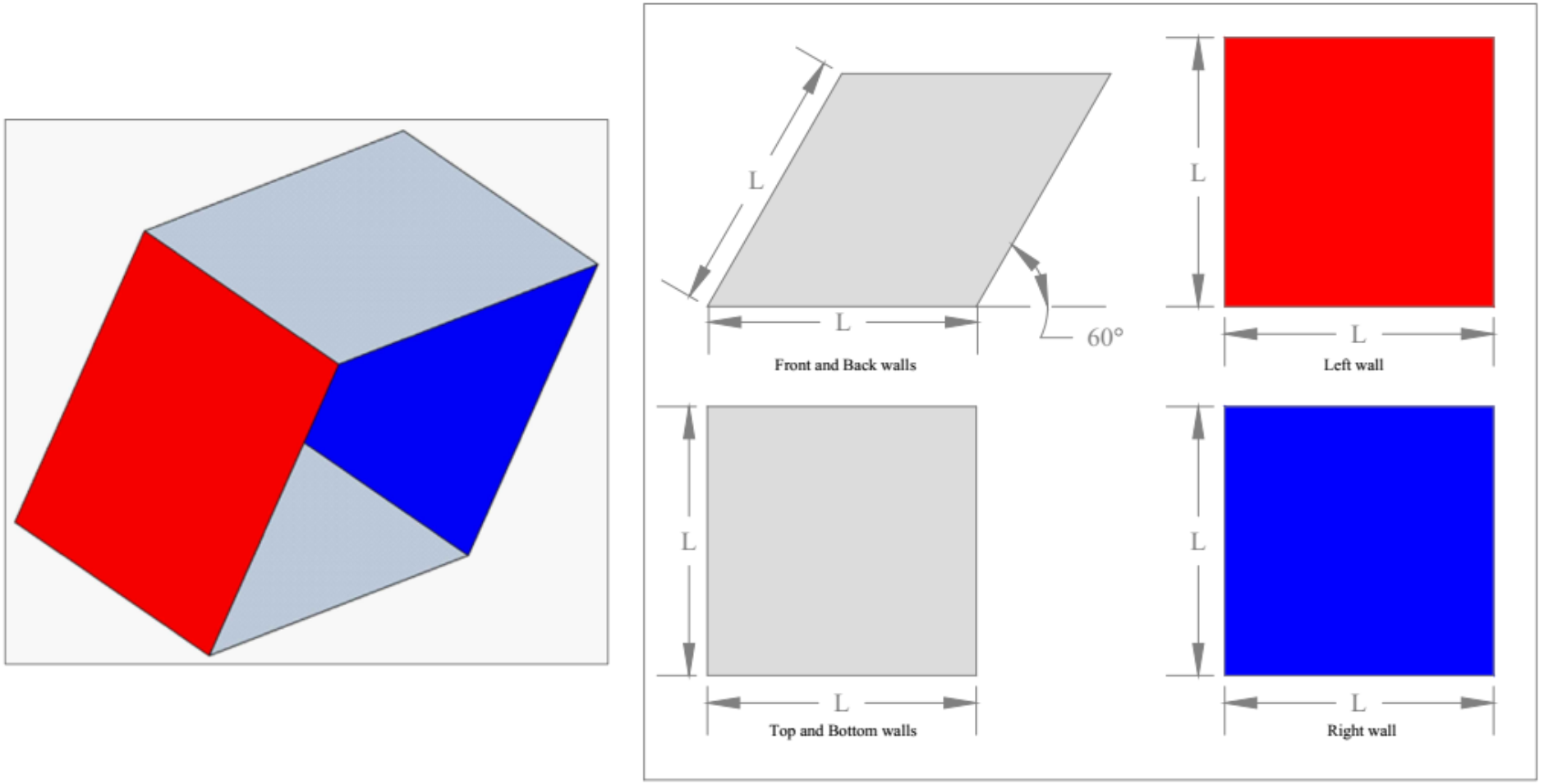

Figure (3.1): The 3D and side projection for the parallelogrammical cavity of (γ= 60º) at constant side length (L).

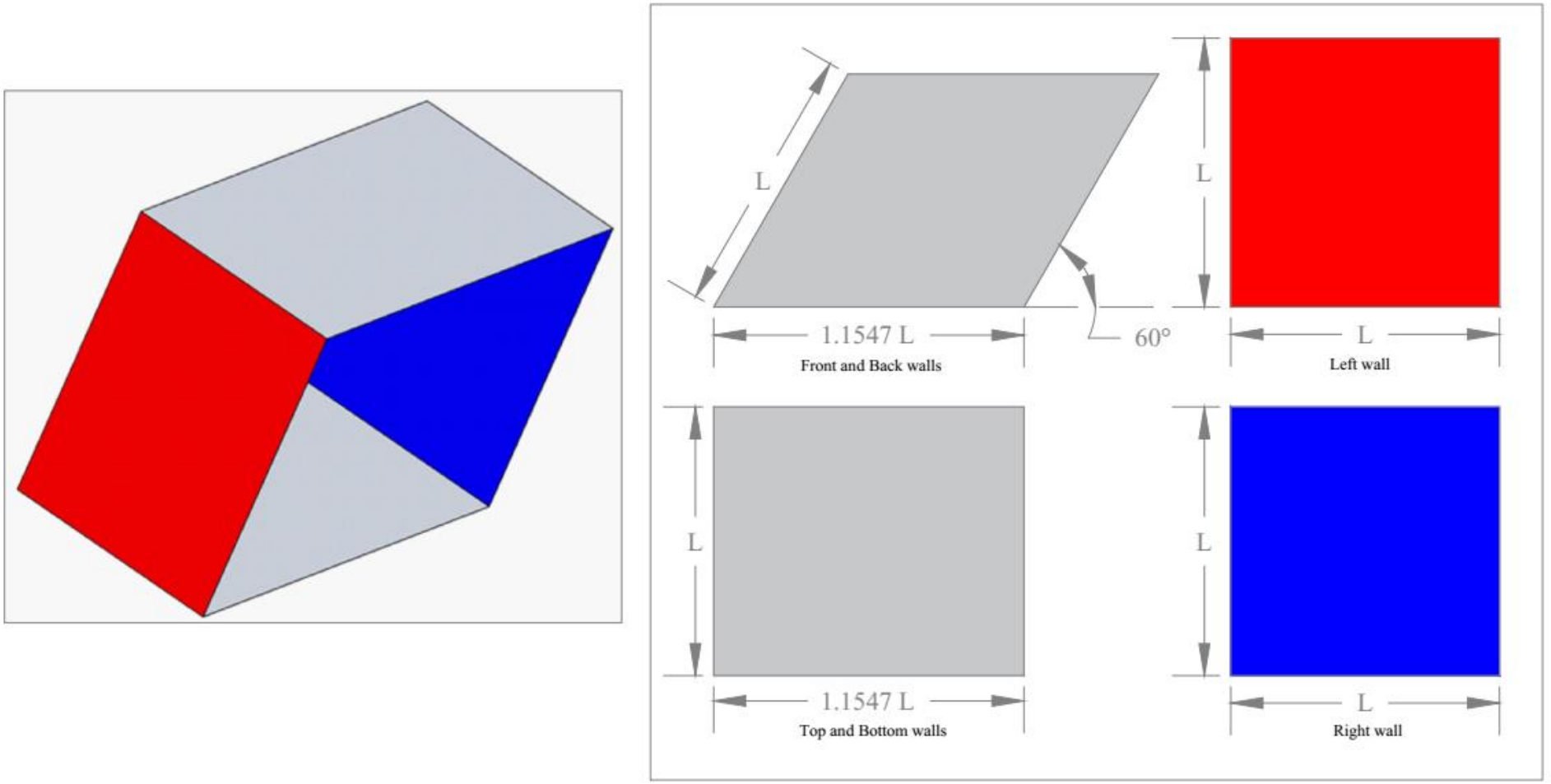

Figure (3.2): The 3D and side projection for the parallelogrammical cavity of (γ= 60º) at constant volume (L^3).

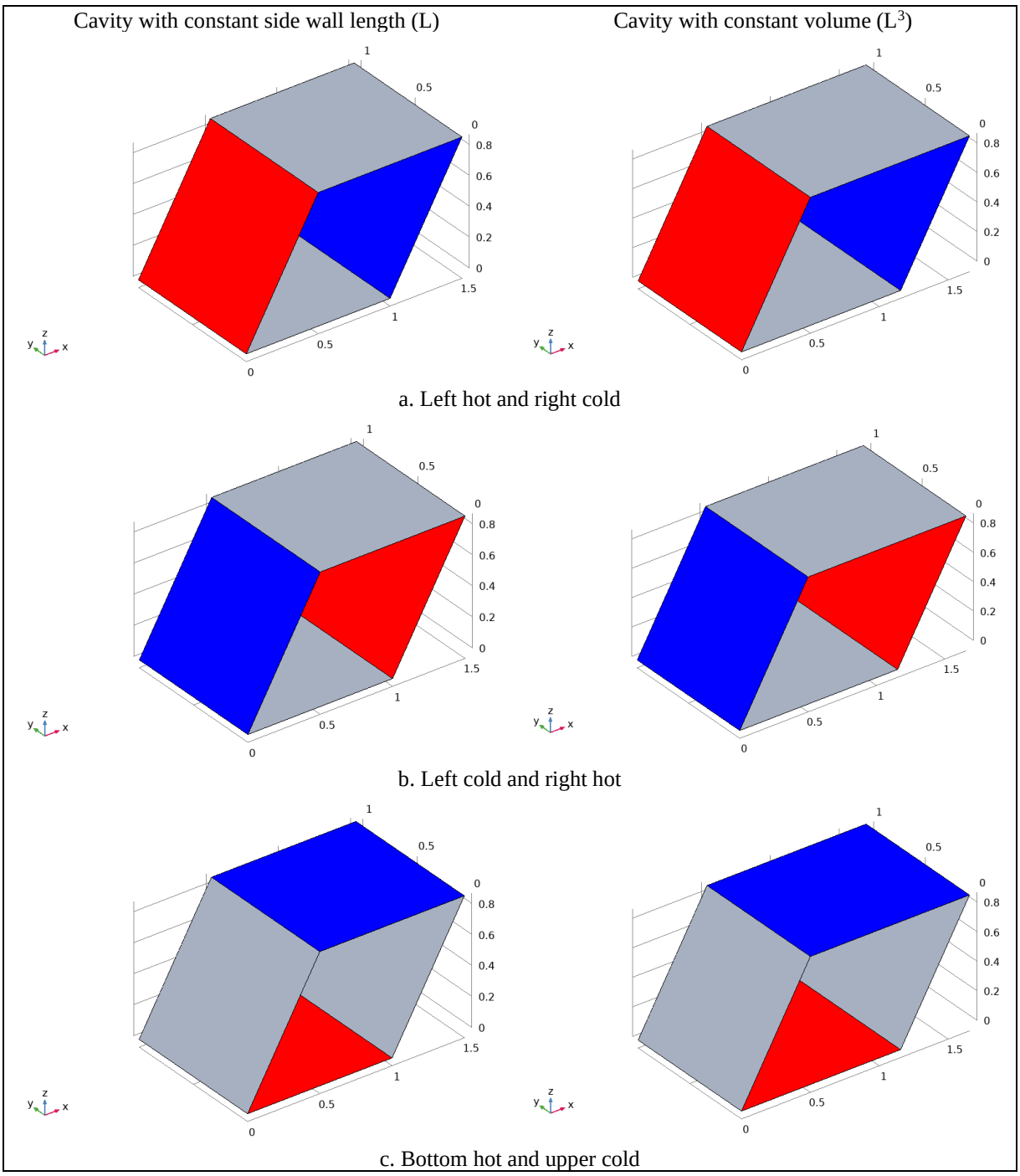

Figure (3.3): The heating and cooling sections arrangements on the 3D parallelogrammical cavity of (γ= 60º).

3.2.1.2. The Parallelogrammical Cavities with different (γ)

To cover the study field from all sides, the effect of the skew angle variation is distinguished. Two cases of the parallelogrammical walls skews are examined together with the (γ=60º) which are (γ = 45º

and 30º) as shown in Fig. (3.4). For all cases, the cavity is heated differentially on its vertical left and right sidewalls. The left wall is kept at constant hot temperature, while the right at constant cold temperature. The parallelogrammical front and back like the top and bottom walls are kept insulated. All the cavities have heating and cooling sections side lengths of (L) and areas of (L^2). While, the volumes can be calculated by multiplying the front wall area by the cavity depth which equals to ($0.866L^3$, $0.7071L^3$ and $0.5L^3$) as tabulated in Appendix B. The second case of the cavities are considered with constant volume (L^3) and constant heating and cooling sections side lengths (L) and area (L^2) but different other side lengths. The heights (along the X-axis) and the other horizontal dimension (along the Z-axis) are changed in accordance with the skew angle (γ). Where the heights are (0.866L, 0.7071L, 0.5L) and the horizontal dimensions are (1.154L, 1.414L and 2L), respectively. While, the depth (along Y-axis) is fixed at length of (L) to ensure the same area of the heating and cooling sections (L^2).

3.2.1.3. The Parallelogrammical Cavity at (γ = 60º) with an Internal Objects

The third case is the insertion of insulated solid body inside the cavity in different counts, locations and distributions. These inner objects are presented in Fig. (3.5); single circular cylinder with diameter of (0.24L), double cylinders with diameters of (0.12L) and triple cylinders with diameters of (0.08L). In each case, the volume of the inners is equal. Three properties are discovered by the nine cases: the location of the inner body (lower left corner – center – upper right corner). Also, the distribution of the inner body volume inside the cavity (single – double – triple). The distance between the centers of these

inners is (0.12L, 0.09L and 0.06L) for double cylinders cases as presented in Appendix B.

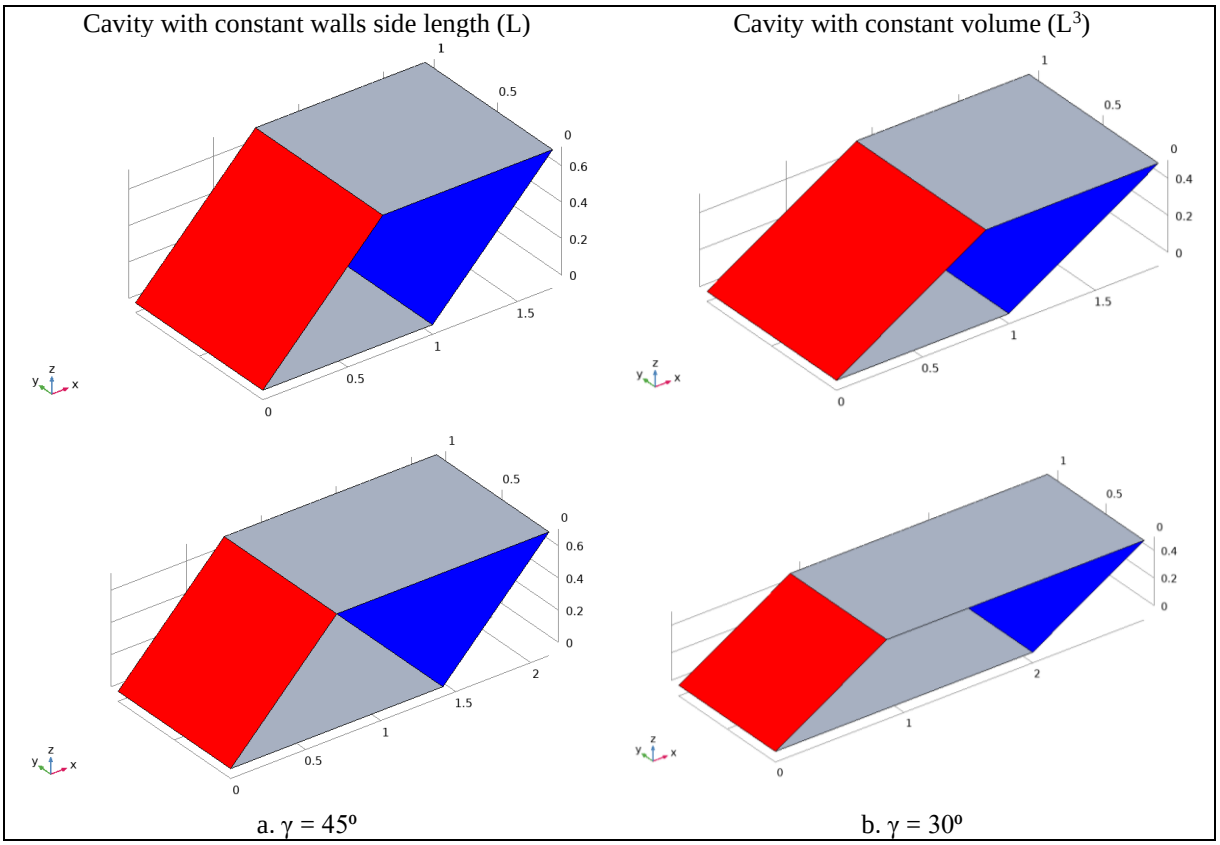

Figure (3.4): The 3D configuration of the parallelogrammical cavity of different (γ).

3.2.2. The Physical Domain of Another Different Geometrical Cavities

The parallelogrammical cavity shape is compared with another different geometry cavities which are varied as eight or ten walls cavity. Three geometries with different front cross section are designed; hexagonal, octagonal and elliptical. These cavities have the same volume (L^3) and the same heating and cooling sections (L^2). But they have a different surface area as it is presented in Appendix B. Similar to the parallelogrammical cavity the heating and cooling arranged as the left wall is hot and the right wall is cold.

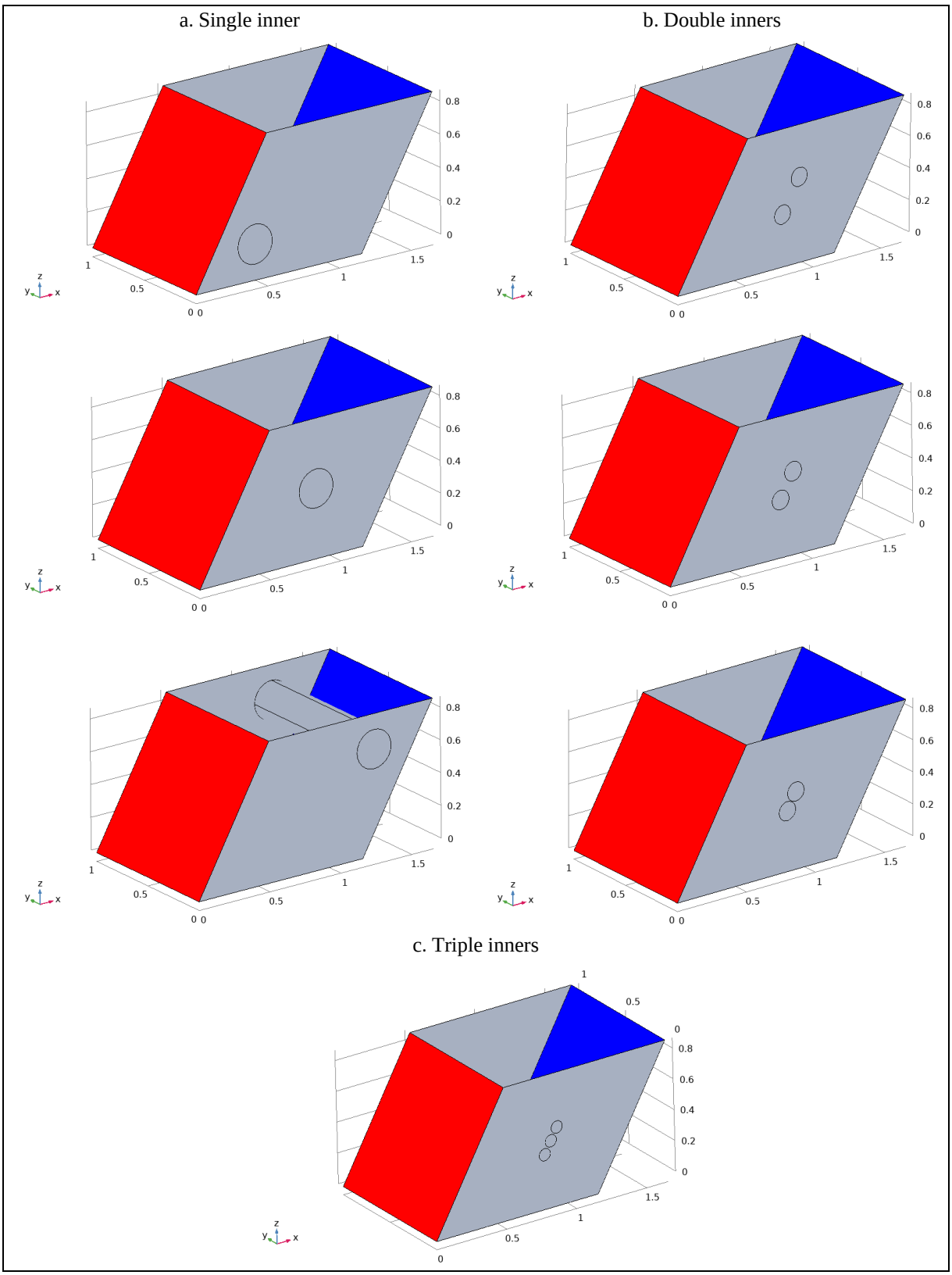

Figure (3.5): The 3D parallelogrammical cavity of (γ= 60º) with different inners distribution.

3.2.2.1. Hexagonal Cavity

This cavity has eight walls as shown in Fig. (3.7). The front and back cavity walls have a six non-equal length sides. It has the same volume, heating and cooling sections arrangement and area as the previous cavities but with different overall surface area.

3.2.2.2. Octagonal Cavity

Fig. (3.8) introduces the octagonal cavity which has ten walls. The front and back walls have eight non-equal sides. Also, it has the same constant study parameters; the volume and the heating and cooling arrangement and area except the overall surface area which is different.

3.2.2.3. Elliptical Cavity

This cavity has ten walls as it is presented in Fig. (3.9). It has only two straight walls; the front and back, having an elliptical shape with the longer diameter parallel to the (Z-axis). The other eight walls are shells of different dimensions. Two of the left side shells are considered hot while the opposite right shells are kept cold.

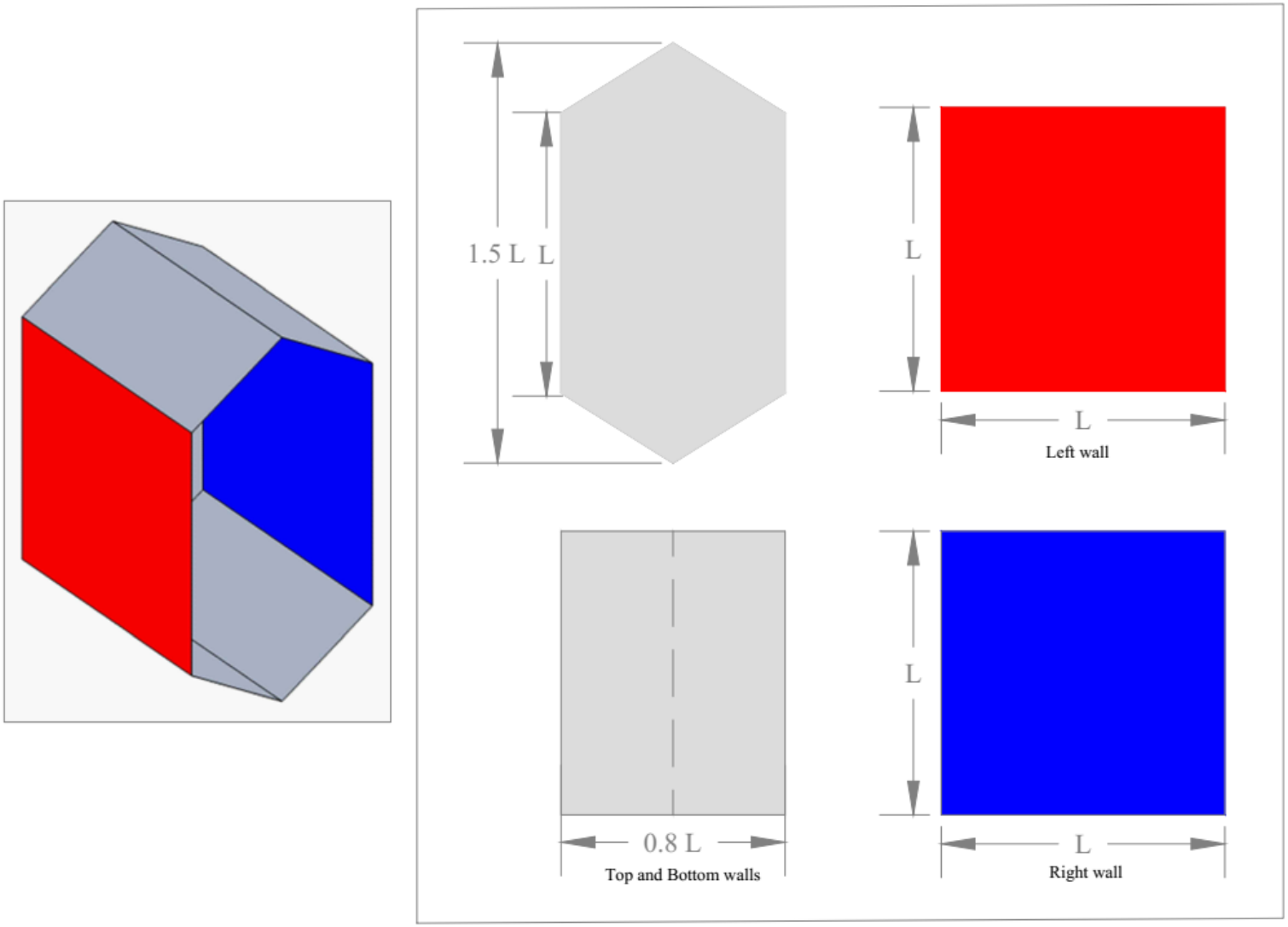

Figure (3.7): The 3D configuration and sides projection of the hexagonal cavity.

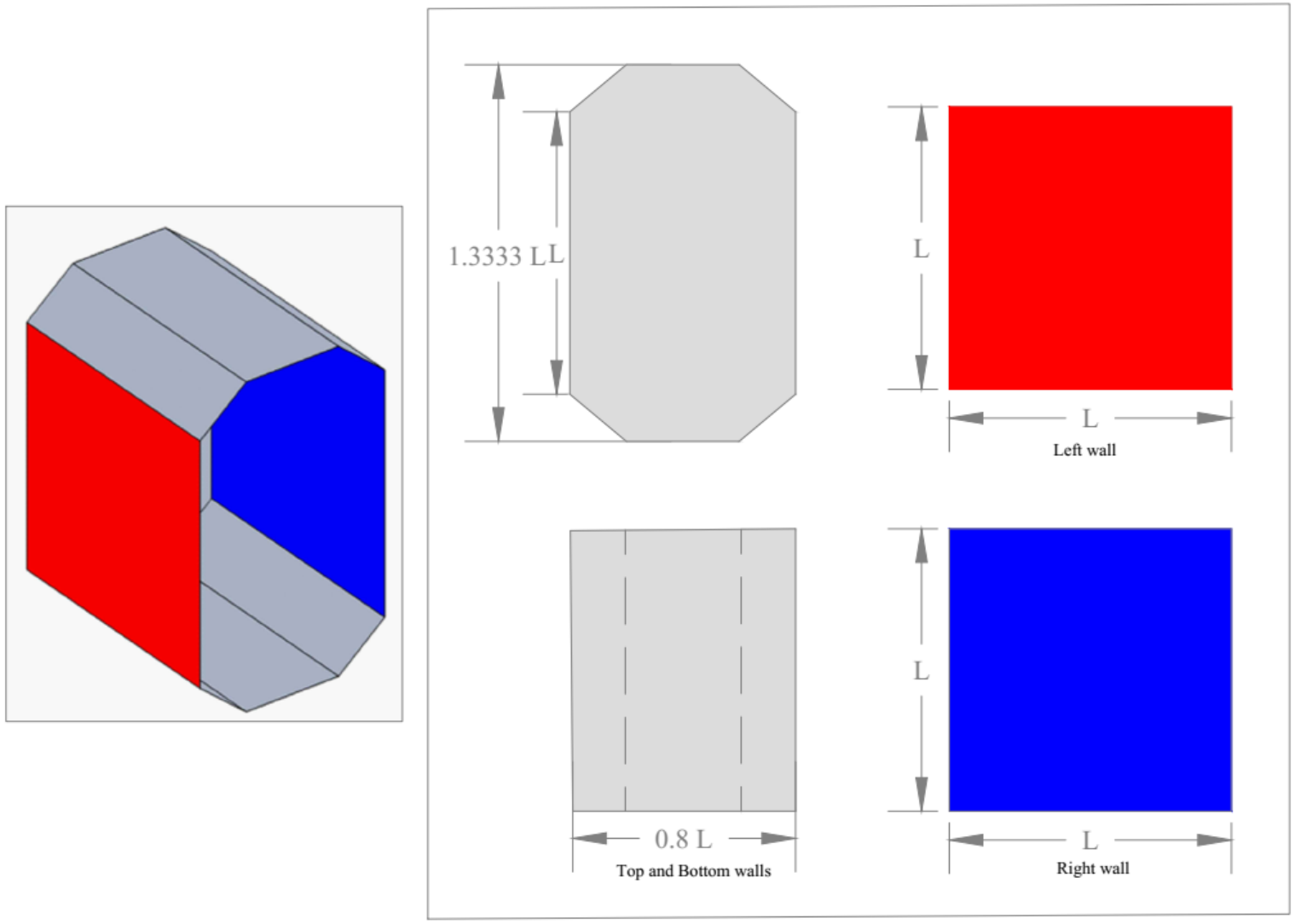

Figure (3.8): The 3D configuration and sides projection of the octagonal cavity.

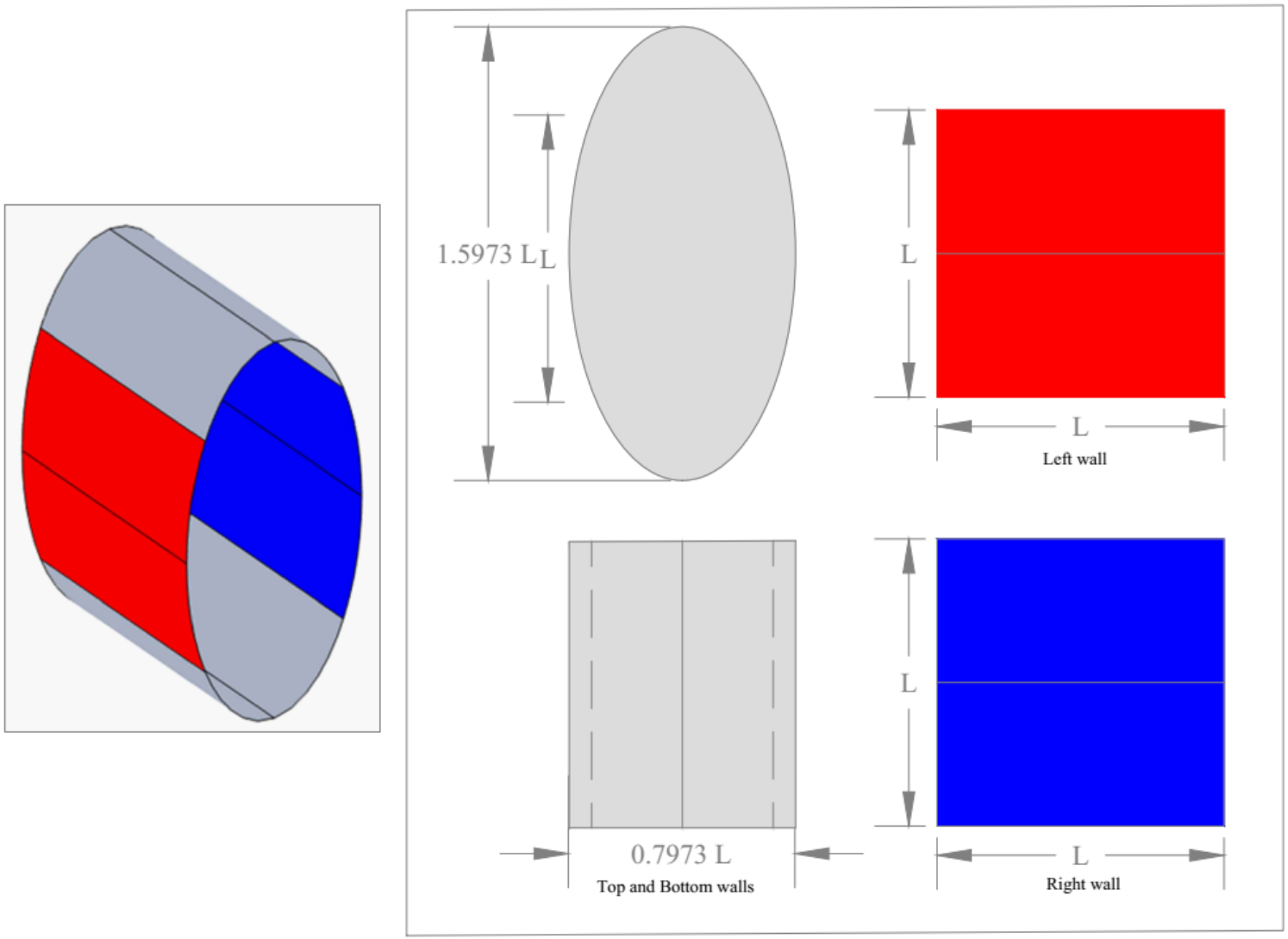

Figure (3.9): The 3D configuration and sides projection of the elliptical cavity.

3.3. The Governing Equations

In the present study a steady-state laminar flow of water (de-ionized) based (Al_2O_3) nanofluid is considered. It is assumed that:

1. A steady, three-dimensional, laminar, Newtonian incompressible flow.
2. The heat generation and the radiation heat transfer are neglected.
3. The base fluid and the nanoparticles are assumed in a thermal equilibrium state.
4. The thermophysical properties of the mixture are considered constant. While the density variation determined based on the Boussinesq approximation.

The system of the dimensional governing equations is the continuity, the momentum in the three dimensions and the energy equations [56]:

The continuity equation:

$$\frac{\partial u}{\partial x}+\frac{\partial v}{\partial y}+\frac{\partial w}{\partial z}=0 \tag{3.1}$$

The momentum equation in the x-axis:

$$\rho_{nf}\left(u\frac{\partial u}{\partial x}+v\frac{\partial u}{\partial y}+w\frac{\partial u}{\partial z}\right)=-\frac{\partial P}{\partial x}+\mu_{nf}\left(\frac{\partial^2 u}{\partial x^2}+\frac{\partial^2 u}{\partial y^2}+\frac{\partial^2 u}{\partial z^2}\right) \tag{3.2}$$

The momentum equation in the y-axis:

$$\rho_{nf}\left(u\frac{\partial v}{\partial x}+v\frac{\partial v}{\partial y}+w\frac{\partial v}{\partial z}\right)=-\frac{\partial P}{\partial y}+\mu_{nf}\left(\frac{\partial^2 v}{\partial x^2}+\frac{\partial^2 v}{\partial y^2}+\frac{\partial^2 v}{\partial z^2}\right) \tag{3.3}$$

The momentum equation in the z-axis:

$$\rho_{nf}\left(u\frac{\partial w}{\partial x}+v\frac{\partial w}{\partial y}+w\frac{\partial w}{\partial z}\right)=-\frac{\partial P}{\partial z}+\mu_{nf}\left(\frac{\partial^2 w}{\partial x^2}+\frac{\partial^2 w}{\partial y^2}+\frac{\partial^2 w}{\partial z^2}\right)-\rho_{nf}g \quad (3.4)$$

The energy equation:

$$u\frac{\partial T}{\partial x}+v\frac{\partial T}{\partial y}+w\frac{\partial T}{\partial z}=\alpha_{nf}\left(\frac{\partial^2 T}{\partial x^2}+\frac{\partial^2 T}{\partial y^2}+\frac{\partial^2 T}{\partial z^2}\right) \quad (3.5)$$

In order to limit the number of variables involved in the studied problem, the system of equations is converted to non-dimensional form by considering the following dimensionless parameters:

$$X,Y,Z=\frac{(x,y,z)}{L} \quad (3.6)$$

$$U,V,W=\frac{(u,v,w)}{\alpha_f/L} \quad (3.7)$$

$$P=\frac{p+\rho_f g y}{\left(\rho_{nf}\alpha_f^2/L\right)} \quad (3.8)$$

$$\theta=\frac{T_h-T}{\Delta T} \quad (3.9)$$

Where

$$\Delta T=T_h-T_c \quad (3.10)$$

Therefore, the governing equations of continuity, momentum, and energy conservation for laminar flow in Cartesian coordinates can be written in the following dimensionless form:

$$\frac{\partial U}{\partial X}+\frac{\partial U}{\partial Y}+\frac{\partial U}{\partial Z}=0 \quad (3.11)$$

$$U\frac{\partial U}{\partial X}+V\frac{\partial U}{\partial Y}+W\frac{\partial U}{\partial Z}=-\frac{\partial P}{\partial X}+\frac{\mu_{nf}}{\alpha_f\rho_{nf}}\left(\frac{\partial^2 U}{\partial X^2}+\frac{\partial^2 U}{\partial Y^2}+\frac{\partial^2 U}{\partial Z^2}\right) \quad (3.12)$$

$$U\frac{\partial V}{\partial X}+V\frac{\partial V}{\partial Y}+W\frac{\partial V}{\partial Z}=-\frac{\partial P}{\partial Y}+\frac{\mu_{nf}}{\alpha_f\rho_{nf}}\left(\frac{\partial^2 V}{\partial X^2}+\frac{\partial^2 V}{\partial Y^2}+\frac{\partial^2 V}{\partial Z^2}\right) \quad (3.13)$$

$$U\frac{\partial W}{\partial X}+V\frac{\partial W}{\partial Y}+W\frac{\partial W}{\partial Z}=-\frac{\rho_{nf}}{\rho_f}\frac{\partial P}{\partial Z}+\frac{\beta_{nf}}{\beta_f}Ra\times Pr\times\theta+\frac{\nu_{nf}}{\nu_f}\left(\frac{\partial^2 W}{\partial X^2}+\frac{\partial^2 W}{\partial Y^2}+\frac{\partial^2 W}{\partial Z^2}\right) \quad (3.14)$$

$$U\frac{\partial \theta}{\partial X}+V\frac{\partial \theta}{\partial Y}+W\frac{\partial \theta}{\partial Z}=\frac{\alpha_{nf}}{\alpha_f}\left(\frac{\partial^2 \theta}{\partial X^2}+\frac{\partial^2 \theta}{\partial Y^2}+\frac{\partial^2 \theta}{\partial Z^2}\right) \quad (3.15)$$

For water, the previous equations abbreviate by considering (φ=0).

3.4. The Initial and Boundary Conditions

The previous governing equations were solved by using the initial and boundary conditions which are presented in Fig. (3.10). The initial temperature of the fluid domain is (T_i) which given by:

$$T_i=(T_h+T_c)/2 \quad (3.16)$$

The boundary conditions are given by:

1. All walls have no slip conditions:

$$U=V=W=0 \quad (3.17)$$

2. The left sidewall maintained at hot temperature:

At $X=0$, $\theta=1$, (3.18)

3. The right sidewall maintained at cold temperature:

At X=1, θ=0 (3.19)

4. The remained walls are kept thermally insulated:

$$\frac{\partial \theta}{\partial X} = \frac{\partial \theta}{\partial Y} = \frac{\partial \theta}{\partial Z} = 0 \quad (3.20)$$

5. On the walls of the inserted cylinders:

$$\frac{\partial \theta}{\partial r} = 0 \quad (3.21)$$

3.5. Dimensionless Numbers of Fluid Flow and Heat Transfer

The Rayleigh number (Ra) is a dimensionless number associated with the convection flow which is used to characterize the flow regime in laminar or turbulent flow. It is expressed as the product of the Grashof (Gr) and Prandtle (Pr) numbers [68]:

$$Ra = \frac{g\rho_{nf}^2 c_{p_{nf}} \beta_{nf} \Delta T L^3}{k_{nf}\mu_{nf}} \quad (3.22)$$

The Nusselt number (Nu) represents the ratio of heat transfer by convection to that by conduction. To study the heat transfer characteristics due to the natural convection along the vertical hot wall; the local Nusselt number can be defined as [22]:

$$Nu(yz) = -\frac{k_{nf}}{k_f}\frac{\partial \theta}{\partial x}|Hot\ wall| \quad (3.23)$$

The wall averaged (Nu) on the hot or cold sidewalls is presented as follows [22]:

$$\overline{Nu}(yz) = \frac{1}{A_h}\int_0^{A_h} \mathrm{Nu}(yz)dA_h \quad (3.24)$$

Which also can be given by [68]:

$$Nu = \frac{h_{nf}L}{k_{nf}} \tag{3.25}$$

On the inner surface of the left hot wall, the heat conduction equals the heat convection as shown in Fig. (3.11), where the heat transfer coefficient can be calculated as:

$$h_{nf}A\left(T_{wall} - T_{film}\right) = -k_{wall}A\left(\frac{\Delta T}{\Delta X}\right) \tag{3.26}$$

$$\Delta T = T_{wall} - T_{heater} \tag{3.27}$$

Where (A) is the surface area of the heated wall and (Δx) is the selected film thickness.

3.6. The Working Fluid

The working fluid that contained in the different geometry cavities is the water based nanofluids with Aluminum oxide (Al_2O_3) nanoparticles. The solid volume fraction and the Rayleigh number ranges of the current study are ($0.01 \leq \varphi \leq 0.05$) and ($10^3 \leq Ra \leq 10^6$), respectively.

The thermophysical properties of the base fluid and nanoparticles are presented in Table (3.1). While, the physical properties of the nanofluid which include density, dynamic viscosity, heat capacity, thermal diffusivity and the thermal expansion are given by [76-77]:

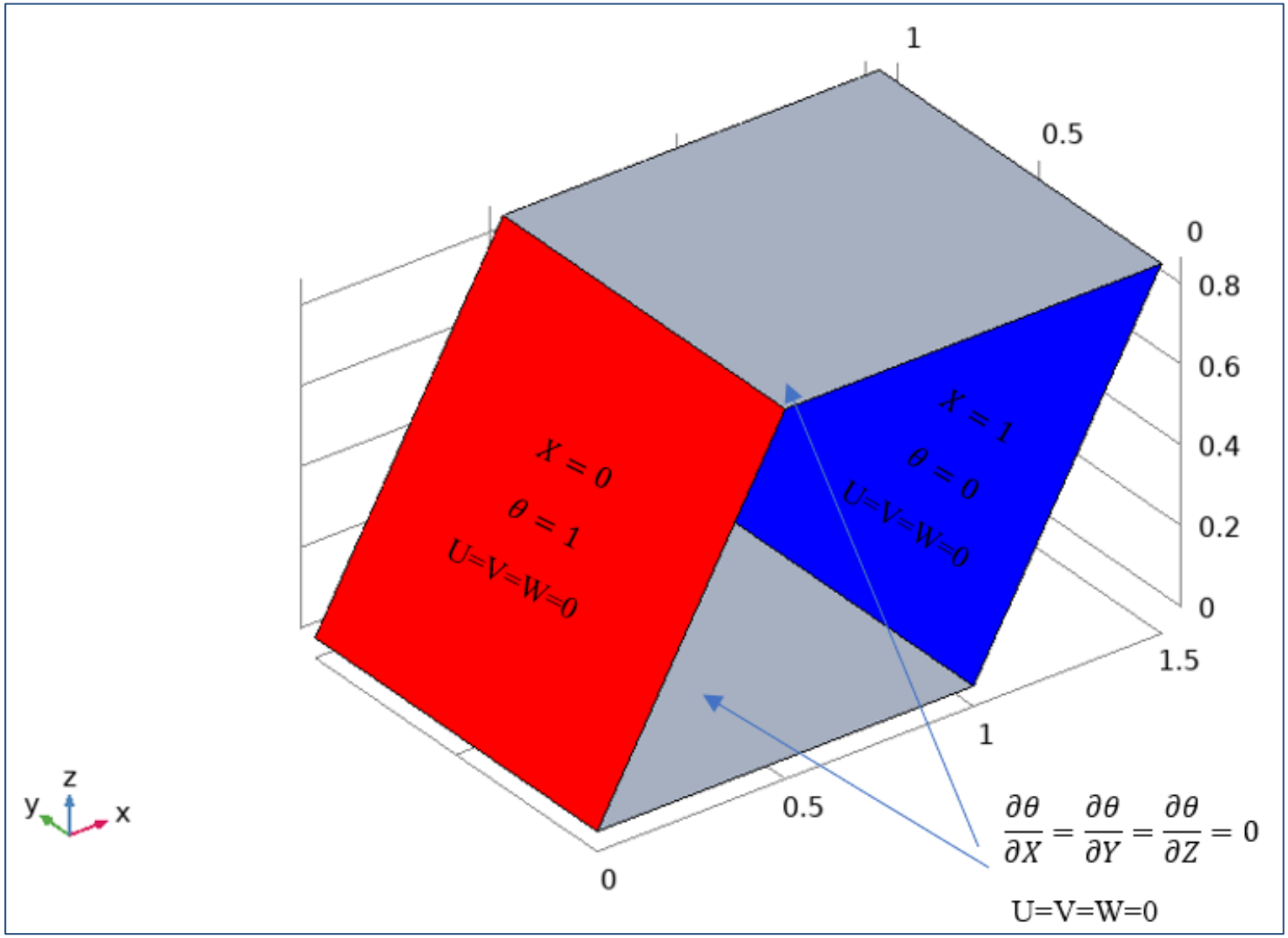

Figure (3.10): The boundary conditions on the 3D parallelogrammical cavity of (γ=60º) and constant side length (L).

$$\rho_{nf} = (1-\varphi)\rho_f + \varphi\rho_s \quad (3.28)$$

$$\mu_{nf} = \frac{\mu_f}{(1-\varphi)^{2.5}} \quad (3.29)$$

$$(\rho C_p)_{nf} = (1-\varphi)(\rho C_p)_f + \varphi(\rho C_p)_s \quad (3.30)$$

$$\alpha_{nf} = \frac{k_{nf}}{(\rho C_p)_{nf}} \quad (3.31)$$

$$(\rho\beta)_{nf} = (1-\varphi)(\rho\beta)_f + \varphi(\rho\beta)_s \quad (3.32)$$

The suggested model of the thermal conductivity for suspensions proposed firstly by Maxwell as [78]. Also, it can be approximated for spherical nanoparticles by the Maxwell-Garnetts model as [79]:

$$\frac{k_{nf}}{k_f} = \frac{k_s + 2k_f - 2\varphi(k_f - k_s)}{k_s + 2k_f + \varphi(k_f - k_s)} \quad (3.33)$$

The Rayleigh and Prandtl numbers of nanofluid can be expressed as [58]:

$$Ra_{nf} = \frac{(\rho\beta)_{nf}}{(\rho\beta)_f}\frac{k_{bf}}{k_{nf}}\frac{(\rho c_p)_{nf}}{(\rho c_p)_f}\frac{\eta_{bf}}{\eta_{nf}}Ra_f \quad (3.34)$$

$$Pr_{nf} = \frac{k_f}{k_{nf}}\frac{c_{p_{nf}}}{c_{p_f}}\frac{\eta_{nf}}{\lambda_f}Pr_f \quad (3.35)$$

Table (3.1): The physical properties of the working base fluid and nanoparticles [80].

	ρ	C_p	K	β	μ
Pure Water	997.1	4179	0.613	0.0002100	0.000855
Al_2O_3	3880	765	40	0.0000085	-

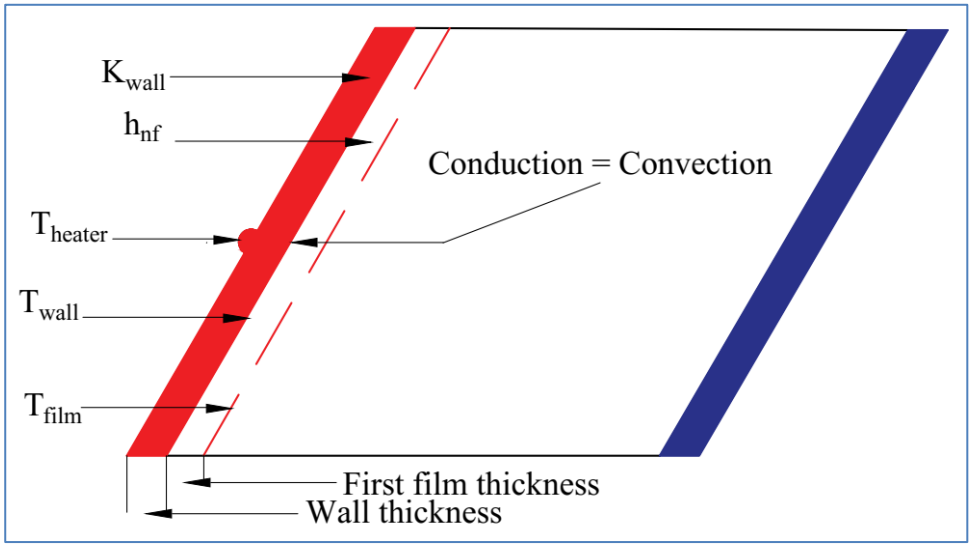

Figure (3.11): The calculation of (h_{nf}) and the average (Nu) on the left hot wall.

3.7. The Numerical Analysis

To obtain an approximate solution numerically, one has to use a discretization technique that approximates the differential equations by a system of algebraic equations at only discrete points in the domain, which can then be solved on a computer code. The first step to numerically solve a mathematical model of physical phenomena is its numerical discretization.

This means that each component of the differential equations is transformed into a numerical analogue which can be represented and then processed by a computer program, built on some algorithm. The powerful computational technique finite element method (FEM) is employed to solve the problem of natural convection inside a closed domain that are described by a partial differential equation.

The basic idea of the finite element method that the domain is broken into a set of finite elements that are generally triangular or quadrilaterals.

3.7.1. The Numerical Solver

The present work is an attempt to bring the (FEM) technique into light through a novel formulation of three-dimensional incompressible and steady thermal flow problems.

The commercial code solver (COMSOL) has been used to solve the differential equations. The (FEM) is a technique for solving a numerical solution to a boundary value problem described by differential equations. In order to solve the problem numerically, the geometry in which the equations will be solved must be broken down into a stiffness matrix.

This is a series of points within the boundaries of the geometry. The equations will be solved on each of these individual points. Once the points are set in place, they are connected to one another. The connections sometimes form rectangular mesh elements, other times they form triangular mesh elements. (COMSOL) almost uses a triangular connectivity pattern.

3.7.2. Controlling the Solving Parameters

In (COMSOL) the segregated approach is selected automatically to solve the (3D) Multiphysics models. That is subdivided solving the unknowns in many time steps. The main controlling factor is the time step which is set to give a small number of iterations as possible.

Whilst maintaining a smoothly converging solution. Inside each time step, number of iterations which is carried out to resolve the transparent equations for the time step. As long as the time step is small enough to get convergence. The smaller time step means less iterations per time step are required. The current time steps are the temperature in

the heat transfer field, the pressure and the three components of velocity (U, V, W) in the flow field.

A measure of how the solution converged can be obtained by plotting the residuals for each equation. The maximum error obtained are set to be around (10^{-5}-10^{-8}) as shown in Fig. (3.12). The number of iterations increased with Rayleigh number.

$$\left|\frac{\lambda_{i+1}-\lambda_i}{\lambda_{i+1}}\right| \leq Maximum\ Error \qquad (3.36)$$

Where (λ) is any calculated parameter.

3.7.3. The Mesh Generation and The Grid Independence Test

The (FEM) is based on the idea that a continuous function may be approximated by solving it at discrete points. Since the solutions for finite element analysis are based for these individuals meshes elements, the space between the nodes directly affects the accuracy of the solution.

The closer the nodes are, the smaller the mesh area of the elements. Also, the smaller the distance across which the governing equations must be approximated. So, the more refined meshes, the better the solution. However, the more mesh elements present, the more equations must be solved and the greater the computing time required to arrive the better solution.

A triangular mesh on all the cavities is generated. The grid independence study was presented for the number of elements in the entire cavity domain for the cavity of (γ = 60º) and of (L) walls side length as presented in Appendix B.

Considering the accuracy and time consumed, a mesh of (198036) elements including (14756) boundary elements and (564) edge elements has been selected as shown in Fig. (3.13) for all computations of this cavity. This mesh specifications were selected duo to the error and the time consumption where the final mesh in the table was consumed about twice the selected mesh while the error in accuracy was only (0.02%).

Whereas, the selected mesh has an error of about (0.58%) from the previous mesh and consuming about (1.3) of its time of running. For other cavities the selected meshes are presented in Fig. (3.14) to Fig. (3.17). The elements at the edges were paid a special attention due to its important rule in guiding the results. As it is shown in Appendix B these elements are increased with the complexity of the cavity. The flow chart of the solution process is presented in **Fig.** (3.18).

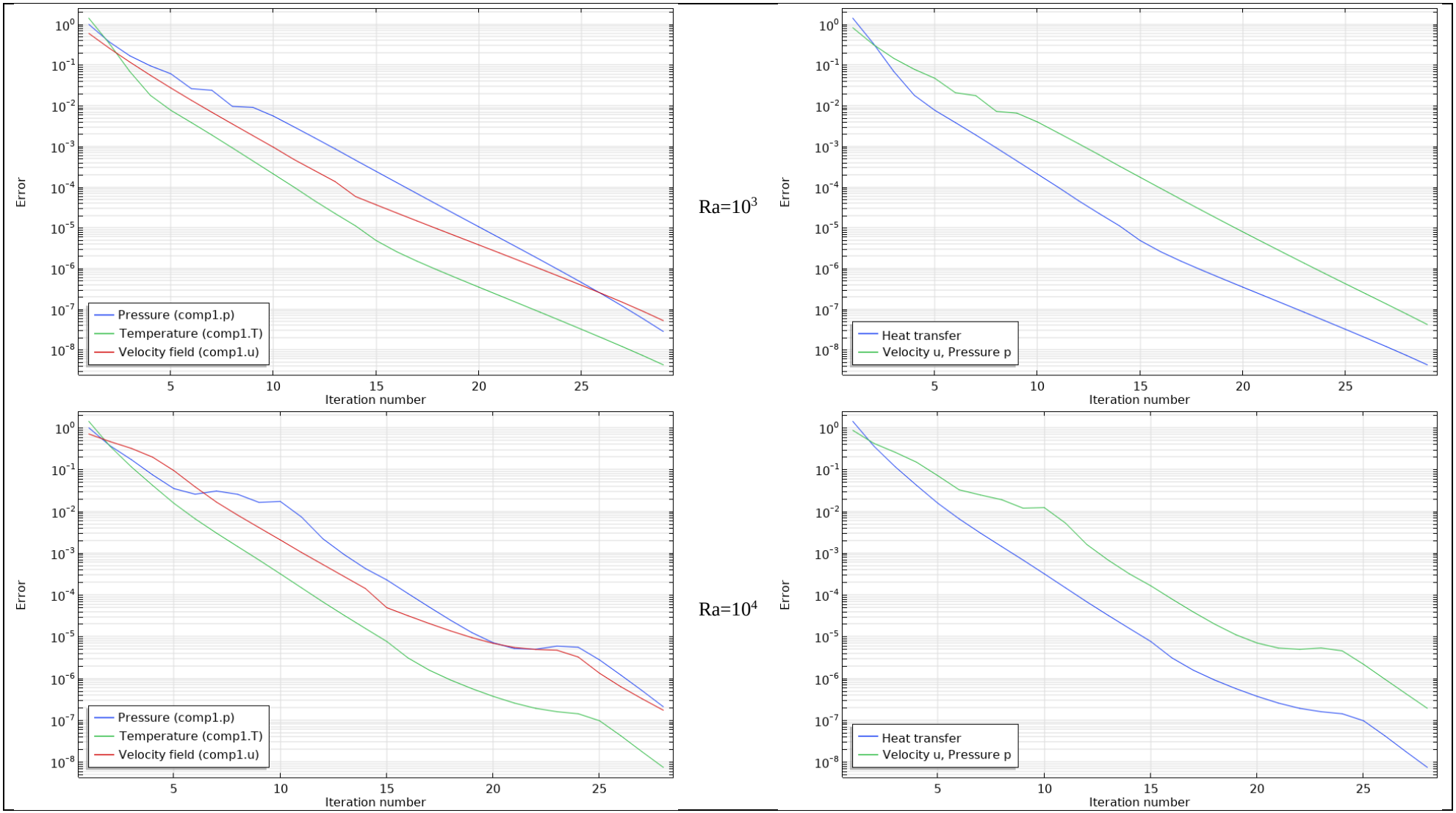
Error
Iteration number
Pressure (comp1.p)
Temperature (comp1.T)
Velocity field (comp1.u)
Heat transfer
Velocity u, Pressure p
Ra=10^3
Ra=10^4

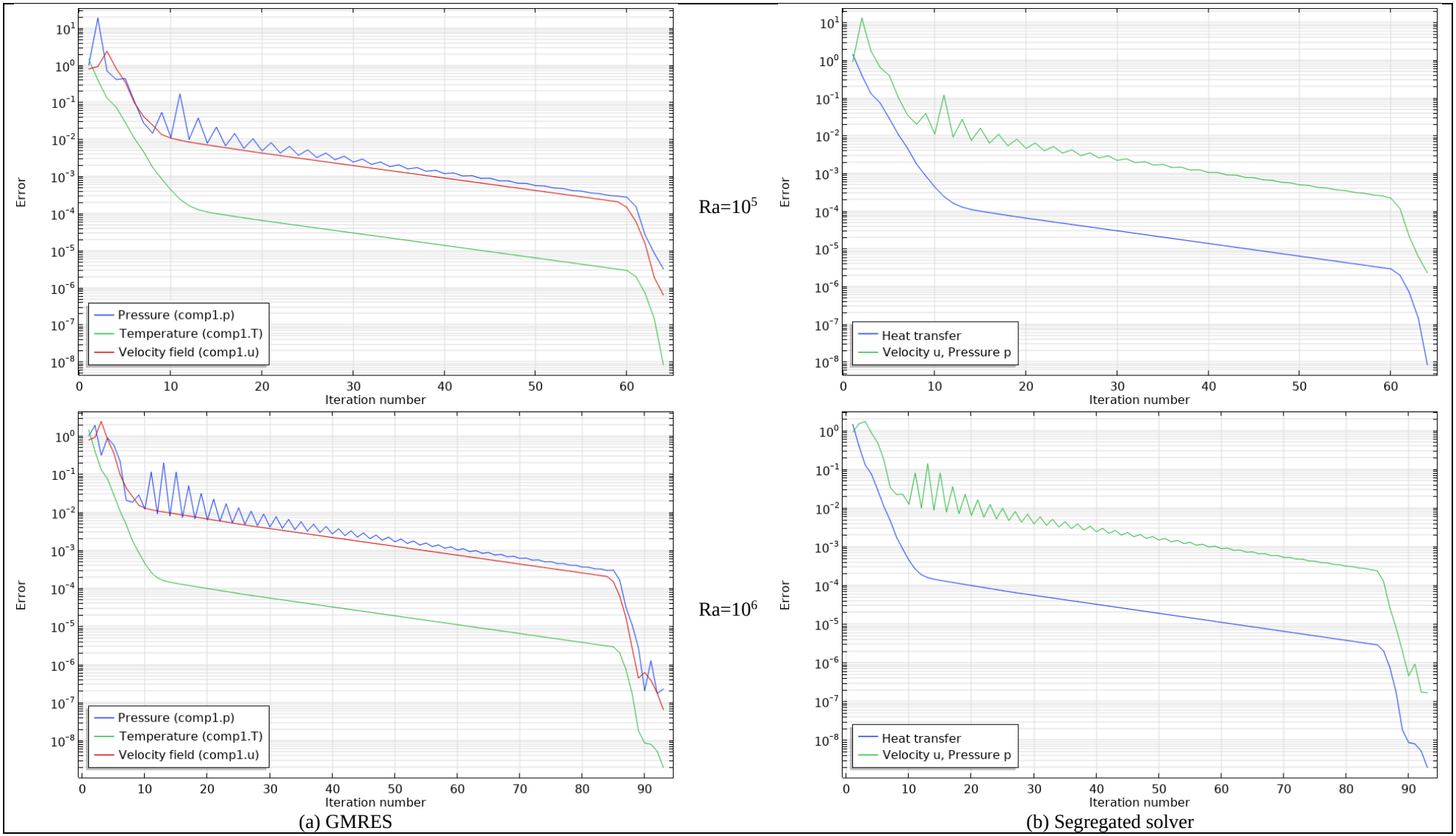

Figure (3.12): The convergence plot for the parallelogrammical cavity of (γ=60º) and constant walls side length (L) at (φ=0.05) and different (Ra).

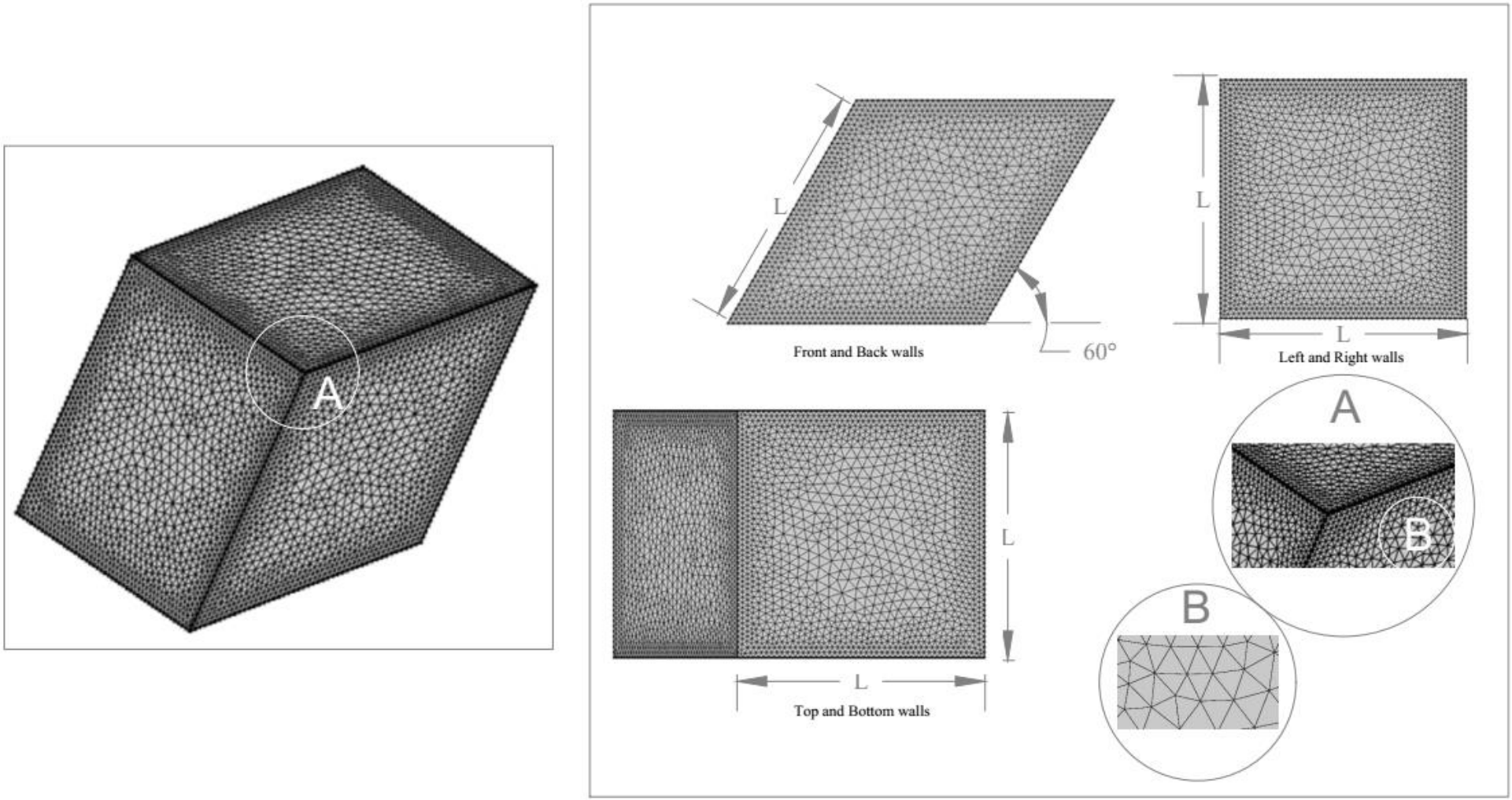

Figure (3.13): The selected mesh of the parallelogrammical cavity of (γ=60º) and constant walls side length (L).

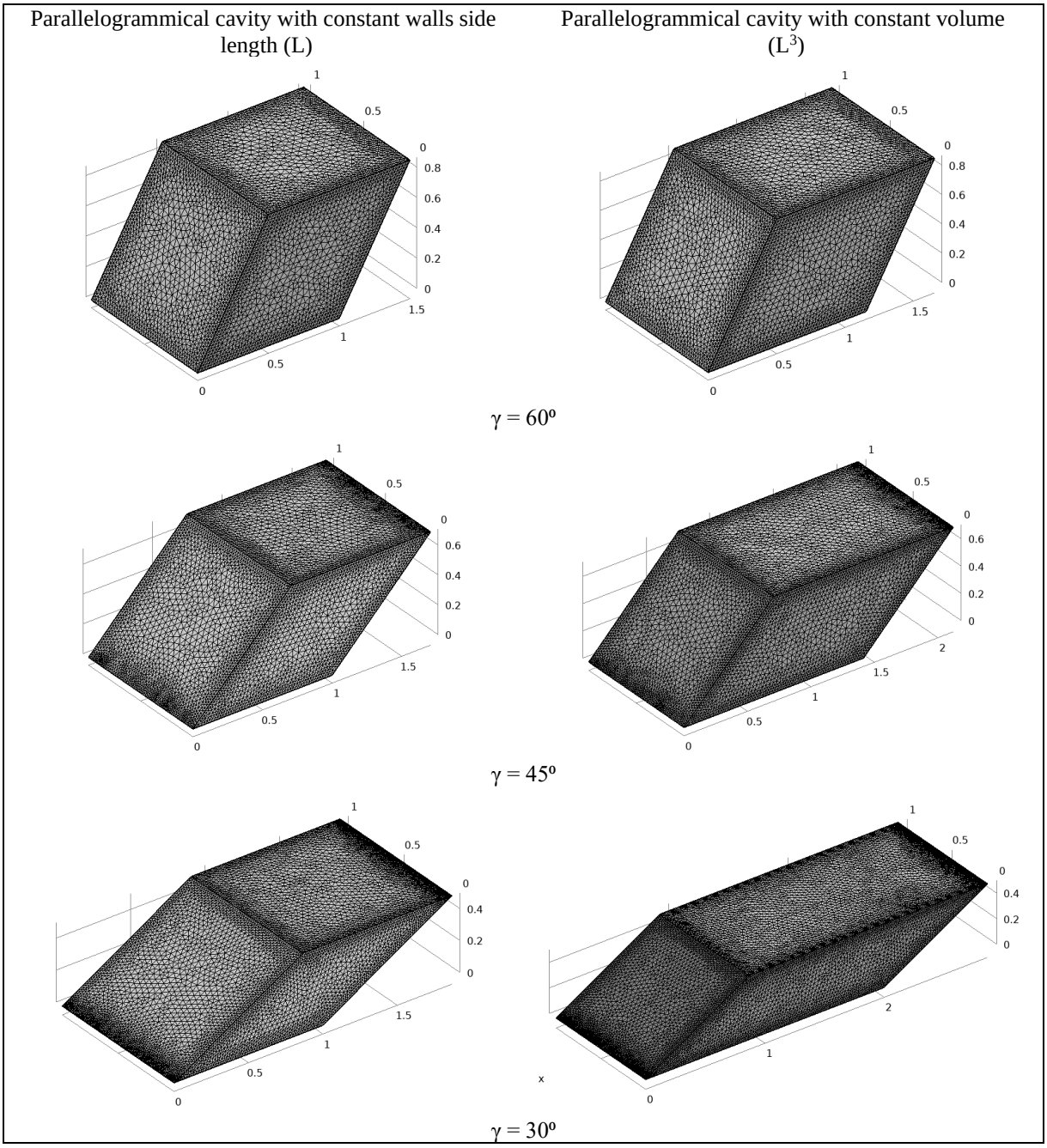

Figure (3.14): The selected mesh of the parallelogrammical cavity with different (γ).

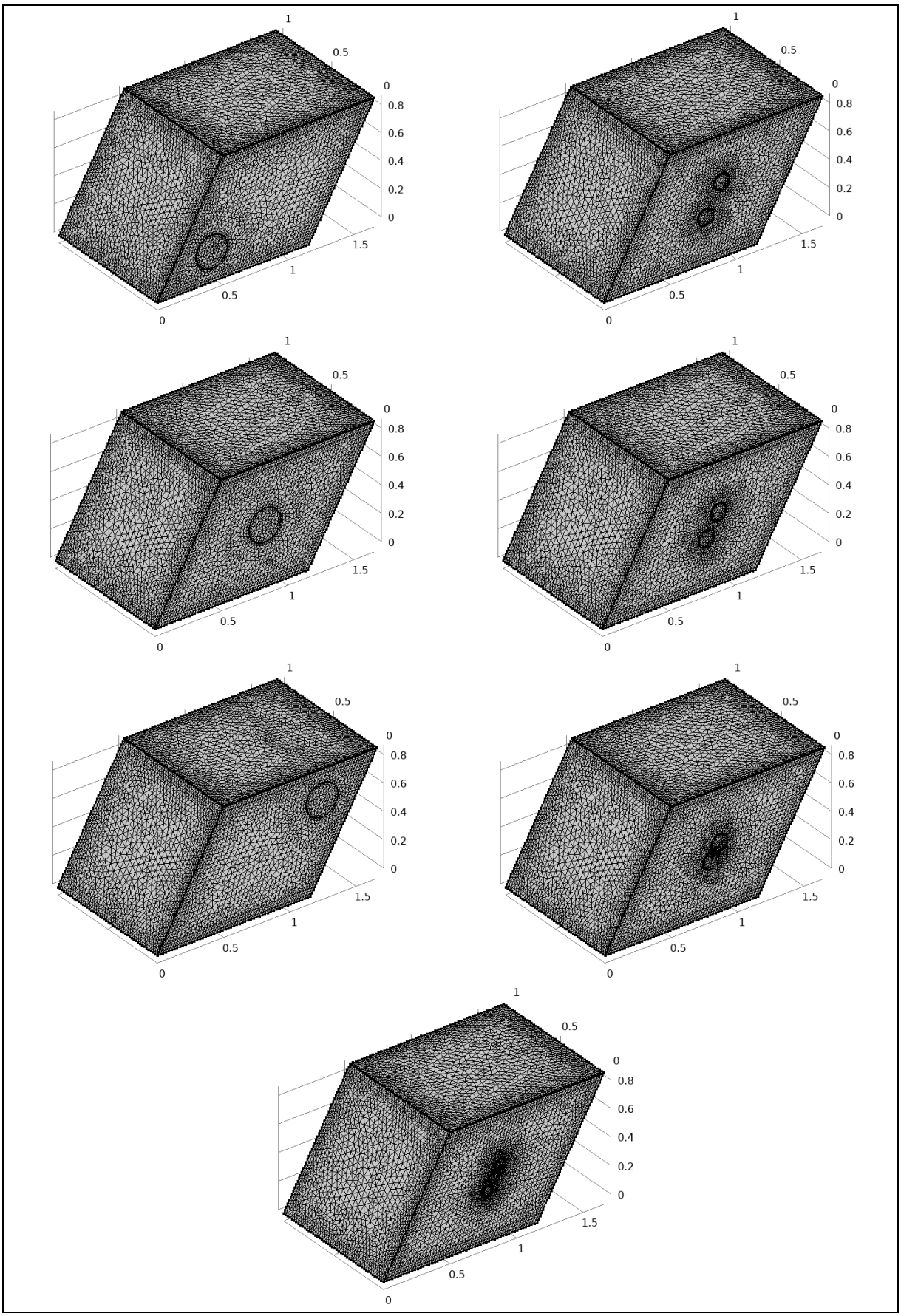

Figure (3.15): The selected mesh of the parallelogrammical cavity of ($\gamma = 60^{o}$) with different inners.

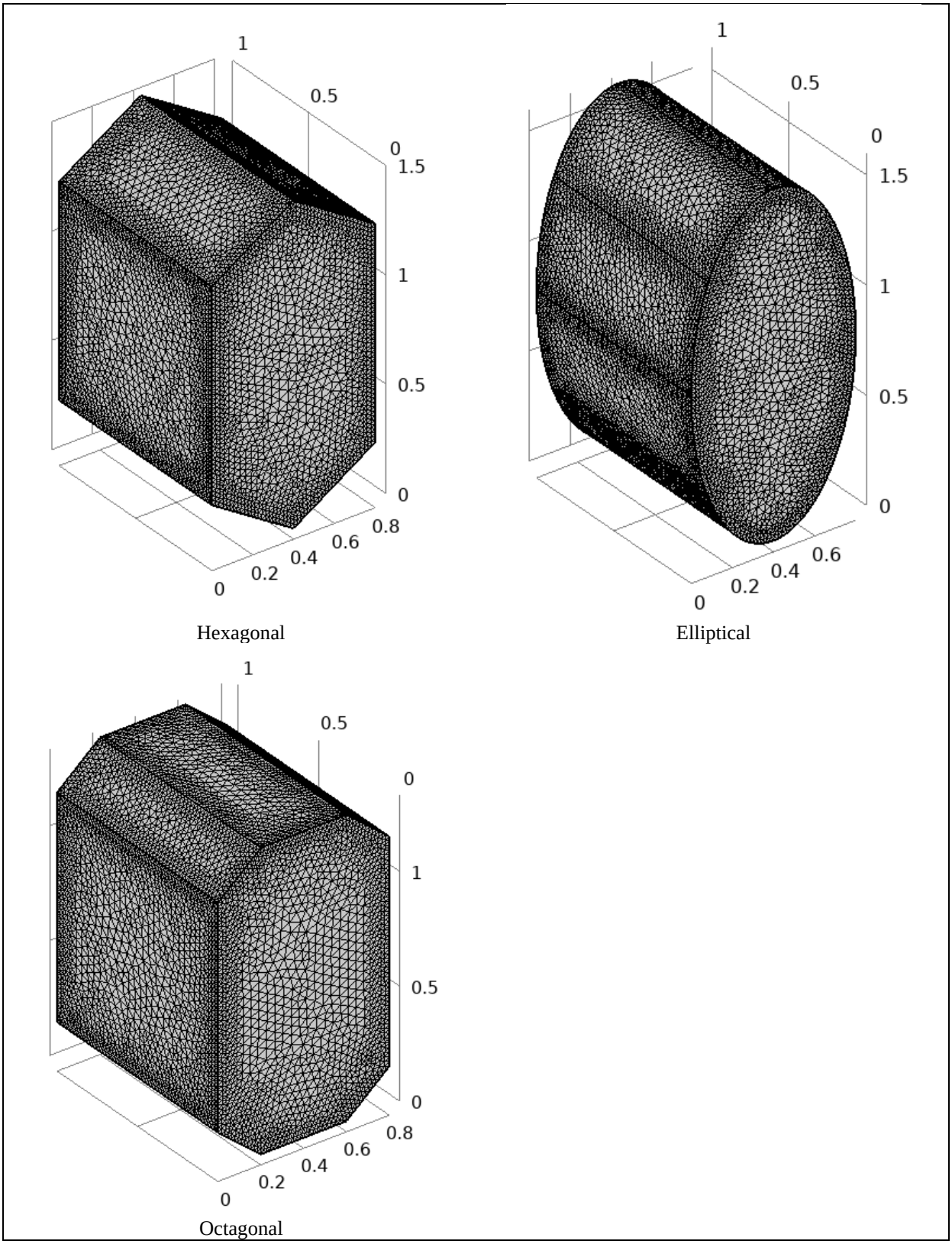

Figure (3.17): The selected mesh for the different geometry cavities.

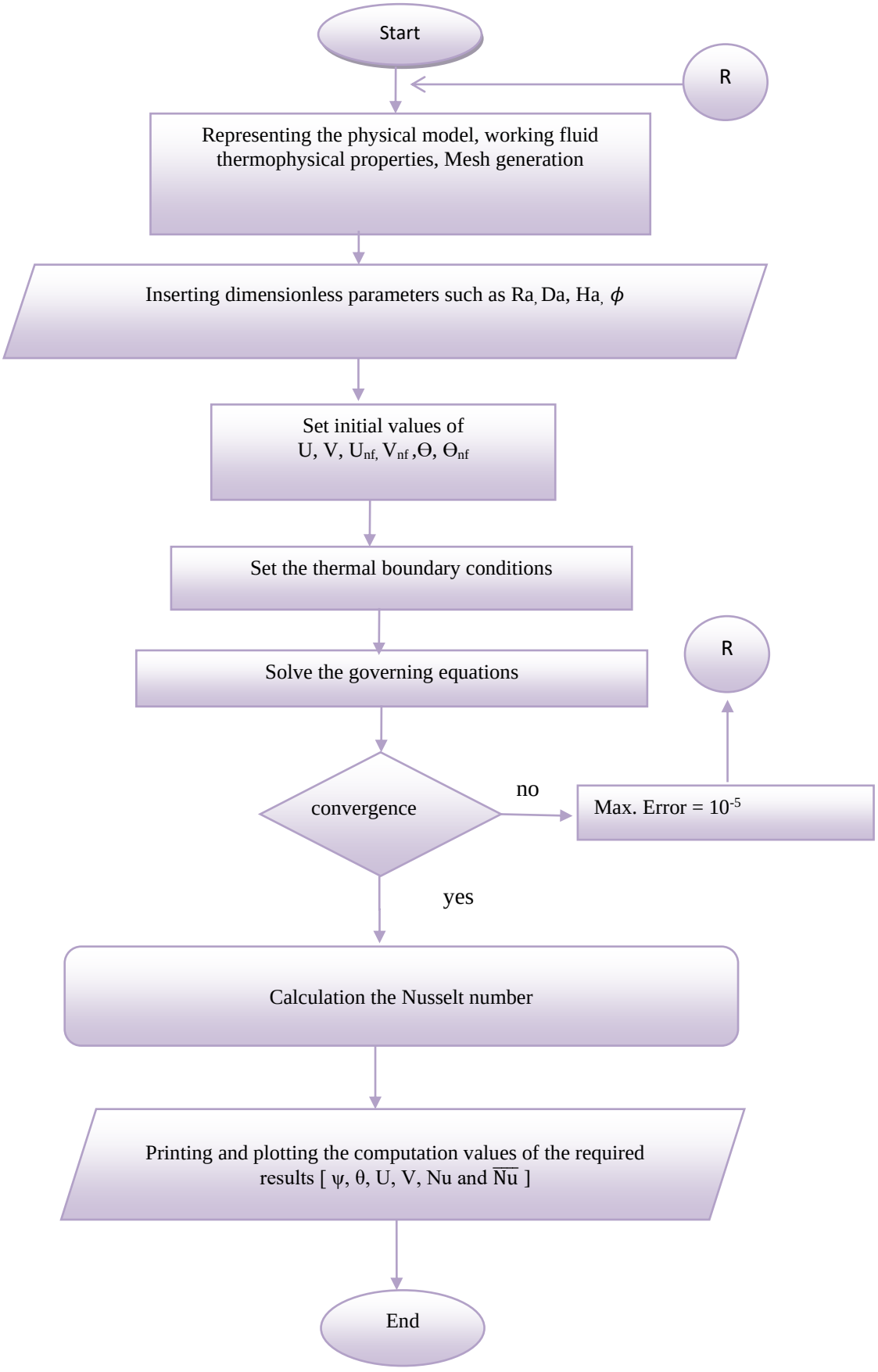

Figure (3.18): The flow chart of the simulation.

Chapter Four: The Experimental Work

4.1. Introduction

This chapter introduce the experimental work facilities and procedure which consumed time about fourteen months from the rig building to reading results in the labs of the Mechanical Engineering Department / University of Babylon. Detailed description of the rig setup parts is explained in the following sections. The working fluid preparation and the experimental procedure are presented. This rig is built to study the laminar natural convection inside a 3D novel parallelogrammical cavity filled with (Al_2O_3-deionized water) nanofluid of three different concentrations (φ=0.01, 0.03 and 0.05) and the Rayleigh number range of ($10^5 \leq Ra \leq 10^6$).

4.2. The Experimental Rig

The experimental rig consists of four parts as shown in the schematic diagram and the experimental set-up in Fig. (4.1) and Fig. (4.2) respectively. The main part is the parallelogrammical cross section cavity. The cavity is differentially heated along the vertical left and right sidewalls. The other parts of the rig are the heating and the cooling systems. The last part is the measuring and control system.

4.2.1. The Cavity

The cavity has a parallelogrammical front and back walls and square other walls, the building steps of the cavity is presented in Fig. (4.3). All walls have (15cm) side lengths except the horizontal lengths of the front and back parallelogrammical sidewalls or the cavity width are (16cm). The walls are made of Perspex glass of (0.5cm) thick except the left and right walls. Which are made of Aluminum sheet of (1cm) thick. The left wall loaded by the heating system to keep a constant hot temperature. The right wall carrying the cooling system to produce constant cold temperature. he transparent cavity has a circular hole at the upper wall (close to the cold wall) to fill the cavity by the working fluid. A drainage hole at the lower (base) wall (close to the hot wall) for emptying it through a rubber hose. Fourteen (14) mini holes are drilled on the upper wall to enter the temperature sensors. The cavity is fixed by iron stand on a fiber plate to prevent movement during the experiments.

4.2.2. The Heating System

This system is formed by two components; the electrical heater and the control system which are shown in Fig. (4.4). The heater consists of eight-point heaters with specifications introduced in Appendix C distributed on the left Aluminum plate. The electrical heater is powered by (DC) current. The heaters are designed as that each two heaters are works together with the specified thickness of the plate to ensure regular and homogeneous distribution of temperature. The stability of the temperature is satisfied by stitching three thermocouples with depth (3mm) along the inner central height of the hot wall. These thermocouples are distributed as that near the base called (H1), at the center called (H2) and near the tip called (H3).

The control system represents by keyboard and monitor which has many functions. One of these functions are setting the left wall to the desired temperature. Which is designed to be in the range of (30ºC-80ºC) and controlling it to stay constant along the run of each experiment. These functions are entered by the keyboard and display on the monitor.

4.2.3. The Cooling System

The cooling system shown in Fig. (4.5) on the right-side wall is accomplished by inserting cross counterflow heat exchanger to ensure a better heat exchange. The heat exchanger is formed by Aluminum plate of (1cm) thick digging of grooves to allow the flow of cooling water. The cooling water is provided from the cooling equipment through counter rubber pipes of (1cm) diameter.

The cooling equipment is a chiller unit of (9L) capacity with specifications presented in Appendix C. It filled by the green water (radiator cooling water). This water has good physical properties. Also, it is with no salts which protecting the inner body and increasing the boiling temperature to about (120ºC). Although, to satisfy the stability three thermocouples are stitched at depth of (3mm) along the inner central height of the cold wall. These thermocouples are distributed like that of hot wall and called (C1) at the base, (C2) at the center and (C3) at the tip.

4.2.4. The Measuring System

This system consists of three components which are; thermocouples, control system and computer as shown in Fig. (4.6). Thermocouples of type-K are used which are the most common type of thermocouples. It is accurate, reliable and has a wide temperature range.

The current type capacity range is (0ºC-100ºC) with accuracy of (+/-1.1ºC). The specifications of thermocouples are presented in Appendix C.

Twenty-seven (27) thermocouples are divided into three groups as shown in the Fig. (4.7). Fourteen (14) thermocouples are distributed along the width (X-axis) of cavity from the center of the left hot wall to the center of the right cold wall at (1cm) apart. These are called (X1 to X14). Eight (8) thermocouples are distributed along the central depth (Y-axis) of the back half of the cavity called (Y1 to Y8) from the cavity center to the back wall, (1cm) apart also. Five (5) thermocouples are distributed along the central vertical height (Z-axis) from the bottom to the top parallel to the inclined side walls called as (Z1 to Z6). Six reading for the height can be recorded because of the combined thermocouple at the center of cavity where (Z4=Y1).

The control system consists from Arduino board, monitor and software setup on the computer. Two cables are connected from the Arduino to the computer, one of them for the X-axis thermocouples and the other to the Y and Z axes thermocouples. If the reading of X-axis appears in the computer, the reading of Y-axis and Z-axis appears on the control monitor and vice versa. The reading is repeated each (20sec) in the computer while it repeats each (5sec) at the monitor. The readings are recorded after the repeated values being stable with no variation.

The thermocouples are calibrated at laboratory of The Ministry of Planning / Central Organization for Standardization and Quality Control (C.O.S.Q.C). The calibration certificate is presented in Appendix C.

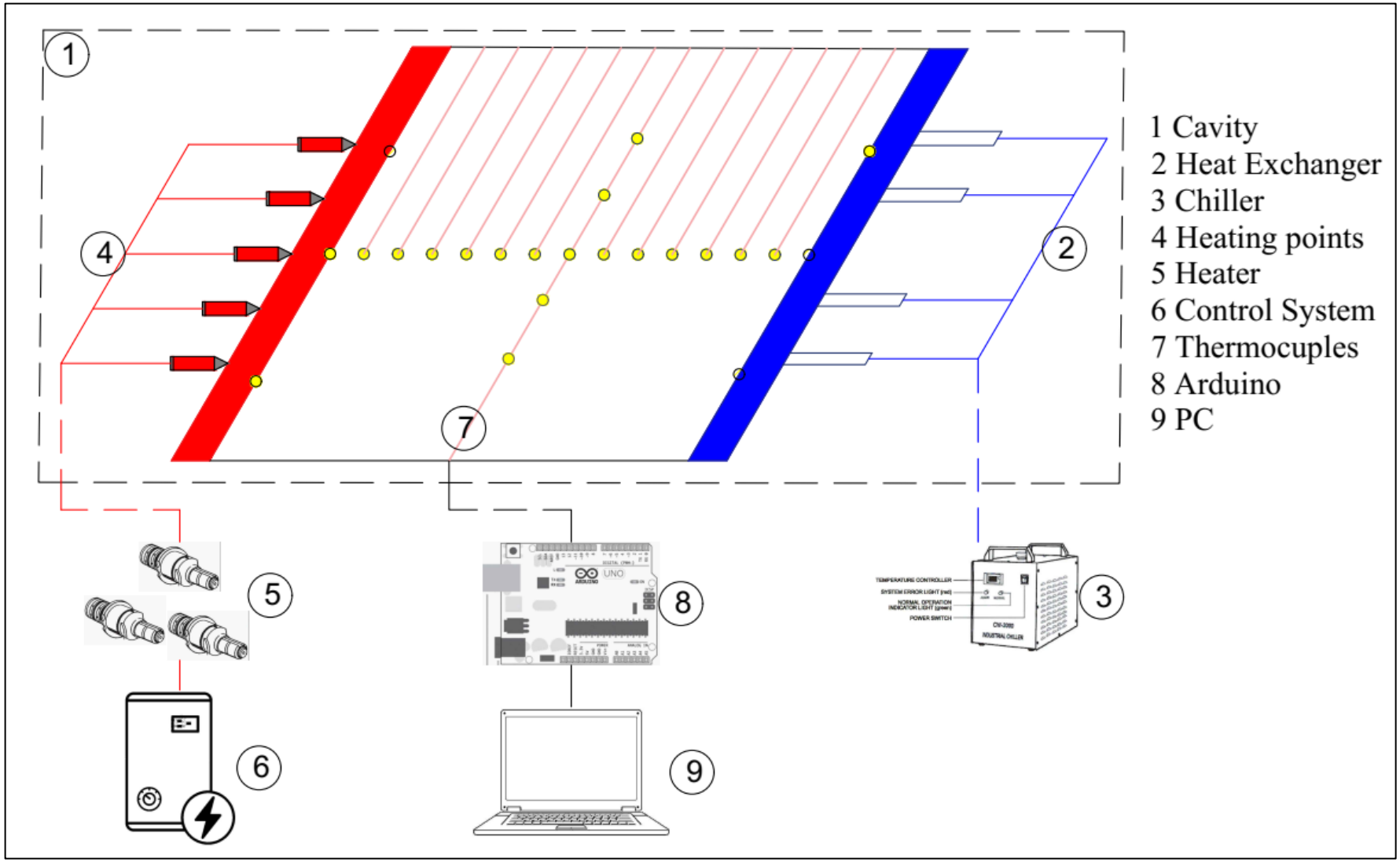

Figure (4.1): Schematic diagram of the experimental setup.

Figure (4.2): The experimental set-up apparatus.

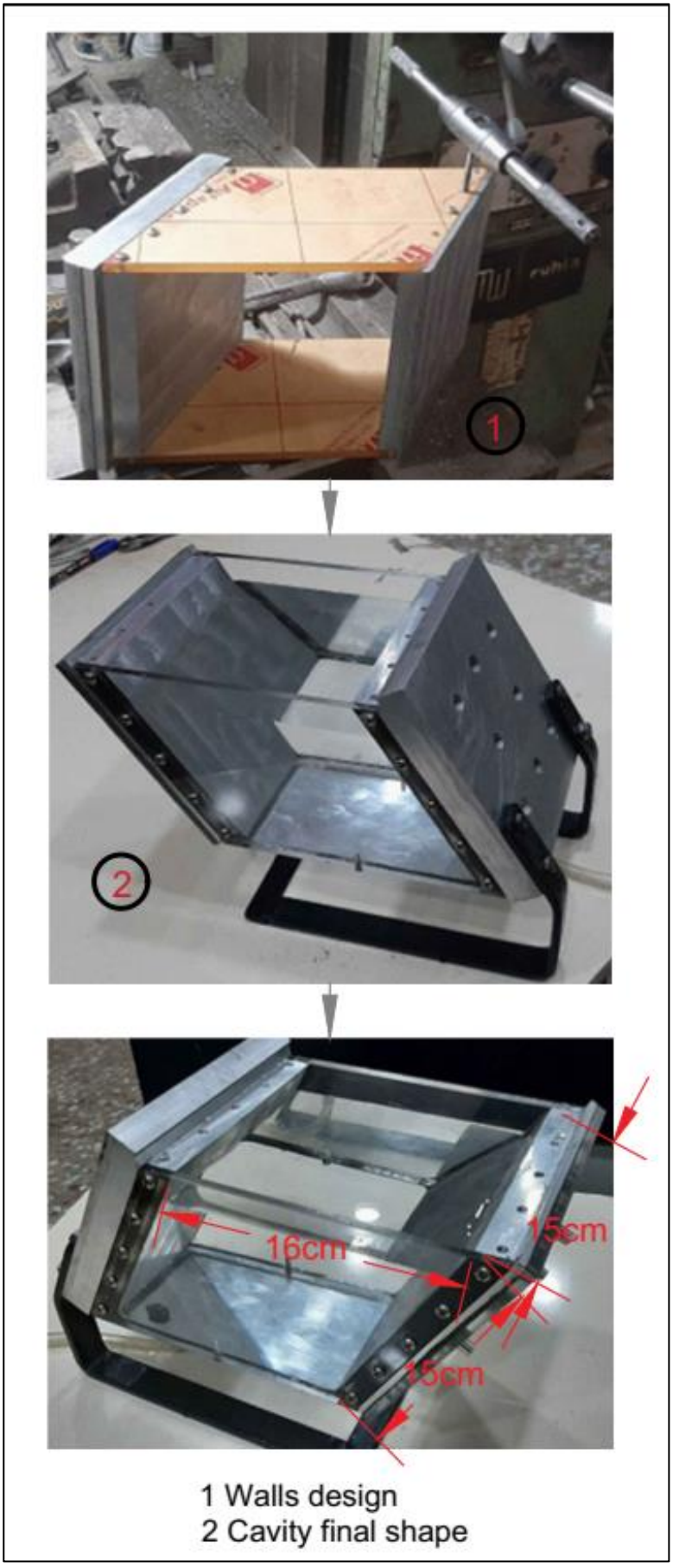

Figure (4.3): The cavity building.

Figure (4.4): The heating system.

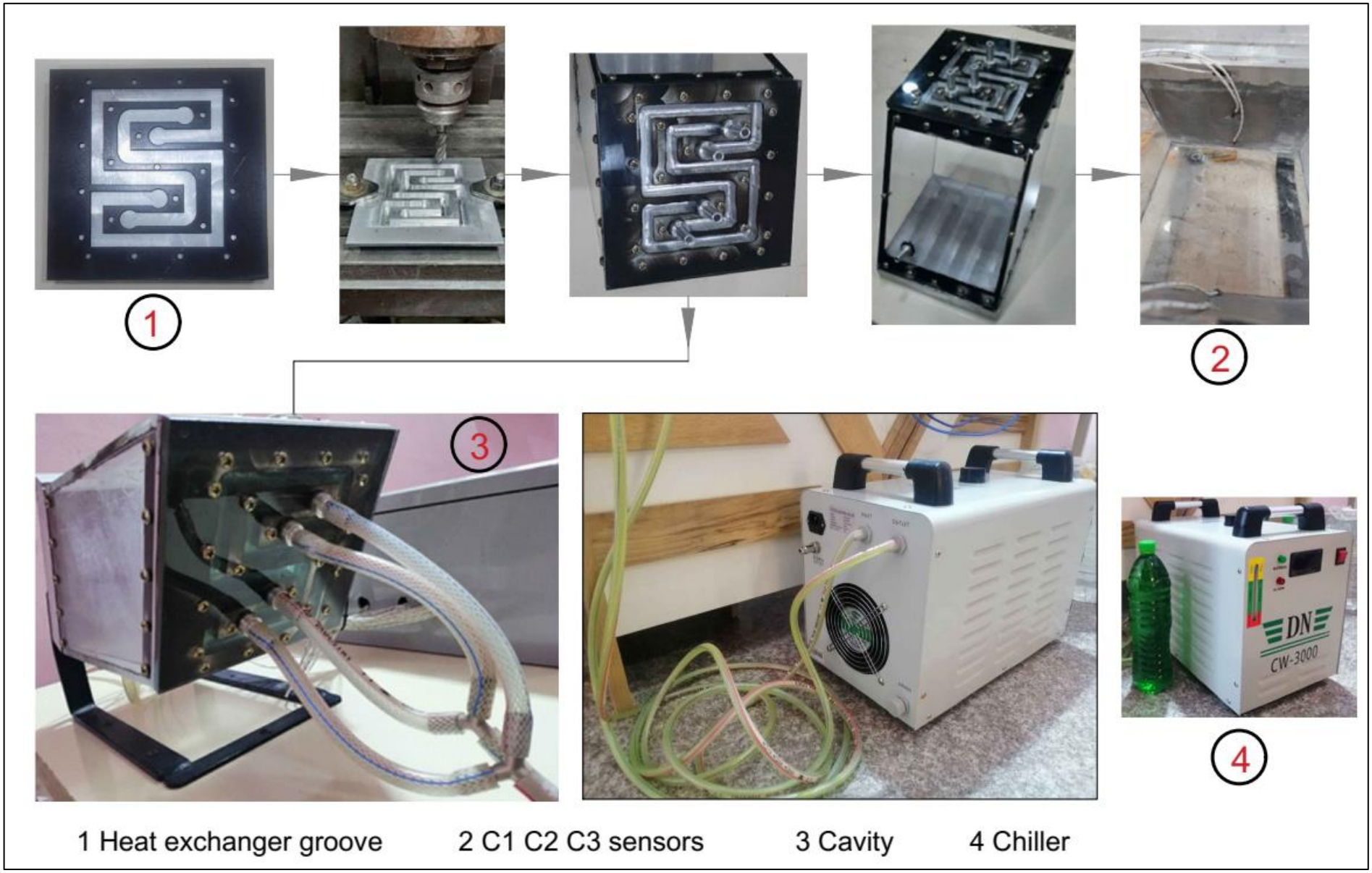

Figure (4.5): The cooling system.

Figure (4.6): The measuring and control systems.

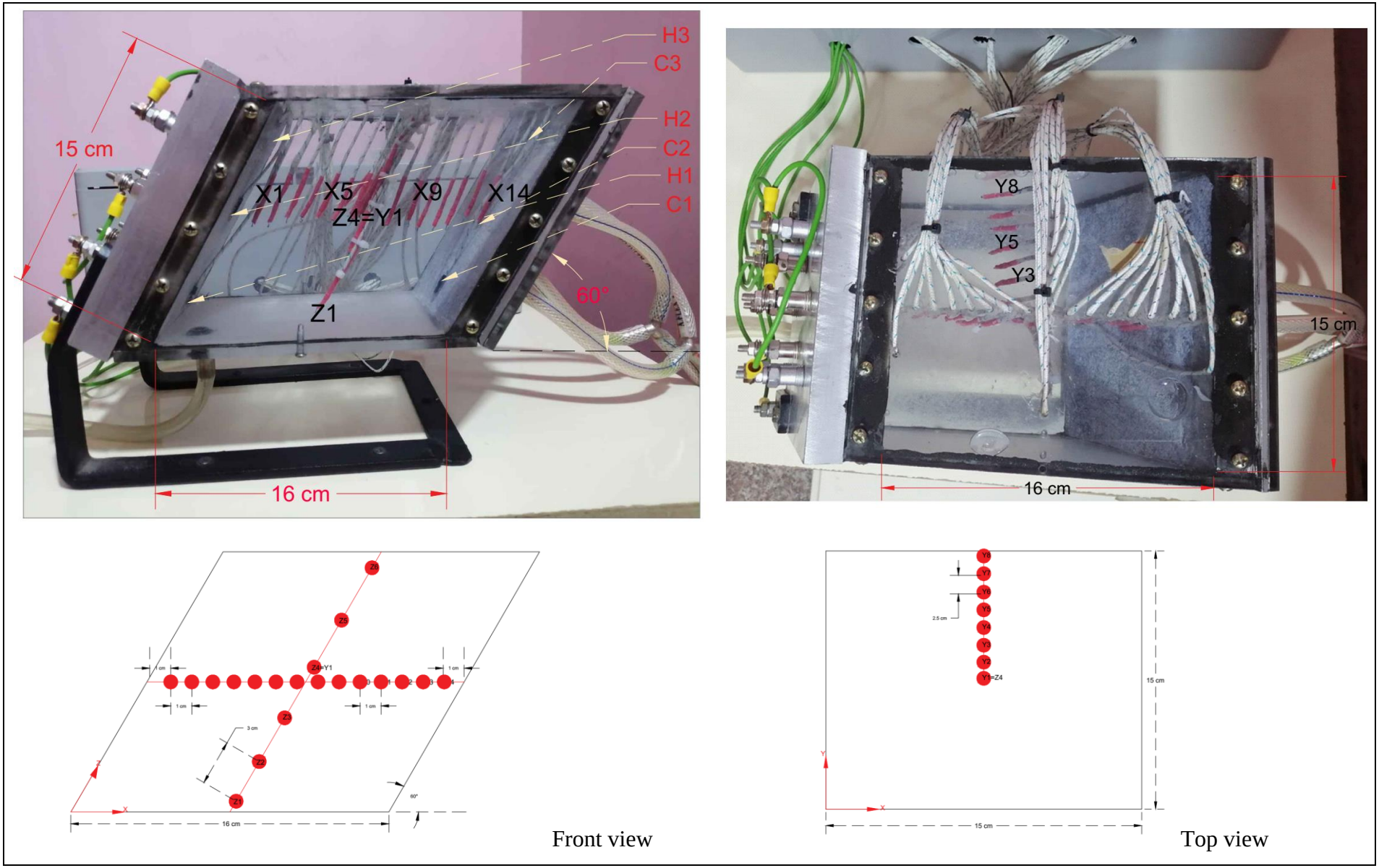

Figure (4.7): The cavity dimensions and thermocouples distribution.

4.3. The Working Fluid

The Al_2O_3 nanoparticles varied in the range of (13nm - 302nm) to prepare nanofluids, and the observed enhancement in the thermal conductivity is (2% - 36%).

The most important criterion of nanofluid is agglomerate-free stable suspension for long durations without causing any chemical changes in the base fluid. This can be achieved by minimizing the density between solids and liquids or by increasing the viscosity of the liquid using nanometer-sized particles. This prevents particles from agglomeration effects [9-10].

4.3.1. The Nanoparticles Properties Tests

The current working fluid is the Alumina particles suspended in Deionized water as a base fluid (Al_2O_3-H_2O) with three different concentrations (φ = 0.01, 0.03 and 0.05).

The Al_2O_3 nanoparticles used are of Gama type with (99.9%) purity and having a particle size of (d_p<45nm). The nanoparticles size is analyzed utilizing the X-ray apparatus (SHIMADZU X-RAY DIFFRACTOMETER, XRD-6000) that shown in Fig. (4.8). The report of X-ray is presented in Appendix D.

The Scanning Electron Microscope (SEM) apparatus of type (VEGA 3 SBU / No. 118-0014) from TESCAN that shown in Fig. (4.9) which is of maximum 500 times magnification as illustrated in Appendix C is used to provide the micro scale image (10^{-6} m) of particles as presented in Appendix D.

Figure (4.8): The X-ray apparatus.

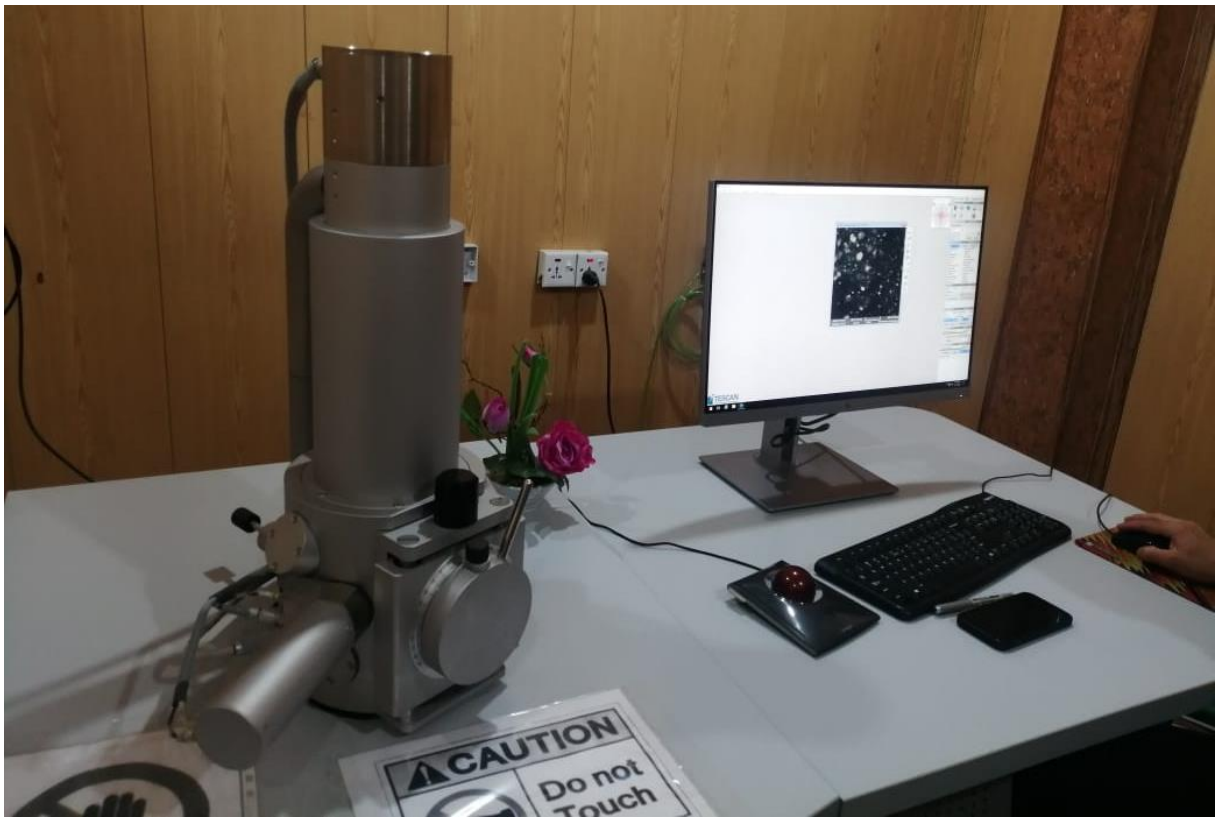

Figure (4.9): The microscope apparatus.

4.3.2. The Nanofluid Preparation

In this work, the two-step method for preparing the nanofluid is used which explained as that, the nano particles are first produced and

then dispersed in the base fluid. The commercial product nanoparticles are used and follow the following points in preparation of the nanofluid:

1. Calculating the nano particles weight for each considered concentration namely (φ = 0.01, 0.03 and 0.05) as given by:

$$\varphi\% = \frac{(m_p/\rho_p)}{(m_p/\rho_p)+(m_f/\rho_f)} \quad (4.1)$$

The calculated amounts of nanoparticles are for (1L) of deionized water which will multiplied by the cavity capacity (3L) to get the total amount of nano particles for each concentration. The calculated amounts are presented in Appendix D.

2. The calculated amounts of nanoparticles are weighted using the analytical balance from (Sartorius) which is presented in Fig. (4.10) and its specifications described in Appendix C.

3. Dispersing the weighted nano particles for each concentration into (3L) of the deionized water base fluid.

4. Distributing the nanoparticles uniformly by using the ultrasonic waves through the continuous flow ultrasonic homogenizer for half hour at the room temperature (35ºC-38ºC). This apparatus shown in Fig. (4.11) from (MTI) corporation with the specifications presented in Appendix C.

5. To homogenate the nanofluid, the mechanical stirrer from (Heidolph / RZR line) is used to do this task, for one hour. The stirrer head is carried by (H) frame stand. The mixing shaft has two cross blades impeller at the end and its length is controlled by chuck with a key. The apparatus is presented in Fig. (4.12) and its specifications included in Appendix C. The cycle of preparing the nanofluid is shown in Fig. (4.13).

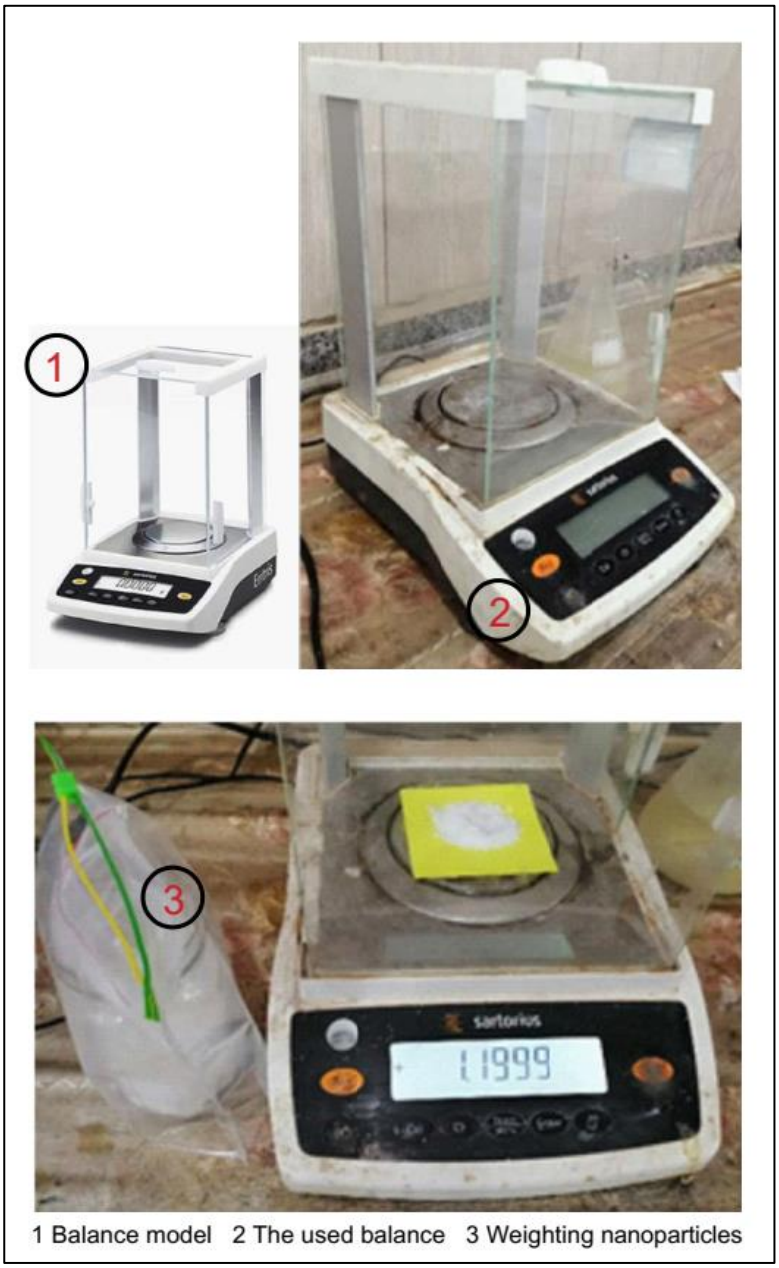

Figure (4.10): The sensitive balance.

4.3.3. The Sedimentation and Agglomeration Tests

The period of the nanoparticles spread and distribution inside the liquid is a very important property of nanofluid experiments. Three samples of the three nanofluid concentrations are left still for three days.

It is re-photographed every day to observe the difference in its homogeneity. Or, the possibility of mass gatherings/deposition at the

bottom. The nanofluid keeping its physical properties for about (30) hour. After this period, the nanofluid needs to re-homogenize where the nanoparticles begin to participate as shown in Fig. (4.14).

4.3.4. The Nanofluid Thermophysical Properties

The thermophysical properties of the nanofluid are playing a strong effect on the flow and thermal fields. These properties are including mainly the effective density, the effective dynamic viscosity and the effective thermal conductivity.

The first two parameters are calculated from the equations (3.28) and (3.29) that introduced by Oztop et al. [75]. While the thermal conductivity calculated by the equation (3.32). The calculated values are presented in Appendix D.

4.4. The Experimental Procedure

The following experimental procedure is repeated for three concentrations of working fluid, (Al_2O_3-H_2O) nanofluid (φ=0.01, 0.03 and 0.05). To ensure convection and avoiding turbulent flow, the temperature differences between the hot and cold walls are chosen as (ΔT=16ºC, 26ºC) which corresponding to ($Ra \approx 10^5$ and 10^6) respectively.

Each of these two values is studied for the named concentrations. All the studied cases are discovered for two different values of the cold wall temperature that is selected near the average room temperature of Iraq weather (T_c=28ºC and 30ºC). The overall cases become (12) as presented in Appendix D. The error analysis of the experimental measured data by the temperature sensors are presented in Appendix C

through the repeatability analysis of (10) experiments. The experimental procedure can be outlined as follows:

1. The cavity is cleaned by distilled water to remove impurities. The washing is repeated after each run.

2. The cavity is filled completely by the working fluid and ensuring that its initial temperature is equal to the cold wall temperature.

3. The cold wall is set to a constant temperature (T_c = 28ºC) by running the chiller through the designed heat exchanger. The studies repeated for (T_c = 30ºC). This temperature can be satisfied by observing the control system monitor and to be sure that all the thermocouples (C1, C2, C3) having the same readings and stable.

4. The hot wall temperature is set to its desired value by entering the temperature from the keyboard of the control system. The hot temperatures are selected according to the temperature differences which are (T_h=44ºC and 54ºC) for (T_c=28ºC). While they are (T_h=46ºC and 56ºC) for (T_c=30ºC). For all cases; the hot temperature is satisfied by observing the control system monitor and to be sure that all the thermocouples (H1, H2, H3) having the same readings and stable.

5. The Arduino cables are connecting to the personal computer and waiting few seconds. Then start of recording the thermocouples readings.

6. Emptying the cavity from the working fluid through its bottom hole that designed for this purpose.

7. Fill the cavity by distilled water completely then emptying it. The experiment procedure steps are presented in Fig. (4.15).

Figure (4.11): The ultrasonic device.

Figure (4.12): The mechanical overhead stirrer.

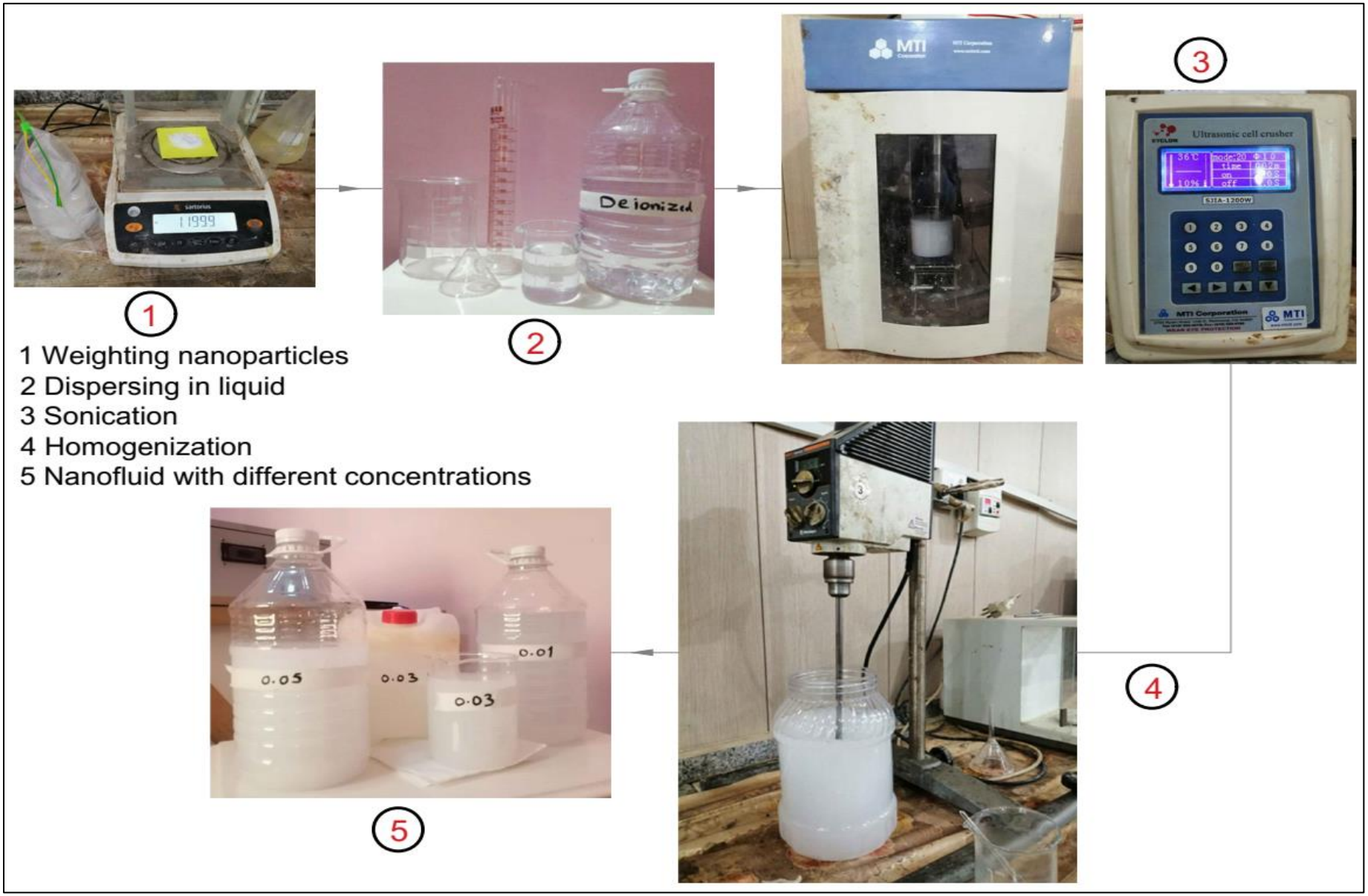

Figure (4.13): The cycle of the nanofluid preparation processes.

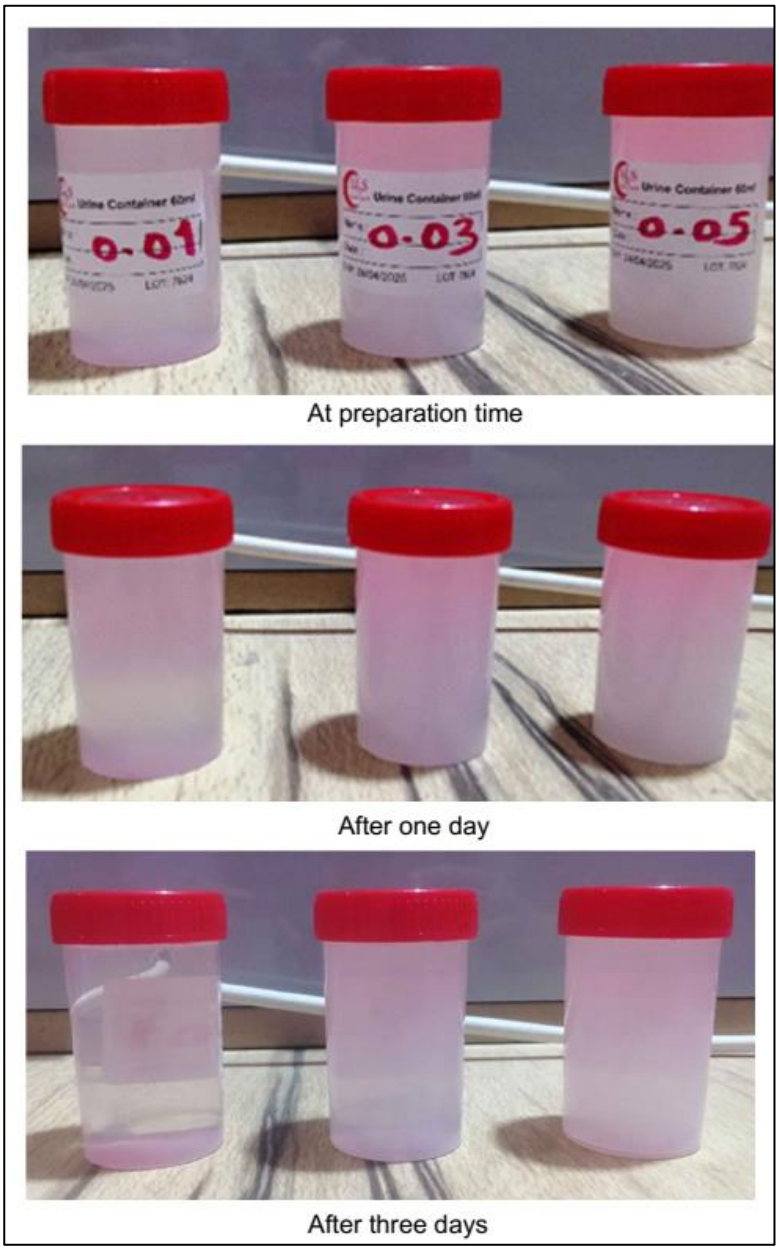

Figure (4.14): The participations test

Figure (4.15): The experiment procedure.

Chapter Five: Results and Discussion

5. 1. Introduction

This chapter consists of three major parts; the validation of the numerical code, the presentation and discussion of both the numerical and the experimental cases. The simulated results of the model with related to the steady laminar natural convection inside four different 3D geometry cavities are introduced. The main cavity configuration is the parallelogrammical cavity which also visualized experimentally.

Theoretically, the effects of many parameters on the fluid flow and heat transfer fields are studied. These parameters are the heating and cooling system arrangements, the solid volume fraction ($0.01 \leq \varphi \leq 0.05$), the Rayleigh number ($10^3 \leq Ra \leq 10^6$) and the inclination angle of the parallelogrammical side walls from the horizon; the skew angle ($\gamma=30^o$, 45^o and 60^o). After selecting the better conditions for the heat transfer enhancement, additional modifications on the parallelogrammical cavity are studied. These are the inserted bodies and its distribution. Finally, a comparison of the parallelogrammical cavity with other shape cavities for the same volume are accomplished. The other three considered cavities are: hexagonal, octagonal and elliptical.

On the other hand, the best design of the parallelogrammical cavity is accomplished and manufactured experimentally at ($\varphi=0.01$, 0.03 and 0.05) and ($Ra=10^5$ and 10^6). The numerical and experimental results are based on the flow and thermal fields presented as the stream lines and the isotherms contours. As like as, the average Nusselt number (Nu) along the hot wall and the local (Nu) plots. The temperature

distribution along the central width (X-axis), central height (Z-axis) and central depth (Y-axis) are presented too.

5. 2. The Code Validation

The present numerical model has been validated against benchmark solutions obtained in the literature. The validation was done according to the average Nusselt number on the hot wall and the fluid velocity components when the fluid moves from the hot to the cold walls horizontally or vertically. For more accuracy, the pattern of the streamlines and the isotherms are satisfied also. The first considered case is that of Sannad et al. [55]. The natural convection of (Al_2O_3-water) nanofluid inside a square cubical cavity which had a localized hot region while the rest of it kept insulated. The right vertical side was set to the lower temperature. The other walls were kept adiabatic. The streamlines are presented in **Fig.** (5.1). While the vertical velocity component (V) along the horizontal dimension and the average (Nu) along the hot wall are presented in **Figs.** (5.2) and (5.3), respectively.

The second case is that of Sannad et al. [54]. The natural convection of (Al_2O_3-water) nanofluid inside a square cubical cavity with cold left and right vertical sidewalls. A rectangular hot block is inserted inside the cavity to be the heat source. The other walls are adiabatic. This case presents the including of inner bodies inside the domain of cavity. The vertical velocity component along the horizontal dimension and the average (Nu) are presented in the **Figs.** (5.4) and (5.5). A second degree of validation was done for (CuO-water) nanofluid inside a square cavity. The case is that of Rahimi et al. [51] which is a classic case for validation. The left and right vertical sides are set to different temperatures, the higher and the lower respectively. While keeping the front, back, top and bottom surfaces at adiabatic

conditions. The isotherms, the 2D plane flow structure are shown in the **Figs.** (5.6) and (5.7). From the above validations; it is clear that there is a good agreement between the previous works and the current work. That's mean the effectivity of the current commercial numerical tool (COMSOL) for solving the problem.

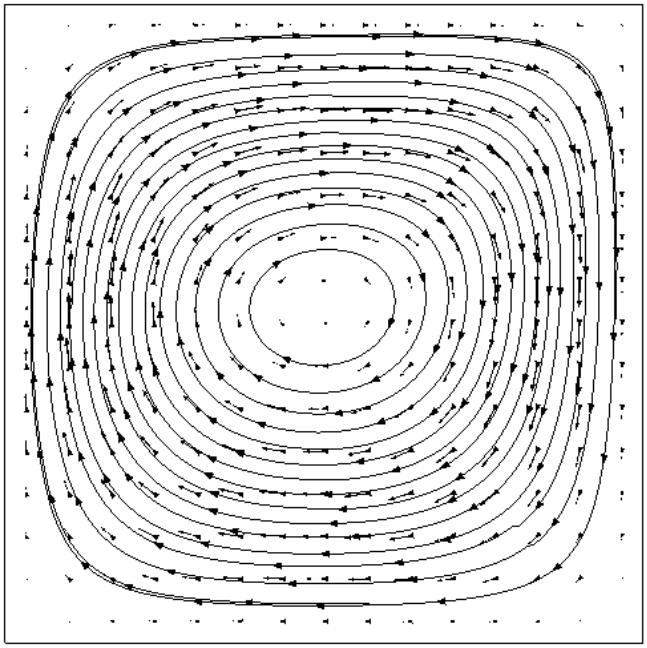

a. Present

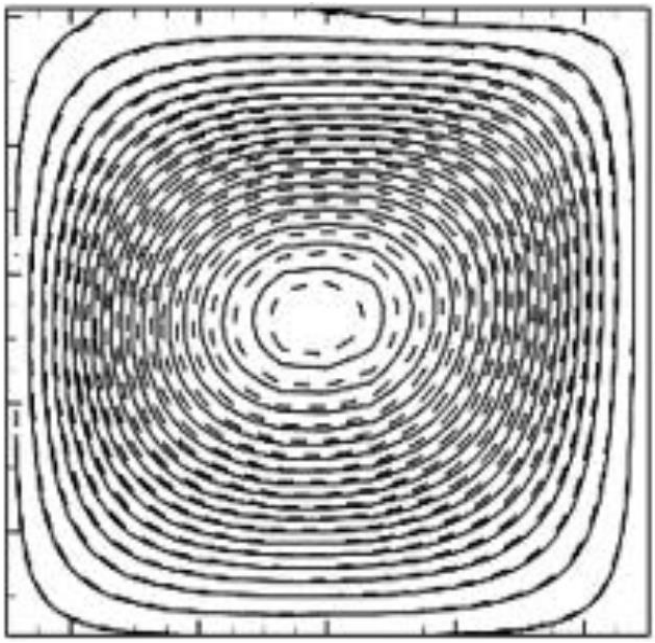

b. Sannad et al. [55]

Figure (5.1): Comparison of the streamlines contour with Sannad et al. [55] for Al_2O_3-water of ($Ra=10^4$ and $\varphi=0.04$) for ($Z=0.5$).

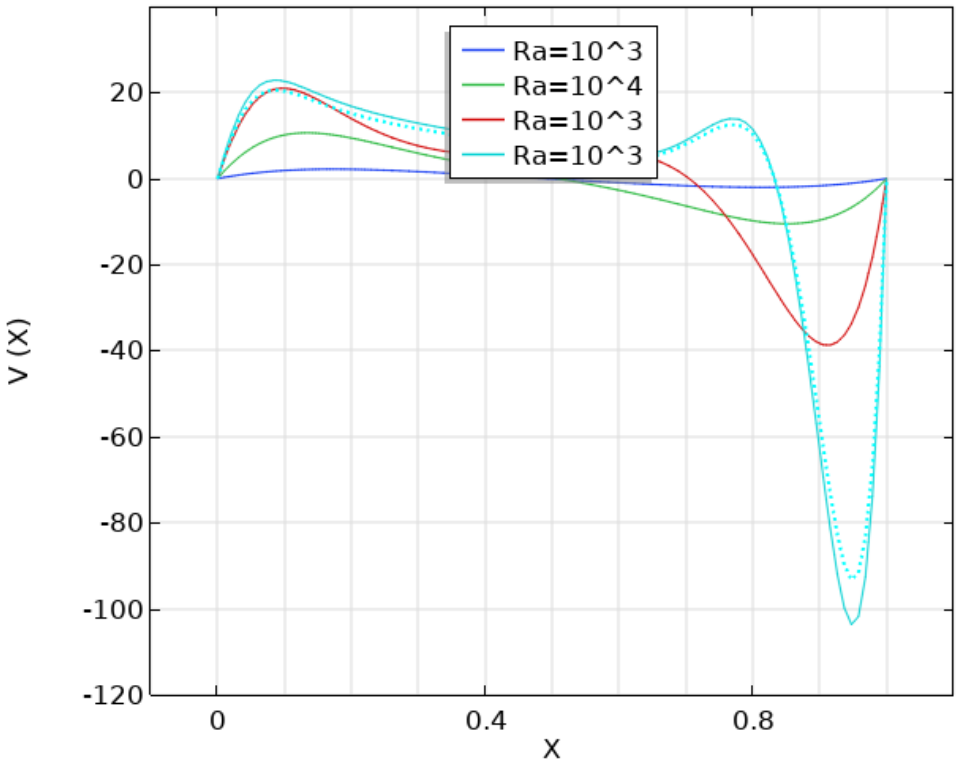

Figure (5.2): Comparison of the vertical velocity component (V) (—) along the central (x-y) plane with Sannad et al. [55] (---) for (Al_2O_3-water) nanofluid at (φ=0.04).

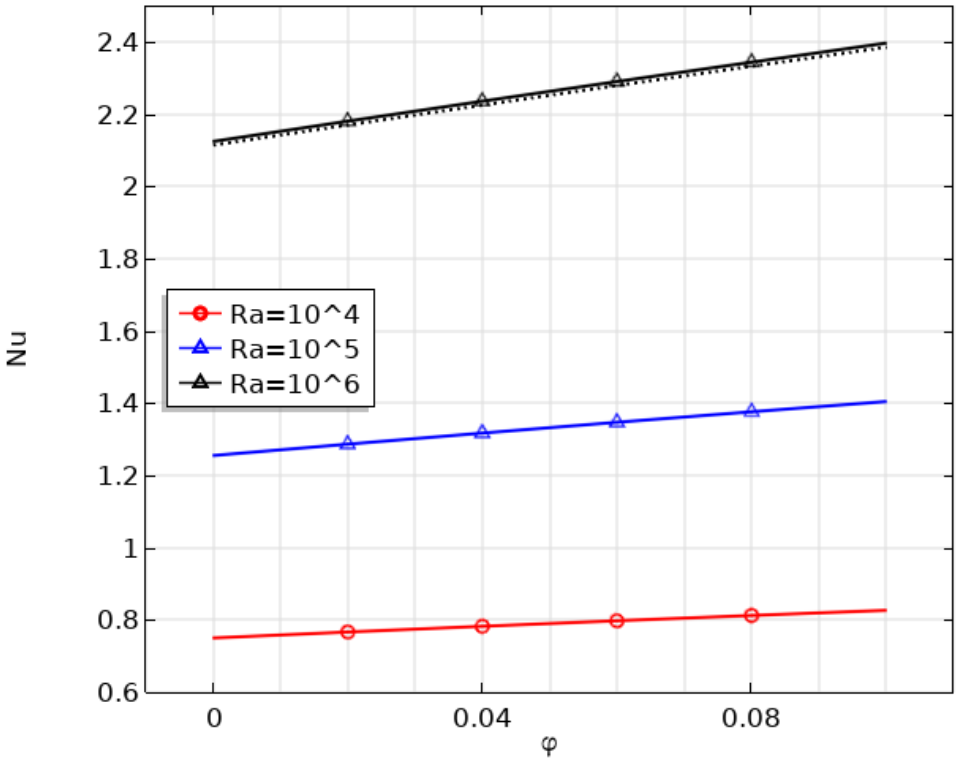

Figure (5.3): Comparison of the average (Nu) (—) with Sannad et al. [55] (---) for (Al_2O_3-water) nanofluid.

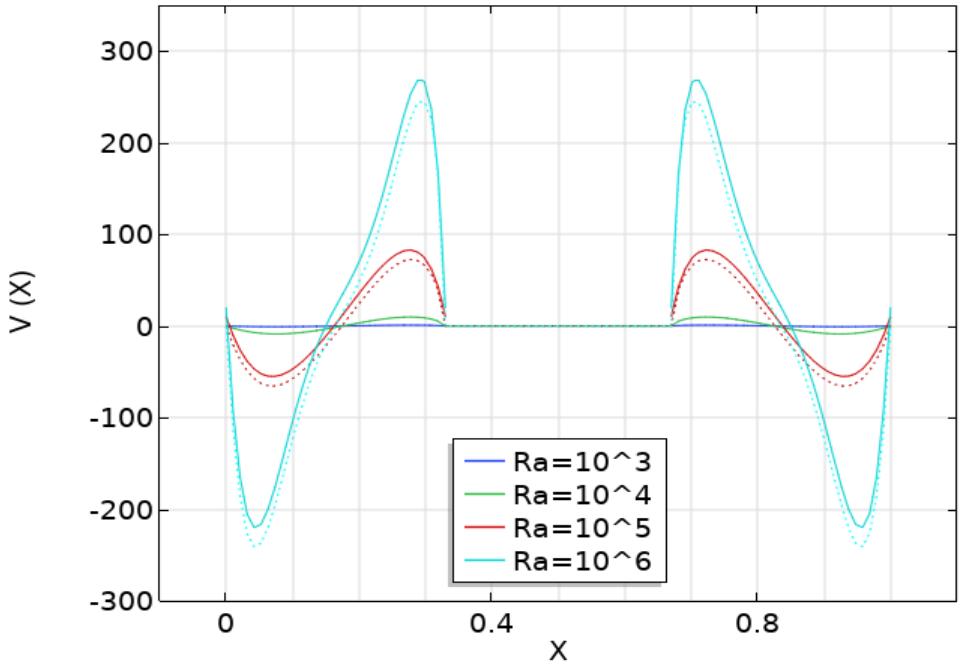

Figure (5.4): Comparison of the vertical velocity component (V) along the central x-axis (—) with Sannad et al. [54] (---) for (Al_2O_3-water) nanofluid at (φ=0.04) and (d=0.5).

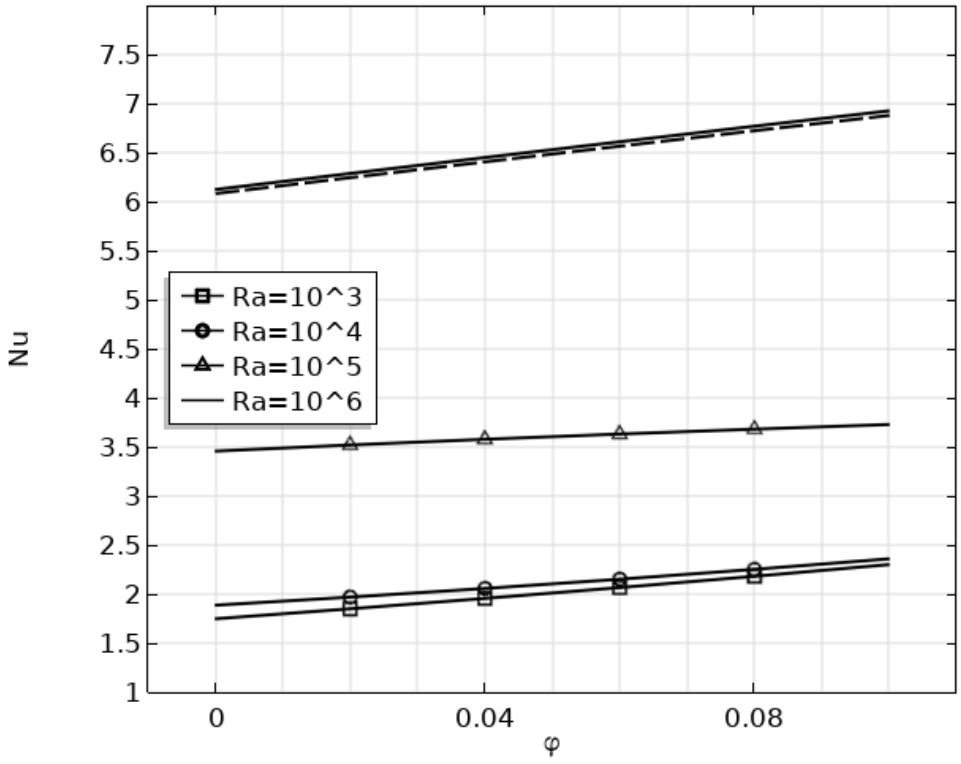

Figure (5.5): Comparison of the average Nu (—) with Sannad et al. [54] (---) for (Al_2O_3-water) nanofluid at (d=0.5).

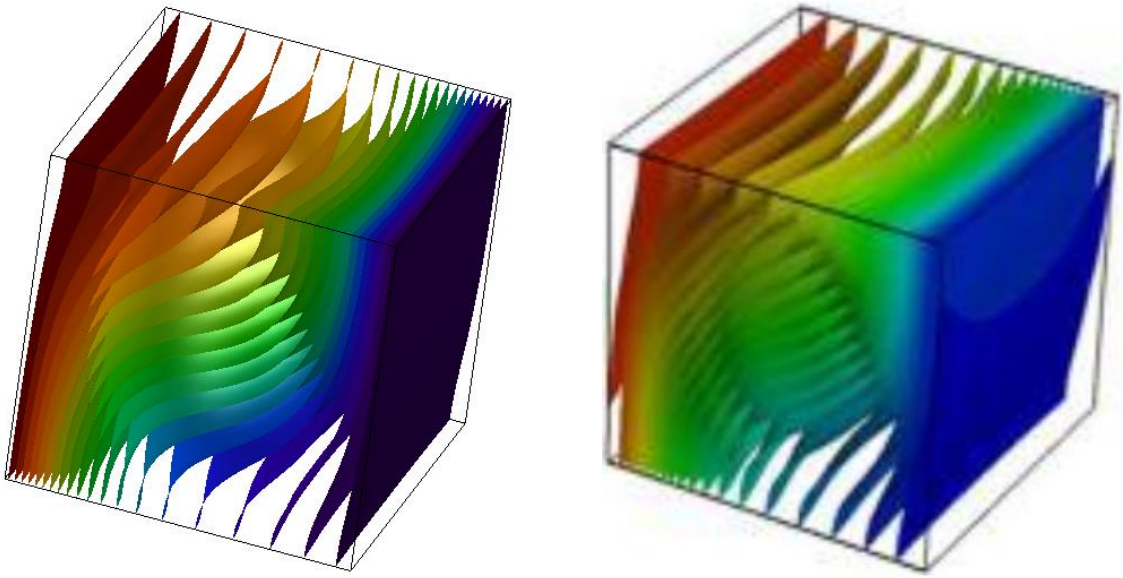

a. Present b. Rahimi et al. [65]

Figure (5.6): Comparison of the temperature surfaces with Rahimi et al. [51] for CuO-water of ($Ra=10^4$ and $\varphi=0.04$).

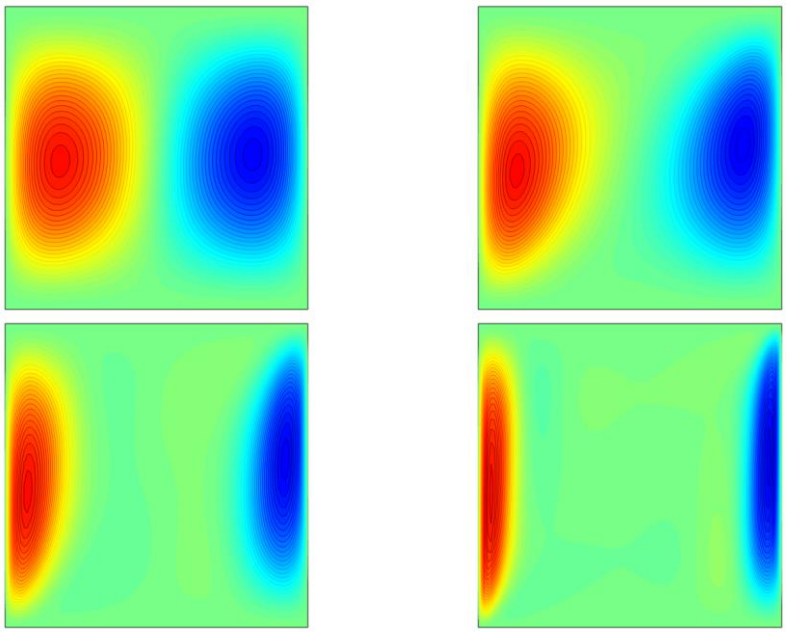

a. Present

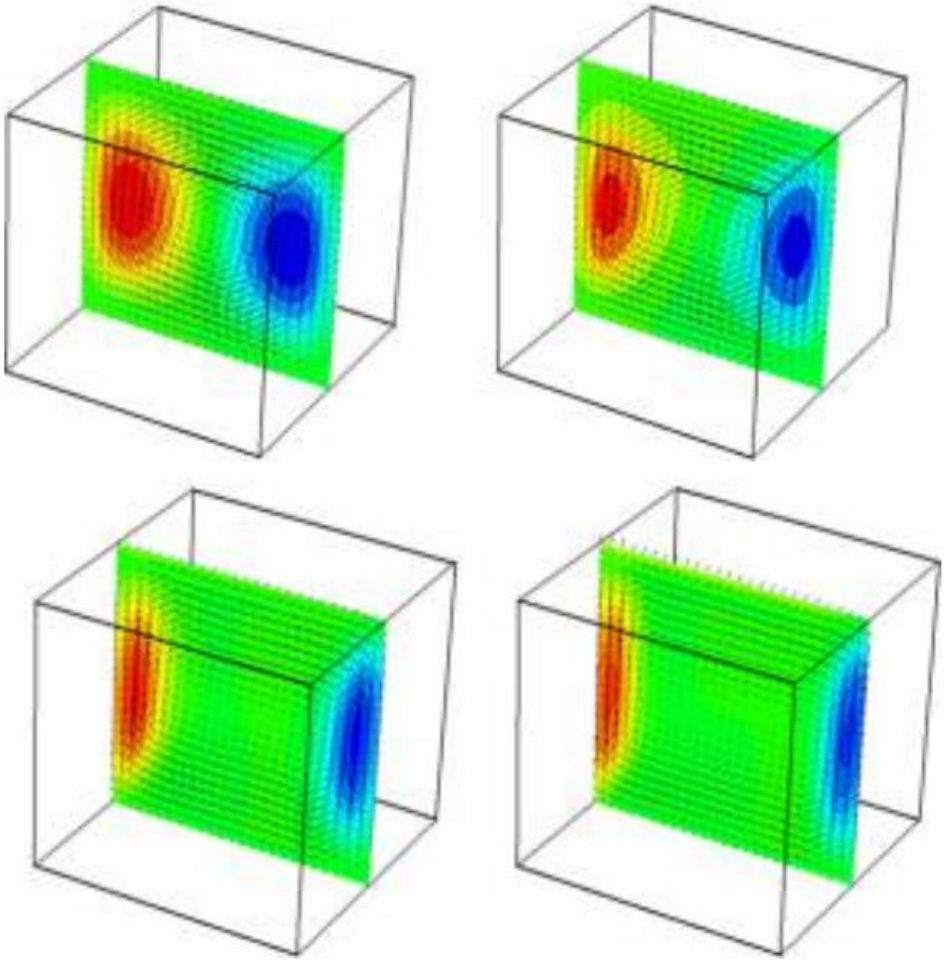

b. Rahimi et al. [51]

Figure (5.7): Comparison of the flow structure along the y-z plane at (x=0.5) with Rahimi et al. [51] for CuO-water of (φ=0.04).

5. 3. The Numerical Study

The numerical study involves two main parts, the parallelogrammical cavity and the other shape or geometry cavities. The parallelogrammical cavity is examined for two main facilities, the heated and the cooled walls arrangements and the skew angle value. Then, other modifications are studied like inserting bodies of many shapes and distributions. These cases are presented in the following sections.

5.3.1. Natural Convection inside a Parallelogrammical Cavity

To optimize the better design of cavity according to the geometry, dimensions and the differential heating walls arrangement. Two cases of the study by means of the constant parameter are considered as presented in Chapter Three. The first is cavity with specified skew angle (γ) has walls with constant side lengths (L). The second is also of specified (γ) but has constant volume (L^3). Observing that for the two cases, the axial dimension (depth) is (L). For the first case the horizontal dimension (width) also (L). But the vertical dimension (height) varied with (γ) variation. For the second case, it has unfixed horizontal or vertical dimensions, both are changed according to (γ) to satisfy the constant volume condition. The following subsections are discovering the effects of different parameters on the fluid flow and thermal fields.

5.3.1.1. The Optimum Differentially Heating System Arrangements Selection

First of all, it must specify the ideal differentially heating arrangement, by means of the location of the hot wall and the opposite cold wall. Three cases for the hot wall are examined. These cases are; on the left vertical wall, on the right vertical wall and on the bottom horizontal wall. The opposites walls are kept cold. All the heated/cooled walls of the cavity have fixed side lengths (L) and area (L^2). This property is investigated on the parallelogrammical cavity at ($\gamma=60^o$) and constant volume (L^3) filled with (Al_2O_3-water) nanofluid. **Fig**. (5.9) presents the flow field by means the 3D stream lines and the thermal field by means the 3D temperature iso-surfaces for the three heating/cooling arrangements of the cavity at ($\varphi=0.05$) and ($Ra=10^5$). The streamlines are the lines that tangential to the instantaneous velocity direction where the velocity is a vector and it has a magnitude and direction. It is noticed from the streamlines that the flow circulation of

the first and the third arrangements are in clock wise direction. While the second case flow is in counter clock wise. This motion of the working fluid can be explained by the physical phenomenon of the flow from the hot region to the cold region due to the difference in density where the temperature inversely proportional to the density. For the case of right hot wall, the flow is counter clock wise due to the tendency of the hotter fluid which is lighter to flow up while the colder is heavier, so the fluid is flowing down.

The fluid flow inside the cavity is controlled by the horizontal velocity (U) along the (X-axis) and the vertical velocity (W) along the (Z-axis) which accelerates the flow circulation between the deferentially heated walls regardingless the axial velocity (V) along the depth of cavity Y-axis. These velocities are introduced for the three cases in **Fig**. (5.10). Both the two average velocities are increased with (Ra) increase for all the considered cases. For the cases of left or right vertical hot walls, at ($Ra<10^4$) these velocities are (U>W) but it becoming inverse at ($Ra>10^4$) while for the case of bottom horizontal hot wall this phenomenon occurs at ($Ra<6\times10^4$). This phenomenon represents the region where the starting point of the convection dominant which appears lately for the case of bottom hot wall. Another observation is that, these velocities for the two vertically heated cases (left or cold) are close to each other at all the (Ra) range which are higher than that of the third case for ($Ra<10^4$) but less than it for other (Ra) values. The higher velocity values of the third case are due to the shorter distance between the differentially heated walls. By observing the region ($10^3\leq Ra\leq10^4$) where the velocities of the case of bottom hot wall is higher than those of other cases, this is due to the conduction dominant where the effect of gravity have the highest effect on the fluid flow by the density

difference, while after this region when the convection dominates the effect of cavity design become the more affecting parameter.

On the other hand, the distribution of the iso-surfaces of thermal field is in harmony with the flow behavior. The iso-surfaces represent the constant temperature regions which is presented by the normalized temperature (θ) on surfaces parallel to the hot and cold walls. At the left wall, the normalized temperature is (1) which takes the red color while on the cold wall it is (0) that represents by blue color. The other normalized temperatures are represented by the graduated colors from higher red to lower cold. To indicate the heat transfer enhancement; the average (Nu) on the hot wall is calculated as shown in **Fig**. (5.11). As it observed from the horizontal (U) and vertical (W) velocities, the convection initiates earlier at the cases of vertical hot walls, and as it known that the average (Nu) represents the ratio of convection to conduction, the higher average (Nu) is recorded for the cases of vertical hot walls. But it is higher for the case of left hot wall, that is due to the design of the hot wall with respect to the cavity. The left wall inclination making a smaller distance between the higher and lower points of the hot wall from the farthest bottom horizontal wall, where the gravitational acceleration is strong, while inverse situation is observed for the right hot wall case. Around the region ($Ra=10^4$), the average (Nu) is nearly the same for all the considered cases which is the region where the effect of gravity for the bottom heated cavity become equal to the effect of walls design for the vertical walls heated cavities.

From the previous discussion, it is concluded that the case of hot left vertical wall is the more suitable case to improve the heat transfer by natural convection. This will be depended on in whole study.

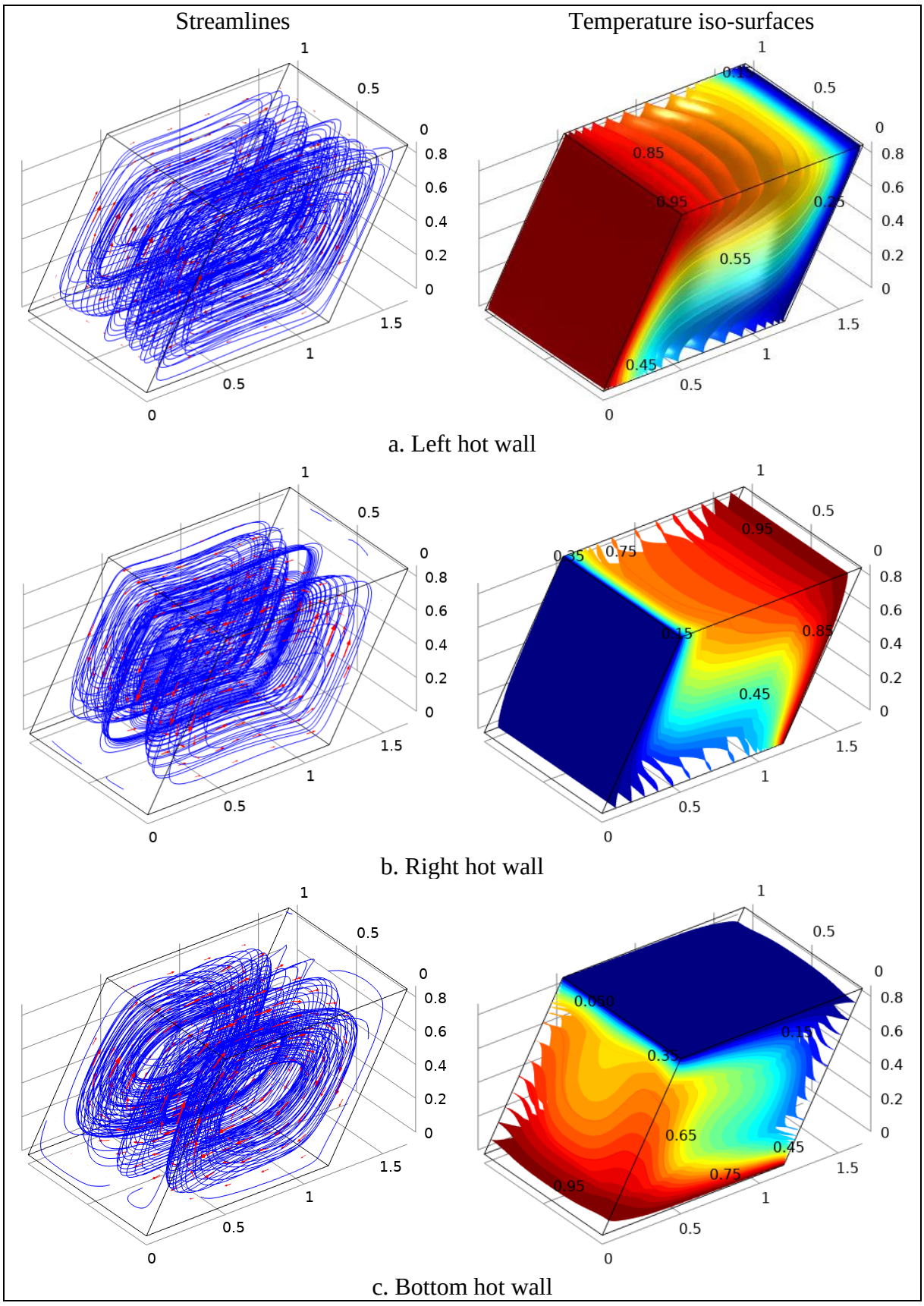

Figure (5.9): The 3D stream lines and temperature iso-surfaces for the three heating/cooling arrangements of the parallelogrammical cavity of (γ=60º) and (L) side length at (Ra=10^5) and (φ=0.05).

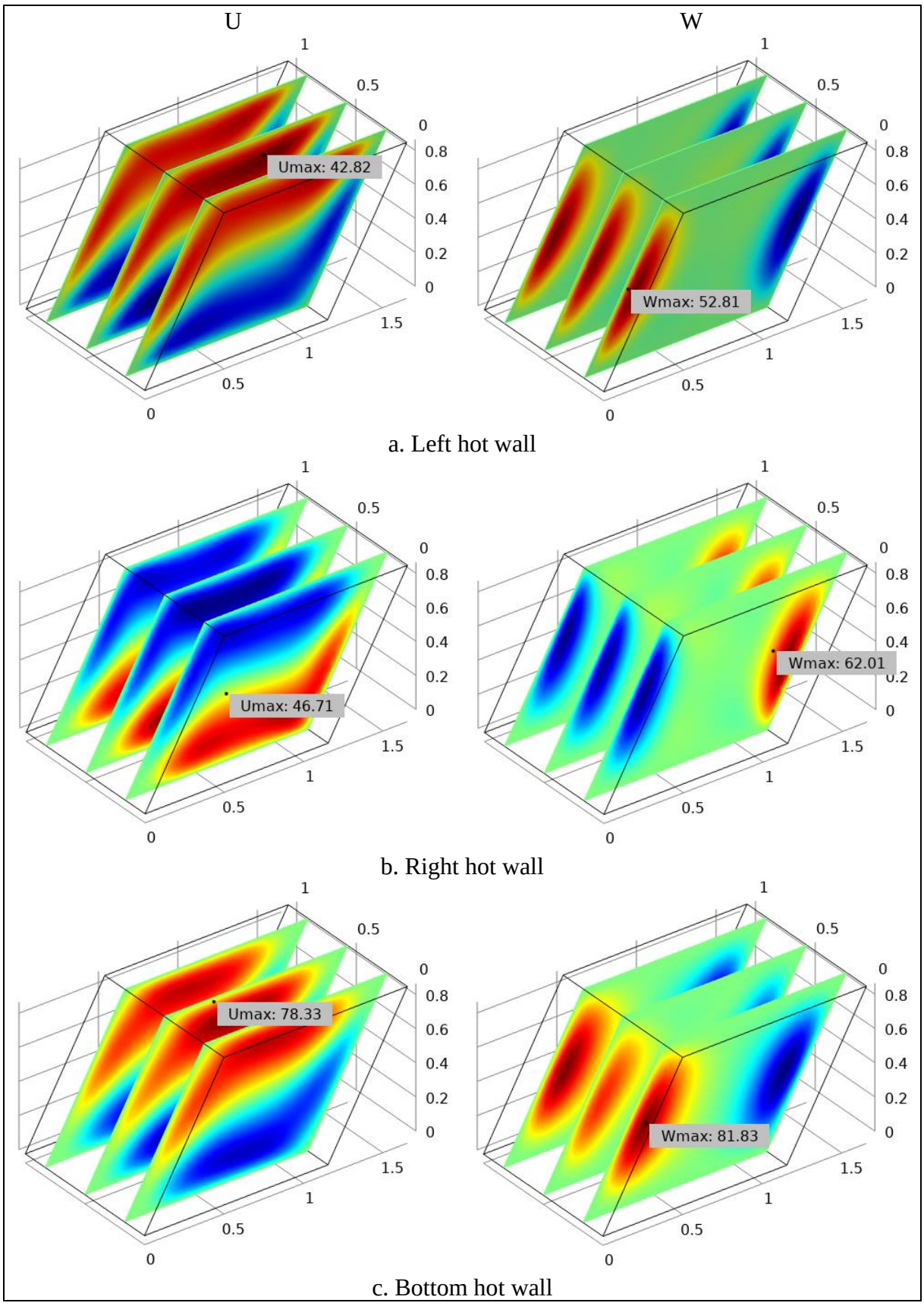

Figure (5.10): The 3D stream lines and temperature iso-surfaces for the three heating/cooling arrangements of the parallelogrammical cavity of (γ=60º) and (L) side length at (Ra=10^5) and (φ=0.05).

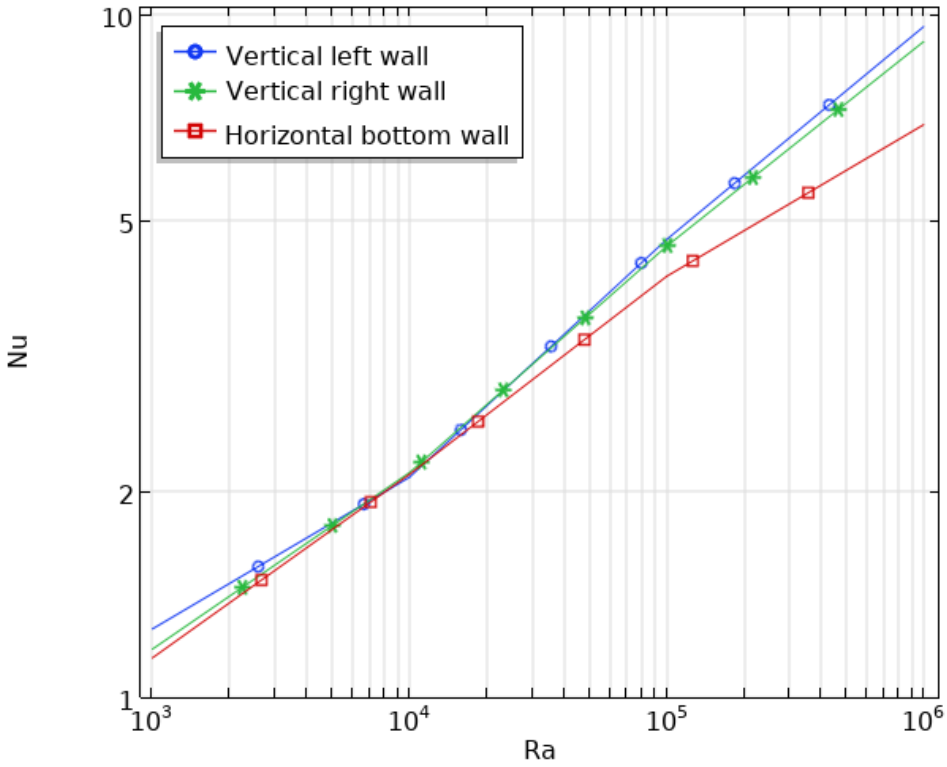

Figure (5.11): The average (Nu) on the hot wall versus (Ra) for the three heating/cooling arrangements of the parallelogrammical cavity of (γ=60º) and (L) side length at (φ=0.05).

5.3.1.2 The Optimum Parallelogrammical Skew Angle Selection

Another important selection must be done which is the better skew angle (γ) choice. The angles that are accomplished on the differentially heated parallelogrammical cavities are (γ=30º, 45º and 60º). The left vertical wall of the cavity is kept hot, while the opposite right wall is kept cold and the other walls are adiabatic. This property is examined for the two situations of cavities; that of constant side lengths (L) and that of constant volume (L^3) and both have equal heating and cooling areas (L^2). The flow field represented by the 3D stream lines and the thermal field represented by the temperature iso-surfaces at ($Ra=10^5$) and (φ=0.05) are presented in **Figs**. (5.12) and (5.13).

The 3D streamlines for the situation of constant side length (L), the cavities with (γ=45º and 30º) have two separated large circulations of flowing fluid that nearly similar around the central plane of the cavity

between the vertical hot and cold walls. The left lower and upper right corners regions are considered idler regions which not permit an effective heat exchange due to the very little vertical height of cavity comparing to the horizontal distance between the hot and cold vertical walls. Unsimilar to the cavity with (γ=60º), where the two terminal large circulations are separated by a third thick one at the central plane between the two others which enforce the flow to distribute inside the cavity even at the corners. This behavior increasing the turbulence inside the cavity which in turn increasing the convection.

For the situation of constant volume (L^3), nearly the same behavior is observed but for the cavity of (γ=30º), the two circulations are not of the same intensity, the very long distance between the hot and cold walls with the lower height effecting the flow to increase the idler regions and decelerating the flow propagation between the differentially heated walls. In the velocity field, the cavity of (γ=60º) has the higher horizontal (U) and vertical (W) average velocities for the two considered situations of cavities, but that of constant side length have the heist average velocities. This is because that the other skew angles make the hot walls inclined strongly towards the domain and due to the decreased height of the cavity which causing subside of the flow. These walls work as like as obstacles that absorbs the energy in the path of the flow.

On the other side, the thermal field by means of the temperature iso-surface profiles is obeys the fluid flow behavior. For the two situations of cavities with (γ=60º), the temperature iso-surfaces curvature from the hot wall towards the cold is more than that of the cavities of (γ=45º) and (γ=30º), respectively. As it mentioned earlier, the high inclination of the hot side wall on the inner fluid works as energy dissipation. As like as, the average (Nu) on the hot wall the values of the

average (Nu) for the cavities with constant side lengths (L) are higher than that of cavities with constant volume (L^3) as shown in **Fig**. (5.14). Generally, it has the highest values for the cavity of ($\gamma=60^o$). The enhancements of the average (Nu) are (32.49%) and (43.04%) for constant side length and constant volume cavities when the skew angle increased from (30^o) to (60^o) at ($Ra=10^6$) respectively. But for the same ($\gamma=60^o$), the two situations give the same range of average (Nu) at all the considered (Ra). As like as for the case of constant volume (L^3), the convection lates in appearance for the cavities of (30^o and 45^o) which appears at ($Ra\geq 5\times10^4$ and $Ra\geq6\times10^5$) respectively.

The previous observations are led to the conclusion that the cavity of ($\gamma=60^o$) is the best among the other cavities bothering with constant side length or with constant volume. So, in the coming sub-sections, the parallelogrammical cavity of constant volume (L^3) is selected to be the main cavity in order to make the comparisons easier with other geometry cavities for the same volume. While experimentally, the cavity of ($\gamma=60^o$) and with constant side length are accomplished.

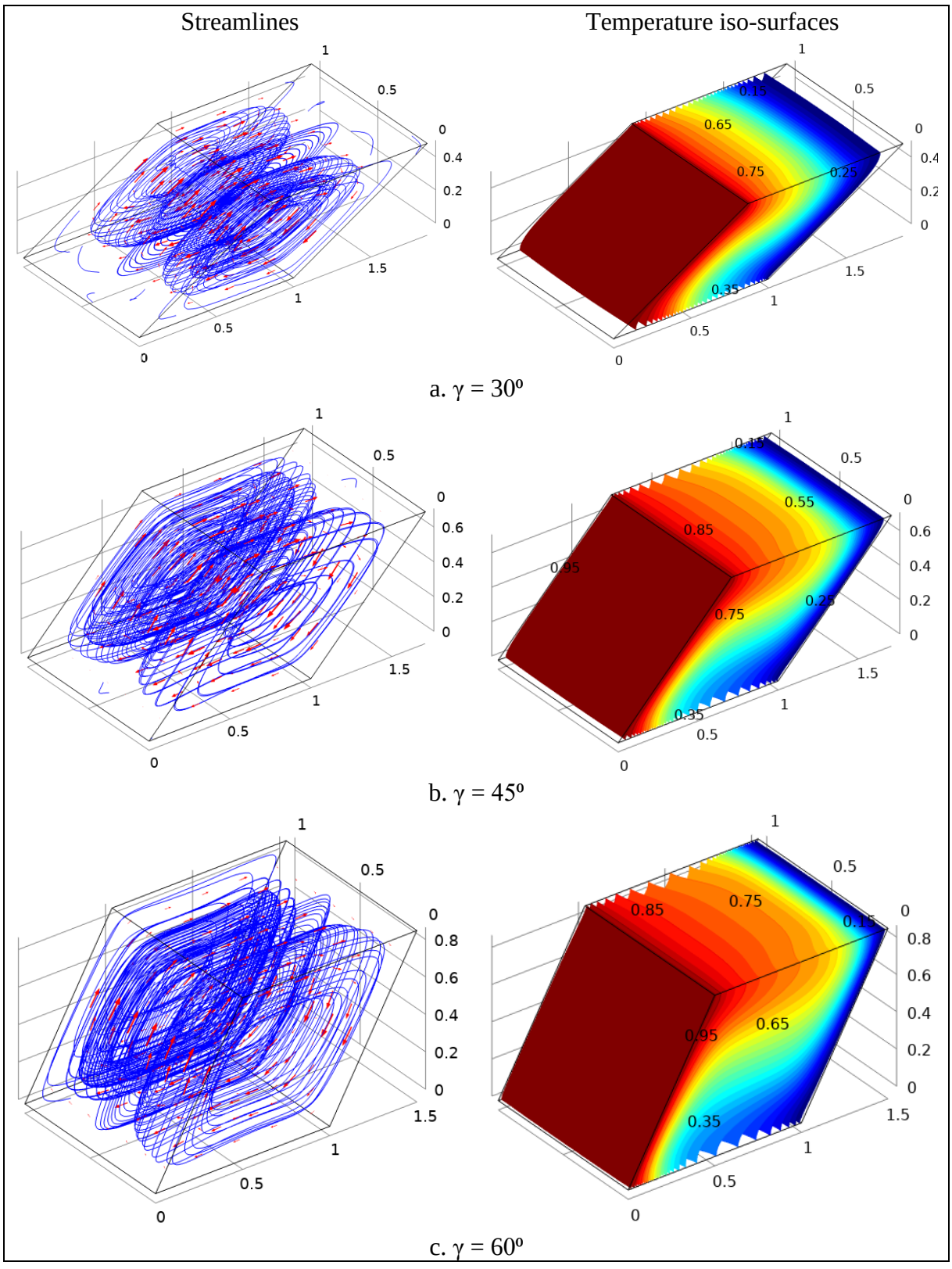

Figure (5.12): The 3D stream lines and temperature iso-surfaces for the parallelogrammical cavity of constant side length (L) and different (γ) at (Ra=10^5) and (φ=0.05).

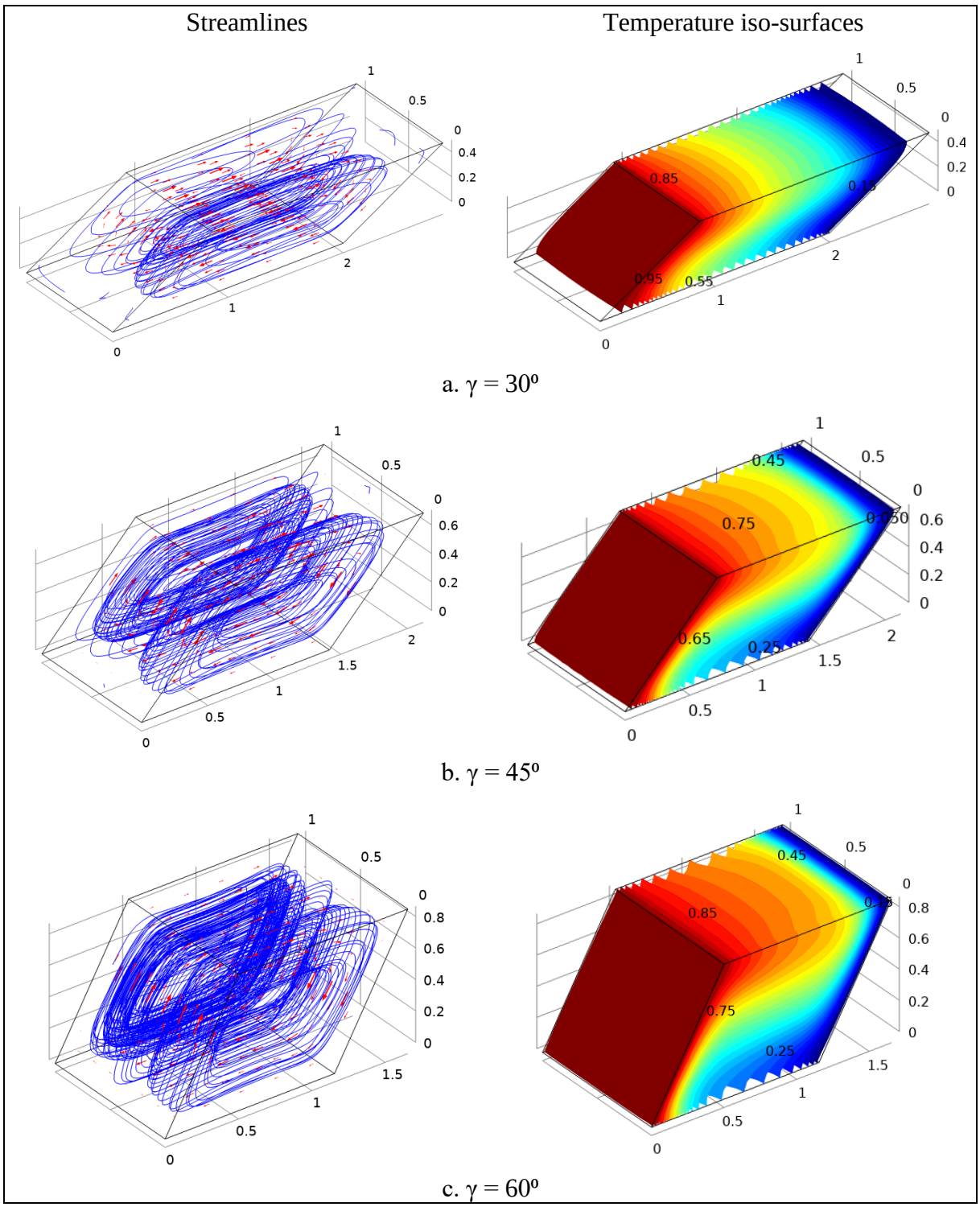

Figure (5.13): The 3D stream lines and temperature iso-surfaces for the parallelogrammical cavity of constant volume (L^3) and different (γ) at ($Ra=10^5$) and (φ=0.05).

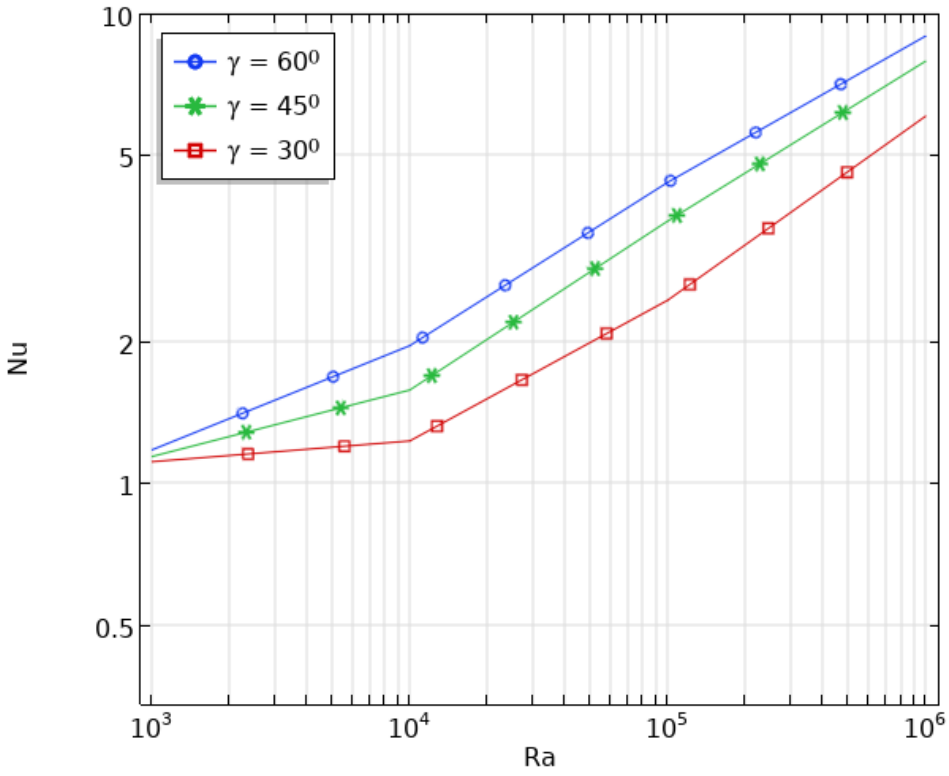

a. Constant side length (L) cavities.

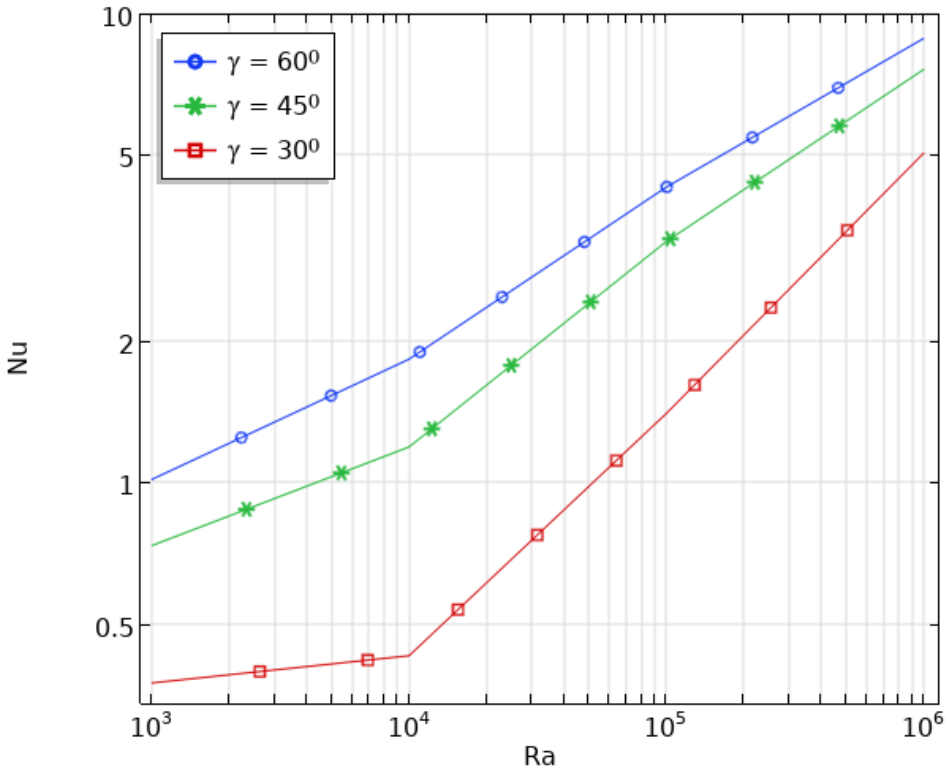

b. Constant volume (L^3) cavities.

Figure (5.14): The average (Nu) on the hot wall versus (Ra) for the parallelogrammical cavity with different (γ) at (φ=0.05).

5.3.1.3. The Effect of the Rayleigh Number

The effects of (Ra) on the fluid flow streamlines and the temperature iso-surfaces contours inside the parallelogrammical cavity with ($\gamma=60^{o}$) at ($\varphi=0.05$) are demonstrates in **Fig**. (5.15). The circulation cells or vortices are formed in the clockwise direction for all the (Ra) range. For more observation, three planes parallel to the front wall of the cavity at (Y=0.25, Y=0.5 and Y=0.75) are depended on to view the streamlines as shown in **Fig**. (5.16). All the planes introduce nearly similar configuration but the central plane at (Y=0.5) has the denser lines which indicate lower velocities and more uniform flow. The more intensity of lines in central plane can be explained as the faraway from the cavity walls which work as a flow deceleration and their effect become weak at the center. The shape of the core of these vortices is changed from circular to elliptical with (Ra) increase. This core represents the steady or constant temperature region. This region increases in area with increasing (Ra). It is clear that; the flow strength is highly influenced by the (Ra) increase.

As it mentioned earlier, the flow is consisting of three velocity components, the horizontal (U) along the (X-axis), the vertical (W) along the (Z-axis) and the axial (V) along the (Y-axis) as shown in **Fig.** (5.17). The axial velocity (V) is varied in limited range along its direction where for this case, the depth is suitable to maintain the axial velocity in accepted range to keep uniform distribution between the hot and cold walls. In other words, the flow circulations between the differentially heated walls are large enough to overcome the axial direction circulations which in general very small comparing to the main flow direction circulations (between the hot and cold walls along the cavity width (X-axis)). Both (U) and (W) are flowing in two main circulations in reverse direction to each other inside the cavity domain.

These circulations are number of circles between the hot and cold walls along the vertical direction for (U) and between the top and bottom along the horizontal direction. Where the positive velocities mean clockwise direction while the minus sign referred to counterclockwise flow. The maximum (U) or (W) velocities located at the center of each circulation. By observing the maximum velocities, the maximum (U) always located aligned to the centers of the bottom and top walls of cavity unlike the maximum (W) which located parallel to the center of the hot and cold walls. At ($Ra=10^6$) it is noticed that, the maximum velocities (U and W) and their main circulations become close to the cavity walls due to the increase of convection with increase of (Ra) and due to no slip boundary conditions unlike the center of cavity where the steady flow region initiates. While at ($Ra=10^3$) the flow circulation becomes weak where the two vortices of the same size were occupying the whole cavity. In general, the horizontal velocity (U) is higher than the vertical velocity (W) at ($Ra \leq 4\times10^4$) and vice versa at higher (Ra) values because of the increase in convection at this region which exceed the gravity action and leading to lift the flow adjacent to the hot wall upward and the flow adjacent to the cold wall downward in high rates. In other words, when buoyancy forces overcome the resistance induced by viscous forces, the natural convection occurs.

With respect to the 3D iso-surfaces that presented in **Fig.** (5.16), are becoming more curved when (Ra) increased lines where the high nonlinearity of these surfaces means the increase in the steady region core (laterally between the differentially heated walls) or convection dominant. At high (Ra) it clustered strongly near the cavity sidewalls where a thermal boundary layer can be observed and the high circulation causes the convection heat transfer is dominant. From the other hand, as the (Ra) decreases, the reduction in flow circulation leads to make these

isothermal surfaces parallel and symmetrical where the pure heat conduction dominates.

The heat transfer enhancement was measured by the average (Nu) along the heated wall of the cavity as shown in **Fig**. (5.18). Similar to the iso-surfaces, the average (Nu) is enhanced with (Ra) augmentation which in turn mean that the heat transferred by convection inside the cavity was enhanced. This notation can be seen for various arrangements of partially active vertical sidewalls. This is due to the natural convection heat transfer and the buoyancy force enhancement when the Rayleigh number increases. The average (Nu) increased to about (10) times when increasing from ($Ra=10^3$ to 10^6).

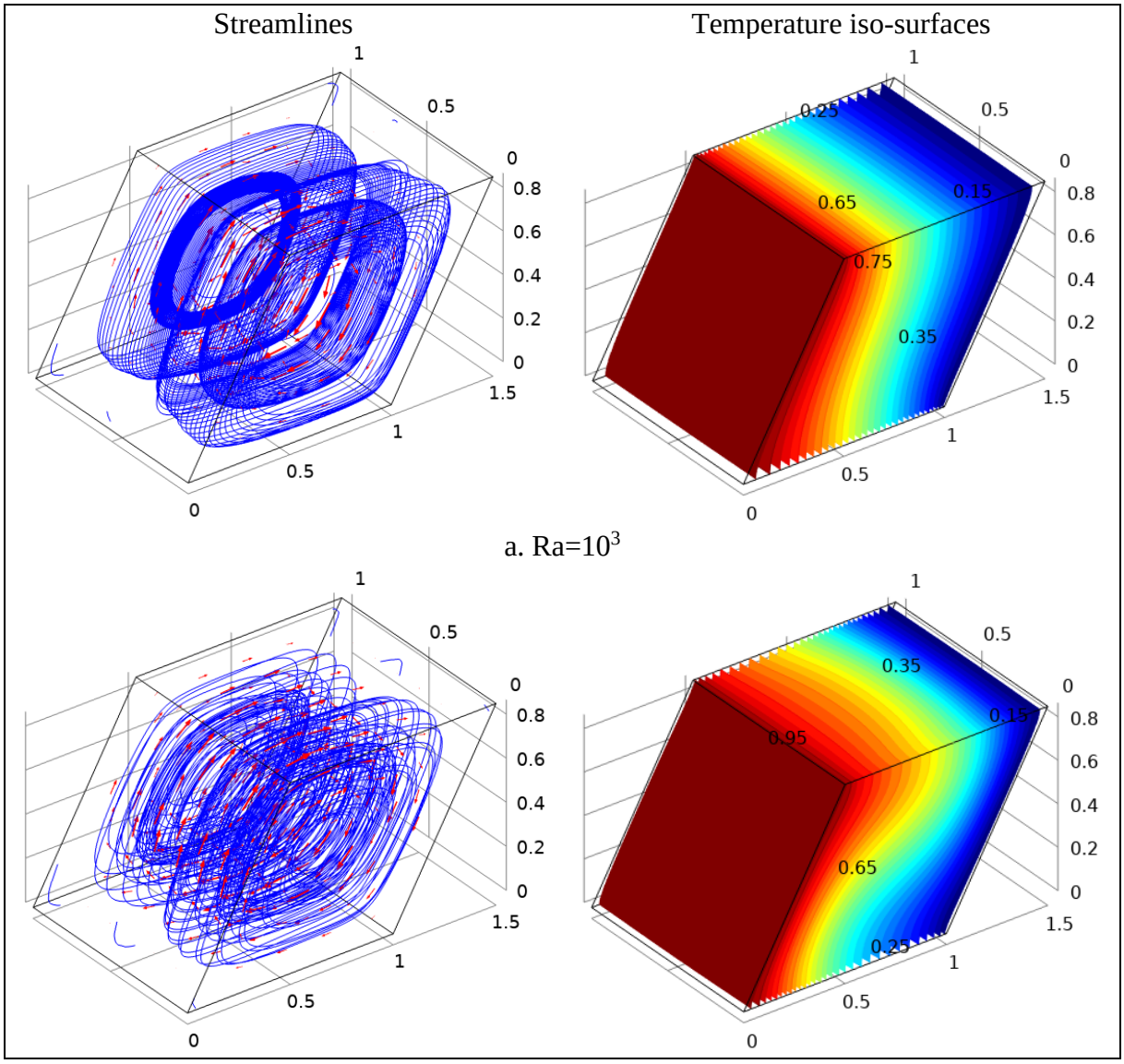

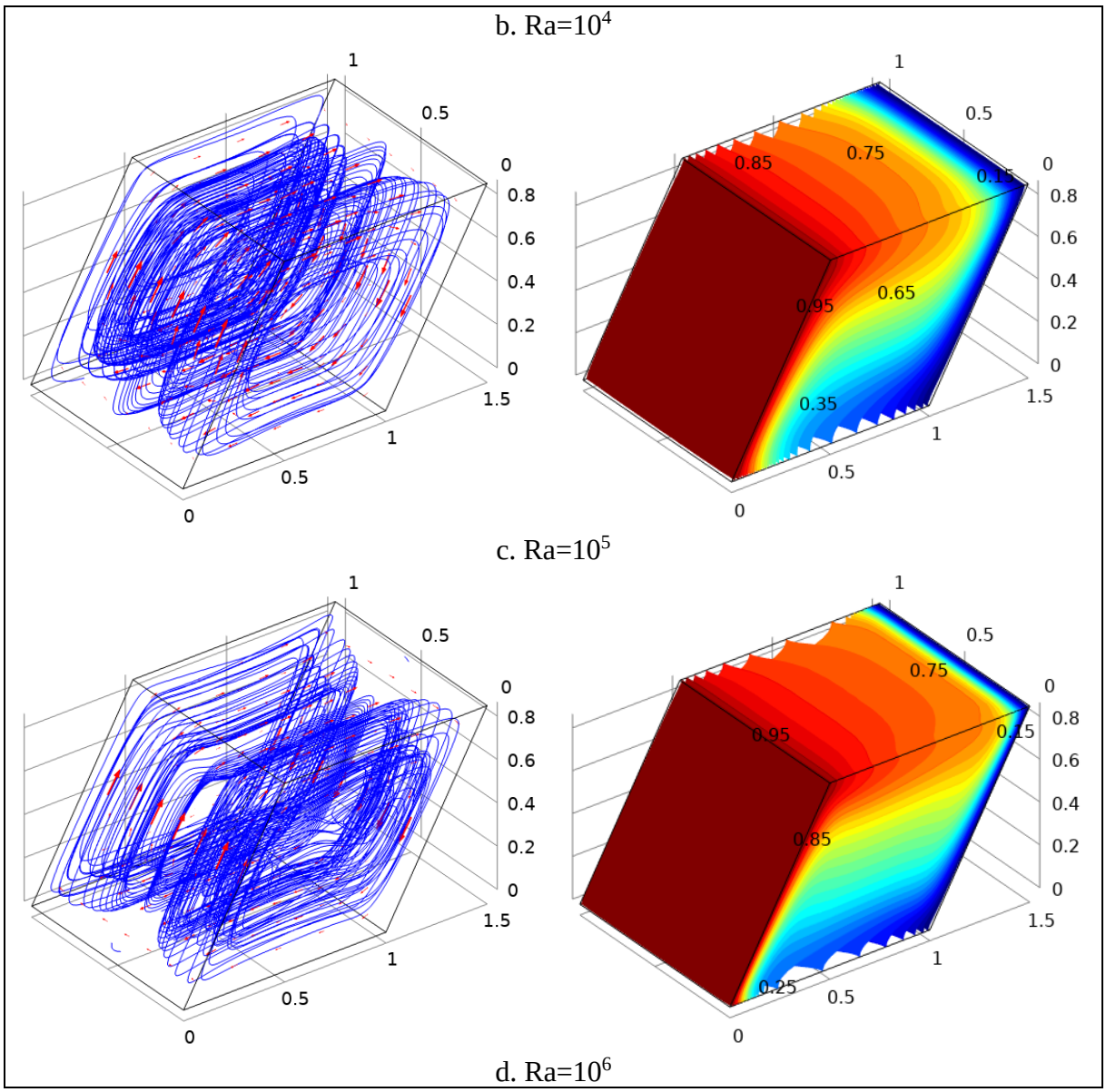

Figure (5.15): The parallelogrammical cavity and (L) side lengths with (γ=60º) at (φ=0.05).

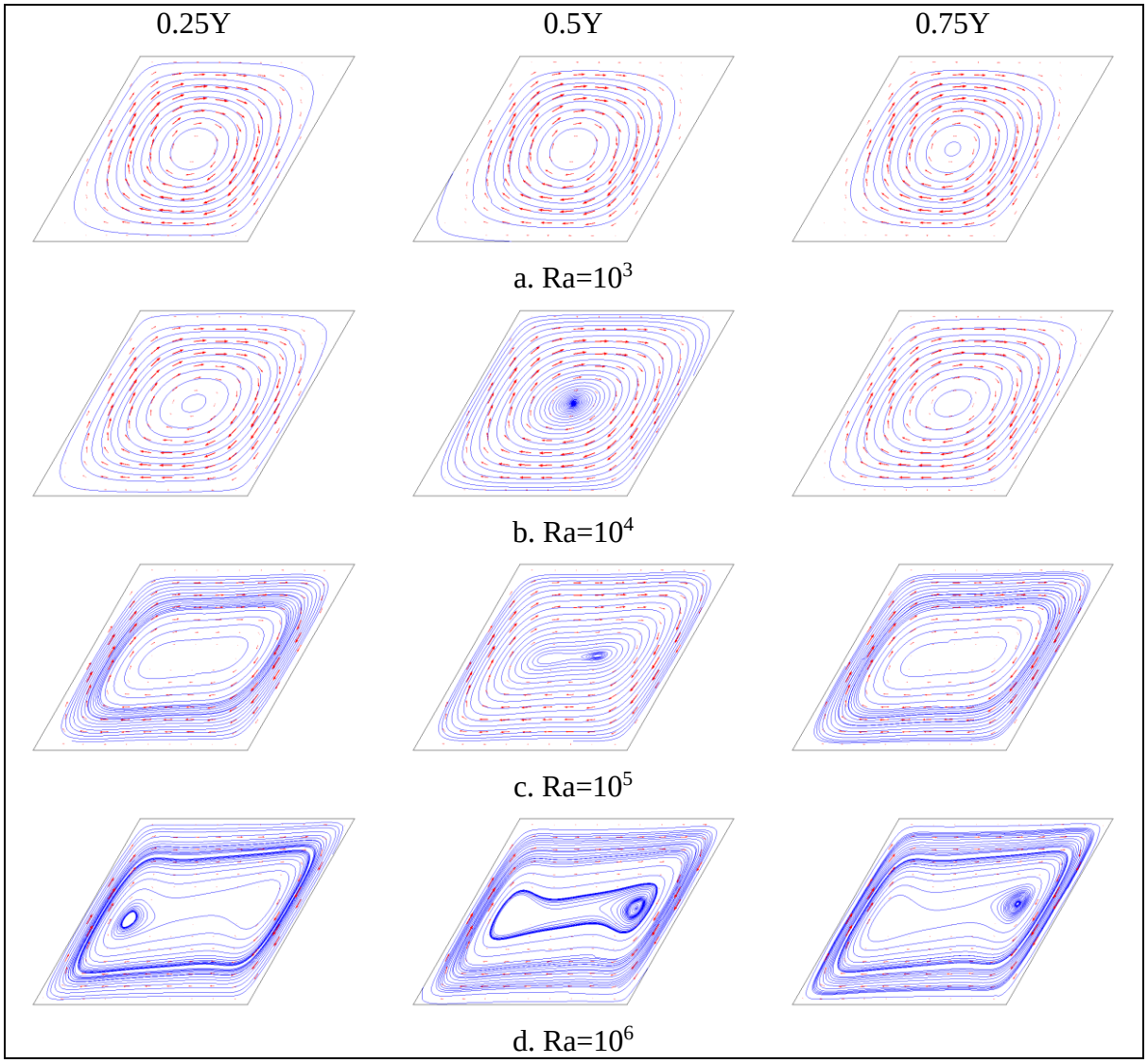

Figure (5.16): The 2D stream lines projection on the plane (X-Z) of the parallelogrammical cavity of (γ=60º) at (φ=0.05) and different (Ra).

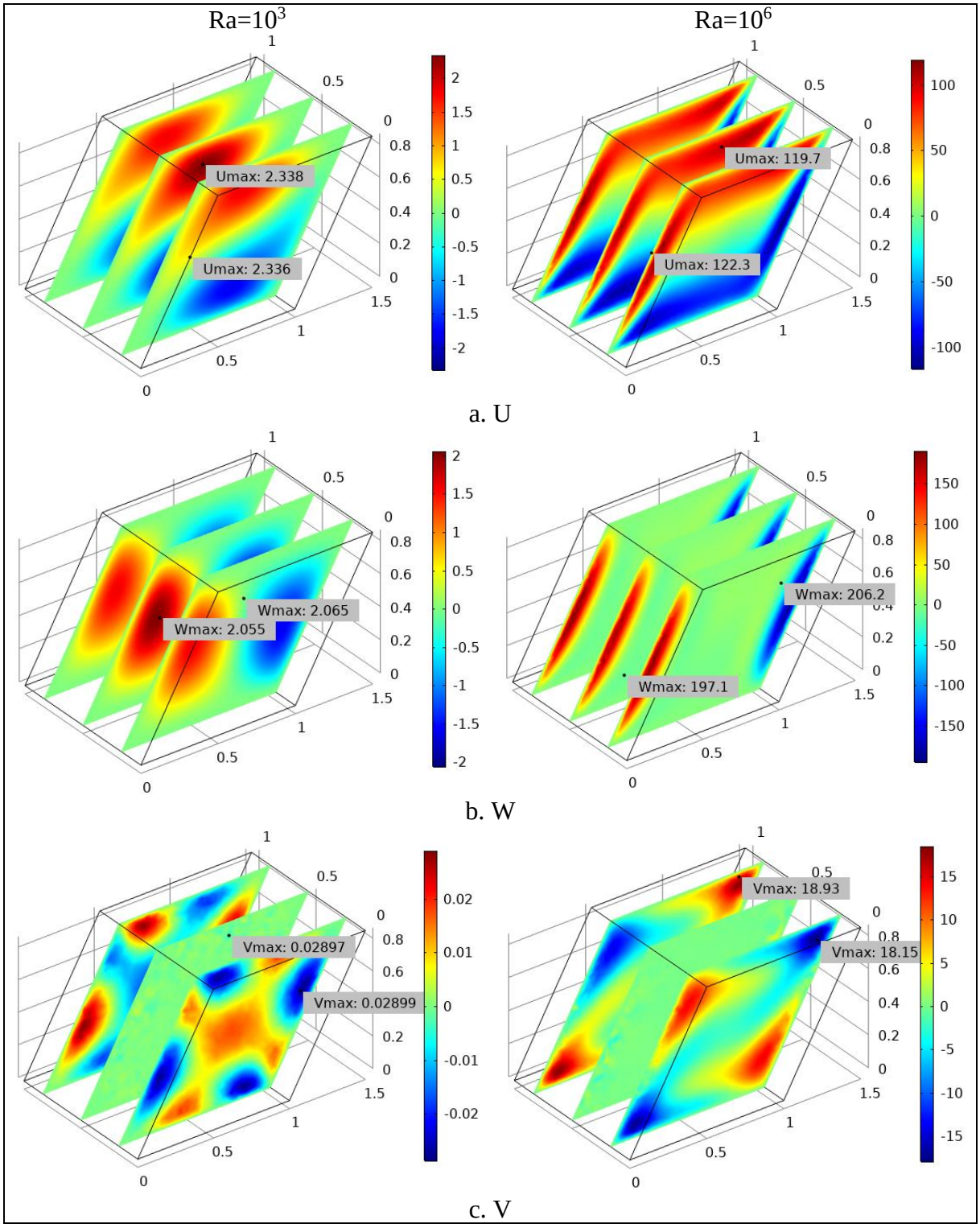

Figure (5.17): The 3D velocities (U, V and W) for the parallelogrammical cavity of (γ=60º) at (φ = 0.05).

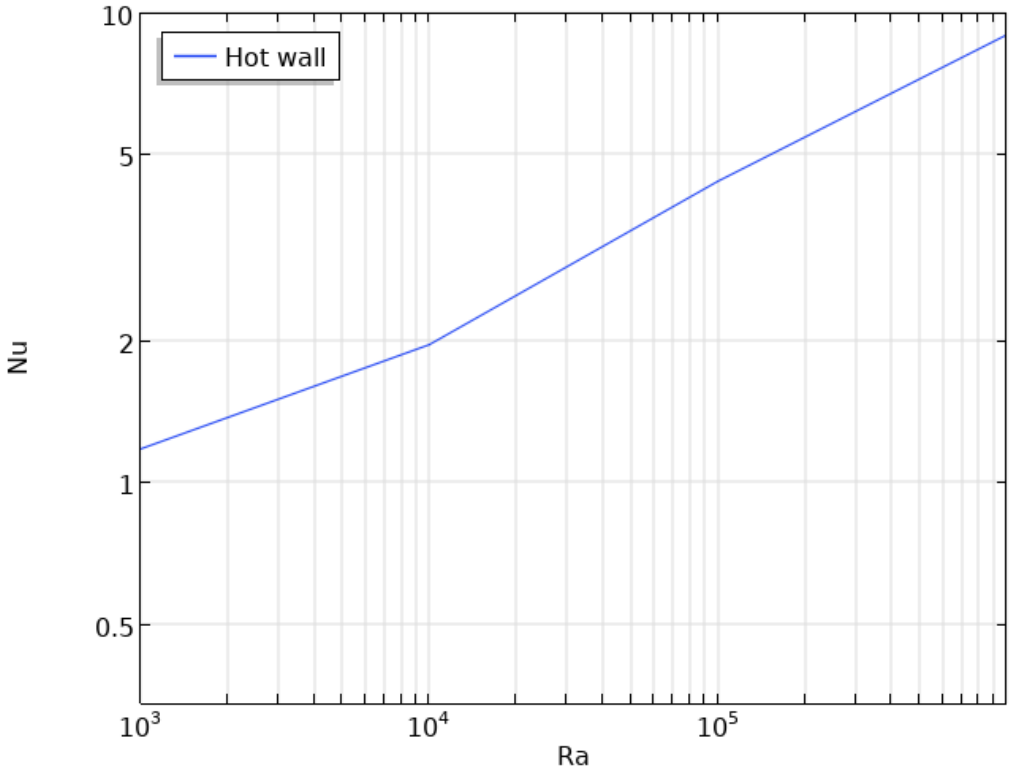

Figure (5.18): The average (Nu) versus (Ra) for the parallelogrammical cavity of (γ=60º) at (φ=0.05).

5.3.1.4. The Effect of the Solid Volume Fraction and Comparison with Pure Water

Figs. (5.19) and (5.20) are presented the 3D streamlines and the temperature iso-surfaces at (Ra=10^4 and 10^6) respectively. The cavity filled by nanofluid with different solid volume fractions ($0.01 \leq \varphi \leq 0.05$) or pure water ($\varphi$=0). The configuration of the streamlines is nearly identical for all the cases of the nanofluid. It is differing clearly with increasing (Ra) as it discussed in the previous section. The core of the streamlines that shown in **Fig.** (5.21) takes a circular shape at (Ra=10^3) while it was tending to have an elongated elliptical shape with longer axis parallel to the horizontal direction at higher (Ra) values. The elliptical core which represents the steady or stagnant region increases in width and height with increasing (Ra). The intensity of these lines is becoming thicker with increasing (Ra) and solid volume fraction of

nanofluid. For water, the vorticity core was nearly circular even when ($Ra>10^5$) where no steady region is occurring and conduction still dominant.

Unlike the (Ra) effect on the horizontal velocity (U), it decreases with the solid volume fraction (φ) increase as shown in **Fig**. (5.22) as like as the vertical velocity (W) that presented in **Fig**. (5.23). These velocities are decreased when increasing the solid volume fraction (φ) due to the increasing weight and density of the flowing fluid while it reinforces the heat transfer coefficient because of the high thermal conductivity of the added nanoparticles. But, the advantage of the nanoparticles exceeding the disadvantage of the higher weigh and density effect. Generally, for all nanofluid concentrations (U>W) at ($Ra\leq10^4$) and vice versa for ($Ra>10^4$). While for water the (U>W) always because of the weak buoyancy effect of water comparing to the gravity effect.

With respect to the 3D temperature iso-surfaces that presented in **Fig**. (5.24), the temperature is transferred higher at the tip of the cavity towards the cold wall in clockwise direction for nanofluid while those of water transferred from the bottom of the left hot wall towards the cold wall in counter clock wise because of the higher gravity effect comparing to the convection effect due to the lower heat transfer coefficient of the pure water. To observe the enhancement of the heat transferred through the cavity, the average (Nu) along the left hot wall for all nanofluid concentrations and water is presented in **Fig**. (5.23). The average (Nu) is enhanced with the solid volume fraction (φ) increase. Where, at ($Ra=10^6$) the average (Nu) is increased to about (12) times the average (Nu) of water when increasing to ($\varphi=0.01$) while it increased to (13) times when increases to ($\varphi=0.05$).

For more observations, the local (Nu) along the central height of the left hot wall is presented in **Fig**. (5.24) for the concentrations (φ=0.05, 0.03, 0.01 and 0). It is noticed that the maximum local (Nu) or the peak value occurs at the lower part of the wall close to the base of cavity except for ($Ra=10^3$) where it occurs at the tip of the wall. Where the peak values of the local (Nu) appears around (0.1L, 0.2L and 0.4L) for ($Ra=10^4$, 10^5 and 10^6) respectively for all the nanofluid considered concentration cases. For water at ($Ra=10^3$, 10^4 and 10^5), as like as the case of nanofluid at ($Ra=10^3$) it is occurring at the tip of the wall for all the (Ra) considered. The local (Nu) of the nanofluid reach about more than (10) times that of the water. The described behavior of the local (Nu) can be analyzed due to the reasons of thermal field or the heat transfer behavior for the different considered cases. Where for the water case and the low (Ra) nanofluid cases, because of the high gravity effect comparing to the buoyancy effect, the heat transferred in uniform distribution which parallel to the hot wall. And due to that the region on the tip of wall are flow more freely than the lower regions where the effect of the liquid column are considered. For nanofluid cases at ($Ra>10^3$), the maximum peak value of the local (Nu) is appeared at the point where the maximum curvature of the isotherm lines occurs. At this point, the stagnant region has been initiated. A special behavior for water at ($Ra=10^6$) was appeared, the maximum convex peak value occurs at the region (0.4L) and another concave appeared at the region (0.9L), the drop in the local (Nu) at this region occurs because of the deceleration of velocity against the gravity effect. Where after the region of maximum local (Nu) and due to the far away from the base, the convection fails to overcome the gravity, so the local (Nu) drops. Then, the local (Nu) began to increase due to the close location from the upper wall which hit the flow stream causing increase in its velocity to overcome gravity.

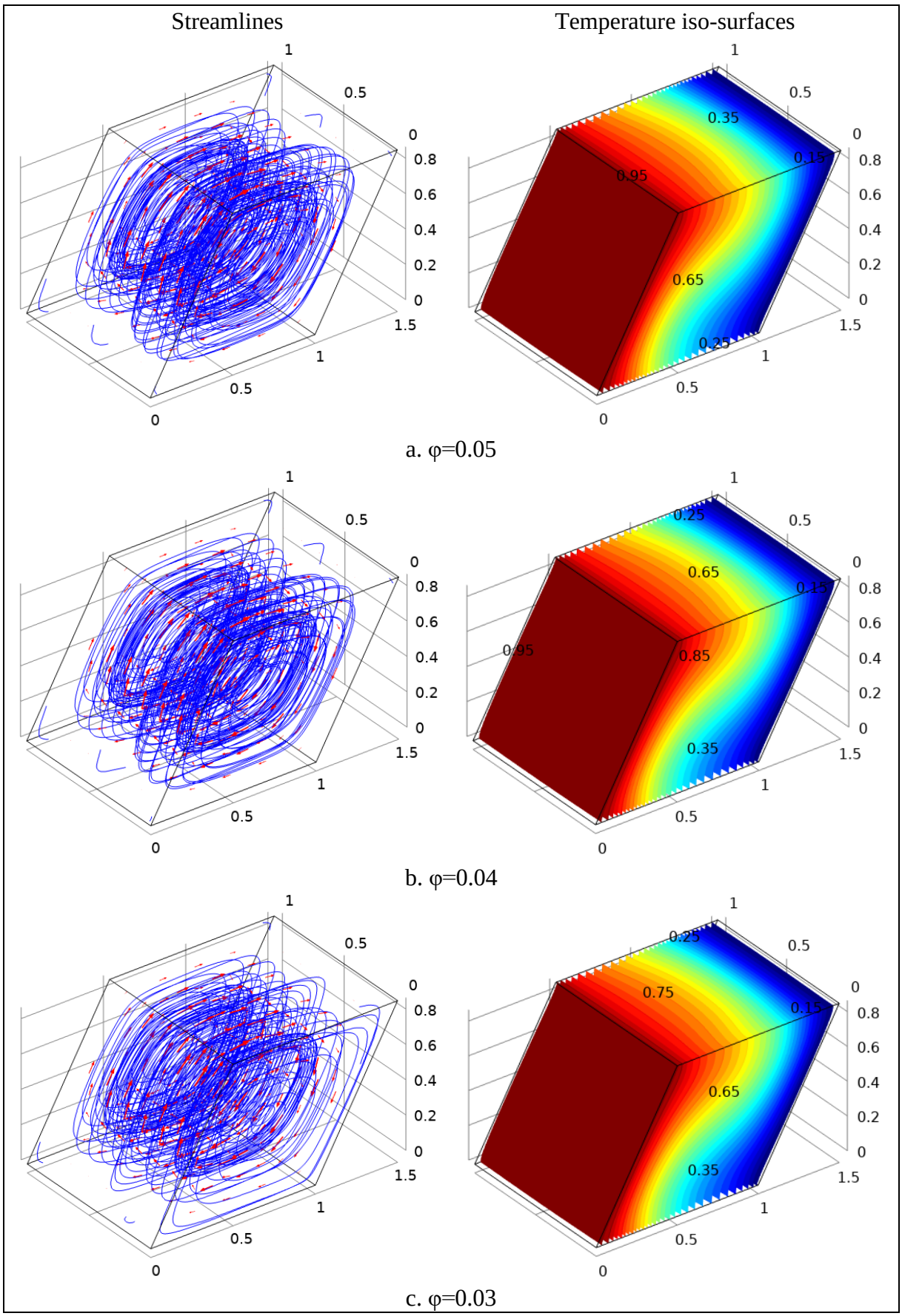

a. φ=0.05

b. φ=0.04

c. φ=0.03

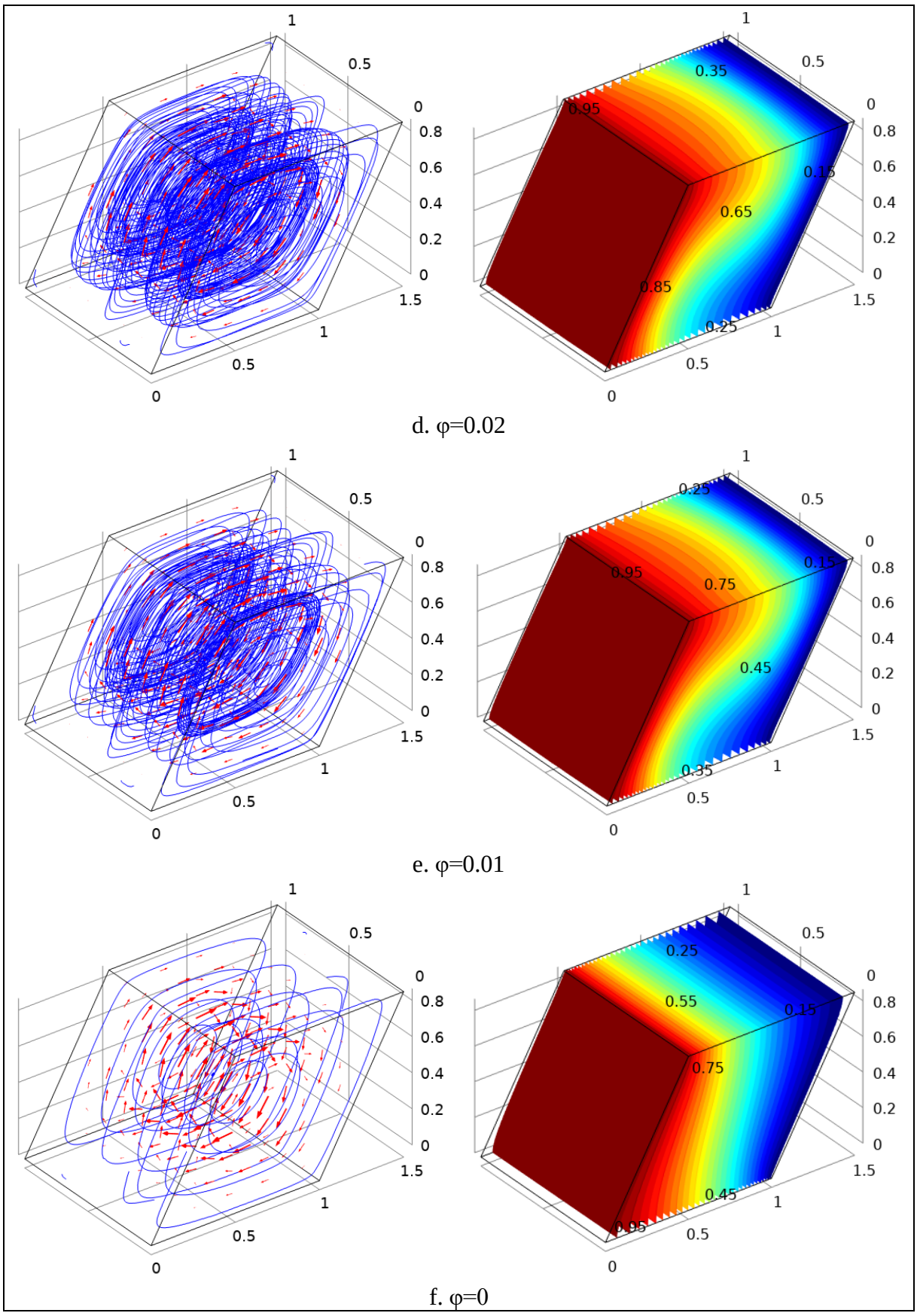

Figure (5.19): 3D streamlines and temperature iso-surfaces of the parallelogrammical cavity at (γ=60º) with different (φ) and (Ra=10^4).

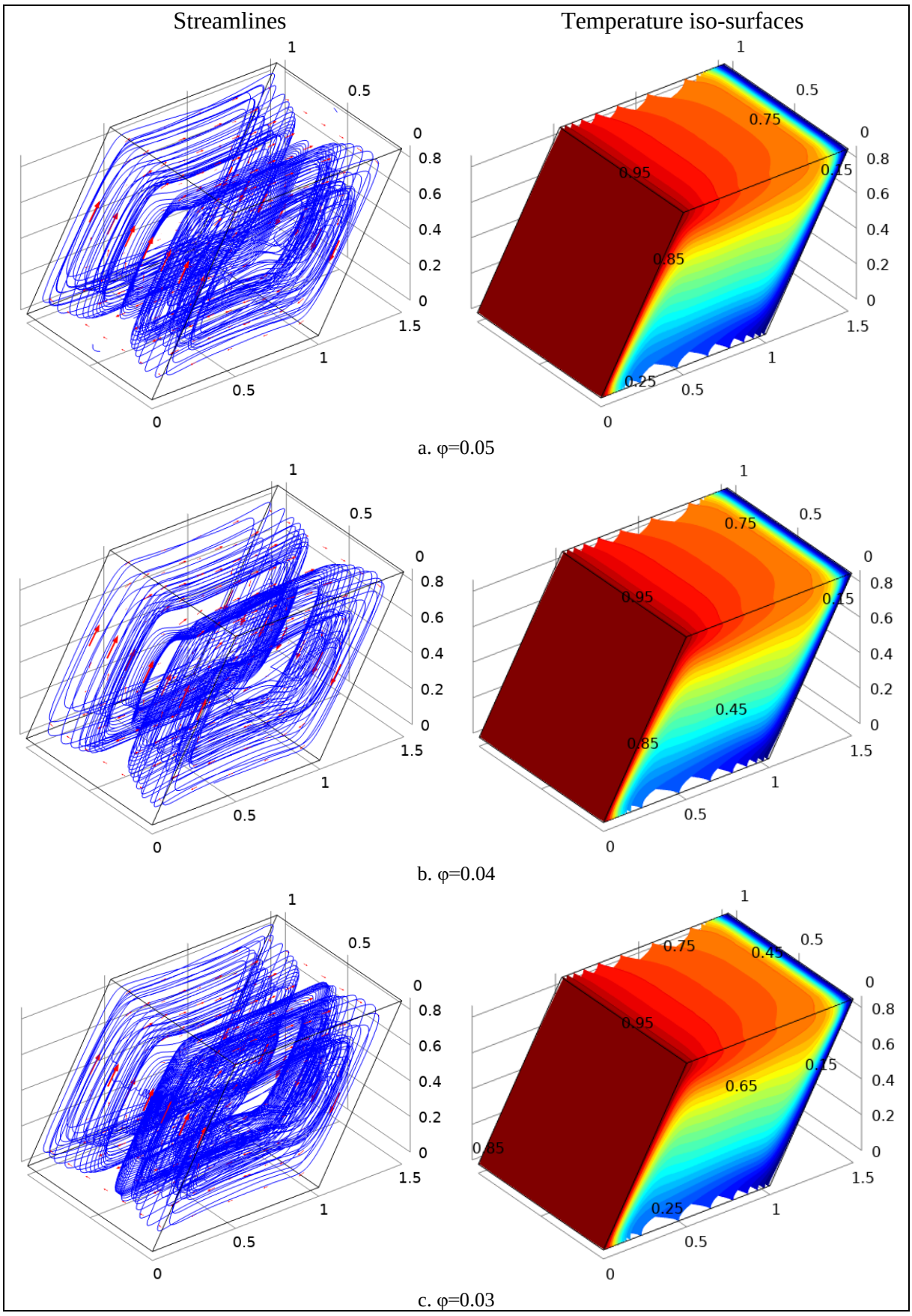

a. φ=0.05

b. φ=0.04

c. φ=0.03

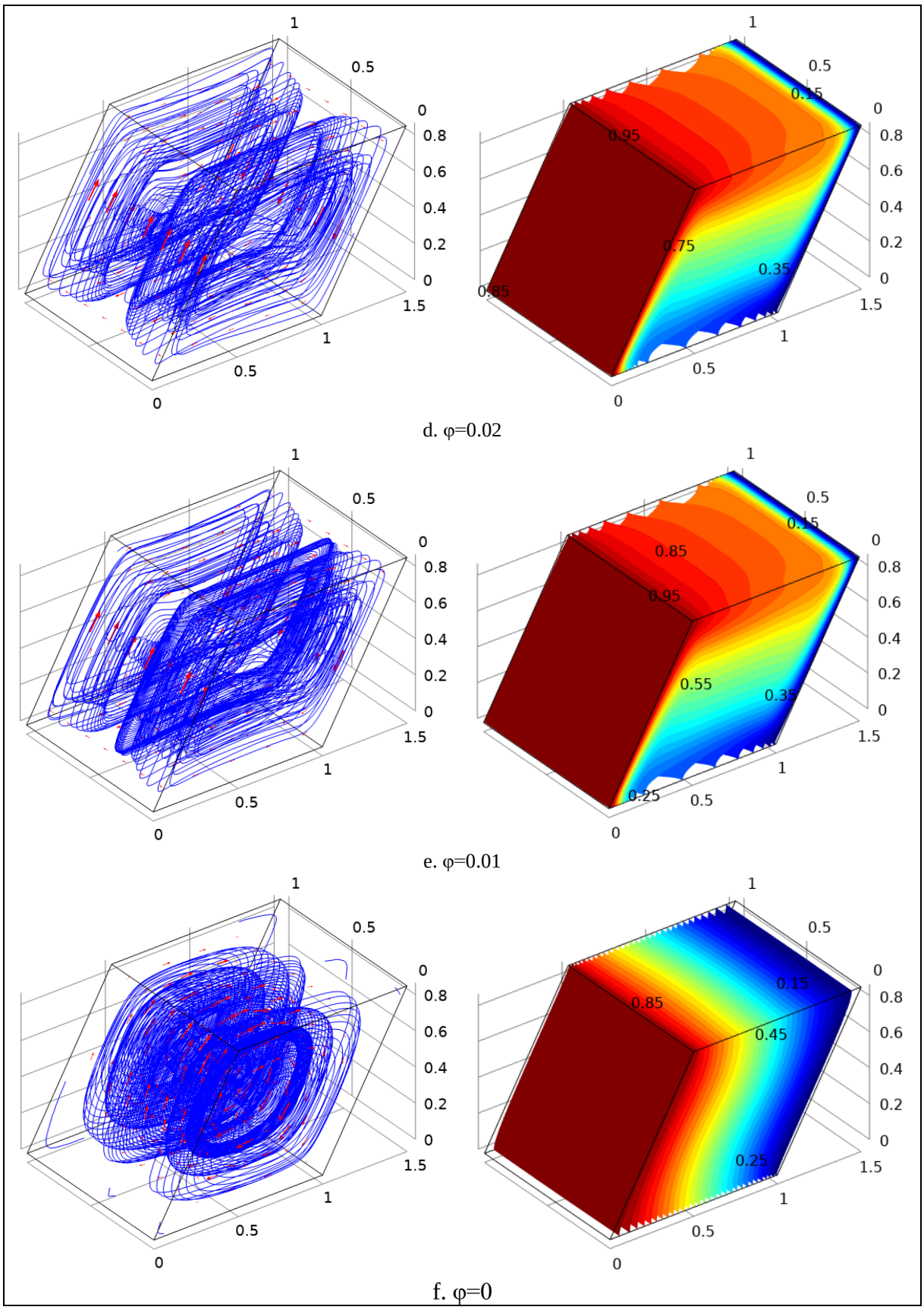

Figure (5.20): 3D streamlines and temperature iso-surfaces of the parallelogrammical cavity at (γ=60º) with different (φ) and (Ra =10^6).

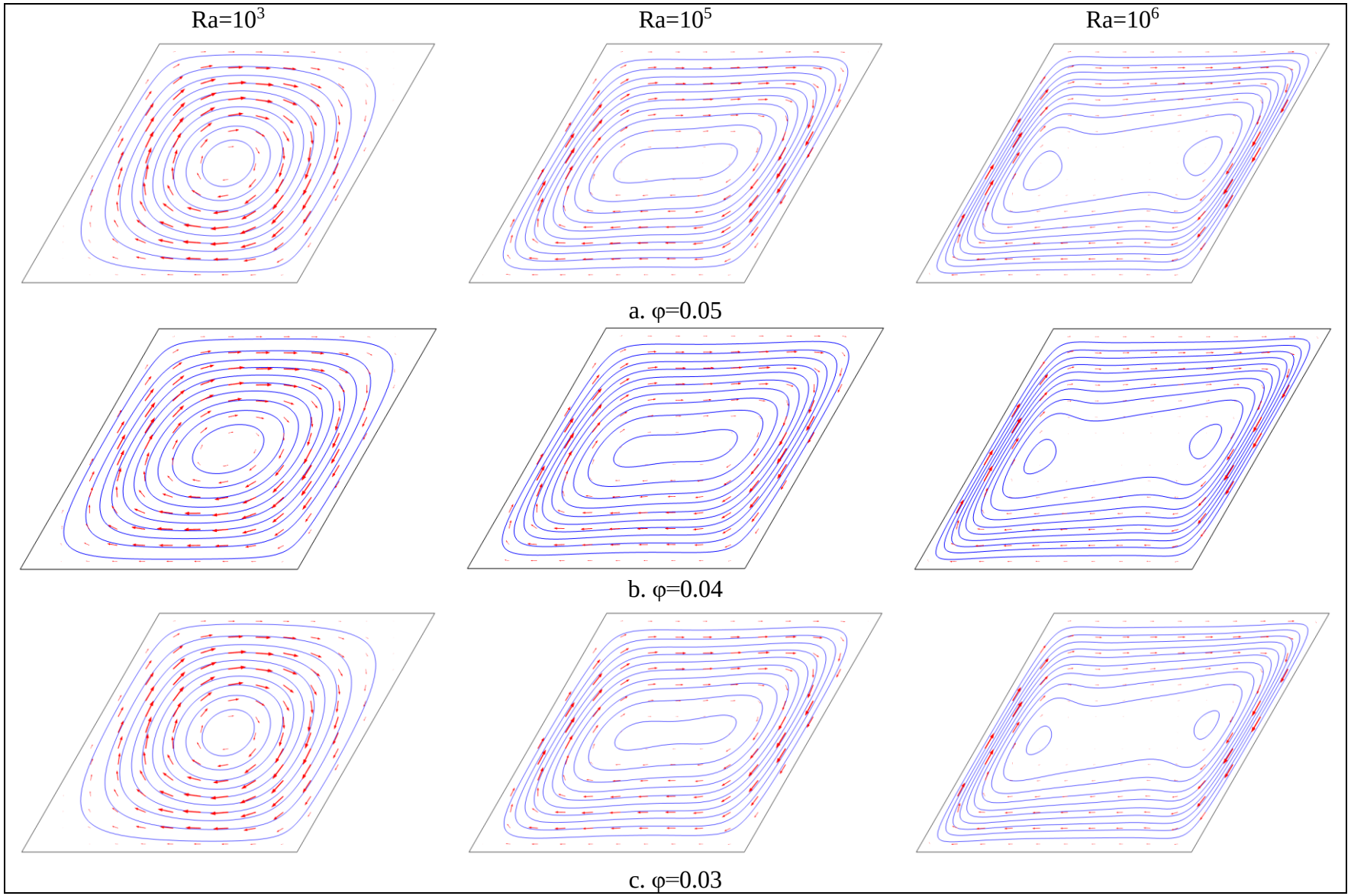
Ra=10^3
Ra=10^5
Ra=10^6
a. φ=0.05
b. φ=0.04
c. φ=0.03

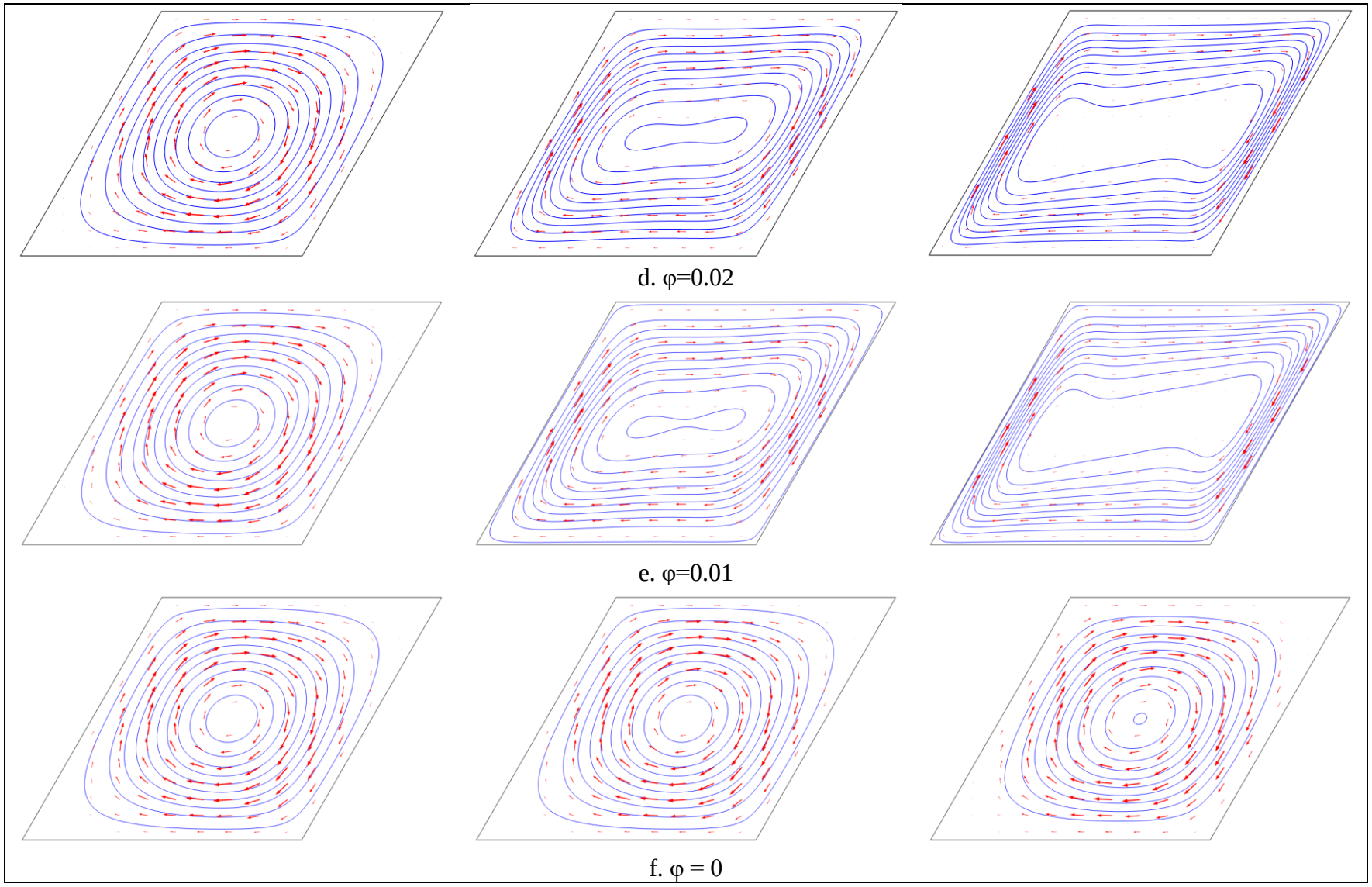

Figure (5.21): 2D stream lines projection for the parallelogrammical cavity at (γ=60º) on the plane (X-Z) at different (φ) and (Ra).

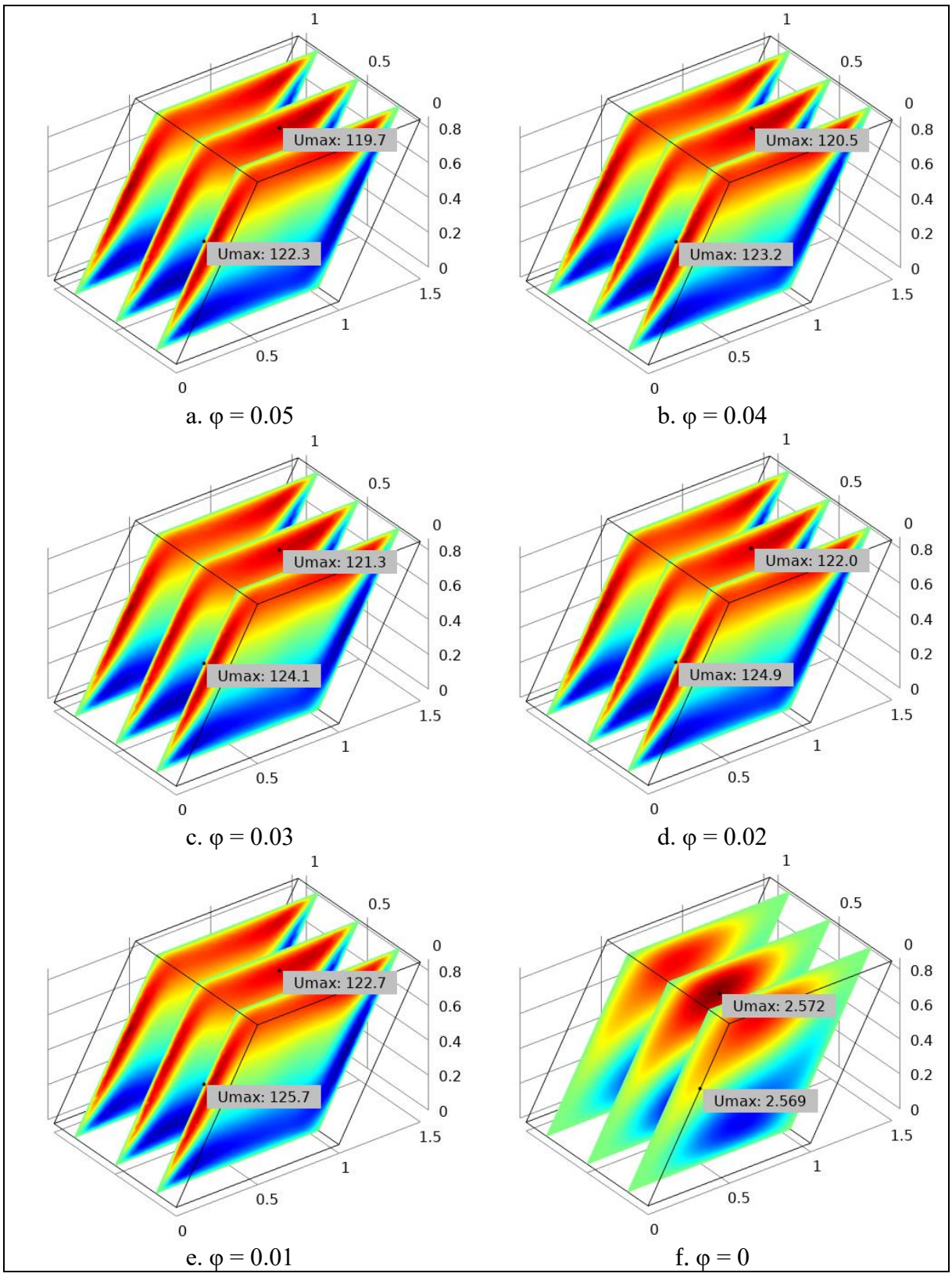

Figure (5.22): The horizontal velocity (U) for the parallelogrammical cavity at ($\gamma=60^{o}$) with ($Ra=10^{6}$) and different (φ).

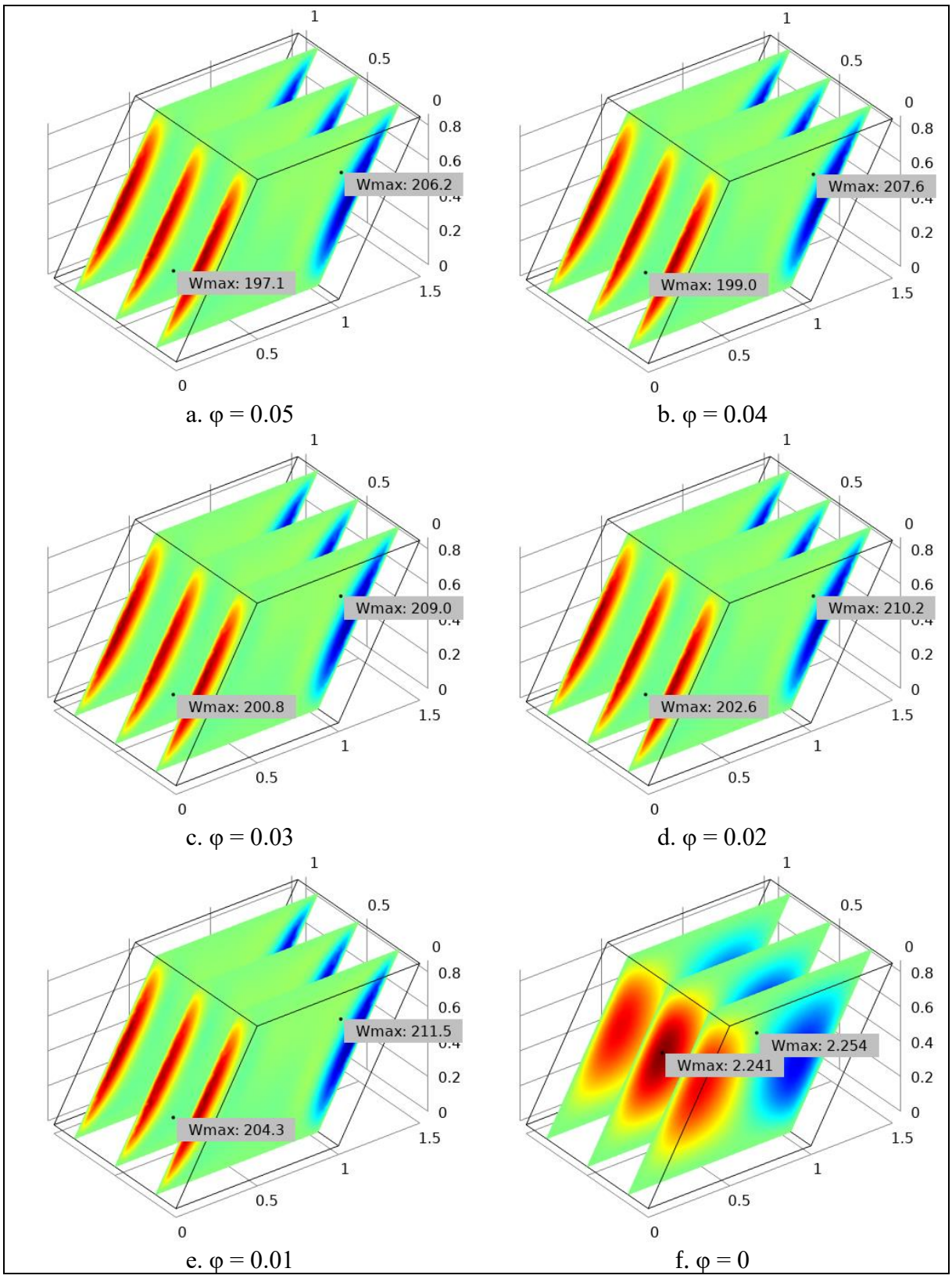

Figure (5.23): The vertical velocity (W) for the parallelogrammical cavity at ($\gamma=60^{o}$) with ($Ra=10^{6}$) at ($\gamma=60^{o}$) and different (φ).

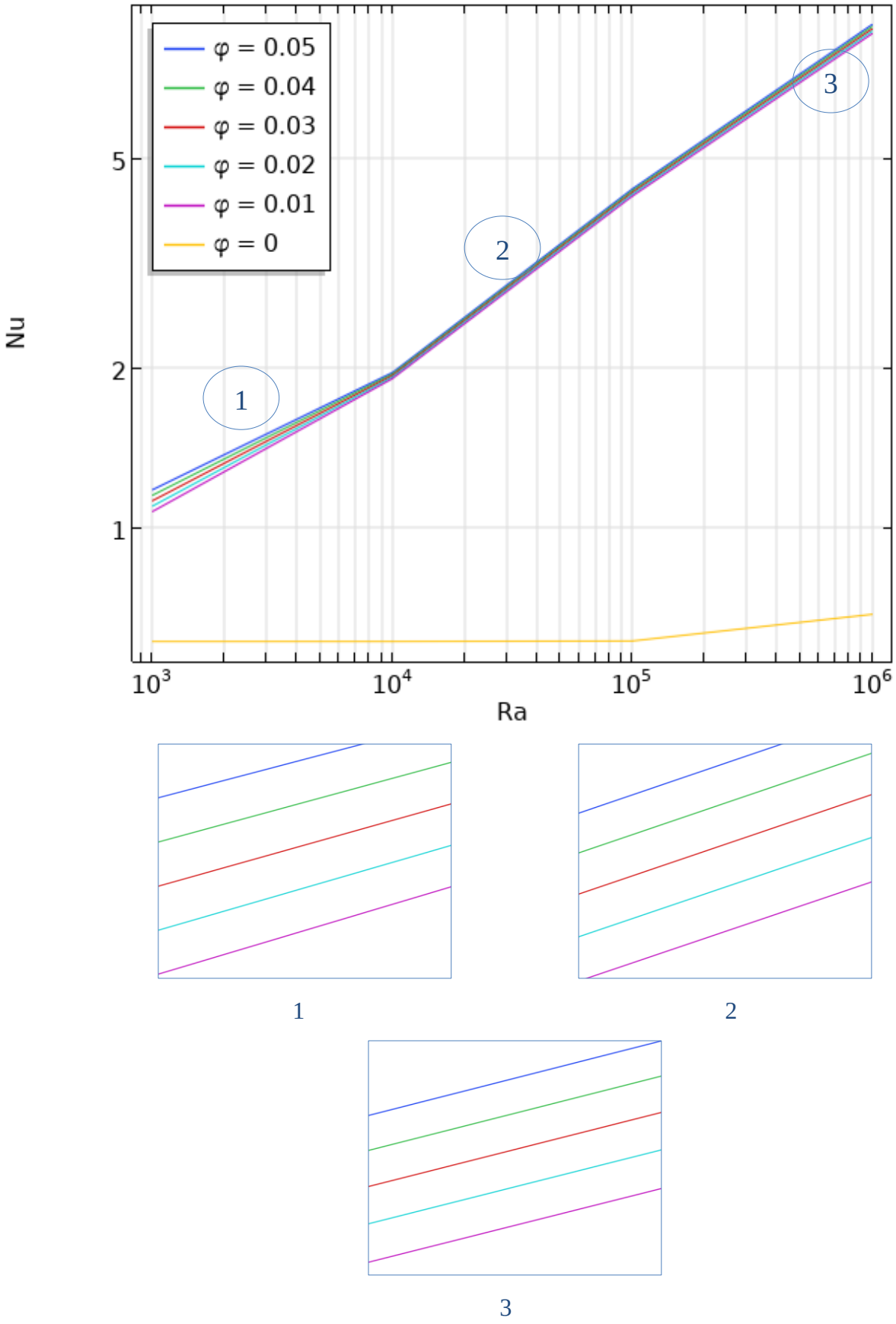

Figure (5.24): The average (Nu) on left hot wall versus (Ra) for the parallelogrammical cavity at (γ=60º) with different (Ra) and (φ).

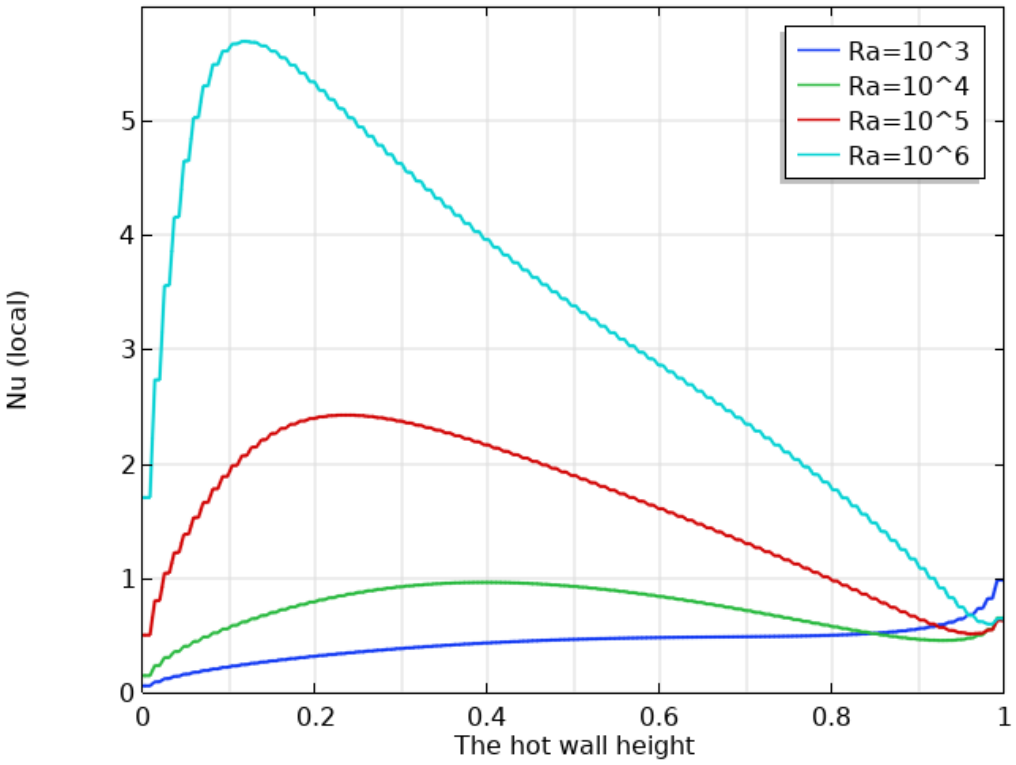
Ra=10^3
Ra=10^4
Ra=10^5
Ra=10^6
Nu (local)
The hot wall height
0
1
2
3
4
5
0
0.2
0.4
0.6
0.8
1

a. φ = 0.05

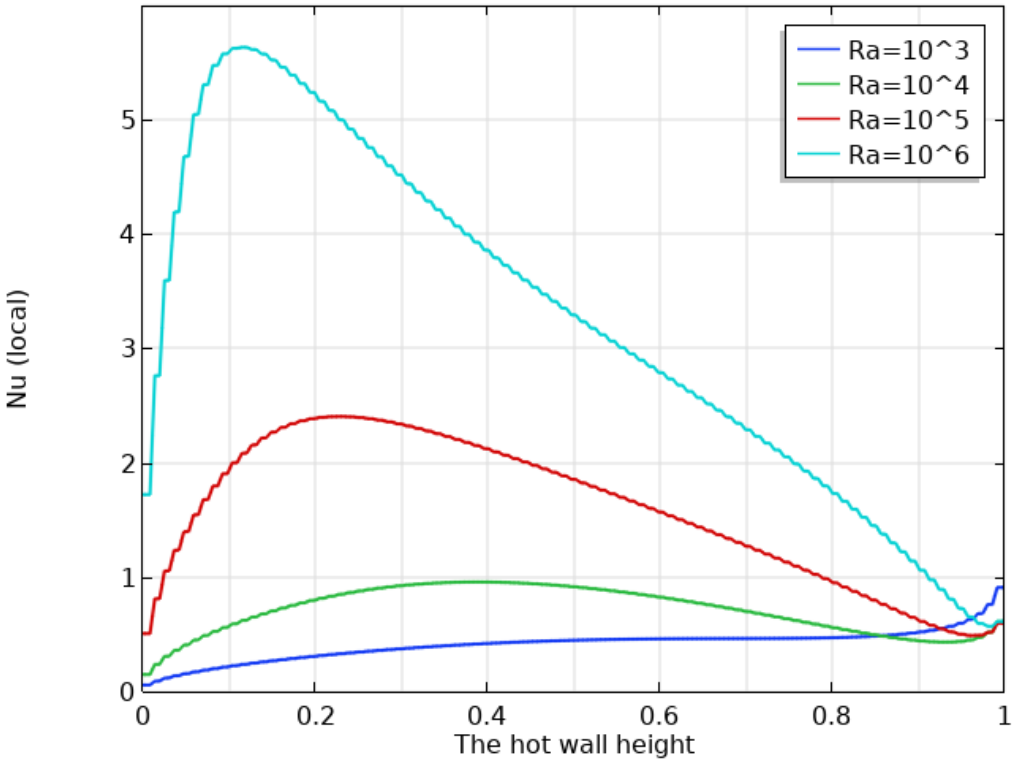
Ra=10^3
Ra=10^4
Ra=10^5
Ra=10^6
Nu (local)
The hot wall height
0
1
2
3
4
5
0
0.2
0.4
0.6
0.8
1

b. φ = 0.03

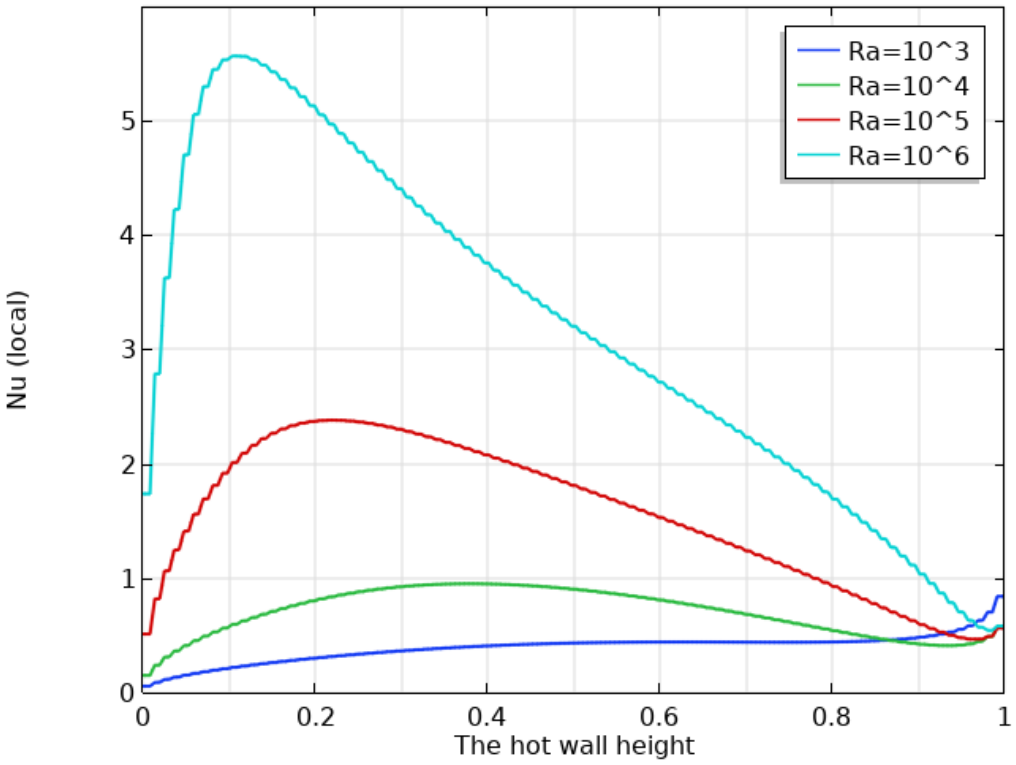

c. φ = 0.01

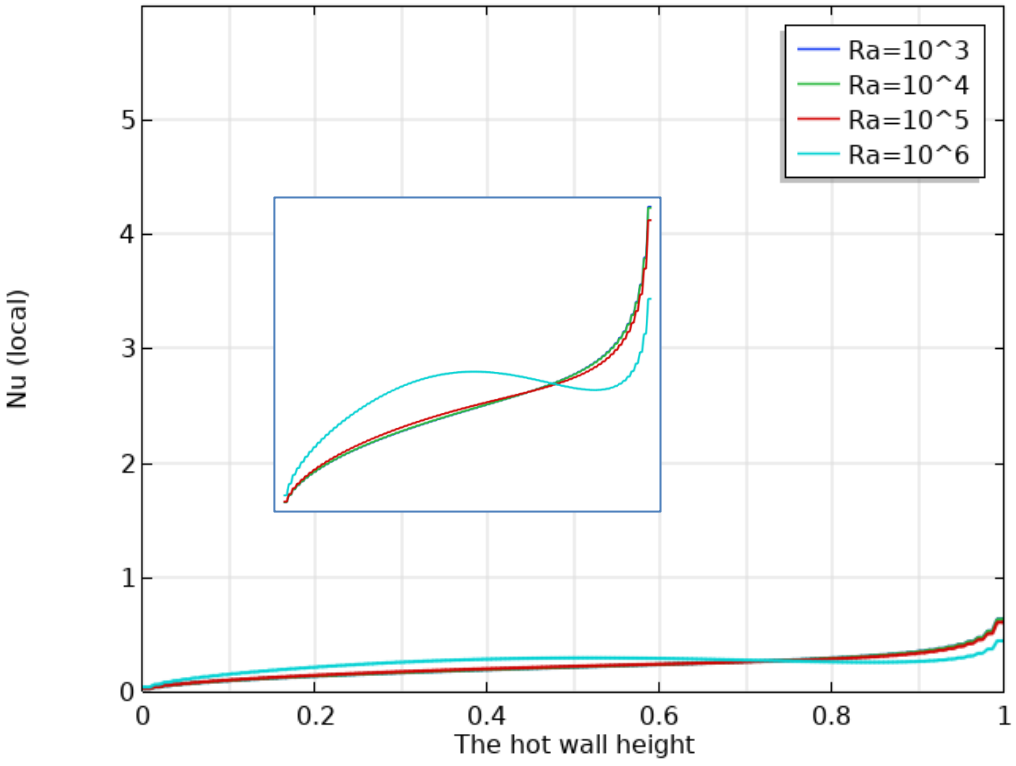

d. H_2O

Figure (5.25): The local (Nu) on the central line along the left hot wall for the parallelogrammical cavity at (γ=60º) with different (Ra) and (φ).

5.3.1.5 The Effect of Location and Distribution of Inserted Solid Bodies

Other modification of the parallelogrammical cavity at (γ=60º) is discussed in the present section. The considered inserted solid bodies are seven cases of circular inserted cylinders that had different radius but have the same volume together as explained previously in Chapter Three. The 3D streamlines and the temperature iso-surfaces of the seven cases at (φ=0.05) and ($Ra=10^5$) are presented in **Fig**. (5.26). The 2D projection of the streamlines on the plane (X-Z) for all the considered cases at (φ=0.05) and ($Ra=10^5$) are presented in **Fig**. (5.27).

The streamlines configuration is changing due to the inner shape count and location. But the less change satisfied in the case of central location where it keeps the similarity around the center as like as the case with no inners. The terminal locations producing unsimilar flow in the two halves of the cavity around the center. It is producing additional vortices that encourage the convection initiation. Also, it is observed that the cases of central concentrated volumes are show similar behavior to the cases with no inners while the two cases of double inner with (0.09L and 0.12L) apart which have relatively high distance between location are introduce a special behavior. This behavior was initiating two separated vortices on the two sides of inners which covering the cavity parts entirely.

Of course, these flow configurations were affecting the horizontal (U) and vertical (W) velocities as shown in **Figs.** (5.28) and (5.29) which presented the 2D projection on the plane (X-Z). The location of the maximum (U) and (W) for the corner single cylinder cases are located between the inserted cylinder and the adjacent horizontal wall whereas the core of the two main circulations that parallel to the inclined vertical walls are less than it. These variations of velocity making non homogeneous fluid flow inside the cavity. The vertical

velocity (W) enhancement is necessary to push the flow to grow up and forming the circulation from the hot to the cold walls.

In general, the inners are delaying the region where the vertical velocity (W) being higher than the horizontal (U) which occurs at ($5\times10^4 \leq Ra \leq 10^5$). The more enhancement of (W) is noticed for the central location for the single cylindrical inner cases. For the two inners cases, the maximum (W) is recorded for the case of two inners of (0.06L) apart. The increased distance has reverse effect on the flow where the higher distance permits another mini circulation between the inners. That absorb the flow energy causing flow deceleration. The second stage of comparisons are accomplished for the central location and for single, double and triple inners. The triple inners case introduced the maximum (U) and (W) while from the single inner case the lower values are satisfied. The increased count of inners means increasing the surface area of inners for the same volume producing good technique to enhance the flow inside cavities.

With respect to the thermal field, by observing the 3D temperature iso-surfaces for all cases that presented in **Fig**. (5.26). The location of inners is affecting the isotherm lines configuration where the inner cylinders are working as obstruction that changes the flow direction and the energy transformation. For the two and three inner cases, it is generating more nonlinearity which works as convection increasing phenomenon. The single inner is producing the less effect on the isotherm configuration. The average (Nu) in turn obeys the same behavior of the isotherms towards location of the inner cylinder where the central location is giving the higher average (Nu) comparing to the other two terminal locations which in turn giving nearly the same range of the average (Nu). With respect to the number of inners, the average (Nu) is augmented with increasing the inners inside the cavity as shown

in **Fig.** (5.30) (c) for all the considered (Ra) range except for ($Ra \leq 10^4$). Where at this range, the increased surface area means the flow will hit large obstacles which causing deceleration in energy where it absorbs by these obstacles, so the flow stream becoming unable to overcome the gravity effect. At higher (Ra) values, invers effect of these obstacles is appeared, where it works as velocity accelerator due to that these velocities already increased with (Ra) increase and overcoming the gravity effect. So, when the flow stream hit these inner walls, accelerates and increasing convection.

By comparing the average (Nu) of the different cases of inners with the case of cavity without inners and filled with water at ($Ra=10^6$), it was founded that, for the single inner cases with the considered locations (left, center and right) the average (Nu) was about (12.4, 12.9 and 12.5) times, respectively. For double inner with (0.06L, 0.09L and 0.12L) apart distances between them, it was about (13, 12.9 and 12.8) times, respectively. While it was about (13.2) times for the triple inners case. It concluded that the enhancement of convection that represented by the average (Nu) is decreases with (Ra). But still, that of triple inners have about (2) times the enhancement of the single case for all considered (Ra).

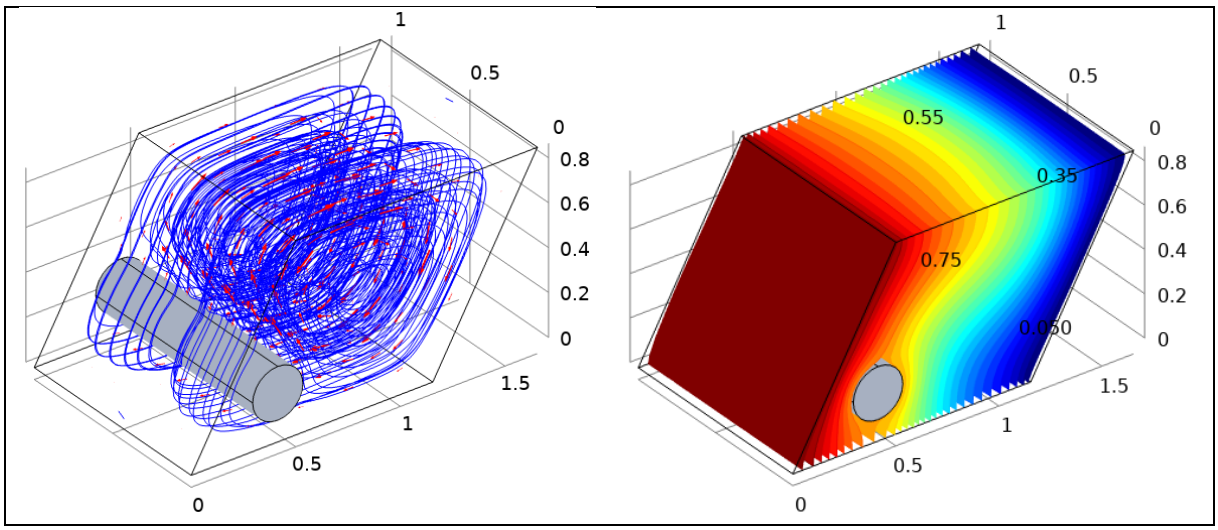

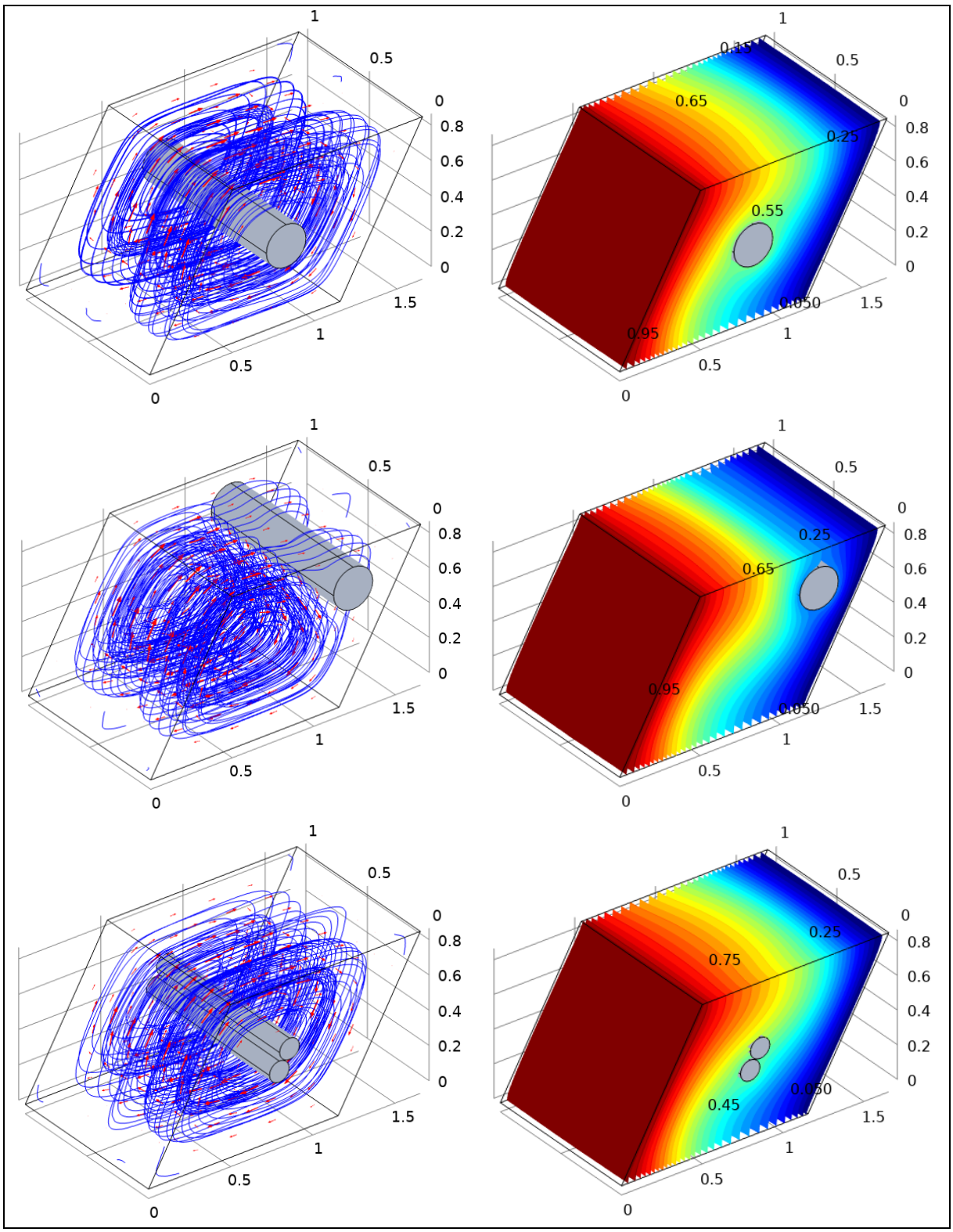
1
0.5
0
0.8
0.6
0.4
0.2
0
1.5
1
0.5
0
0.15
0.65
0.25
0.55
0.95
0.050
0.75
0.45

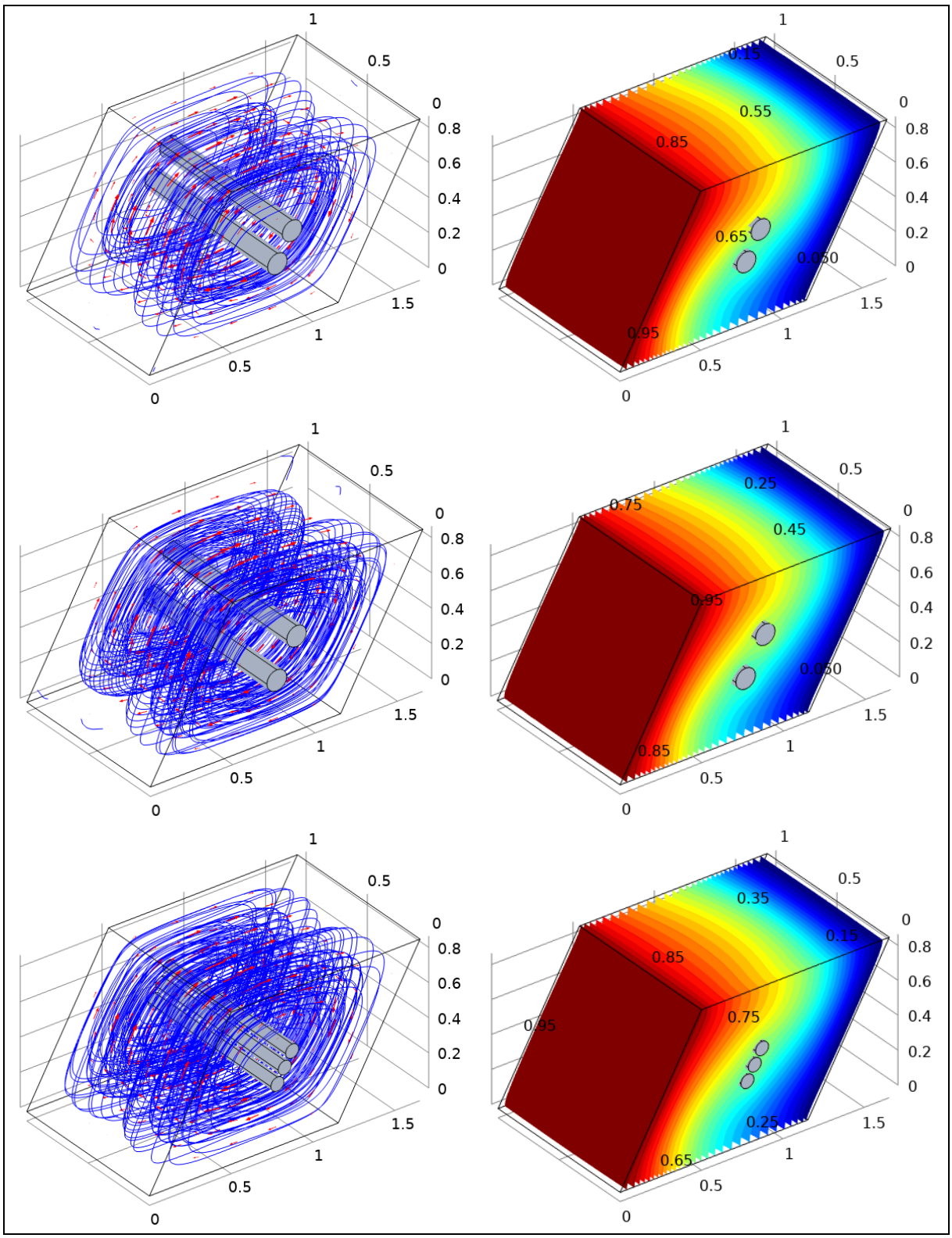

Figure (5.26): 3D streamlines and iso-surfaces of the parallelogrammical cavity at (γ=60º) with different inserted bodies and (φ=0.05, Ra=10^5).

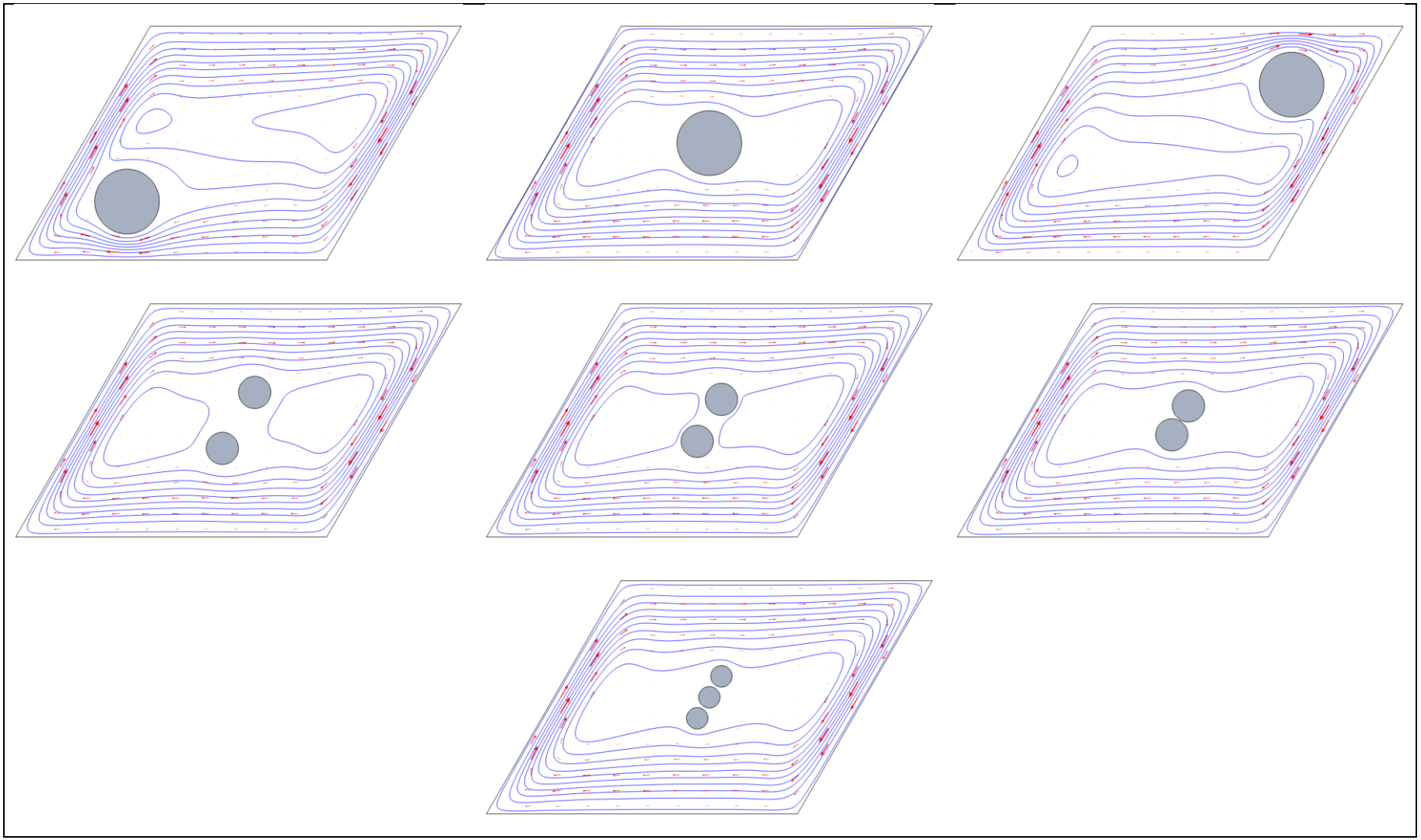

Figure (5.27): The streamlines of the parallelogrammical cavity of (γ=60º) with different inserted bodies on the plane (Y = 0.5) at (φ=0.05) and ($Ra=10^5$).

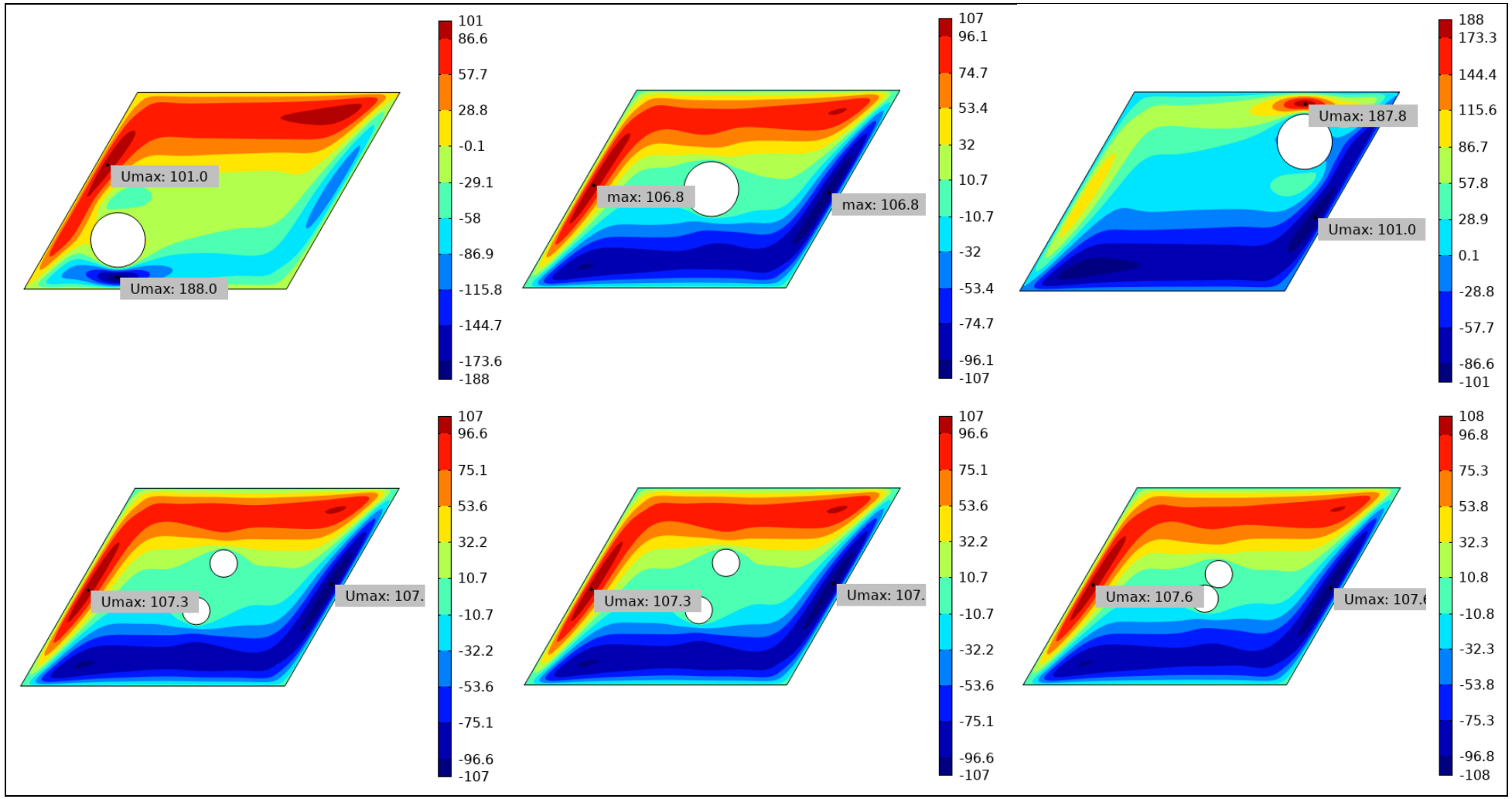
Umax: 101.0
Umax: 188.0
101
86.6
57.7
28.8
-0.1
-29.1
-58
-86.9
-115.8
-144.7
-173.6
-188
max: 106.8
max: 106.8
107
96.1
74.7
53.4
32
10.7
-10.7
-32
-53.4
-74.7
-96.1
-107
Umax: 187.8
Umax: 101.0
188
173.3
144.4
115.6
86.7
57.8
28.9
0.1
-28.8
-57.7
-86.6
-101
Umax: 107.3
Umax: 107.
107
96.6
75.1
53.6
32.2
10.7
-10.7
-32.2
-53.6
-75.1
-96.6
-107
Umax: 107.3
Umax: 107.
107
96.6
75.1
53.6
32.2
10.7
-10.7
-32.2
-53.6
-75.1
-96.6
-107
Umax: 107.6
Umax: 107.
108
96.8
75.3
53.8
32.3
10.8
-10.8
-32.3
-53.8
-75.3
-96.8
-108

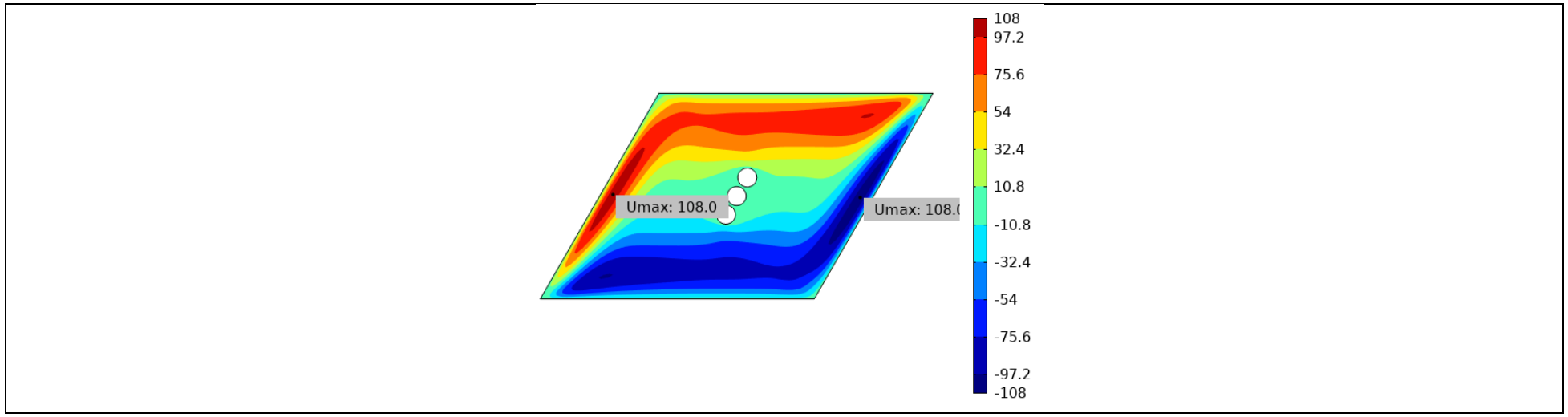

Figure (5.28): 2D projection of the horizontal velocity (U) on the plane (X-Z) for the parallelogrammical cavity at (γ=60º) with different inserted bodies and (φ=0.05, Ra=10^6).

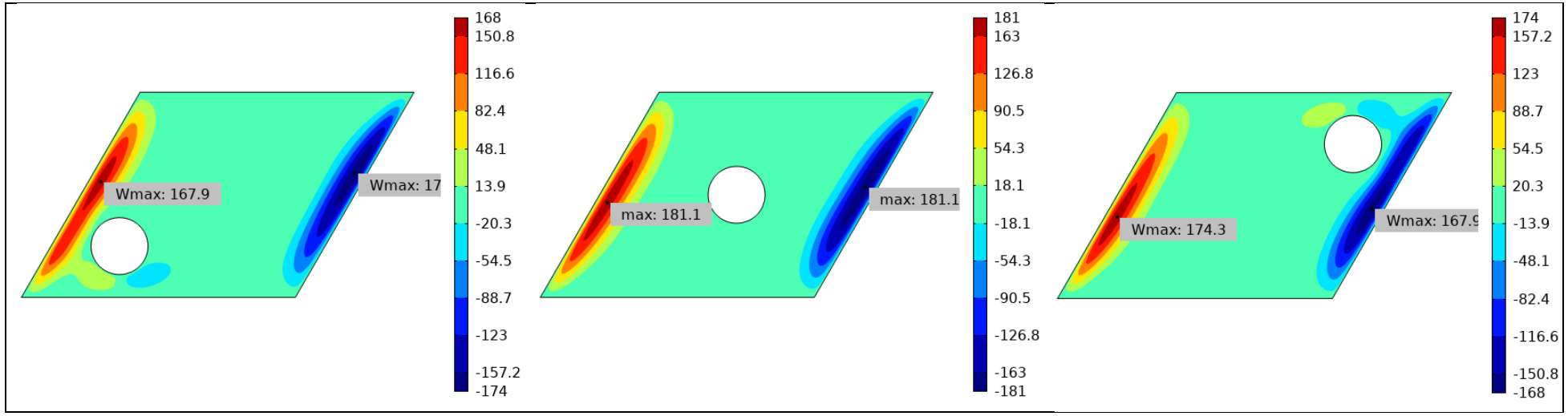

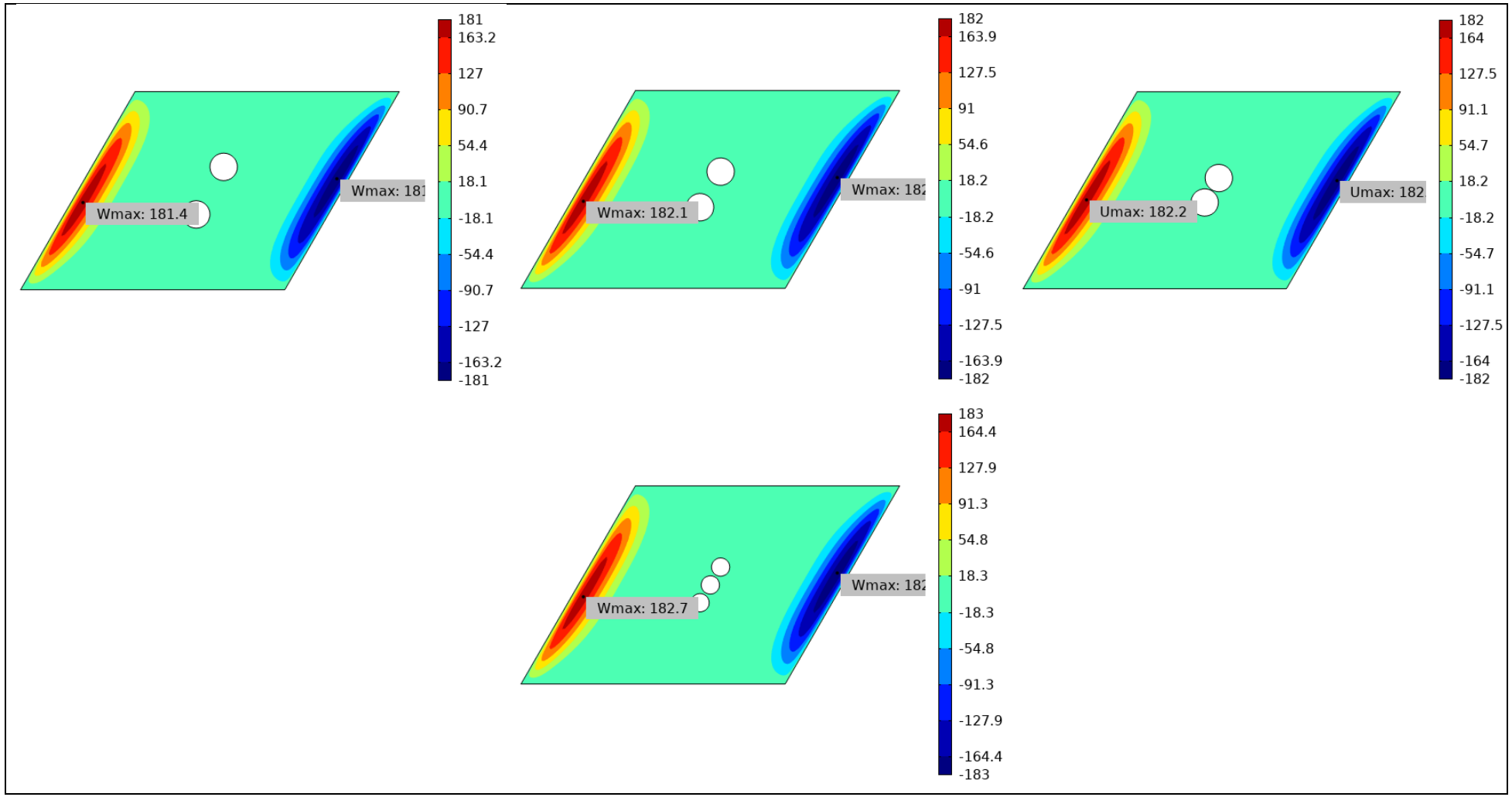

Figure (5.29): 2D projection of the vertical velocity (W) on the plane (X-Z) for the parallelogrammical cavity at (γ=60º) with different inserted bodies and (φ=0.05, Ra=10^6).

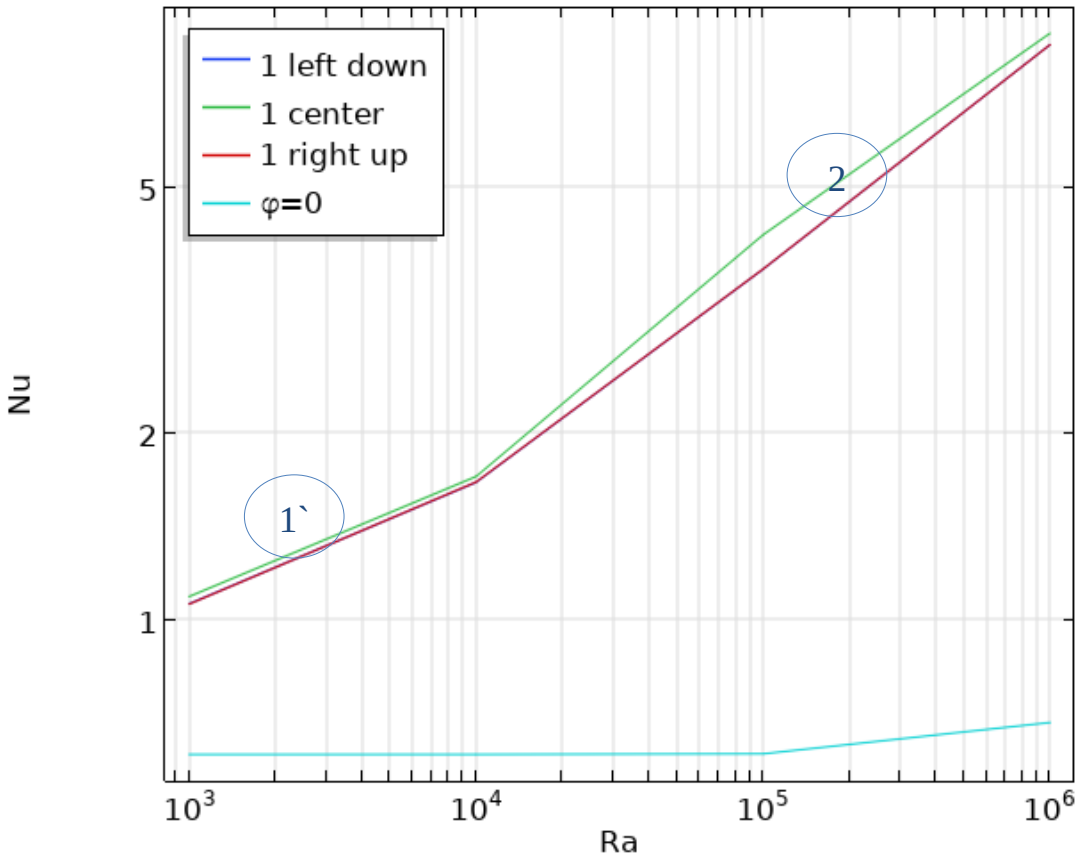

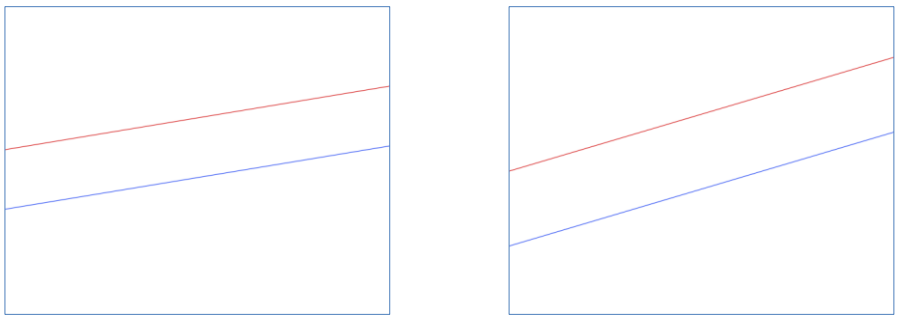

1 2

a. Single with different locations

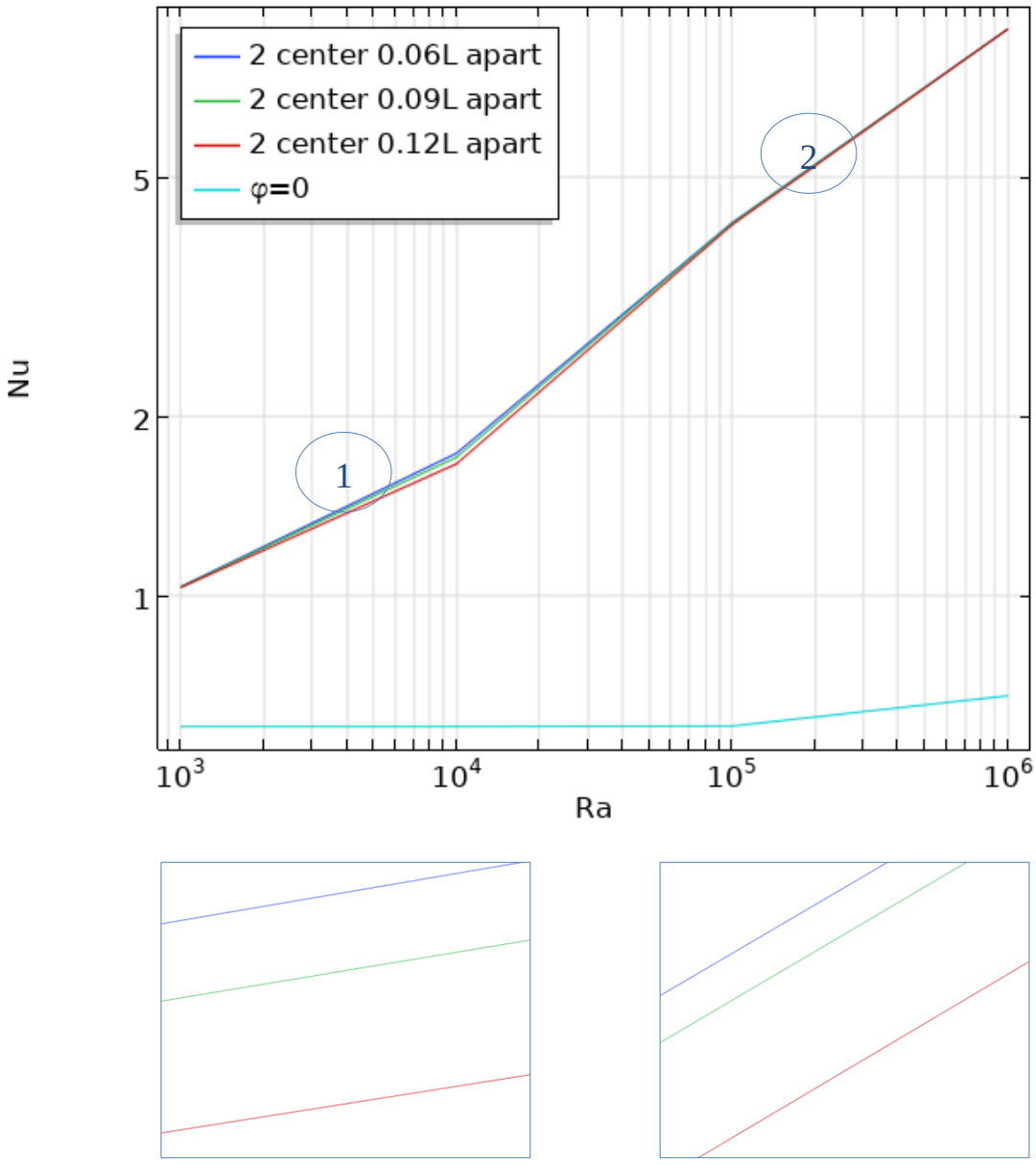

1 2

b. Douple with deferent apartments

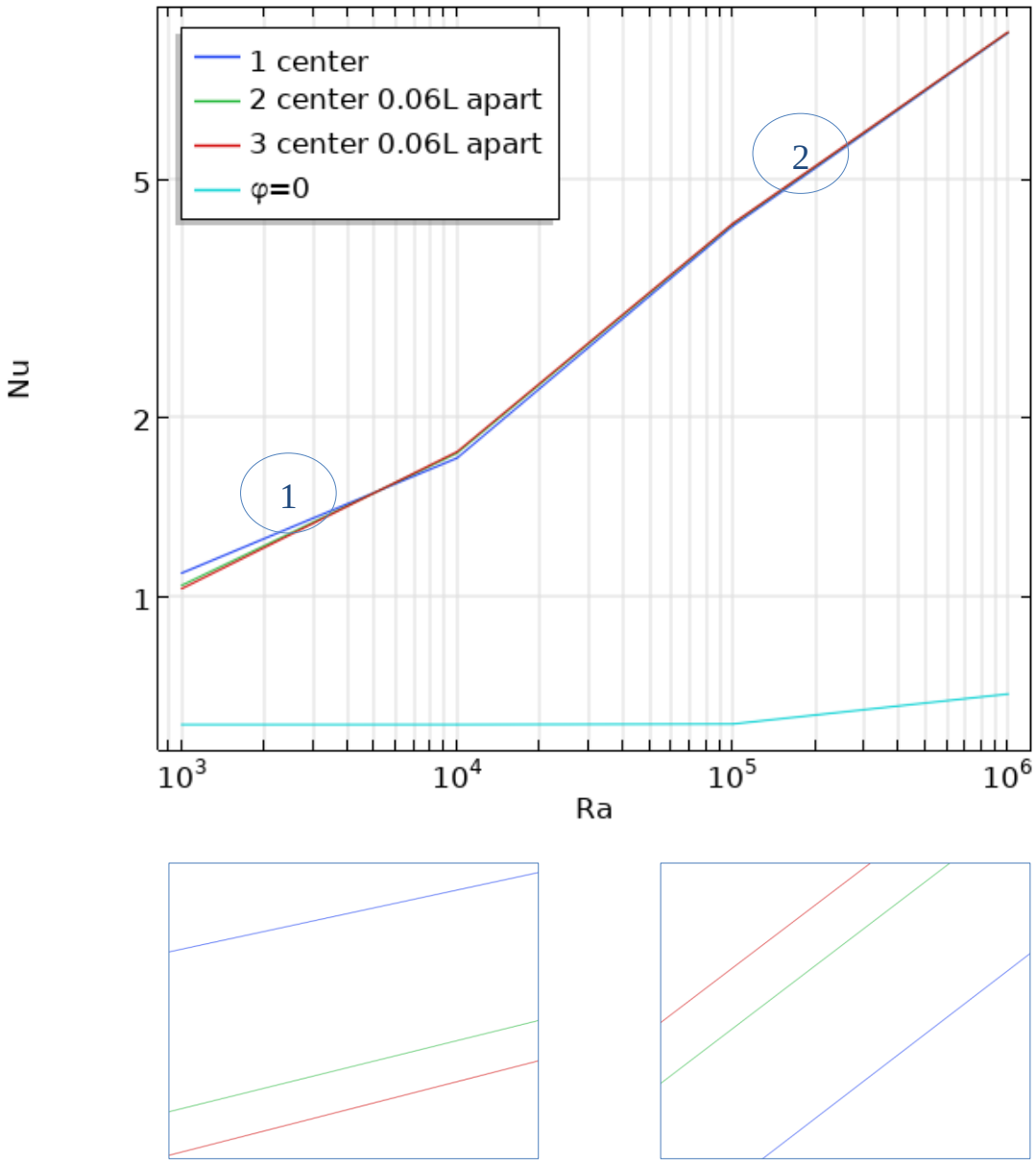

1 2

c. Different inner counts

Figure (5.30): The average (Nu) on the left hot wall versus (Ra) for the parallelogrammical cavity at (γ=60º) with different inserted bodies and (φ=0.05).

5.3.2. Natural Convection inside Other Complex Cavities and Comparison with the Parallelogrammical cavity

The natural convection inside the other considered complex geometry cavities that introduced in Chapter Three is presented and discussed in the current section. These cavities have the same volume (L^3) with different number of walls. It is named according to the shape of the front wall that located between the vertical left hot and right cold walls (i.e., hexagonal, octagonal and elliptical). All these cavities have equal areas (L^2). The effect of three variables on the laminar natural convection inside them are examined in the current section. These variables are the number of walls, the overall surface area and the width to height parameter as presented in **Fig**. (5.31).

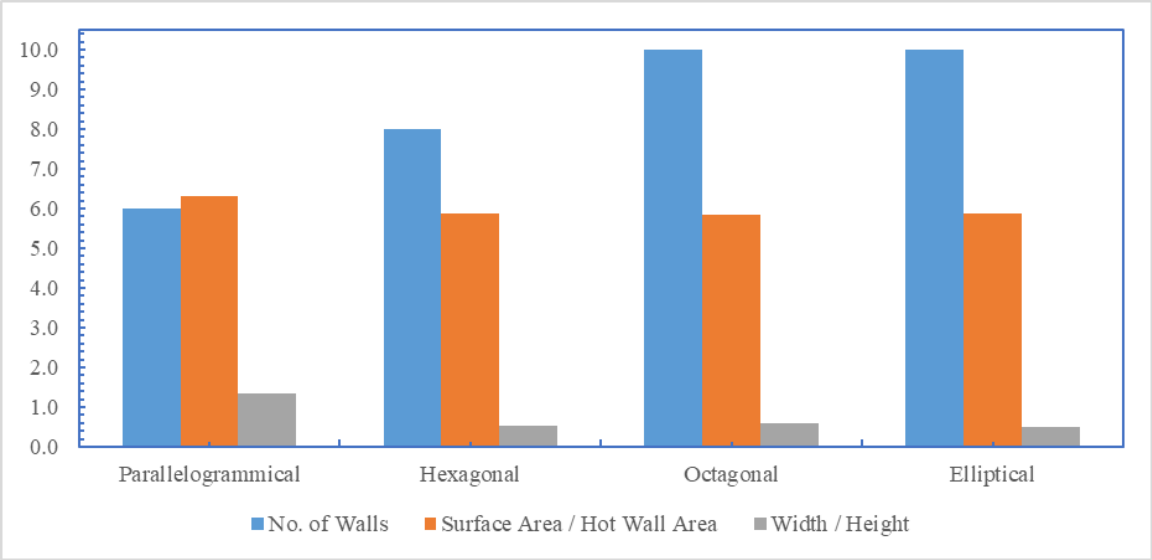

Figure (5.31): The number of walls and the overall surface area of cavities and the width to height.

The number of walls is as that, the octagonal cavity with ten walls, the hexagonal cavity with eight walls while the elliptical cavity has two straight walls and eight shells. The surface area of these cavities is nearly equal which in turn less than the previous parallelogrammical cavity surface area. With respect to the width/height parameter, the cavities have nearly the same value also and less than from that of the

parallelogrammical cavity. Where the parallelogrammical cavity has the horizontal dimension is the longer dimension and vice versa to the other cavities that have its vertical dimension is the longer dimension. The width/height ratio has great indication where it specifies the distance between the hot and cold walls which effects the flow behavior strongly when accelerates between them.

The 3D streamlines of the three cavities are presented in **Figs**. (5.32) and (5.33) at (φ=0.05) and ($Ra=10^4$) and ($Ra=10^5$) respectively. Also, the 2D projection of the streamlines on the plane (X-Z) is presented in **Fig.** (5.34) on three different distances from the front wall (Y=0.25, 0.5 and 0.75) at ($Ra=10^5$ and φ=0.05). As like the parallelogrammical cavity, the streamlines are growing from the hot left wall towards the cold wall in clock wise direction. For all cavities, the streamlines circulations are taking the configuration of horizontal elongated ellipse in parallel with the front and back walls which encounter the stagnant region.

These lines become denser and close to each other near the cavity walls at higher (Ra). A special behavior of these lines is appeared in the core of the cavities, where the lines are becoming of very high intensity and close to the core while the outer circulations are of less intensity at the cavity center. But the circulation of the streamlines at the planes near the front and back walls have moderate and uniform distributed intensity along the entire plane. This phenomenon is occurring due to the high height to width ratio which improve the adhesion of the fluid particles on the cohesion effect especially at high (Ra) and in the center plane where the effect of the walls is poor.

In general, the velocities (U) and (W) are nearly in the same range for all cavities as shown in **Figs**. (5.35) and (5.36) at (φ=0.05) and

($Ra=10^4$, $Ra=10^5$) respectively. The other conclusion is that these velocities are proportional to the longer dimension in their values. For the three cavities, (U) is lower than (W) by observed values for all the considered (Ra) range unlike the parallelogrammical cavity, as like as the locations of the maximum (U) are differed from it also. Where it appeared at the corners at the upper tip of the hot wall and the lower tip of the cold wall with the flow direction. The additional walls that are follow the vertical walls are hitting part of the coming stream from the hot wall in a very short distance from its initiation point which forming a high velocity circulation while the low energy remain stream making the higher circulation.

By observing the temperature iso-surfaces although, the heated and cooled walls have the same area, it is observed that these lines surfaces at ($Ra=10^4$) are of high nonlinearity for the hexagonal cavity than the other which means the convection initiate earlier in the hexagonal cavity. But at ($Ra=10^5$), these surfaces have nearly the same configuration at all the three cavities that means the other cavities propagate the convection lately but in higher rates.

The reason of this behavior is the balancing between the physical properties of flowing fluid and the cavity design. At (Ra) values around (10^4), the width to height ratio is enough to exceed the gravity effect and initiating the convection while it is not enough for the other two cavities. But at higher (Ra), the advantage of low width to height ratio are appearing clearly in the octagonal and elliptical cavities and due to the short distance between the hot and cold walls, making high ratios of convection creation in short time comparing to the hexagonal cavity.

As like as the parallelogrammical cavity, the average (Nu) is directly proportional to (Ra) as shown in **Fig**. (5.37). The higher average

(Nu) is recorded for the cavities with high number of walls, elliptical, octagonal and hexagonal respectively. For ($Ra \leq 10^5$), the best enhancement in the average (Nu) are recorded from the cavities; (elliptical – octagonal – hexagonal) respectively. Two parameters are working together to produce this behavior, the number of walls or the entire surface area and the cavity height where the lateral distance between the hot and cold walls is already the same. Where the surface area is increasing factor while the height id decreasing factor according to the enhancement of the average (Nu). At this region of (Ra) where the flow velocities are low in values so the cavity of the lower height is desirable to overcome the gravity effect.

From other side, the higher surface area and higher walls means additional vortices which increasing convection. The effect of higher surface area for the elliptical cavity exceeds the effect of lower height for the octagonal cavity to produce higher average (Nu). While at ($Ra \geq 10^5$) the best enhancement is becoming in the series; (octagonal – elliptical – hexagonal) and the enhancement of the elliptical and hexagonal become very close to each other. At this region, the height of cavity effect becoming more important by considering that the surface area of all cavities is nearly very close in values unlike the height values. So, the octagonal cavity producing the best enhancement of the average (Nu). Where at ($Ra=10^6$ and $\varphi=0.05$) the enhancement of the average (Nu) over the parallelogrammical cavity for the hexagonal, octagonal and elliptical cavities are (17.6%, 18% and 17.2%), respectively.

These conclusions proved that, the hexagonal, octagonal and elliptical cavities, or generally the cavities with higher vertical dimension in the considered laminar convection and the selected differentially heated arrangements are giving the better heat convection

enhancements comparing to the parallelogrammical cavity which had its dimensions nearly in the same range (width and height).

It is important to mention that the enhancement of heat transfer and the average (Nu) augmented by increasing the solid volume fraction as like as the parallelogrammical cavity for all the considered (Ra) rang. Where at ($Ra=10^6$) by increasing the solid volume fraction (0.05%) from (0 to 0.05%) the average (Nu) increased by the hexagonal, octagonal and elliptical cavities is exceed the increase in the parallelogrammical cavity of the same volume and nanofluid concentration by about (10%) over the parallelogrammical cavity at ($Ra\geq10^4$) as shown in **Fig.** (5.38). For all cavities at ($Ra<10^4$), the augmentation of the average (Nu) due to the increase of the solid volume fraction concentration is higher than the (10%) for the same reason that is explained earlier.

These conclusions proved that, the hexagonal, octagonal and elliptical cavities, or generally the cavities with higher vertical dimension in the considered laminar convection and the selected differentially heated arrangements are giving the better heat convection enhancements.

The local (Nu) along the central height of the left hot wall is presented in **Fig.** (5.39) for all the cavities at ($\varphi=0.05$) and all considered (Ra) range. Unlike the parallelogrammical cavity, the local (Nu) for the hexagonal, octagonal and elliptical cavities are dropped from its maximum value at the base of the hot wall to its minimum value on the tip of the hot wall. The domain inside the parallelogrammical cavity has fetcher of the similarity with the hot and cold walls in height, width, skew angle and all other shape parameters.

While the other cavities are not the same. Where there are regions below and above the height of the hot and cold walls. These different

and unique shapes created the shown behavior for the local (Nu). The reason of the mentioned behavior is that, the parallelogrammical cavity needs the little part of the hot wall that close to the base wall to propagate the flow and enforce the gravity effect and overcome it. So, the maximum peak local (Nu) lates an appearing till distance about (0.1L-0.4L) from the base according to the working (Ra) case.

In the other cavities, the region wanted to propagate the flow and overcome the gravity is already exist below the level of the hot wall. So, the maximum peak of the local (Nu) initiated earlier at the base point of the hot wall for all the considered (Ra) range. The peak local (Nu) of the hexagonal, octagonal and elliptical cavities at ($Ra=10^6$ and $\varphi=0.05$) are about (5.5, 5.5 and 6.8) times that of parallelogrammical cavity at the same conditions, respectively.

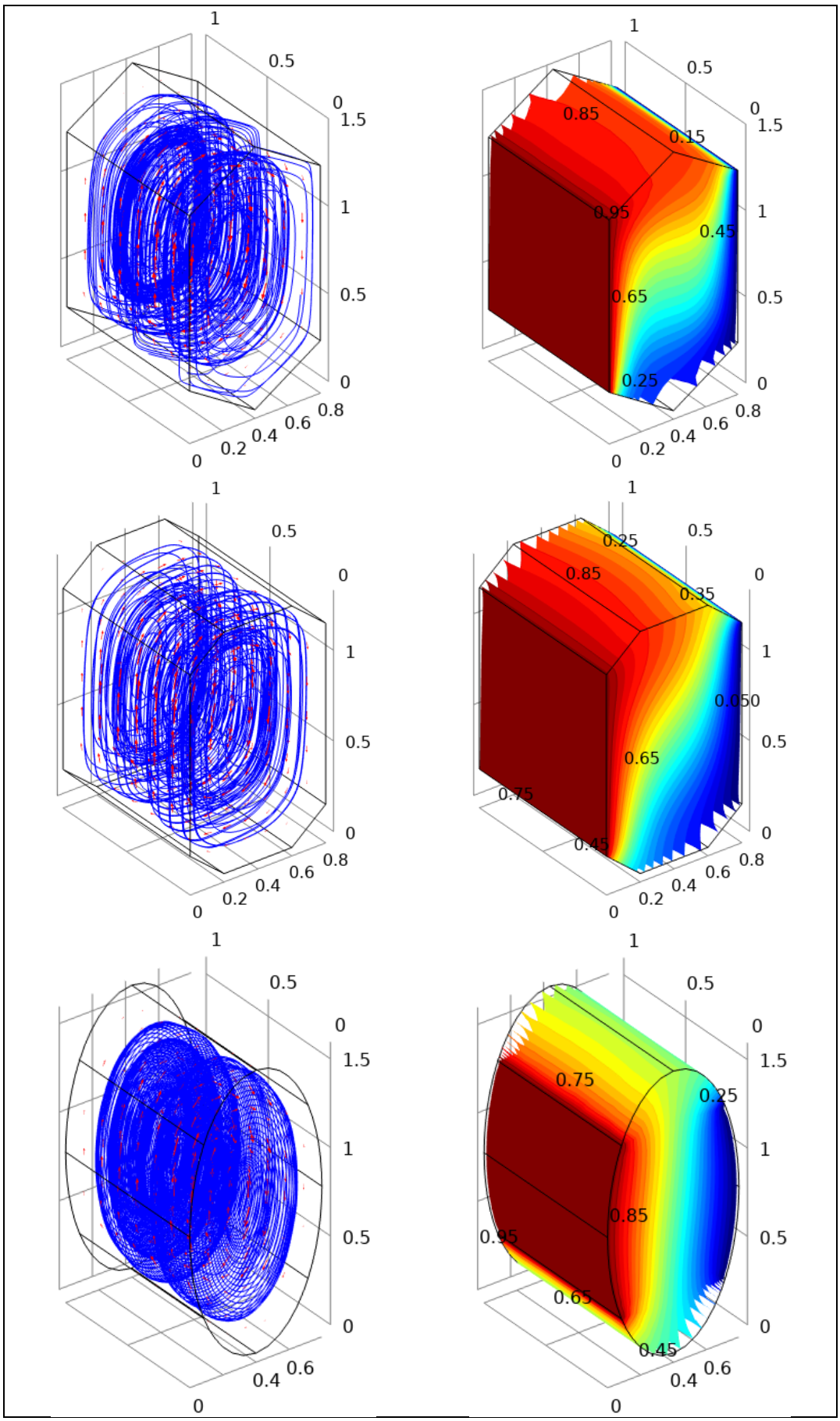

Figure (5.32): 3D streamlines and temperature iso-surfaces for the hexagonal, octagonal and elliptical cavities with (φ=0.05, Ra=10^4).

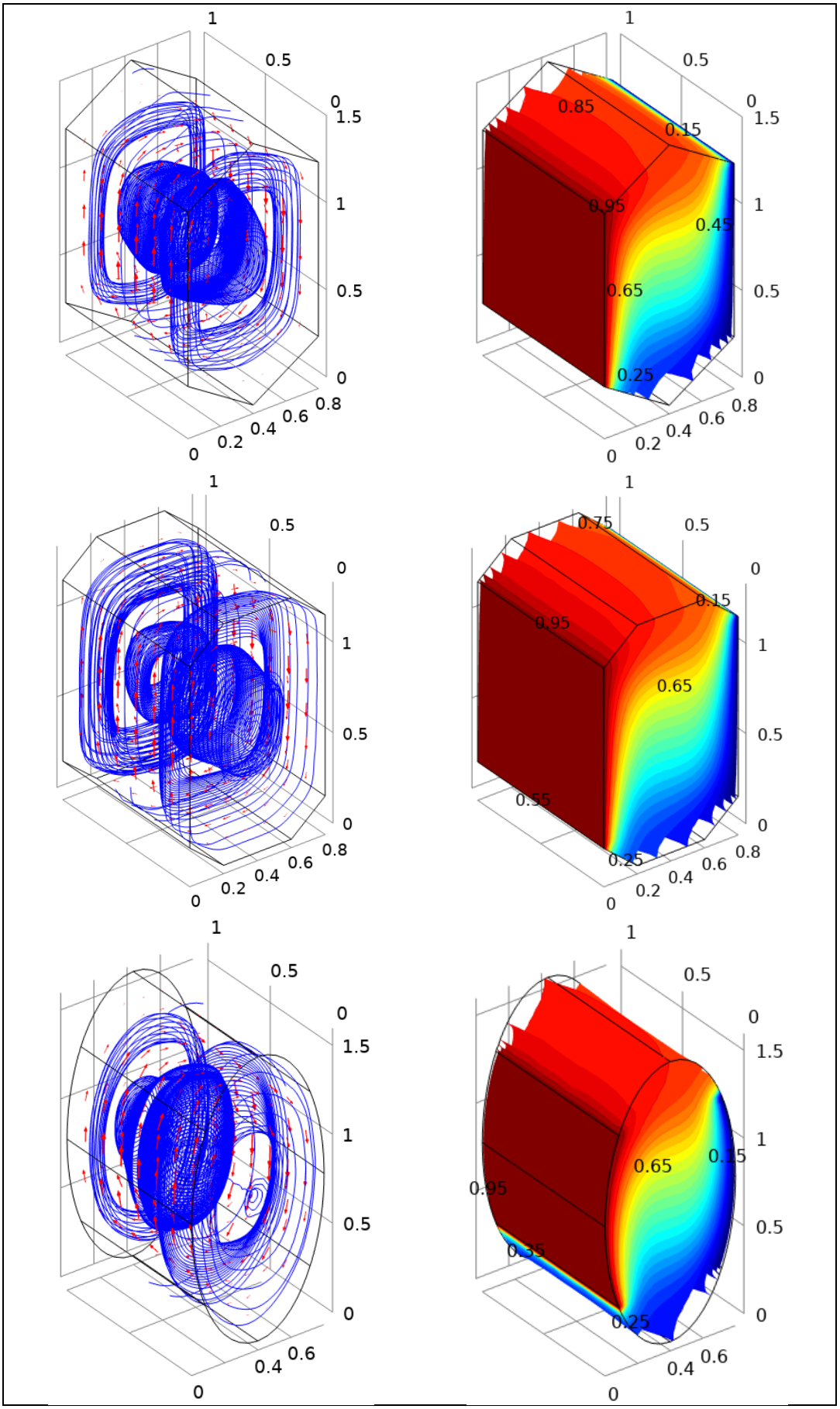

Figure (5.33): 3D streamlines and temperature iso-surfaces for the hexagonal, octagonal and elliptical cavities with (φ=0.05, Ra=10^5).

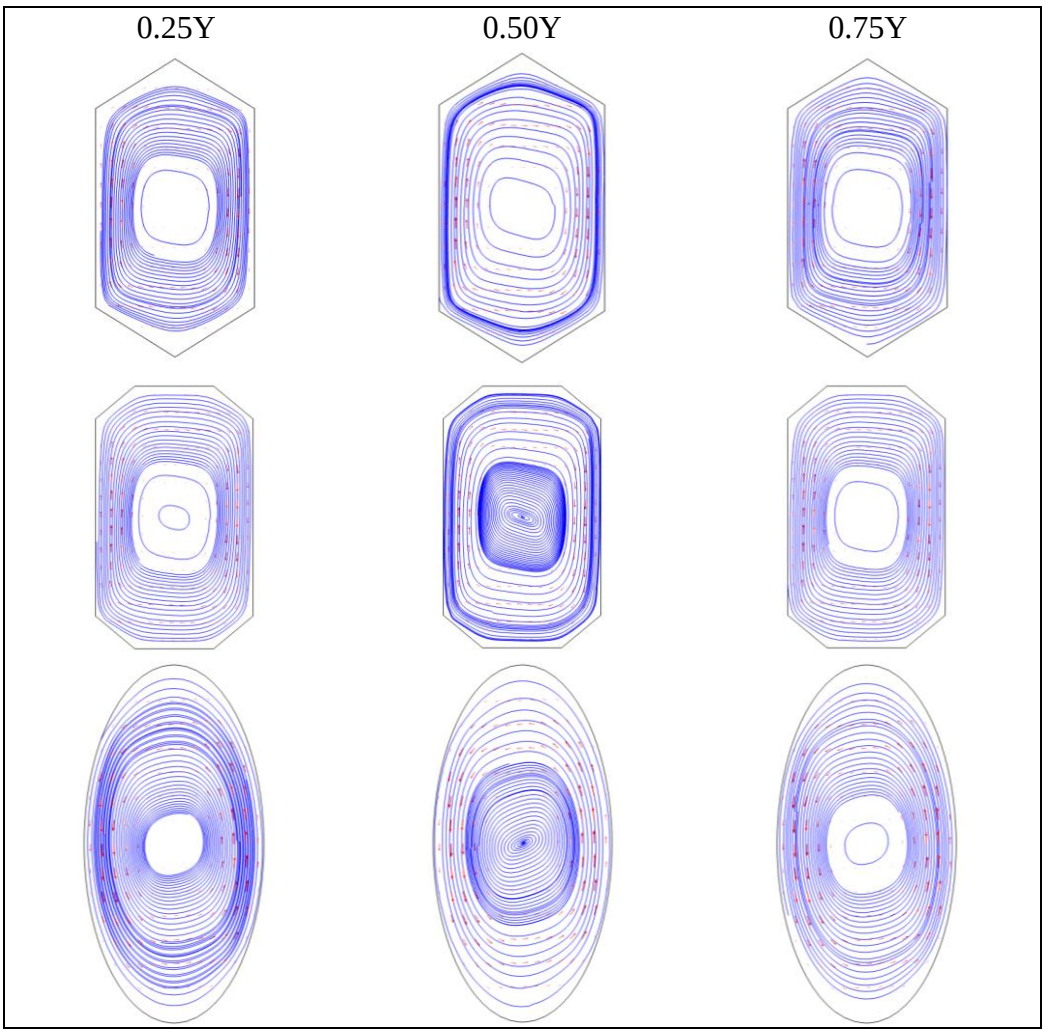

Figure (5.34): 2D projection of the streamlines on different planes in (X-Z) for the hexagonal, octagonal and elliptical cavities with (φ=0.05, Ra=10^5).

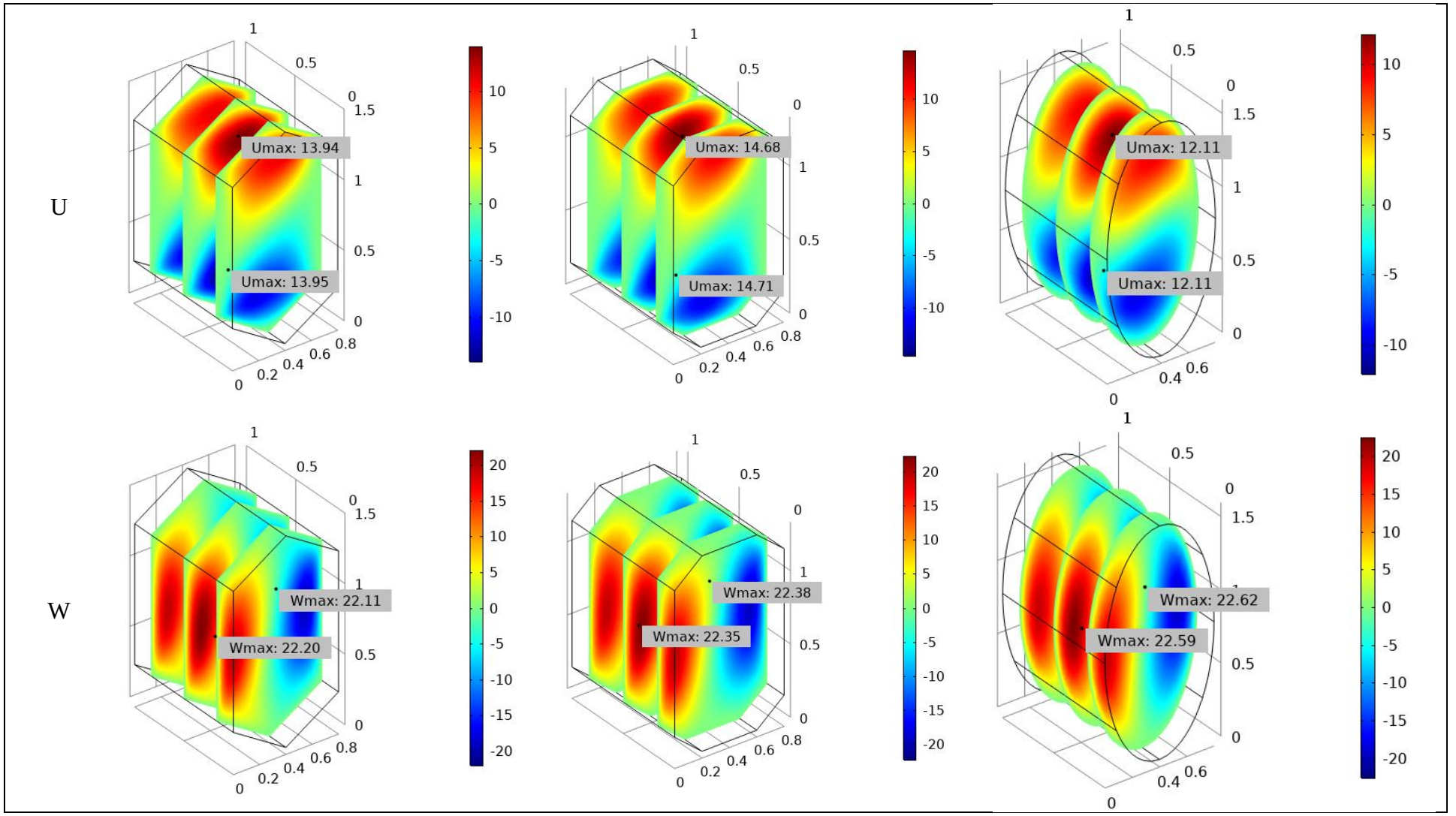

Figure (5.35): 3D horizontal velocity (U) and vertical velocity (W) surfaces for the hexagonal, octagonal and elliptical cavities with (φ=0.05, Ra=10^4).

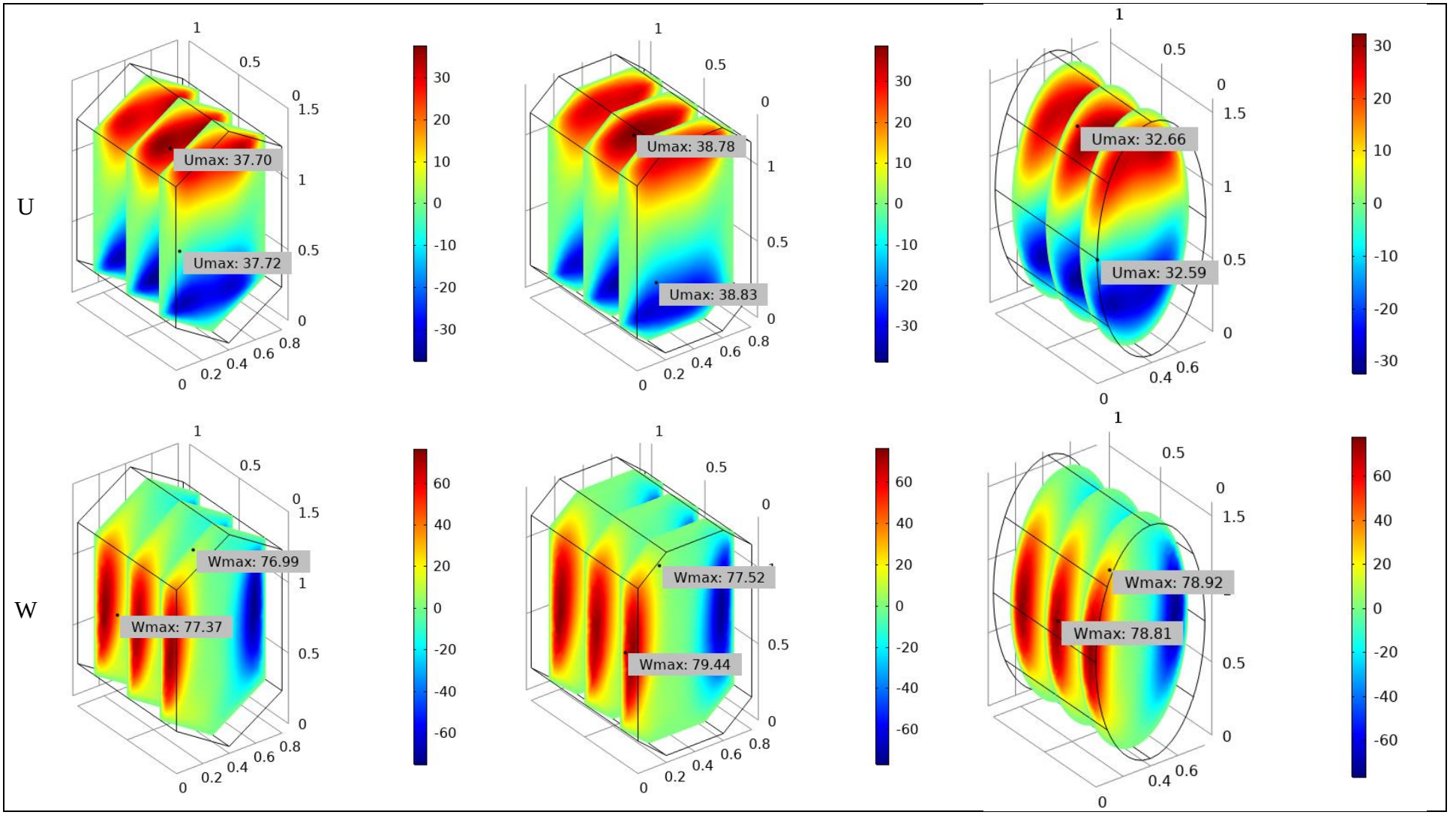

Figure (5.36): 3D horizontal velocity (U) and vertical velocity (W) surfaces for the hexagonal, octagonal and elliptical cavities with (φ=0.05, Ra=10^5).

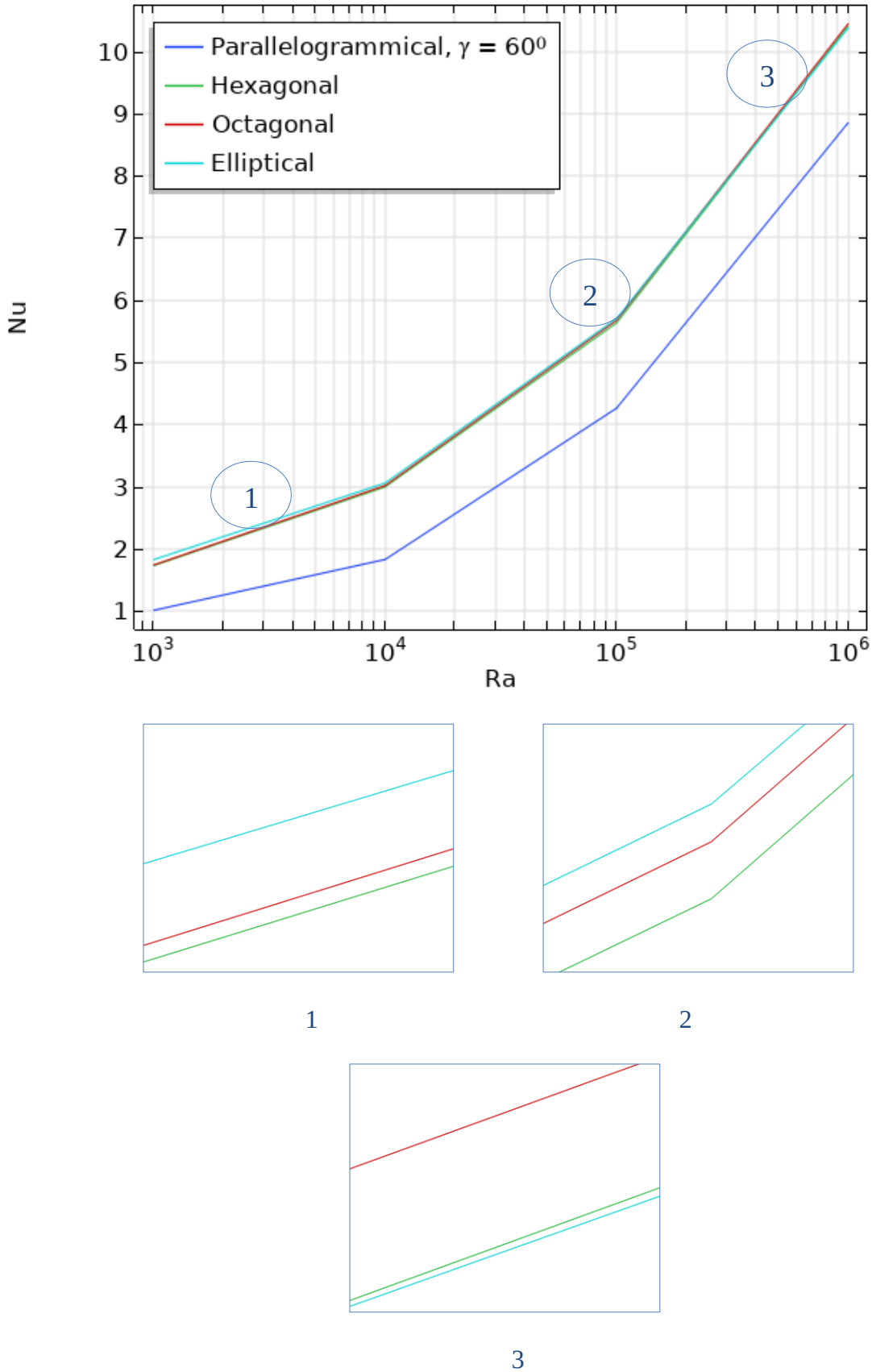

Figure (5.37): The average (Nu) on the left hot wall versus (Ra) for the parallelogrammical, hexagonal, octagonal and elliptical cavities at (φ=0.05).

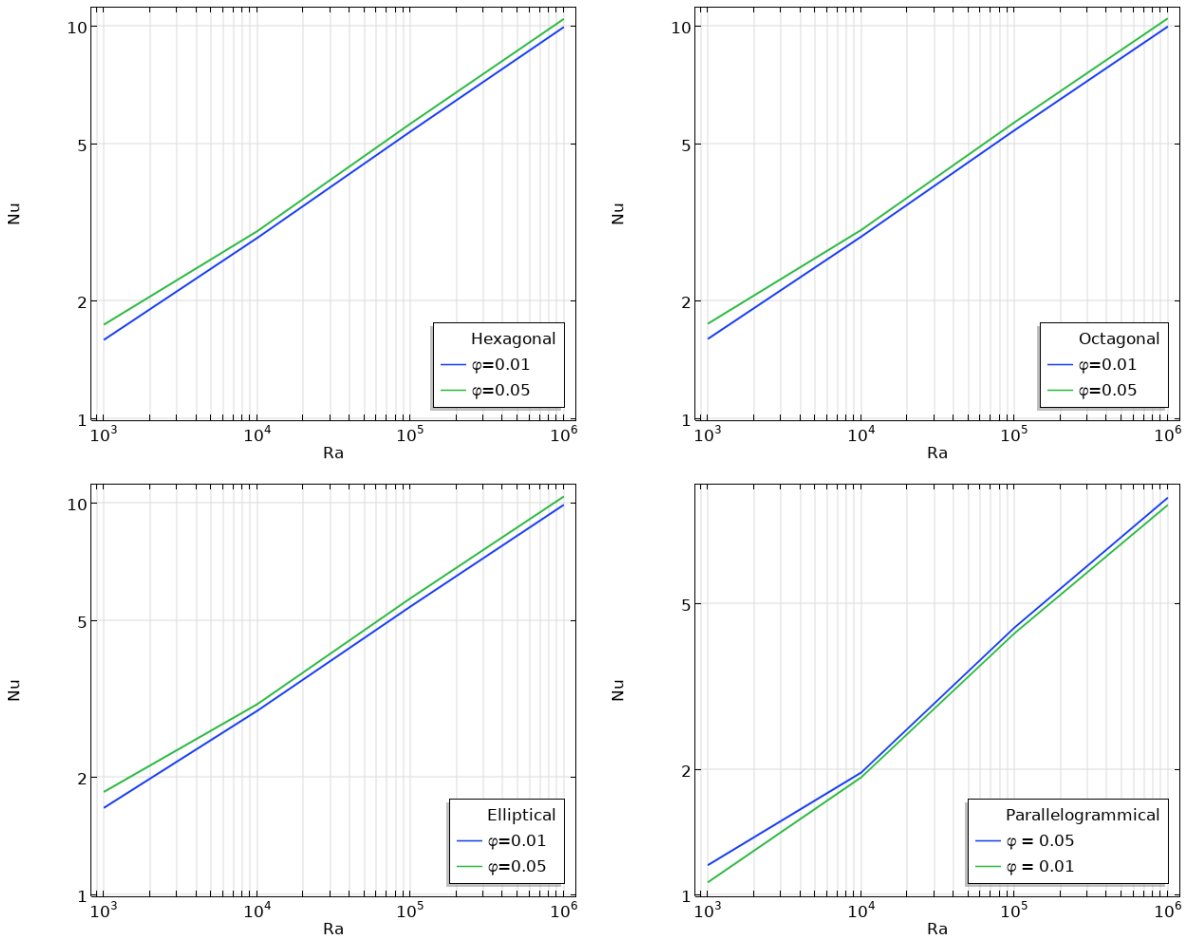

Figure (5.38): The average (Nu) on the left hot wall versus (Ra) for the hexagonal, octagonal, elliptical and parallelogrammical cavities at (φ=0.01 and 0.05).

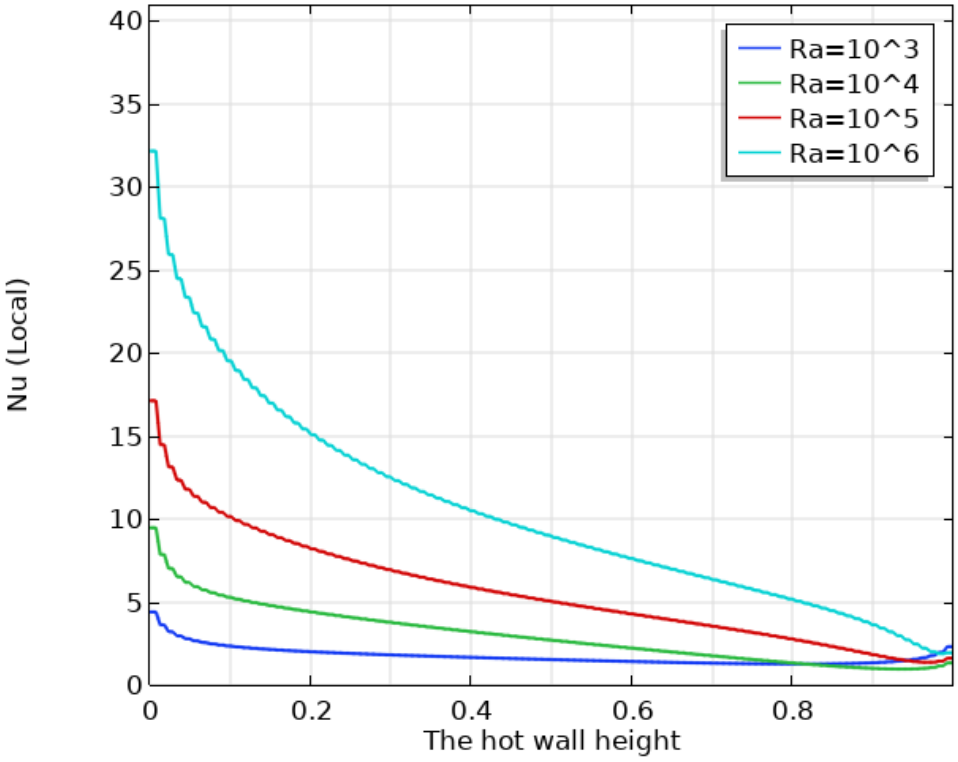

a. Hexagonal

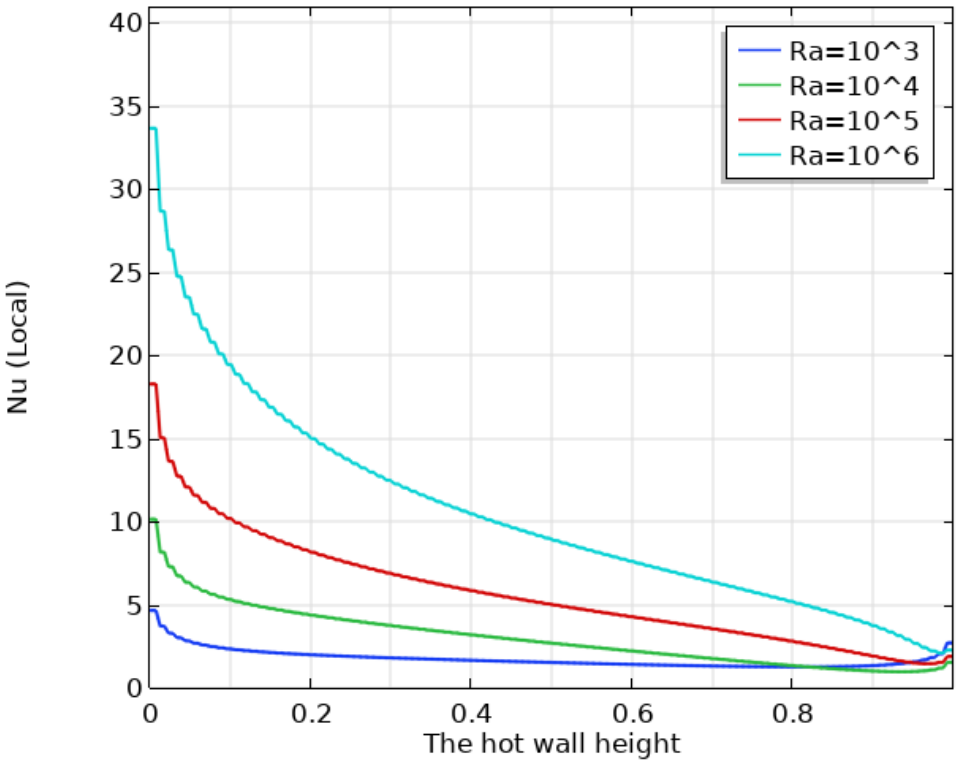

b. Octagonal

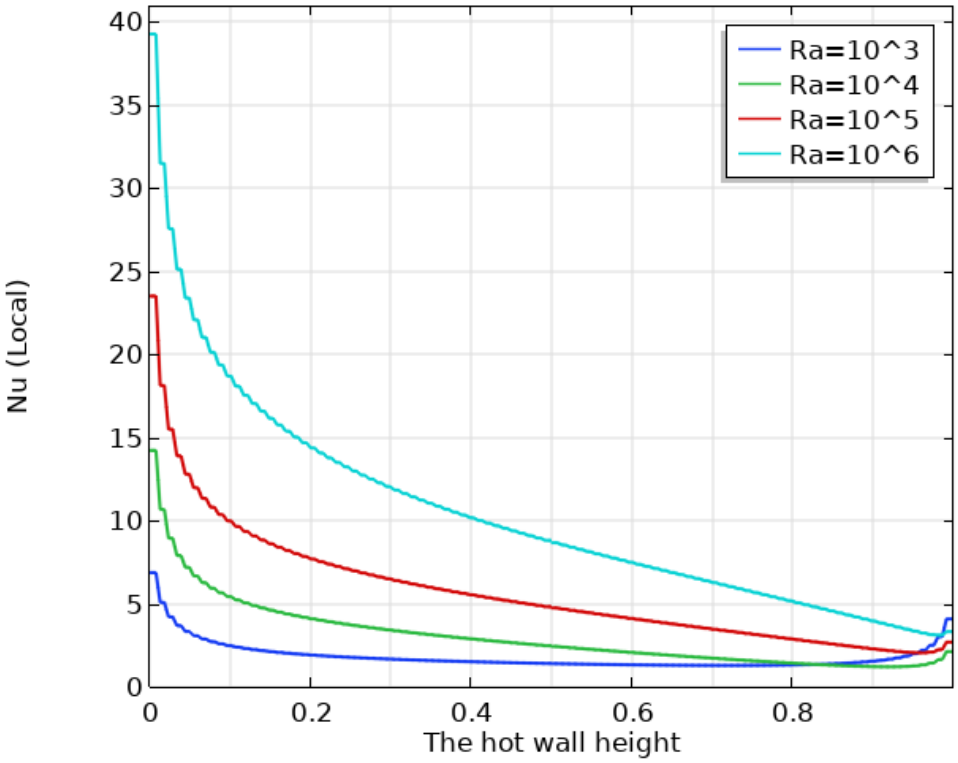

c. Elliptical

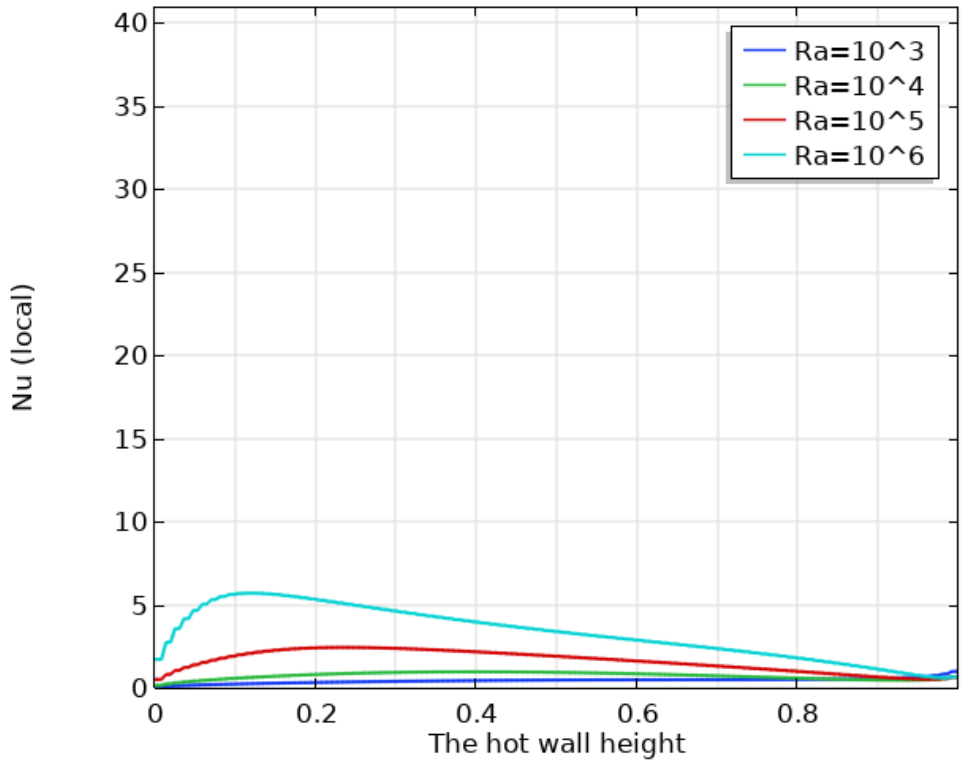

d. Parallelogrammical

Figure (5.39): The local (Nu) on the central height of left hot wall versus (Ra) for the hexagonal, octagonal, elliptical and parallelogrammical cavities at (φ=0.05).

5. 4. The Experimental Results

The parallelogrammical cavity at (γ=60º) is designed and visualized experimentally as described in Chapter Four. Three solid volume fraction concentrations (φ=0.01, 0.03 and 0.05) are considered. Two temperature difference between the hot and cold walls are considered (ΔT=16ºC and 26ºC) which are opposite to ($10^5 \leq Ra \leq 10^6$) as presented in Appendix D. These differences are analyzed for two different cold wall temperature cases which are (T_c=28ºC and 30ºC).

The results are represented by the dimensionless local temperature (θ) distribution along the three dimensions (X, Y and Z) and the average (Nu) on the left hot wall. The results are compared with the related numerical results.

5.4.1. The Temperature Distribution Along the Axis (X, Y, Z)

Figs. (5.40) and (5.41) are presented the dimensionless local temperature (θ) distribution along the central width (X-axis) that located on the plane (Y=0.5) and the center of height (Z) experimentally and numerically. The plots for both the temperature differences (ΔT=16ºC and 26ºC) exhibit nearly a good matching between the numerical and experimental data. Observing that (θ) drops to the half at a distance of about (0.1L-0.3L) from the left hot wall. Then stay constant for the distance from (0.3L-0.7L) where a stagnant region is formed. From (0.7L-L), the temperature drops linearly again.

The dimensionless local temperature (θ) distribution along the central inclined height (Z-axis) that parallel to the hot and cold inclined walls on the planes (X=0.5 and Y=0.5) is presented experimentally and numerically for all the values of (φ) in **Figs**. (5.42) and (5.43). Accepted agreement between results was noticed for both the temperature differences. The (θ) increases approximately linear from the base wall to reach maximum at the upper wall.

Also, (θ) distribution along the back central depth is presented in **Figs**. (5.44) and (5.45) experimentally and numerically. The values of (θ) are nearly steady and constant along the depth, which is meaning that the flow is symmetrical and returned in identical circulations along this depth. The same behaviors are seen for various values of (T_c) and (ΔT).

The results of (θ) for (T_c=30ºC) are generally higher than the case of (T_c=28ºC) for both cases of (ΔT). This behavior is due to the very little difference between the temperature (T_c) and the surrounding ambient temperature, which decreasing the energy needed to overcome this difference initially. But, the difference between these cases being

slight by increasing (φ) because of the higher thermal content of the particles which absorb the energy of the cold wall so decreasing the difference from the ambient temperature. It is clear at (φ=0.01) but slight at (φ=0.05). As like as, being slight by increasing (ΔT). It appeared clearly at (ΔT=16ºC) compared to the case of (ΔT=26ºC).

Concluding that increasing the cold wall temperature for the same temperature difference resulting of enhancement in transferred temperature because of the higher difference in temperature between the hot and cold wall making the initial effect of (T_c) is very little. At the same time, it decreases the cost of cooling by depending on the ambient temperature.

5.4.2. The Average Nusselt Number Along the Hot Wall

The average (Nu) on the left hot wall is presented in **Fig**. (5.46) both experimentally and numerically for the two considered cases of (T_c). For both results, the average (Nu) is enhanced with the increase in (Ra) and (φ). This enhancement is better at (T_c=30ºC) due to the temperature behavior that mentioned in the previous section. At (ΔT=16ºC), the enhancement over the (T_c=28ºC) case are (0.78%, 0.82% and 0.75%) at (φ=0.01, 0.03 and 0.05) respectively. While it is (0.86%, 0.82% and 0.83%) at (ΔT=26ºC).

Generally, the increase in (T_c) by (2ºC) causing an increase in the average (Nu) by about (0.8%) for all the considered parameters and specifications of the current study. Also, increasing (φ) from (0.01 to 0.05) increasing the average (Nu) by about (3.1%-3.6%) for all considered cases.

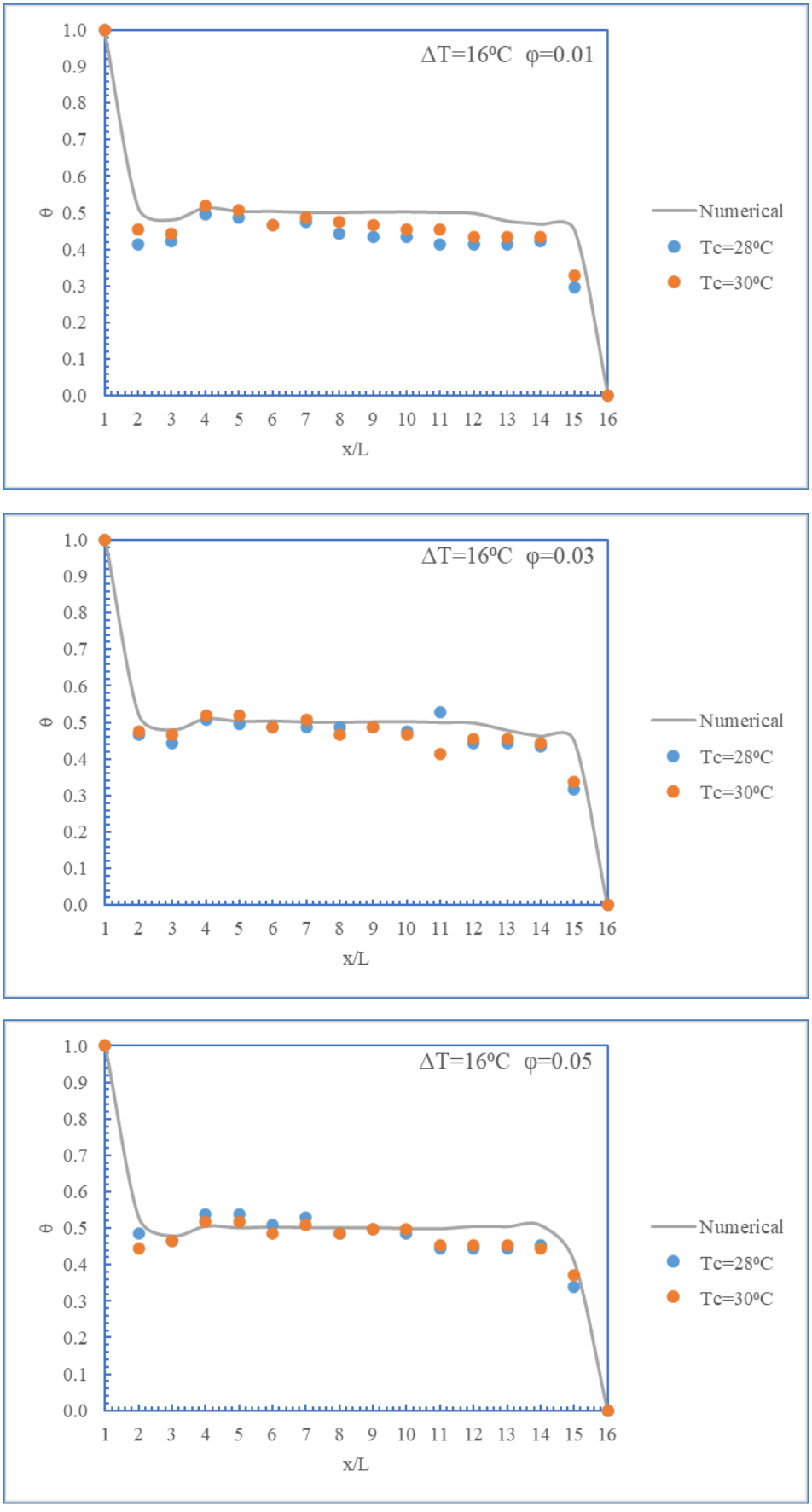

Figure (5.40): The experimental and numerical local dimensionless temperature of local (θ) distribution along the central width (X) for the parallelogrammical cavity at (γ=60º) and (ΔT=16ºC) for various values of (φ).

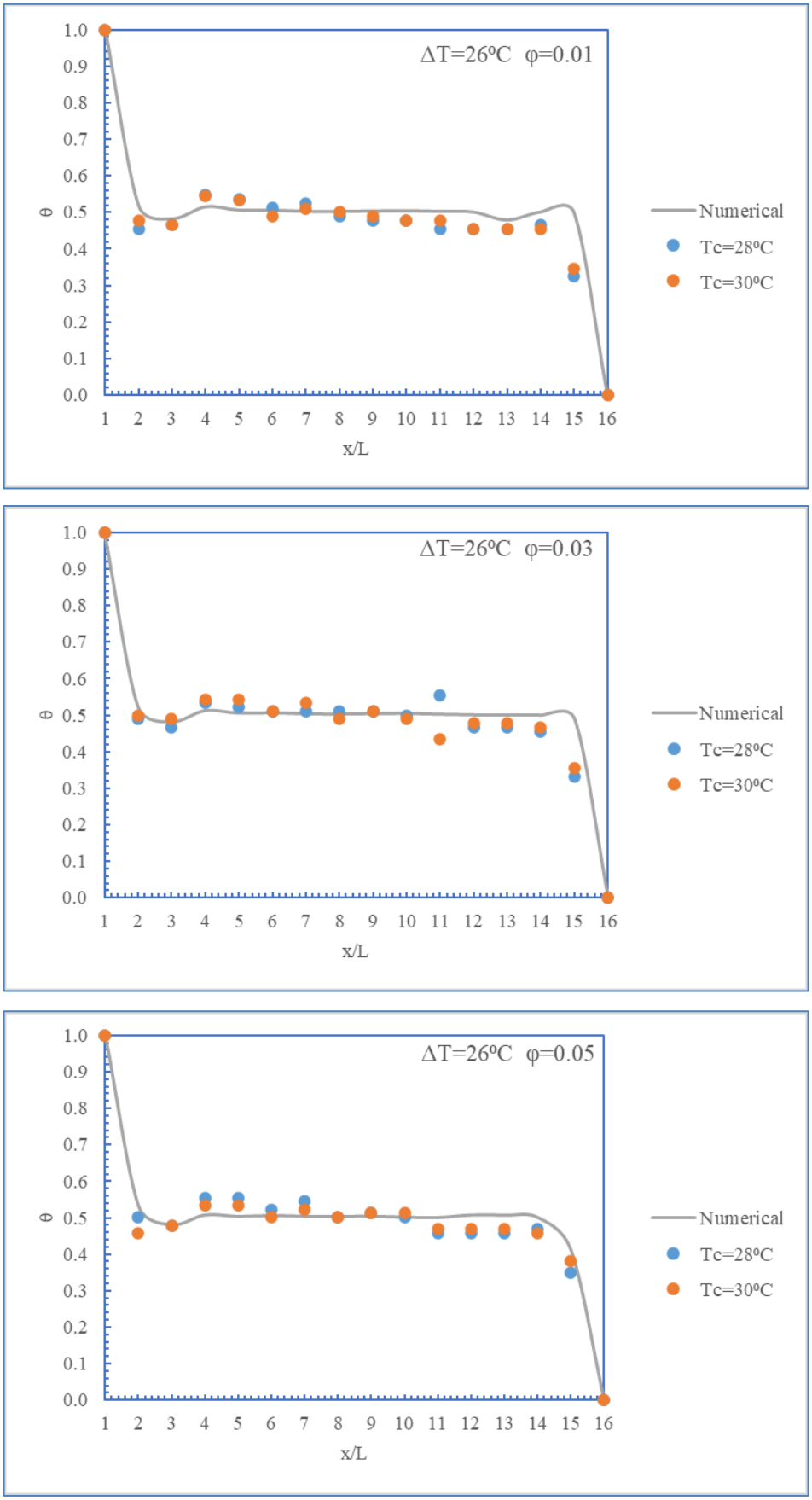

Figure (5.41): The experimental and numerical local dimensionless temperature of local (θ) distribution along the central width (X) for the parallelogrammical cavity at (γ=60º) and (ΔT=26ºC) for various values of (φ).

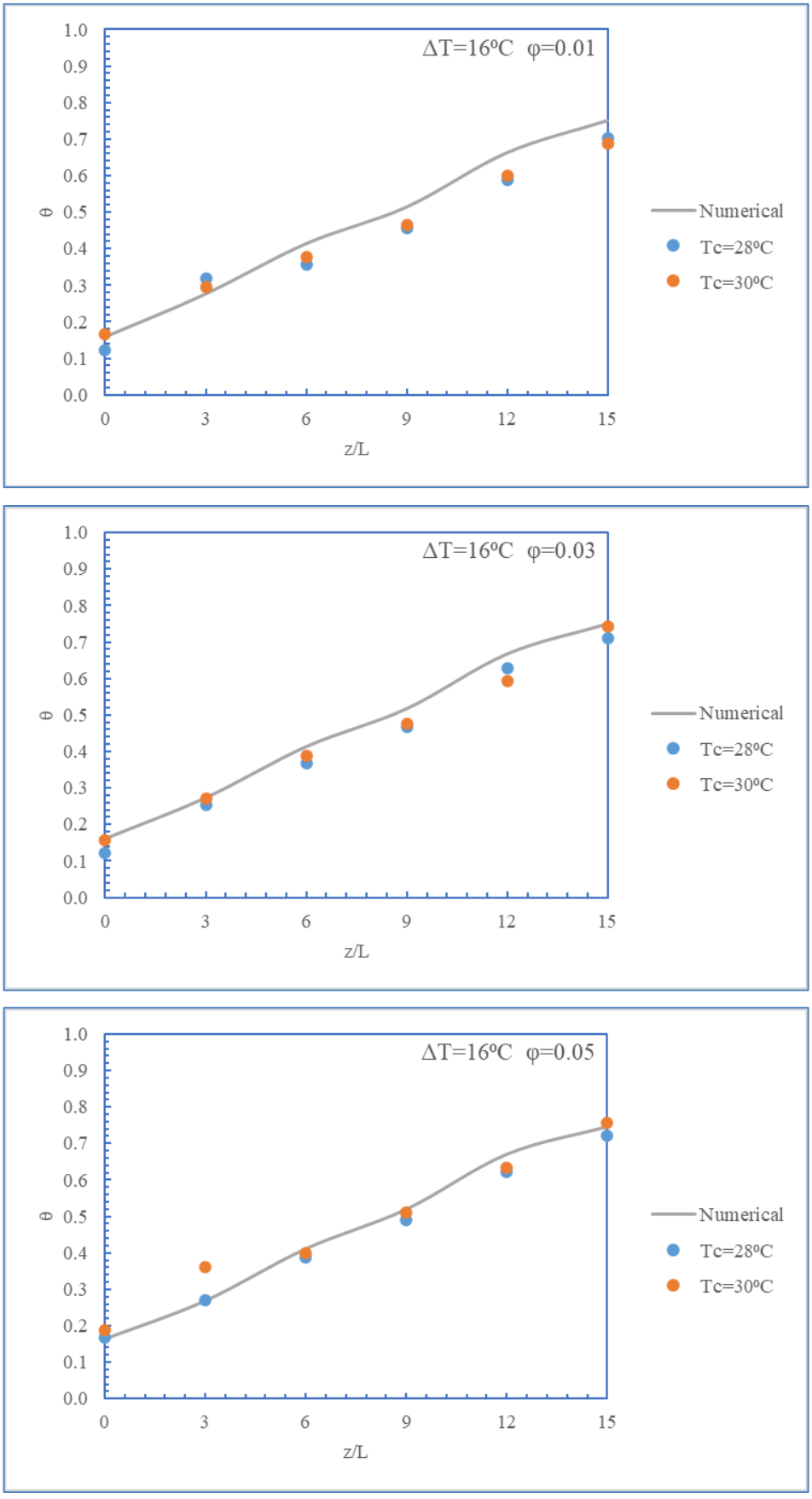

Figure (5.42): The experimental and numerical local dimensionless temperature of local (θ) distribution along the central height (Z) for the parallelogrammical cavity at (γ=60º) and (ΔT=16ºC) for various values of (φ).

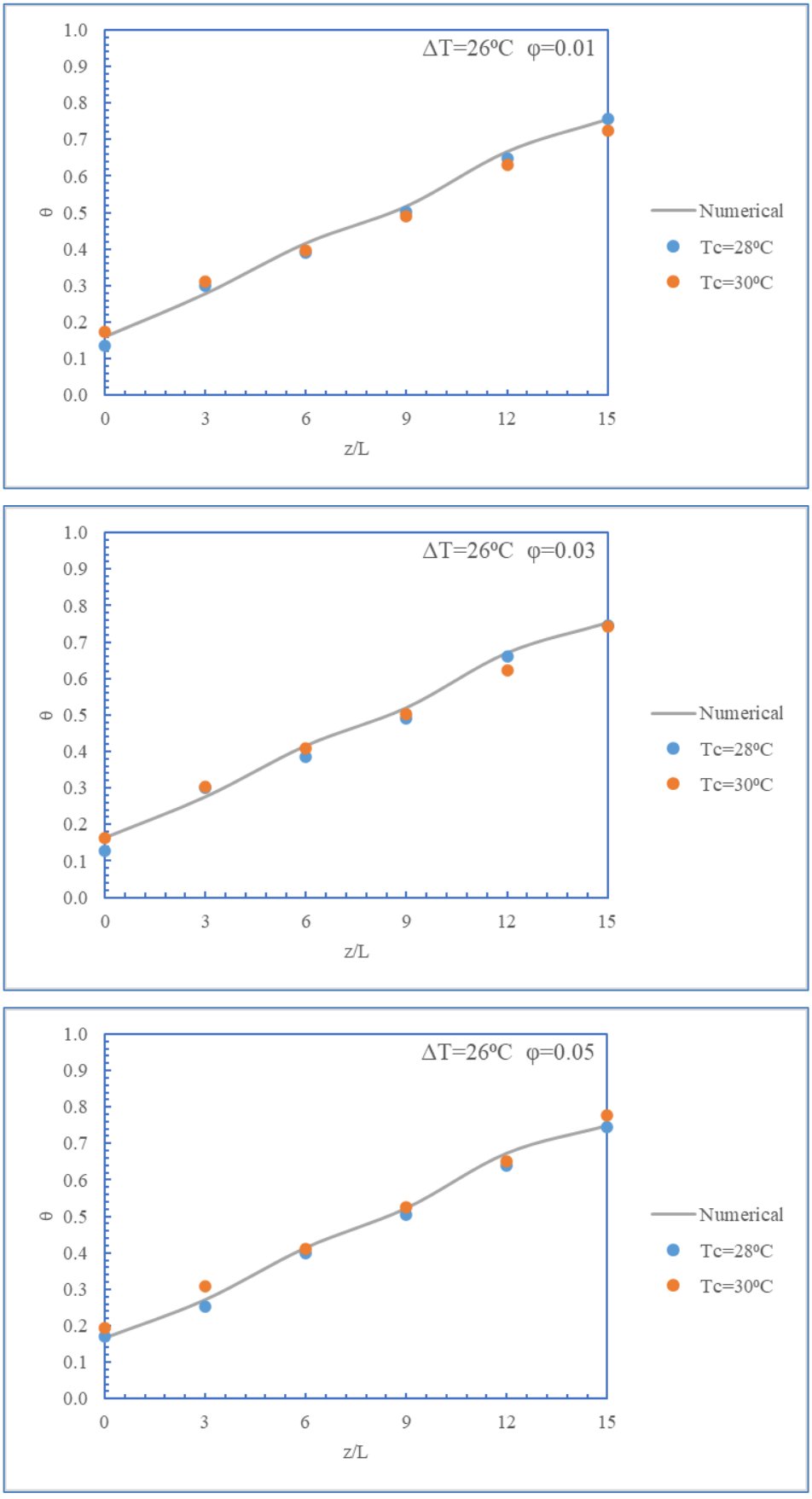

Figure (5.43): The experimental and numerical local dimensionless temperature of local (θ) distribution along the central height (Z) for the parallelogrammical cavity at (γ=60º) and (ΔT=26ºC) for various values of (φ).

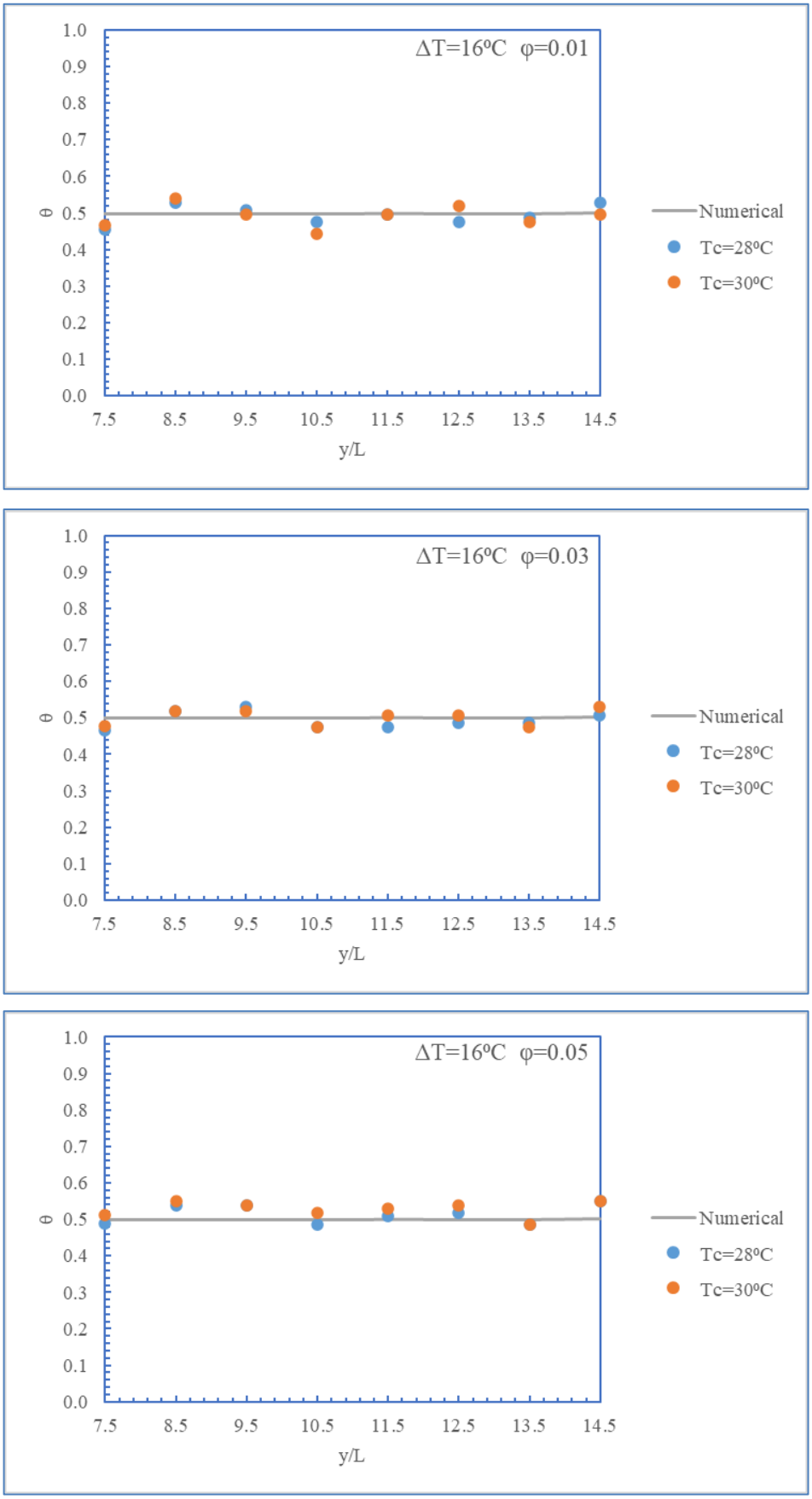

Figure (5.44): The experimental and numerical local dimensionless temperature of local (θ) distribution along the central back depth (Y) for the parallelogrammical cavity at (γ=60º) and (ΔT=16ºC) for various values of (φ).

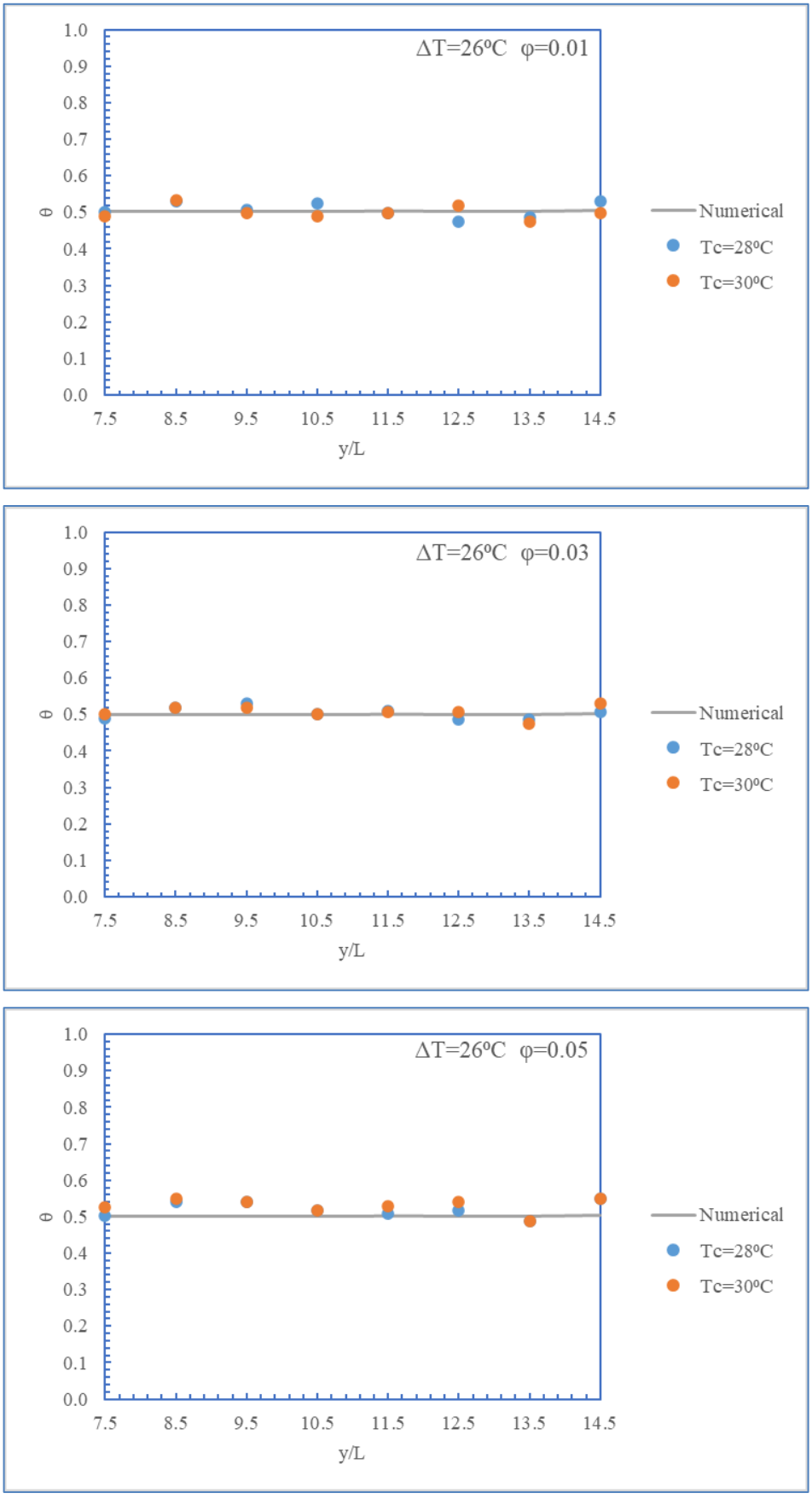

Figure (5.45): The experimental and numerical local dimensionless temperature of local (θ) distribution along the central back depth (Y) for the parallelogrammical cavity at (γ=60º) and (ΔT=26ºC) for various values of (φ).

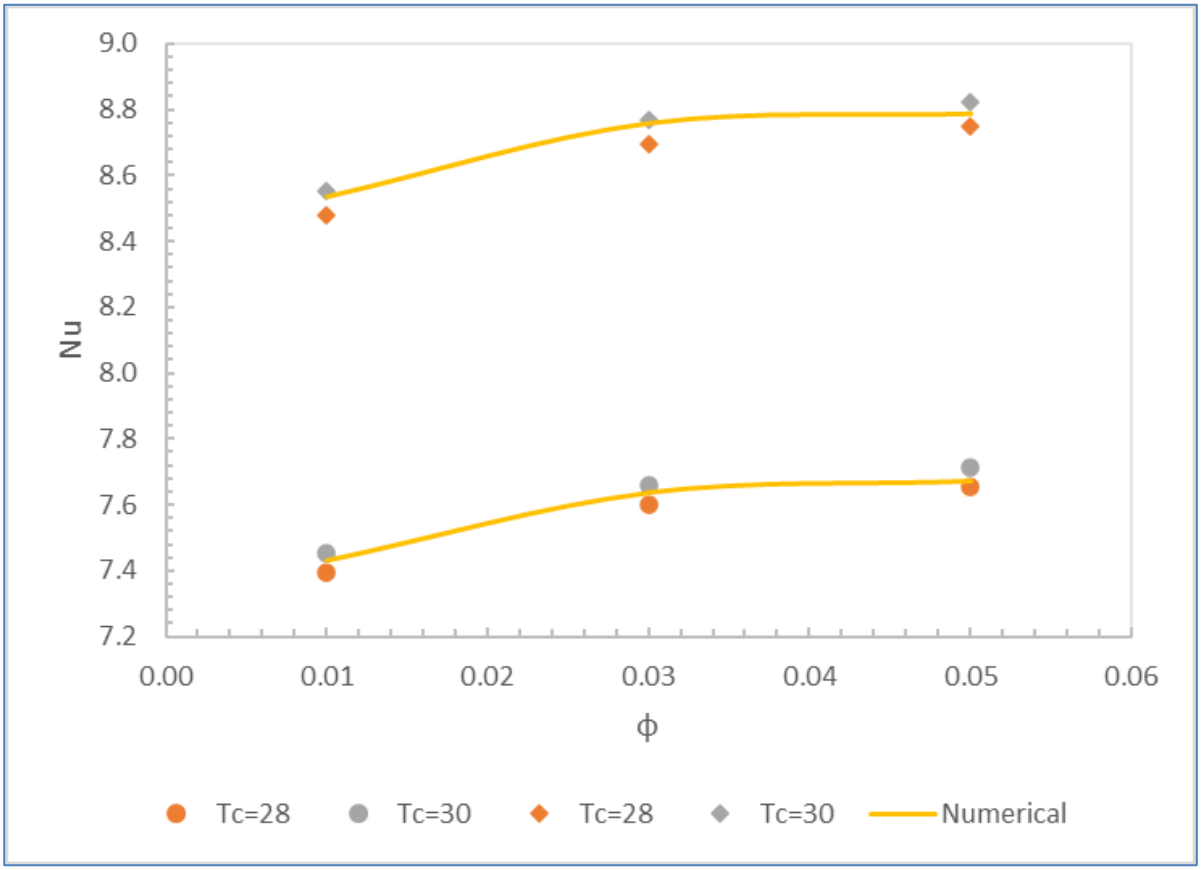

Figure (5.46): The experimental and numerical average (Nu) at the left hot wall for the parallelogrammical cavity at (γ=60º).

Chapter Six: Conclusions and Recommendations for Future Work

6.1. Conclusions

Based on the obtained results, some important conclusions can be presented as follows:

1. The heated left vertical wall case is the more suitable one to improve the natural convection for the selected geometries.
2. The ($\gamma=60^{o}$) of the parallelogrammical cavity is introducing the best convection enhancement.
3. For all the considered cavities, the average (Nu) on the hot wall are enhanced with (Ra) and (φ) augmentation.
4. For parallelogrammical cavity, the average (Nu) increases by about (13) times with increasing the solid volume fraction from ($\varphi=0$ to $\varphi=0.05$) at ($Ra=10^{6}$). While, the local (Nu) increases by about (10) times at all (Ra) range.
5. The higher average (Nu) is recorded for the cavities with higher number of walls and heights; hexagonal, octagonal and elliptical comparing to the parallelogrammical cavity. It was respectively, about (17.6%, 18% and 17.2%) at ($Ra=10^{6}$).
6. The increase in the number of inners by increasing their surface area for the same volume can be considered a good technique to enhance the flow field inside cavities.

7. The triple inners have twice the enhancement in the average (Nu) over the single inner.
8. The experimental local dimensionless temperature (θ) along the cavity axes at (T_c=30ºC) is higher than that at (T_c=28ºC) for both cases of temperature difference (ΔT=16ºC and 26ºC). This difference in temperature decreases with increasing (φ) and (Ra or ΔT) between the hot and cold walls.
9. The experimentally computed average (Nu) is enhanced with the increase in (Ra) and (φ). This enhancement is better for (T_c=30ºC) case.
10. There is good agreement between the numerical and experimental results.

6.2. Recommendations for Future Work

The following recommendations are useful for future work:

- Investigating experimentally and numerically the natural convection inside cavities filled with hybrid nanofluid.

- Studying the effect of supplying an external magnetic field (MHD).

- Investigating the effect of porous medium inside the considered cavities.

- Studying the entropy generation.

References

1. A. Baïri, E. Zarco-Pernia, and J. M. García De María, “A review on natural convection in enclosures for engineering applications. the particular case of the parallelogrammic diode cavity,” Applied Thermal Engineering, vol. 63, no. 1. Elsevier Ltd, pp. 304–322, Feb. 05, 2014. http://doi: 10.1016/j.applthermaleng.2013.10.065
2. D. Das, M. Roy, and T. Basak, “Studies on natural convection within enclosures of various (non-square) shapes – A review,” International Journal of Heat and Mass Transfer, vol. 106. Elsevier Ltd, pp. 356–406, Mar. 01, 2017. http://doi: 10.1016/j.ijheatmasstransfer.2016.08.034.
3. F. Mebarek-Oudina and I. Chabani, “Review on Nano-Fluids Applications and Heat Transfer Enhancement Techniques in Different Enclosures,” Journal of Nanofluids, vol. 11, no. 2, pp. 155–168, Mar. 2022. http://doi: 10.1166/jon.2022.1834.
4. S. Rostami et al., “A review on the control parameters of natural convection in different shaped cavities with and without nanofluid,” Processes, vol. 8, no. 9. MDPI AG, Sep. 01, 2020. http://doi: 10.3390/pr8091011.
5. O. M. Kamiyo, D. Angeli, G. S. Barozzi, M. W. Collins, V. O. S. Olunloyo, and S. O. Talabi, “A comprehensive review of natural convection in yriangular enclosures,” Applied Mechanics Reviews, vol. 63, no. 6. 2010. http://doi: 10.1115/1.4004290.
6. O. Aydin and W.-J. Yang, “Natural convection in enclosures with localized heating from below and symmetrical cooling from sides,” #MCB University Press, 2000.

7. M. Keyhani, V. Prasad, and R. Cox, “An Experimental Study of Natural Convection in a Vertical Cavity With Discrete Heat Sources,” J Heat Transfer, vol. 110, no. 3, pp. 616–624, 1988. http://doi: 10.1115/1.3250537.
8. S. Chakraborty and P. K. Panigrahi, “Stability of nanofluid: A review,” Applied Thermal Engineering, vol. 174. Elsevier Ltd, Jun. 25, 2020. http://doi: 10.1016/j.applthermaleng.2020.115259.
9. I. M. Shahrul, I. M. Mahbubul, S. S. Khaleduzzaman, R. Saidur, and M. F. M. Sabri, “A comparative review on the specific heat of nanofluids for energy perspective,” Renewable and Sustainable Energy Reviews, vol. 38. Elsevier Ltd, pp. 88–98, 2014. http://doi: 10.1016/j.rser.2014.05.081.
10. M. H. Ahmadi, M. Alhuyi Nazari, R. Ghasempour, H. Madah, M. B. Shafii, and M. A. Ahmadi, “Thermal conductivity ratio prediction of Al2O3/water nanofluid by applying connectionist methods,” Colloids Surf A Physicochem Eng Asp, vol. 541, pp. 154–164, Mar. 2018. http://doi: 10.1016/J.COLSURFA.2018.01.030.
11. L. Yang, J. Xu, K. Du, and X. Zhang, “Recent developments on viscosity and thermal conductivity of nanofluids,” Powder Technol, vol. 317, pp. 348–369, Jul. 2017. http://doi: 10.1016/J.POWTEC.2017.04.061.
12. A. K. Hussein and A. W. Mustafa, “Natural convection in fully open parallelogrammic cavity filled with Cu–water nanofluid and heated locally from its bottom wall,” Thermal Science and Engineering Progress, vol. 1, pp. 66–77, Mar. 2017. http://doi: 10.1016/j.tsep.2017.03.002.
13. C. Qi, G. Wang, L. Yang, Y. Wan, and Z. Rao, “Two-phase lattice Boltzmann simulation of the effects of base fluid and nanoparticle size on natural convection heat transfer of nanofluid,” Int J Heat Mass Transf, vol. 105, pp. 664–672, Feb. 2017. http://doi: 10.1016/j.ijheatmasstransfer.2016.10.043.
14. F. Selimefendigil, “Natural convection in a trapezoidal cavity with an inner conductive object of different shapes and filled with nanofluids of different nanoparticle shapes,” Iranian Journal of Science and Technology -

Transactions of Mechanical Engineering, vol. 42, no. 2, pp. 169–184, 2018. http://doi: 10.1007/s40997-017-0083-3.

15. B. Chahrazed and R. Samir, “Simulation of heat transfer in a square cavity with two fins attached to the hot wall,” in Energy Procedia, 2012, vol. 18, pp. 1299–1306. http://doi: 10.1016/j.egypro.2012.05.147.
16. A. Elatar, M. A. Teamah, and M. A. Hassab, “Numerical study of laminar natural convection inside square enclosure with single horizontal fin,” International Journal of Thermal Sciences, vol. 99, pp. 41–51, Jan. 2016. http://doi: 10.1016/j.ijthermalsci.2015.08.003.
17. N. H. Saeid, “Natural Convection in a Square Cavity with Discrete Heating at the Bottom with Different Fin Shapes,” Heat Transfer Engineering, vol. 39, no. 2, pp. 154–161, Jan. 2018. http://doi: 10.1080/01457632.2017.1288053.
18. A. Keyhani Asl, S. Hossainpour, M. M. Rashidi, M. A. Sheremet, and Z. Yang, “Comprehensive investigation of solid and porous fins influence on natural convection in an inclined rectangular enclosure,” Int J Heat Mass Transf, vol. 133, pp. 729–744, Apr. 2019. http://doi: 10.1016/j.ijheatmasstransfer.2018.12.156.
19. W. Safiei, M. M. Rahman, R. Kulkarni, M. N. Ariffin, and Z. A. Abd Malek, “Thermal conductivity and dynamic viscosity of nanofluids: A review,” Journal of Advanced Research in Fluid Mechanics and Thermal Sciences, vol. 74, no. 2. Penerbit Akademia Baru, 2020. http://doi: 10.37934/ARFMTS.74.2.6684.
20. S. M. S. Murshed, M. Sharifpur, S. Giwa, and J. P. Meyer, “Experimental research and development on the natural convection of suspensions of nanoparticles—a comprehensive review,” Nanomaterials, vol. 10, no. 9. MDPI AG, pp. 1–35, Sep. 01, 2020. http://doi: 10.3390/nano10091855.
21. L. Kolsi et al., “Numerical investigation of combined buoyancy-thermocapillary convection and entropy generation in 3D cavity filled with

Al2O3 nanofluid," Alexandria Engineering Journal, vol. 56, no. 1, pp. 71–79, Mar. 2017. http://doi: 10.1016/j.aej.2016.09.005.

22. A. Rahimi, A. Kasaeipoor, E. Hasani Malekshah, M. M. Rashidi, and A. Purusothaman, "Lattice Boltzmann simulation of 3D natural convection in a cuboid filled with KKL-model predicted nanofluid using Dual-MRT model," Int J Numer Methods Heat Fluid Flow, vol. 29, no. 1, pp. 365–387, Jan. 2019. http://doi: 10.1108/HFF-07-2017-0262.
23. M. Hemmat Esfe, R. Barzegarian, and M. Bahiraei, "A 3D numerical study on natural convection flow of nanofluid inside a cubical cavity equipped with porous fins using two-phase mixture model," Advanced Powder Technology, vol. 31, no. 6, pp. 2480–2492, Jun. 2020. http://doi: 10.1016/j.apt.2020.04.012.
24. A. M. Rashad, M. M. Rashidi, G. Lorenzini, S. E. Ahmed, and A. M. Aly, "Magnetic field and internal heat generation effects on the free convection in a rectangular cavity filled with a porous medium saturated with Cu–water nanofluid," Int J Heat Mass Transf, vol. 104, pp. 878–889, Jan. 2017. http://doi: 10.1016/j.ijheatmasstransfer.2016.08.025.
25. M. Bouabid, M. Magherbi, N. Hidouri, and A. B. Brahim, "Entropy generation at natural convection in an inclined rectangular cavity," Entropy, vol. 13, no. 5, pp. 1020–1033, 2011. http://doi: 10.3390/e13051020.
26. M. Bouabid, N. Hidouri, M. Magherbi, and A. B. Brahim, "Analysis of the magnetic field effect on entropy generation at thermosolutal convection in a square cavity," Entropy, vol. 13, no. 5, pp. 1034–1054, 2011. http://doi: 10.3390/e13051034.
27. A. Kasaeian et al., "Nanofluid flow and heat transfer in porous media: A review of the latest developments," International Journal of Heat and Mass Transfer, vol. 107. Elsevier Ltd, pp. 778–791, Apr. 01, 2017. http://doi: 10.1016/j.ijheatmasstransfer.2016.11.074.
28. K. Ghasemi and M. Siavashi, "Lattice Boltzmann numerical simulation and entropy generation analysis of natural convection of nanofluid in a porous

cavity with different linear temperature distributions on side walls," J Mol Liq, vol. 233, pp. 415–430, May 2017. http://doi: 10.1016/j.molliq.2017.03.016.

29. I. M. Abed, A. Abdulkadhim, R. A. Hamzah, H. K. Hamzah, and F. H. Ali, "Natural convection heat transfer for adiabatic circular cylinder inside trapezoidal enclosure filled with nanofluid superposed porous-nanofluid layer," FME Transactions, vol. 48, no. 1, pp. 82–89, 2020. http://doi: 10.5937/fmet2001082M.
30. F. Zemani, A. Sabeur-Bendehina, and M. Boussoufi, "Numerical investigation of natural convection in air filled cubical enclosure with hot wavy surface and partial partitions," in Procedia Computer Science, 2014, vol. 32, pp. 622–630. http://doi: 10.1016/j.procs.2014.05.469.
31. Z. Li, M. Yang, and Y. Zhang, "Lattice Boltzmann method simulation of 3-D natural convection with double MRT model," Int J Heat Mass Transf, vol. 94, pp. 222–238, Mar. 2016. http://doi: 10.1016/j.ijheatmasstransfer.2015.11.042.
32. A. A. A. A. Al-Rashed, L. Kolsi, A. K. Hussein, W. Hassen, M. Aichouni, and M. N. Borjini, "Numerical study of three-dimensional natural convection and entropy generation in a cubical cavity with partially active vertical walls," Case Studies in Thermal Engineering, vol. 10, pp. 100–110, Sep. 2017. http://doi: 10.1016/j.csite.2017.05.003.
33. P. Wang, Y. Zhang, and Z. Guo, "Numerical study of three-dimensional natural convection in a cubical cavity at high Rayleigh numbers," Int J Heat Mass Transf, vol. 113, pp. 217–228, 2017. http://doi: 10.1016/j.ijheatmasstransfer.2017.05.057.
34. A. Spizzichino, E. Zemach, and Y. Feldman, "Oscillatory instability of a 3D natural convection flow around a tandem of cold and hot vertically aligned cylinders placed inside a cold cubic enclosure," Int J Heat Mass Transf, vol. 141, pp. 327–345, Oct. 2019. http://doi: 10.1016/j.ijheatmasstransfer.2019.06.050.

35. A. A. Alnaqi, A. K. Hussein, L. Kolsi, A. A. A. A. Al-Rashed, D. Li, and H. M. Ali, “Computational study of natural convection and entropy generation in 3-D cavity with active lateral walls,” Thermal Science, vol. 24, pp. 2089–2100, 2020. http://doi: 10.2298/TSCI180810346A.
36. A. S. Alshomrani, S. Sivasankaran, and A. A. Ahmed, “Numerical study on convective flow and heat transfer in 3D inclined enclosure with hot solid body and discrete cooling,” Int J Numer Methods Heat Fluid Flow, vol. 30, no. 10, pp. 4649–4659, Aug. 2020. http://doi: 10.1108/HFF-09-2019-0692.
37. O. O. M, S. J. K, O. J. A, and O. J. M, “Enhancement of Natural Convection Heat Transfer in a Square Enclosure with Localized Heating from Below,” International Journal of Science and Research, Accessed: Aug. 12, 2022.
38. M. Ahmadi, “Fluid flow and heat transfer characteristics of natural convection in square 3-D enclosure due to discrete sources,” World Appl Sci J, vol. 29, no. 10, pp. 1291–1300, 2014. http://doi: 10.5829/idosi.wasj.2014.29.10.1578.
39. N. Gibanov and M. Sheremet, “Unsteady natural convection in a cubical cavity with a triangular heat source,” Int J Numer Methods Heat Fluid Flow, vol. 27, no. 8, pp. 1795–1813, 2017. http://doi: 10.1108/HFF-06-2016-0234.
40. N. S. Gibanov and M. A. Sheremet, “Natural convection in a cubical cavity with different heat source configurations,” Thermal Science and Engineering Progress, vol. 7, pp. 138–145, Sep. 2018. http://doi: 10.1016/j.tsep.2018.06.004.
41. N. Gibanov and M. A. Sheremet, “Effect of trapezoidal heater on natural convection heat transfer and fluid flow inside a cubical cavity,” Int J Numer Methods Heat Fluid Flow, vol. 29, no. 4, pp. 1232–1248, Jun. 2019. http://doi: 10.1108/HFF-07-2018-0407.
42. J. Ravnik, L. Kerget, and M. Hriberek, “Analysis of three-dimensional natural convection of nanofluids by BEM,” Eng Anal Bound Elem, vol. 34, no. 12, pp. 1018–1030, Dec. 2010. http://doi: 10.1016/j.enganabound.2010.06.019.

43. A. Arefmanesh and M. Tavakoli, “Nanofluid Natural Convection in a Three-Dimensional Cubic Cavity Using The Meshless Local Petrov-Galerkin Method,” 2012.
44. L. Kolsi, A. K. Hussein, M. N. Borjini, H. A. Mohammed, and H. ben Aïssia, “Computational Analysis of Three-Dimensional Unsteady Natural Convection and Entropy Generation in a Cubical Enclosure Filled with Water-Al2O3 Nanofluid,” Arab J Sci Eng, vol. 39, no. 11, pp. 7483–7493, Oct. 2014. http://doi: 10.1007/s13369-014-1341-y.
45. P. Ternik, “Conduction and convection heat transfer characteristics of water-Au nanofluid in a cubic enclosure with differentially heated side walls,” Int J Heat Mass Transf, vol. 80, pp. 368–375, 2015. http://doi: 10.1016/j.ijheatmasstransfer.2014.09.041.
46. A. Purusothaman, N. Nithyadevi, H. F. Oztop, V. Divya, and K. Al-Salem, “Three dimensional numerical analysis of natural convection cooling with an array of discrete heaters embedded in nanofluid filled enclosure,” Advanced Powder Technology, vol. 27, no. 1, pp. 268–280, Jan. 2016. http://doi: 10.1016/j.apt.2015.12.012.
47. M. Salari, E. H. Malekshah, and M. H. Esfe, “Three dimensional simulation of natural convection and entropy generation in an air and MWCNT/water nanofluid filled cuboid as two immiscible fluids with emphasis on the nanofluid height ratio’s effects,” J Mol Liq, vol. 227, pp. 223–233, Feb. 2017. http://doi: 10.1016/j.molliq.2016.12.004.
48. M. Salari, E. H. Malekshah, and M. H. Malekshah, “Three-dimensional numerical analysis of the natural convection and entropy generation of MWCNTs-H2O and air as two immiscible fluids in a rectangular cuboid with fillet corners,” Numeri Heat Transf A Appl, vol. 71, no. 8, pp. 881–894, Apr. 2017. http://doi: 10.1080/10407782.2017.1309213.
49. L. Kolsi, K. Kalidasan, A. Alghamdi, M. N. Borjini, and P. R. Kanna, “Natural convection and entropy generation in a cubical cavity with twin adiabatic blocks filled by aluminum oxide–water nanofluid,” Numeri Heat

Transf A Appl, vol. 70, no. 3, pp. 242–259, Aug. 2016. http://doi: 10.1080/10407782.2016.1173478.

50. L. Kolsi, H. F. Oztop, A. Alghamdi, N. Abu-Hamdeh, M. N. Borjini, and H. ben Aissia, “A computational work on a three dimensional analysis of natural convection and entropy generation in nanofluid filled enclosures with triangular solid insert at the corners,” J Mol Liq, vol. 218, pp. 260–274, Jun. 2016. http://doi: 10.1016/j.molliq.2016.02.083.
51. A. Rahimi, A. Kasaeipoor, and E. H. Malekshah, “Lattice Boltzmann simulation of natural convection and entropy generation in cavities filled with nanofluid in existence of internal rigid bodies-Experimental thermo-physical properties,” J Mol Liq, vol. 242, pp. 580–593, Sep. 2017. http://doi: 10.1016/j.molliq.2017.07.039.
52. L. Wang, B. Shi, and Z. Chai, “Effects of temperature-dependent properties on natural convection of nanofluids in a partially heated cubic enclosure,” Appl Therm Eng, vol. 128, pp. 204–213, 2018. http://doi: 10.1016/j.applthermaleng.2017.09.006.
53. A. Benabderrahmane and A. Messadi, “NUMERICAL INVESTIGATION OF NATURAL CONVECTIVE HEAT TRANSFER AND ENTROPY GENERATION INSIDE A CLOSED CAVITY USING NANOFLUID.”
54. M. Sannad, B. Abourida, L. Belarche, H. Doghmi, and M. Ouzaouit, “Effect of the heating block position on natural convection in a three-dimensional cavity filled with nanofluids,” Journal of Applied Fluid Mechanics, vol. 12, no. 1, pp. 281–291, 2019. https://doi: 10.29252/jafm.75.253.29026.
55. M. Sannad, B. Abourida, and E. H. Belarche, “Numerical study of the effect of the nanofluids type and the size of the heating sections on heat transfer for cooling electronic components,” Journal of Advanced Research in Fluid Mechanics and Thermal Sciences, vol. 75, no. 2, pp. 168–184, 2020. https://doi: 10.37934/ARFMTS.75.2.168184.

56. M. Sannad, A. Btissam, and B. Lahoucine, “Numerical simulation of the natural convection with presence of the nanofluids in cubical cavity,” Math Probl Eng, vol. 2020, 2020. https://doi: 10.1155/2020/8375405.
57. F. Selimefendigil and H. F. Öztop, “Control of natural convection in a CNT-water nanofluid filled 3D cavity by using an inner T-shaped obstacle and thermoelectric cooler,” Int J Mech Sci, vol. 169, Mar. 2020. https://doi: 10.1016/j.ijmecsci.2019.105104.
58. L. el Moutaouakil, M. Boukendil, Z. Zrikem, and A. Abdelbaki, “Natural convection and thermal radiation influence on nanofluids in a cubical cavity,” International Journal of Heat and Technology, vol. 38, no. 1, pp. 59–68, Mar. 2020. https://doi: 10.18280/ijht.380107.
59. H. Li and S. Tong, “Natural convective heat transfer in the inclined rectangular cavities with low width-to-height ratios,” Int J Heat Mass Transf, vol. 93, pp. 398–407, Feb. 2016. https://doi: 10.1016/j.ijheatmasstransfer.2015.10.027.
60. G. Nardini, M. Paroncini, and R. Vitali, “Experimental and numerical analysis of the effect of the position of a bottom wall hot source on natural convection,” Appl Therm Eng, vol. 92, pp. 236–245, Jan. 2016. https://doi: 10.1016/j.applthermaleng.2015.09.085.
61. O. S. Bharti, A. K. Saha, M. K. Das, and S. Bansal, “Simultaneous measurement of velocity and temperature fields during natural convection in a water-filled cubical cavity,” Exp Therm Fluid Sci, vol. 99, pp. 272–286, Dec. 2018. https://doi: 10.1016/j.expthermflusci.2018.07.039.
62. H. Karatas and T. Derbentli, “Natural convection and radiation in rectangular cavities with one active vertical wall,” International Journal of Thermal Sciences, vol. 123, pp. 129–139, Jan. 2018. https://doi: 10.1016/j.ijthermalsci.2017.09.006.
63. H. Karatas and T. Derbentli, “Natural convection in differentially heated rectangular cavities with time periodic boundary condition on one side,” Int J

Heat Mass Transf, vol. 129, pp. 224–237, Feb. 2019. https://doi: 10.1016/j.ijheatmasstransfer.2018.09.087.

64. S. Z. Heris, M. B. Pour, O. Mahian, and S. Wongwises, “A comparative experimental study on the natural convection heat transfer of different metal oxide nanopowders suspended in turbine oil inside an inclined cavity,” Int J Heat Mass Transf, vol. 73, pp. 231–238, Jun. 2014. https://doi: 10.1016/j.ijheatmasstransfer.2014.01.071.

65. A. Brusly Solomon, J. van Rooyen, M. Rencken, M. Sharifpur, and J. P. Meyer, “Experimental study on the influence of the aspect ratio of square cavity on natural convection heat transfer with Al2O3/Water nanofluids,” International Communications in Heat and Mass Transfer, vol. 88, pp. 254–261, Nov. 2017. https://doi: 10.1016/j.icheatmasstransfer.2017.09.007.

66. A. Rahimi, A. Kasaeipoor, E. H. Malekshah, and L. Kolsi, “Experimental and numerical study on heat transfer performance of three-dimensional natural convection in an enclosure filled with DWCNTs-water nanofluid,” Powder Technol, vol. 322, pp. 340–352, Dec. 2017. https://doi: 10.1016/j.powtec.2017.09.008.

67. A. Rahimi, M. Rahjoo, S. S. Hashemi, M. R. Sarlak, M. H. Malekshah, and E. H. Malekshah, “Combination of Dual-MRT lattice Boltzmann method with experimental observations during free convection in enclosure filled with MWCNT-MgO/Water hybrid nanofluid,” Thermal Science and Engineering Progress, vol. 5, pp. 422–436, Mar. 2018. https://doi: 10.1016/j.tsep.2018.01.011.

68. M. Torki and N. Etesami, “Experimental investigation of natural convection heat transfer of SiO2/water nanofluid inside inclined enclosure,” J Therm Anal Calorim, vol. 139, no. 2, pp. 1565–1574, Jan. 2020. https://doi: 10.1007/s10973-019-08445-9.

69. S. O. Giwa, M. Sharifpur, and J. P. Meyer, “Experimental study of thermo-convection performance of hybrid nanofluids of Al2O3-MWCNT/water in a

differentially heated square cavity," Int J Heat Mass Transf, vol. 148, Feb. 2020. https://doi: 10.1016/j.ijheatmasstransfer.2019.119072.

70. A. K. Hussein et al., "Three-dimensional unsteady natural convection and entropy generation in an inclined cubical trapezoidal cavity with an isothermal bottom wall," Alexandria Engineering Journal, vol. 55, no. 2, pp. 741–755, Jun. 2016. https://doi: 10.1016/j.aej.2016.01.004.
71. V. I. Terekhov and A. L. Ekaid, "Three-dimensional laminar convection in a parallelepiped with heating of two side walls," High Temperature, vol. 49, no. 6, pp. 874–880, Dec. 2011. https://doi: 10.1134/S0018151X11060228.
72. M. D. D. Moura and A. C. P. B. Junior, "HEAT TRANSFER BY NATURAL CONVECTION IN 3D ENCLOSURES", 14th Brazilian Congress of Thermal Sciences and Engineering, 18-22, Nov, 2012.
73. A. A. A. A. Al-Rashed, W. Hassen, L. Kolsi, H. F. Oztop, A. J. Chamkha, and N. Abu-Hamdeh, "Three-dimensional analysis of natural convection in nanofluid-filled parallelogrammic enclosure opened from top and heated with square heater," J Cent South Univ, vol. 26, no. 5, pp. 1077–1088, May 2019. https://doi: 10.1007/s11771-019-4072-0.
74. A. Khaleel and K. Al-Khafaji, "Mixed Convection Heat Transfer Enhancement in Lid-Driven Cavities Filled with Nanofluids," 2018.
75. Wong Yean and P. Darul Ridzuan, "Natural Convection Heat Transfer and Fluid Flow in Enclosures with Varying Aspect Ratios (CFD)."
76. H. F. Oztop, M. Mobedi, E. Abu-Nada, and I. Pop, "A heatline analysis of natural convection in a square inclined enclosure filled with a CuO nanofluid under non-uniform wall heating condition," *Int J Heat Mass Transf*, vol. 55, no. 19–20, pp. 5076–5086, 2012. https://doi: 10.1016/j.ijheatmasstransfer.2012.05.007.
77. E. Ghahremani, R. Ghaffari, H. Ghadjari, and J. Mokhtari, "Effect of variable thermal expansion coefficient and nanofluid properties on steady natural convection in an enclosure," *Journal of Applied and Computational*

Mechanics, vol. 3, no. 4, pp. 240–250, Sep. 2017. https://doi: 10.22055/jacm.2017.21451.1099.

78. Hamilton, R.L., Crosser, O.K. (1962). Thermal conductivity of heterogeneous two-component systems. Industrial and Engineering Chemistry Fundamentals, 1(3): 187-191. https://doi.org/10.1021/i160003a005

79. F. H. Lai and Y. T. Yang, "Lattice Boltzmann simulation of natural convection heat transfer of Al 2O3/water nanofluids in a square enclosure," *International Journal of Thermal Sciences*, vol. 50, no. 10, pp. 1930–1941, Oct. 2011. https:// doi: 10.1016/j.ijthermalsci.2011.04.015

80. Holman JD. Experimental methods for engineers. New York: McGraw-Hill; 1986.

81. Young HD. Statistical treatment of experimental data. New York:McGraw-Hill; 1962. https://doi.org/10.1002/bimj.19650070123

وزارة التعليم العالي والبحث العلمي
جامعة بابل
كلية الهندسة
قسم الهندسة الميكانيكية

التحقيق في الحمل الحراري الطبيعي داخل تجويف ثلاثي الأبعاد ذو أشكال هندسية مختلفة مملوء بموائع نانوية

أطروحة

مقدمة الى كلية الهندسة جامعة بابل كجزء من متطلبات نيل درجة دكتوراه فلسفة في الهندسة الميكانيكية

من قبل
زينب كريم غبن
بكالوريوس في الهندسة الميكانيكية ٢٠٠٩
ماجستير في الهندسة الميكانيكية ٢٠١٣

بإشراف
الأستاذ الدكتور أحمد كاظم حسين

١٤٤٤ هـ - ٢٠٢٣ م